



Synthesis, identification, and biological characterisation of sterol transport protein inhibitors

Whitmarsh-Everiss, Thomas

Publication date:
2022

Document Version
Publisher's PDF, also known as Version of record

[Link back to DTU Orbit](#)

Citation (APA):
Whitmarsh-Everiss, T. (2022). *Synthesis, identification, and biological characterisation of sterol transport protein inhibitors*. DTU Chemistry.

General rights

Copyright and moral rights for the publications made accessible in the public portal are retained by the authors and/or other copyright owners and it is a condition of accessing publications that users recognise and abide by the legal requirements associated with these rights.

- Users may download and print one copy of any publication from the public portal for the purpose of private study or research.
- You may not further distribute the material or use it for any profit-making activity or commercial gain
- You may freely distribute the URL identifying the publication in the public portal

If you believe that this document breaches copyright please contact us providing details, and we will remove access to the work immediately and investigate your claim.

Synthesis, identification, and biological characterisation of sterol transport protein inhibitors

PhD Thesis

Thomas Whitmarsh-Everiss

August 2022

DTU Chemistry

Technical University of Denmark

Kemitorvet, building 207

2800 Kgs. Lyngby

Denmark

PhD Supervisor:

Associate Professor Luca Laraia

In memory of my Dad who passed during the writing of this thesis.

Preface

The work presented in this PhD thesis is the result of experimental work carried out at the Technical University of Denmark from September 2018 - August 2022 as part of a 4+4 PhD programme under supervision of Associate Professor Luca Laraia. A four-month external stay at Umeå University, Sweden in the research group of Professor Yaowen Wu was carried out from February 2022 – May 2022.

A number of project students and group members have contributed to the work presented in the thesis, and have either been acknowledged in the thesis text or in the acknowledgement section. Contributions have included analogue and starting material synthesis, protein expression and purification, and biochemical screening.

Acknowledgements

First and foremost I must thank my supervisor Associate Professor Luca Laraia for providing me the opportunity to carry out my PhD studies in his group. Thank you for the continued supervision and support throughout my time in the group, and for fostering such a great group atmosphere and environment to carry out research in. Thank you to all of the current and former group members of the Laraia group; Cecilia, Mikkel, Elisa, Nianzhe, Ruwei, Joseph, Frederik, and Laura. Thanks for all the conversations, scientific discussions, and problem solving (especially related to western blots) over the years.

For hosting me in his lab for my external stay at Umeå University, I would also like to thank Professor Yaowen Wu. Thank you to all the members of the Wu lab for creating such a welcoming atmosphere. A special thanks to Nastya, Dale, Sergio, Laura, and Shuang for helping to make my short stay in Umeå as incredible as it was and creating so many memories in my 4 month stay.

Thank you to all of the project students I have had the pleasure to supervise throughout my PhD. For their contributions to the synthetic side of the project I would like to acknowledge Anna, Razan, Magnus, Christoffer W., Christoffer T. A., Line, and Christine. For his contributions to establishing and optimising the early biochemistry of the project, I would like to acknowledge Asger.

For their specific contributions, either to the Aster project or to helping to teach me new research skills I acknowledge and thank the following people. Dr. Elisa Sassetti and Dr. Cecilia Rossetti are thanked for their support and supervision in helping me learn how to perform cell culture and biological screening. Dr. Laura Depta is thanked for screening of compounds against a number of STPs and for additional contributions to the overall Aster/STP project. Dr. Dale Corkery is thanked for his extensive help, supervision, and contributions throughout my external stay particularly with all of the confocal microscopy imaging. Frederik Simonsen Bro is thanked for the synthesis of the individual enantiomers of Asterpyrin-1.

Thank you to everyone who offered support during the last year of my PhD, helping me to deal with the death of both my Grandad and Dad, and keeping me motivated and focussed to continue with my research and thesis despite the losses. Finally, I would like to thank all of my family for their continued support throughout my PhD, especially my little brother who has helped to keep me going through particularly challenging parts of my studies.

Abstract

Sterol transport proteins (STPs) are an important class of proteins performing an integral role in a range of cellular processes including cholesterol homeostasis, vesicular and non-vesicular trafficking, and regulating organelle contact sites. Despite their importance, the identification of selective modulators of STPs has proved challenging, owing to the high degree of structural similarity in their sterol binding domains. To overcome this challenge, an approach was developed to synthesise a screening collection of sterol-inspired compounds enriched in hits against STPs. By fusing a representative steroidal scaffold to a series of heterocyclic scaffolds, a collection of 65 sterol-inspired compounds were prepared for use in screening.

The relevance of the sterol-inspired compound collection in affording selective hits against STPs was demonstrated by screening against the Aster family of STPs (Asters-A, -B, and -C) using a combination of differential scanning fluorimetry (DSF), fluorescence polarisation (FP), and fluorescence resonance energy transfer (FRET)-based assays. Hit compounds were identified and validated against Aster-A and Aster-C which after further optimisation resulted in the discovery of a new chemotype of Aster-A inhibitor, Asterpyrin-1, and the most potent and selective inhibitor of Aster-C known to date, Astercin-2. Finally, the inhibitors were used to investigate Aster-related biology in a cellular setting, revealing differential effects on the levels and localisation of cholesterol and cholesterol esters, and demonstrating the utility of these sterol-inspired compounds as tool compounds.

Resumé

Sterol transportproteiner (STP'er) er en vigtig klasse af proteiner med en essentiel rolle i en række cellulære processer som for eksempel kolesterol homøostase, vesikulær og ikke-vesikulær transport samt regulering af kontakt områder for organeller. På trods af deres betydning har identifikationen af selektive modulatorer af STP'er vist sig udfordrende på grund af den høje grad af strukturel lighed i domænet hvor sterol binder. For at adressere denne udfordring blev en samling af sterol-inspirerede kemiske forbindelser syntetiseret med fokus på at opnå aktivitet mod STP'er. Dette var muligt ved at fusionere en repræsentativ steroid struktur med en række heterocykliske strukturer, der resulterede i 65 sterol-inspirerede forbindelser fremstillet til screening.

Relevansen af de sterol-inspirerede forbindelser med henblik på at opnå selektiv aktivitet mod STP'er blev demonstreret ved at screene forbindelserne mod Aster-familien af STP'er (Aster-A, -B og -C). Til dette blev en kombination af differentiell scanningsfluorimetri (DSF), fluorescenspolarisering (FP) og fluorescensresonansenergioverførsel (FRET)-baserede assays anvendt. Forbindelser med aktivitet blev identificeret og valideret mod Aster-A og Aster-C, hvilket efter yderligere optimering resulterede i opdagelsen af en ny kemotype af Aster-A inhibitor, Asterpyrin-1, og den mest potente og selektive inhibitor af Aster-C til dato, Astercin-2. Endelig blev inhibitorerne brugt til at undersøge Aster-relateret biologi i et cellulært miljø, hvorved differentielle virkninger på niveauerne samt lokaliseringen af kolesterol og kolesterollestere blev opdaget, udover at demonstrere anvendeligheden af disse sterol-inspirerede forbindelser til at studere relaterede biologiske processer.

List of publications

- (1) Whitmarsh-Everiss, T.; Olsen, A. H.; Laraia, L. **Identification of Inhibitors of Cholesterol Transport Proteins through the Synthesis of a Diverse, Sterol-Inspired Compound Collection.** *Angew. Chemie - Int. Ed.* **2021**, 60 (51), 26755–26761 (*Hot Paper*).
- (2) Whitmarsh-Everiss, T.; Laraia, L. **Small molecule probes for targeting autophagy.** *Nat. Chem. Biol.* **2021**, 17 (6), 653–664.
- (3) Depta, L.; Whitmarsh-Everiss, T.; Laraia, L. **Structure, function and small molecule modulation of intracellular sterol transport proteins.** *Bioorg, Med. Chem.* **2022**, 116856.

Manuscripts under preparation

- (1) Whitmarsh-Everiss, T.; Wang, Z.; Hauberg Hansen, C.; Sassetti, E.; Rafn Dan, O.; Pahl, A.; Sievers, S.; Laraia, L. **Synthesis and evaluation of a chemically and biologically diverse estrogen-inspired compound library.** (Submitted to ChemBioChem)
- (2) Whitmarsh-Everiss, T.; Simonsen Bro, F; Depta, L; Corkery, D; Wu, Y.-W; Laraia, L. **Manuscript in preparation.**

Table of Contents

Abbreviations	xi
Part I – Introduction	1
1.1 Bioactive compound discovery	1
1.2 Steroids in drug discovery	2
1.3 Synthesising natural product-like compounds	3
1.3.1 Ring distortion and Complexity-to-Diversity	3
1.3.2 Diversity oriented synthesis approaches	5
1.3.3 Biology-oriented synthesis	7
1.3.4 Natural product fragment-based approaches	8
1.3.5 Pseudo-natural products	9
1.4 Sterols and sterol homeostasis	11
1.4.1 Cholesterol biosynthesis	11
1.4.2 Cholesterol uptake	12
1.4.3 Regulation of cholesterol homeostasis	13
1.5 Sterol transport proteins	14
1.5.1 Aster proteins	15
1.5.2 Functions of the Aster proteins	16
1.5.3 Small molecule inhibitors of sterol transport proteins	17
Part II – Synthesis of a sterol-inspired compound collection	20
2.1 Project aims and outline	20
2.2 Designing a sterol-inspired compound collection	21
2.2.1 Synthesis of a sterol-inspired building block	22
2.2.2 Synthesis of intermediate building blocks	24
2.2.3 Analogue synthesis from the sterol-inspired ketone	26
2.2.4 Analogue synthesis from the sterol-inspired α -bromoketone	32
2.2.5 Analogue synthesis from the sterol-inspired hydroxymethylenes	33
2.2.6 Analogue synthesis from the sterol-inspired β -ketoester	36
2.3 Sterol-inspired compound collection summary	37
Part III – Biochemical screening and optimization of sterol transport protein inhibitors	40

3.1 Aster proteins as a screening target	40
3.2 Differential scanning fluorimetry	40
3.2.1 Preliminary screening of the sterol-inspired collection by DSF	41
3.3 Fluorescence polarization	43
3.3.1 Hit validation by fluorescence polarization	44
3.4 Identification of the active enantiomer of (±)-Astercin 1	48
3.4.1 Synthesis of (<i>S</i>)- and (<i>R</i>)-Wieland-Miescher Ketone	48
3.4.2 Synthesis of (+)- and (-)-Astercin 1	49
3.4.3 Screening of Astercin 1 enantiomers by fluorescence polarization	50
3.5 Inhibition of Aster-mediated sterol transfer by (-)-Astercin 1	51
3.5.1 Liposomal FRET assays	51
3.5.2 Liposomal FRET assay optimization	52
3.5.3 Modulation of Aster-mediated cholesterol transfer by Astercin 1	53
3.6 Optimisation of Astercin 1	55
3.6.1 Variation of phenyl substituents	55
3.6.2 Modifications to the pyrazole ring and sterol A/B ring	57
3.6.3 Synthesis of pyrazolopyrimidine Aster-A inhibitor enantiomers	62
3.7 Biochemical analysis of Astercin 1 SAR compounds	63
Part IV – Biological characterisation of sterol-inspired Aster inhibitors	68
4.1 Inhibition of autophagy by Asterpyrin-1	68
4.2 Relevance of Aster-C in autophagy	70
4.3 Cellular localization of Aster-A and Aster-C	71
4.4 Cellular cholesterol	72
4.5 Modulation of free cholesterol by Asterpyrin-1 and Astercin-2	74
4.6 Modulation of lipid droplets by Asterpyrin-1 and Astercin-2	79
4.7 Discussion of Aster inhibitor biology	84
Summary and conclusions	86
Future work	87
Experimentals	89
References	162

Abbreviations

25-HC	25-hydroxycholesterol
ABC	ATP-binding cassette
ACAT	acyl-CoA cholesterol acyltransferase
ALO	Anthrolysin O
AMPK	AMP-activated protein kinase
ApoA-1	Apolipoprotein A1
BIOS	Biology-oriented synthesis
Boc	<i>tert</i> -butyloxycarbonyl
cAMP	cyclic adenosine monophosphate
CDC	Cholesterol-dependent cytolysin
CE	Cholesteryl ester
CERT	Ceramide transport protein
CETSA	Cellular thermal shift assay
CoA	Coenzyme A
CREBH	cAMP-responsive element-binding protein H
CtD	Complexity-to-diversity
DBDMH	1,3-Dibromo-5,5-dimethylhydantoin
DCC	<i>N,N</i> -dicyclohexylcarbodiimide
DEG	Diethylene glycol
DGAT	Diacylglycerol O-acyltransferase
DHEA	Dehydroepiandrosterone
DIPEA	<i>N,N</i> -Diisopropylethylamine
DMF	Dimethylformamide
DMP	Dess-Martin periodinane
DMSO	Dimethyl sulfoxide
DOPC	1,2-dioleoyl-sn-glycero-3-phosphocholine
DOS	Diversity-oriented synthesis
DSF	Differential scanning fluorimetry

EBSS	Earle's balanced salt solution
EDC	1-Ethyl-3-(3-dimethylaminopropyl)carbodiimide
ee	Enantiomeric excess
EEA1	Early endosome antigen 1
ER	Endoplasmic reticulum
ERC	Endocytic recycling compartment
ESCRT	Endosomal sorting complexes required for transport
FP	Fluorescence polarisation
FRET	Fluorescence resonance energy transfer
Fsp³	Fraction of sp ³ hybridised carbon atoms
Gal3	Galectin-3
GLUT	Class 1 glucose transporter
HATU	1-[Bis(dimethylamino)methylene]-1H-1,2,3-triazolo[4,5-b]pyridinium-3-oxide hexafluorophosphate
HDL	High-density lipoprotein
HMG	3-hydroxy-3-methylglutaryl
HOBt	Hydroxybenzotriazole
HOSA	Hydroxylamine- <i>O</i> -sulfonic acid
HPLC	High performance liquid chromatography
HTS	High-throughput screening
IC₅₀	Half maximal inhibitory concentration
IDOL	Inducible degrader of LDLR
IF	Immunofluorescence
INSIG	Insulin-induced gene
ITDRF	Isothermal dose-response fingerprint
K_d	Dissociation constant
KO	Knockout
LAMP1	Lysosomal-associated membrane protein 1
LAMP2	Lysosome-associated membrane protein-2
LC3	Microtubule associated protein 1 light chain 3

LCMS	Liquid chromatography-mass spectrometry
LD	Lipid droplet
LDA	Lithium diisopropylamide
LDL	Low-density lipoprotein
LDLR	Low-density lipoprotein receptor
LiHMDS	Lithium bis(trimethylsilyl)amide
M	Molar
<i>m</i>CPBA	<i>meta</i> -chloroperoxybenzoic acid
MEM	Methoxyethoxymethyl
mTORC1	Mammalian target of rapamycin complex 1
NBS	<i>N</i> -bromosuccinimide
NCI-60	National Cancer Institute 60 cancer cell lines
NIS	<i>N</i> -iodosuccinimide
NMR	Nuclear magnetic resonance
NP	Natural product
NPC	Niemann-pick type C
NPC1L1	Niemann-Pick type C1-like 1
nSREBP2	Nuclear SREBP2
Oly A	Ostreolysin A
ORP	OSBP-related protein
OSBP	Oxysterol-binding protein
PCR	Polymerase chain reaction
PCTP	Phosphatidylcholine transfer protein
PE	Phosphatidylethanolamine
PFA	Paraformaldehyde
PFO	Perfringolysin O
PI3K	Phosphoinositide 3-kinase
PIP₂	Phosphatidylinositol 4,5-bisphosphate
PLIN2	Perilipin 2
PM	Plasma membrane

PMI	Principal moment of inertia
POI	Protein of interest
PPARα	Proliferator-activated receptor α
PS	Phosphatidylserine
ROS	Reactive oxygen species
RXRα	Retinoid X receptor α
S1P/S2P	Site-1/2 protease
SAR	Structure-activity relationship
SBD	Sterol-binding domain
SCAP	SREBP-cleavage activating protein
SCONP	Structural classification of natural products
SM	Squalene monooxygenase
SR-BI	Scavenger receptor class B type 1
SRE	sterol-regulatory elements
SREBP2	Sterol regulator element-binding protein 2
StAR	Steroidogenic acute regulatory protein
STARD	START-related domain
START	StAR-related lipid transfer
STP	Sterol transport protein
TBAF	tetra- <i>n</i> -butylammonium fluoride
TBS	<i>tert</i> -butyldimethylsilyl
THF	Tetrahydrofuran
THIQ	Tetrahydroisoquinoline
TLC	Thin-layer chromatography
T_m	Melting temperature
TM	Transmembrane
Tosyl	<i>p</i> -Toluenesulfonyl
ULK1	Unc51-like kinase
VT-NMR	Variable temperature NMR
WMK	Wieland-Miescher ketone

Part I – Introduction

The introductory sub-chapters “Sterols and sterol homeostasis”, “Cholesterol biosynthesis”, “Cholesterol uptake”, “Regulation of cholesterol homeostasis”, and “Functions of the Aster/GRAMD1 proteins” were originally written for use in and subsequently published in the review article “Structure, function and small molecule modulation of intracellular sterol transport proteins” (Depta, L.; Whitmarsh-Everiss, T.; Laraia, L. Structure, Function and Small Molecule Modulation of Intracellular Sterol Transport Proteins. *Bioorg. Med. Chem.* **2022**, 116856.) The passages of text remain largely unchanged for what was written in the review, however additions and modifications to the text were made throughout.

1.1 Bioactive compound discovery

The discovery of biologically active small molecules is a significant aspect of both chemical biology and medicinal chemistry, ultimately leading to the development of chemical probes to study select biological processes and forming the starting point of drug discovery campaigns. The identification of bioactive compounds has traditionally been performed in a low-throughput manner utilising crude natural product (NP) extracts, with subsequent purification and characterisation of active components.^{1,2} Significant technological and scientific advancements throughout the 20th century culminated in the advent of high-throughput screening (HTS), wherein tens to hundreds of thousands of compounds could be screened per day against a chosen biological target or pathway.³ The widespread adoption of HTS by pharmaceutical companies necessitated larger numbers of screening compounds, to which end combinatorial chemistry was viewed as a potential solution. Combinatorial chemistry is a technique allowing for the synthesis of large numbers of compounds using both solution phase and solid supported synthesis to assemble different monomeric building blocks into vast numbers of compounds.⁴ Despite the promise that combinatorial libraries held, the technique dropped out of favour in the early 2000s owing to several factors. It was often found that the time required to synthesise and characterise new combinatorial libraries as part of structure-activity relationship (SAR) studies often lasted longer than the initial chemical hit remained relevant, resulting in a significant loss of time and resources.⁵ Combinatorial libraries were also found to have poor structural and shape diversity, often being derived from flat heteroaromatic core scaffolds, and as a result the biological diversity of these libraries was limited, resulting in poor performance and hit rates in screening efforts.⁶

To improve the quality of screening compounds, cheminformatics analysis studies were performed on typical screening collections, synthetic drugs, and NPs in order to determine whether any specific properties were associated with producing bioactive compounds. This analysis revealed several key properties of small molecules that confer favourable assay performance to a compound library.^{7,8} Some key features contributing to improved hit rates and protein selectivity include the fraction of sp³ hybridised carbons (Fsp³), increased stereochemical complexity, and high levels of scaffold diversity – features that are enriched in natural products.⁹ Natural products have historically been a significant source of bioactive compounds, and to this day remain an important source of drugs with over 34% of small-molecule drugs approved between 1981 – 2019 being NPs or NP-derived.¹⁰

1.2 Steroids in drug discovery

Steroids are an important class of natural product typically derived from the tetracyclic gonane **1.01** core scaffold (Figure 1.1). Mammalian steroid derivatives decorate this core scaffold with additional substituents, often by oxidation of the A- and B-rings or through appendage of alkyl chains to the D-ring. Prototypical steroids include the cholestanes cholesterol **1.02**, estranes such as estradiol **1.03**, and the androstane testosterone **1.04**.¹¹ Steroids possess a vast range of bioactivities, spanning from the anti-inflammatory properties of the corticosteroids, to the anabolic effects of the androgens including testosterone.¹² This rich bioactivity has resulted in the direct therapeutic use of many endogenous steroids with progestogens, estrogens, and androgens alike having extensive uses in hormone therapy targeting a multiplicity of disease areas.^{13,14} In addition to the use of endogenous steroids as drugs, synthetic steroid derivatives have also seen extensive use. Commonly used synthetic steroidal drugs include the immunosuppressant methylprednisolone **1.05**, as well as the androstane-derived abiraterone acetate **1.06** that is used in a combination therapy for treatment of metastatic castration-resistant prostate cancer.^{15,16}

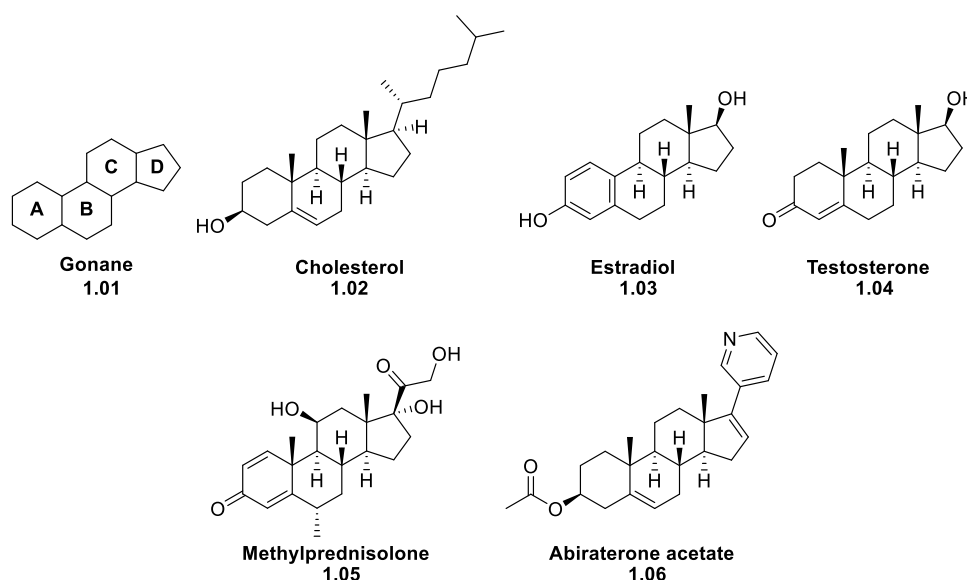


Figure 1.1 Chemical structures of Gonane, the representative steroids cholesterol, estradiol, and testosterone, and of two synthetic steroid drugs methylprednisolone and abiraterone acetate.

The range and diversity of steroid bioactivities suggests that the steroid core itself could serve as an excellent privileged scaffold for the basis of a small-molecule screening library. Privileged scaffolds can be defined as a molecular scaffold with the capability to bind multiple protein targets, resulting in a range of different bioactivities.¹⁷ Use of the steroid scaffold in library synthesis is typically limited to the fusion or appendage of heterocycles to either the A-ring or D-ring of the steroid scaffold via short synthetic sequences (i.e. 2 – 5 synthetic steps) from commercially available building blocks. Steroidal ketones hydrocortisone **1.07**, dehydroepiandrosterone (DHEA) **1.08**, and estrone **1.09** have been used as core building block scaffolds to afford series of pyrazole-fused glucocorticoid modulators **1.10**, cytotoxic thiadiazoles **1.11**, and antiproliferative triazolopyrimidines **1.12**, with the exemplified chemistries being representative of the use of these building blocks (Figure 1.2).^{18–20}

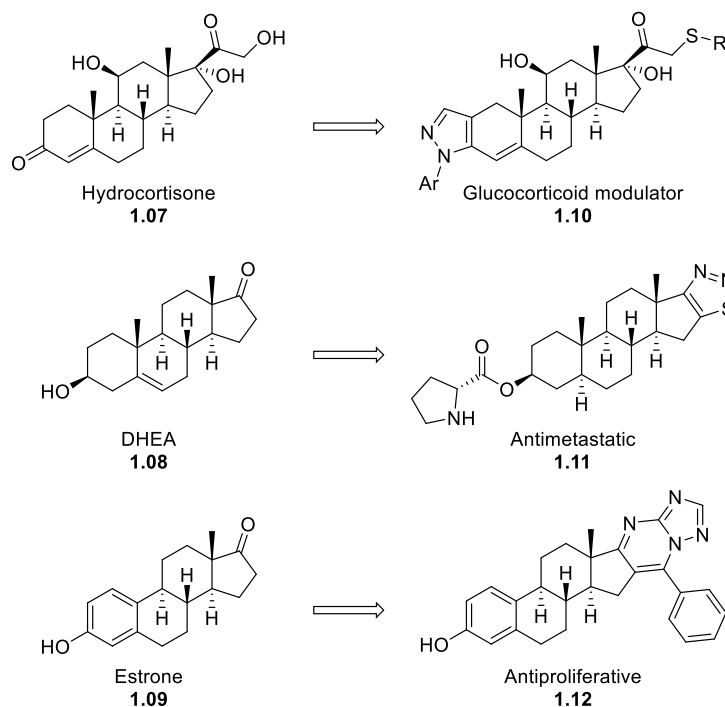


Figure 1.2 Representative examples of steroid building blocks used for synthesis of screening collections and resulting bioactive steroidal compounds.

Whilst using the complete steroid scaffold as a basis for library synthesis is a viable approach to access new bioactive compounds, the approach does suffer from some limitations. One major limitation is that the number of commercial steroids amenable for use in library synthesis is limited, and as such, the chemical and biological space explored by steroidal compound libraries remains poor.

1.3 Synthesising natural product-like compounds

Given the inherent biological activities and favourable molecular properties presented by NPs, including steroids, significant research has been performed on developing methods to synthesise more NP-like screening libraries, with the aim of affording compound libraries capable of probing uncharted chemical and biological space.²¹ The following sections will introduce several of these key techniques, with an emphasis on examples utilising steroidal compounds where applicable.

1.3.1 Ring distortion and Complexity-to-Diversity

One approach to synthesise NP-like compound libraries was introduced by the Hergenrother lab, wherein NPs available on commercial scales are utilised as the starting point of library synthesis. The approach termed Complexity-to-Diversity (CtD) takes a stereochemically complex natural product with multiple points of reactivity, and through a series of synthetic steps transforms it into a range of diverse products retaining the complexity of the parent NP.²² The diversity of the compound library is a result of the application of chemoselective ring-distortion reactions that can be further classified as either ring expansion, ring rearrangement, ring cleavage, or ring fusion reactions. The CtD approach has been thoroughly exemplified with multiple types of NPs including terpenes, alkaloids, and steroids.^{23–25}

The steroid hormone adrenosterone **1.13** is one such example of a steroidal-NP used in the CtD approach (Figure 1.3).²³ Inspection of the adrenosterone structure identifies three major points of possible diversification that could be exploited in the CtD approach: the A-ring enone, C-ring ketone, and the D-ring ketone. Analogue **1.14** was synthesised by ethylene glycol protection of the A and D-ring ketones in a ring fusion reaction, treatment with phenyl lithium which adds in a 1,2-addition to the C-ring ketone, and a final *meta*-chloroperoxybenzoic acid (*m*CPBA) epoxidation of the migrated double bond in the B-ring. Treatment of adrenosterone with typical Schmidt conditions (NaN₃ and sulfuric acid) gave rise to a tandem ring-expansion of the A-ring via a Beckmann rearrangement and cleavage of the D-ring via Schmidt reaction with dehydration of the resulting amide. The D-ring enone was selectively reduced by a Luche reduction and the resulting secondary alcohol and amide were acetylated with acetic anhydride to afford lactam **1.15**. Oxidative cleavage of the A-ring enone with sodium periodate and potassium permanganate, followed by coupling of the resulting acid with 2-bromobenzyl alcohol and a final selective Baeyer-Villiger reaction with peracetic acid gives rise to the A-ring cleaved and B-ring expanded lactone **1.16**.

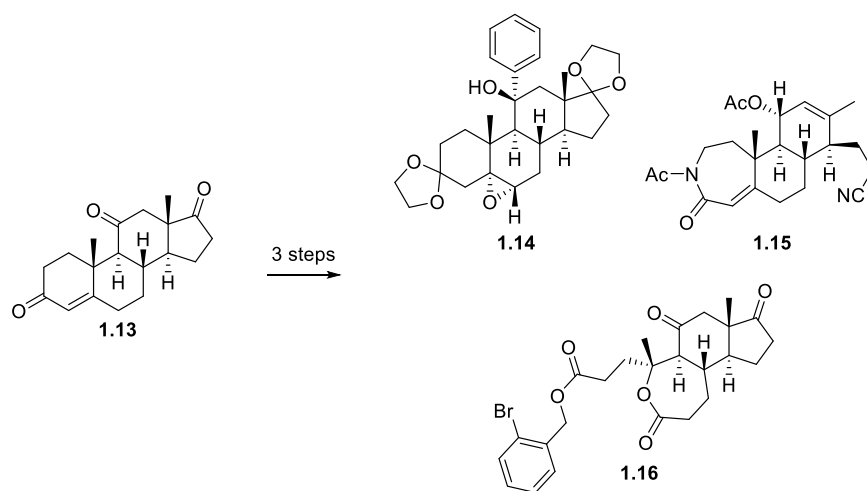


Figure 1.3 The Complexity-to-Diversity approach applied to the commercial steroid hormone adrenosterone and resulting diversified products.²³

Cheminformatics analysis of CtD-derived compound libraries reveals that properties such as the Fsp³ and number of stereocentres are more favourable compared to commercial screening collections, and the compounds thus ideal for use in screening.²³ Though the biological activity of these steroid-derived compounds was not investigated, the CtD approach has been shown to afford novel bioactive compounds. Application of CtD to the antibacterial diterpene pleuromutilin **1.17**, resulted in the identification of a novel inducer of ferroptosis **1.18**, acting through inhibition of thioredoxin (Figure 1.4).²⁶

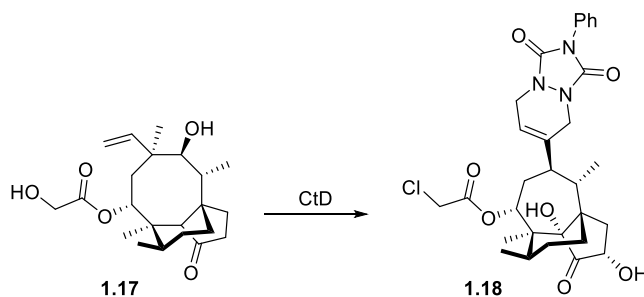


Figure 1.4 CtD applied to the antibacterial NP pleuromutilin and the resulting inducer of ferroptosis.²⁶

The inherent limitations of the CtD approach include the requirement for a commercial NP available at a sufficient scale and price to permit its use as a library precursor as well as a sufficient number of reactive sites to facilitate the outlined ring-distortions and allow diversification of the parent NP. These two requirements severely limit the scope of the CtD approach, and other techniques to synthesise NP-like compound libraries have therefore largely moved away from the direct use of NPs as a starting material.

1.3.2 Diversity Oriented Synthesis approaches

One of the first techniques to arise from the need to synthesise structurally complex and diverse compound collections, and the most widely adopted technique, was diversity-oriented synthesis (DOS). The DOS approach is focussed upon accessing compound libraries that probe a large degree of chemical space; the theoretical space covering all plausible small molecules.²⁷ This exploration of chemical space is achieved by targeting different types of diversity: appendage diversity, scaffold diversity, functional group diversity, and stereochemical diversity.²⁸ Taken together, these four main types of diversity contribute to the overall shape diversity of DOS libraries, however analysis has revealed that the main driver of library shape diversity and therefore biological performance stems from scaffold diversity. The molecular complexity arising from stereochemical and appendage diversity was also identified as a major contributing factor towards target specificity.^{6,29}

Synthesising scaffold diverse compound libraries via DOS can be achieved using either reagent-based DOS or substrate-based DOS (Figure 1.5). The reagent-based DOS approach uses a common starting material for library synthesis, and through changing combinations of reagents, allows access to a range of different core scaffolds. Two types of starting materials are utilised in the reagent-based approach, starting materials that are either densely functionalised or that possess pluripotent functional groups.²⁸ Densely functionalised starting materials tend to bring together different parts of the molecule in the assembly of the core scaffold, exploiting the reactivity of different functional groups. Pluripotent starting materials depend upon differences in the reactivity of one functional group under a range of different conditions to assemble the core scaffold. In contrast to reagent-based DOS, substrate-based DOS uses starting materials with designed “pre-encoded” reactivity that when subjected to a common set of conditions will react and cyclise to afford a range of core scaffolds.³⁰

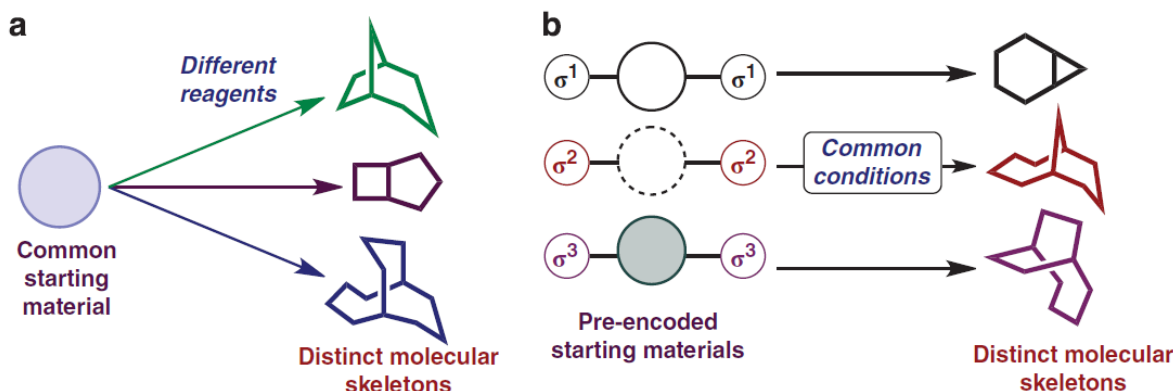
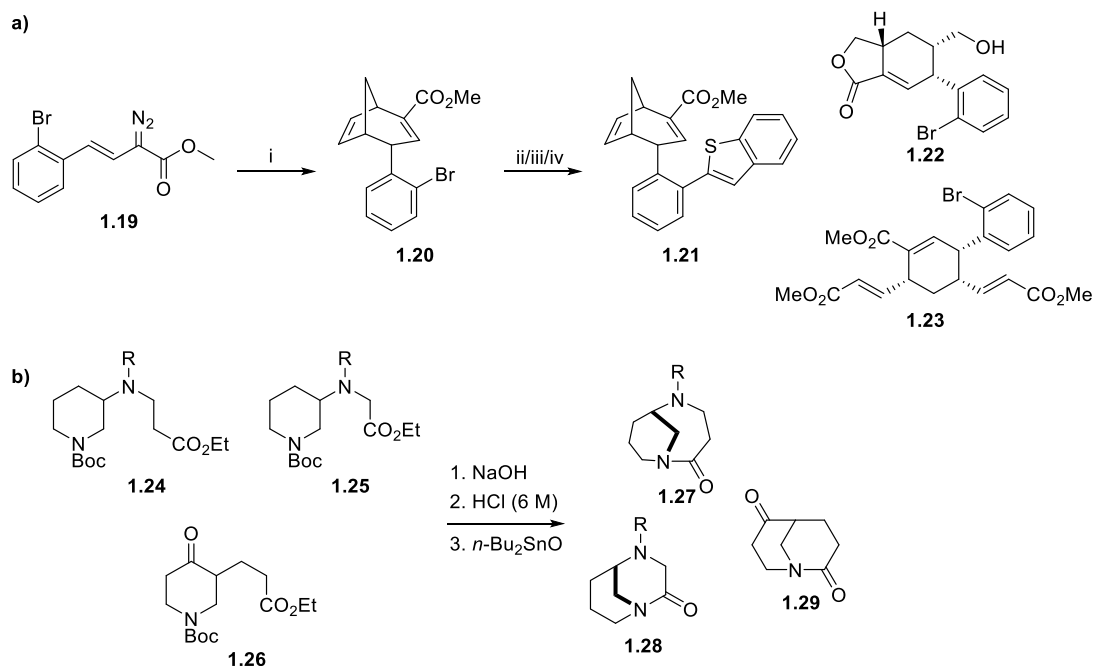


Figure 1.5 Two main types of DOS to achieve scaffold diversity. Schematic representations of the (a) reagent-based DOS approach and (b) the substrate-based DOS approach. Figure reproduced with permission from reference.²⁸ Copyright (2010) Springer Nature.

Using the reagent-based DOS approach, a library of 35 complex and diverse small molecules were synthesised from the diazoester **1.19** (Scheme 1.1a).³¹ A rhodium-catalysed tandem cyclopropanation-cope rearrangement of diazoester **1.19** with cyclopentadiene gave access to the bridged ester **1.20**. From this pluripotent intermediate, a number of scaffolds were synthesised using different combinations of reagents. Suzuki couplings with arylboronic acids gave rise to compounds such as **1.21**, whereas subjecting ester **1.20** to oxidative ring cleavage conditions gave rise to the bicyclic lactone **1.22** after hydride reduction of the intermediate ester and spontaneous transesterification. The highly-substituted cyclohexene **1.23** was synthesised in a ring opening/cross metathesis with a 2nd generation Hoveyda-Grubbs catalyst. Screening of the resulting DOS library by phenotypic screening and subsequent target identification identified a new class of mitosis modulators based upon compound **1.21**. Substrate-based DOS has been applied in the synthesis of a library of three-dimensional alkaloid-derived fragments based around bicyclo[3.3.1]nonane and bicyclo[4.3.1]decane core scaffolds. Commercial piperidones were converted into their corresponding tethered-amino esters **1.24**, **1.25**, and **1.26**, from which the lactam fragments including **1.27**, **1.28**, and **1.29** were synthesised in a ester hydrolysis/nitrogen deprotection/amide formation sequence (Scheme 1.1b).³² Whilst the compound collection was not subjected to screening efforts, the utility as a fragment set was demonstrated through the synthesis of a number of additional analogues featuring both heterocycle fusions and N-functionalisation.



Scheme 1.1 Representative examples of reagent-based DOS and substrate-based DOS. **(a)** Reagent-based DOS employing a pluripotent intermediate building block **1.20**. i) cyclopentadiene, Rh₂(OAc)₄; ii) Pd(OAc)₂, PPh₃, K₂CO₃; iii) NMO/OsO₄/PhI(OAc)₂ then NaBH₄; iv) alkene, Hoveyda-Grubbs (II) catalyst, ethylene **(b)** Substrate-based DOS using a common set of reagents for a “hydrolysis/deprotection/cyclisation” pathway.

While there is no doubt that the DOS approach is capable of affording new bioactive compounds, it has often been found that many DOS libraries underperform when used in screening – with the increased chemical diversity of collections not always translating to biological performance.³³ As such, there has been a push to synthesise compound libraries not only focussed upon achieving chemical diversity, but that also consider features favourably contributing to selectivity and target diversity, summarised as the biological

performance diversity of the library.³⁴ In response to shortcomings of the DOS approach, additional concepts for library synthesis with a greater focus on achieving biological performance diversity have been developed.

1.3.3 Biology-oriented synthesis

The biology-oriented synthesis (BIOS) approach was developed as one of the first approaches to synthesise compound libraries of higher biological relevance, drawing inspiration from the biological relevance of NPs.³⁵ BIOS avoids the direct use of NPs in library synthesis, as per the CtD approach, and instead builds up a compound library around a simplified NP-inspired scaffold.³⁶ The BIOS approach is based upon the assumption that the biological activity of a NP is related to its core scaffold, as it is the core scaffold that correctly positions a NPs substituents in the protein binding site. Thus, it is to be expected that retention of this core scaffold should, to some extent, retain the biological activity of the parent NP.³⁵ Using cheminformatics based approaches, over 150,000 NPs were analysed and classified according to their core scaffolds in an approach termed the structural classification of NPs (SCONP).³⁷ SCONP simplifies parent NPs in an iterative procedure, removing substituents and gradually removing extra rings, until one ring remains, creating a scaffold branch. A final merger of these individual scaffold branches gives rise to a NP scaffold tree which maps NP chemical space in a logical manner. Moving down a branch of the scaffold tree leads to a simplified scaffold that should retain some of the bioactivity of the parent NP. BIOS utilises SCONP in the selection of biologically relevant scaffolds to serve as a core library building block, from which a library of analogues can be synthesised.³⁸

BIOS has been successfully applied to many different NPs, affording compounds with diverse biological activities.³⁸ One particular class of NPs that has been the subject of multiple BIOS efforts are the steroid-derived Withanolides. Primarily isolated from plants of the nightshade family, the withanolides have a wide range of biological activities ranging from antitumour properties to anti-inflammatory activity.³⁹ Through BIOS, novel withanolide-inspired compounds were identified that could modulate Hedgehog signalling as well as inhibiting Wnt signalling.^{40,41}

Analysis of a number of withanolides identified a conserved *trans*-hydrindane dehydro- δ -lactone scaffold that constituted the C/D-ring of the compounds, and was therefore under the BIOS principles chosen as a core scaffold for library synthesis (Figure 1.6).⁴⁰ Construction of the *trans*-hydrindane core commenced from readily accessible alkene **1.30**, synthesised in three steps from the Hajos-Parrish ketone. Following a short synthetic sequence, including a key ruthenium catalysed ring-closing metathesis to assemble the dehydro- δ -lactone ring, a series of intermediate compounds suitable for further elaboration were yielded. Functionalisation of the A-ring hydroxyl with phenyl isocyanate afforded carbamate analogue **1.31**, which through biological screening, was identified as a potent inhibitor of Hedgehog signalling via direct binding to the G protein-coupled receptor Smoothened. In contrast to this approach, choosing the steroid scaffold of the withanolides for library synthesis has also proved fruitful in affording new bioactive compounds.⁴¹ The intermediate compound **1.32** derived from commercially available pregnenolone facilitated late-stage diversification into over 50 withanolide analogues which were screened for their ability to modulate Wnt signalling. Analogue **1.33** which was synthesised by reaction of **1.32** with cyclopentylamine was identified as a low-micromolar inhibitor of Wnt signalling. These two examples of BIOS highlight one of its advantages, as from the same class of parent NPs two classes of withanolide-inspired analogues were accessed with two very different classes of bioactivity – different to that of the parent NP.

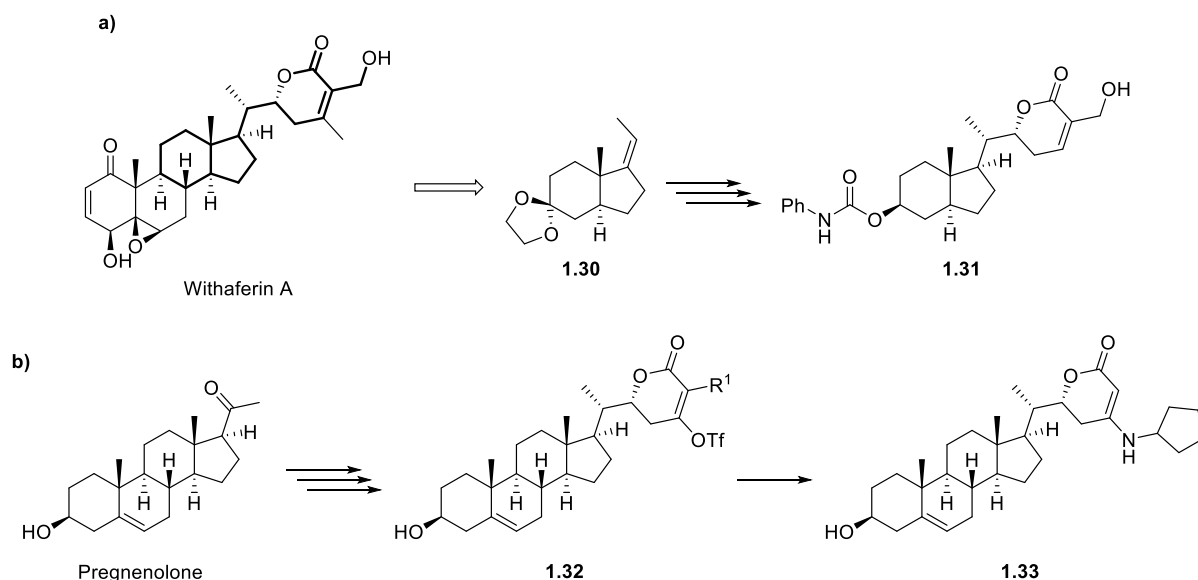


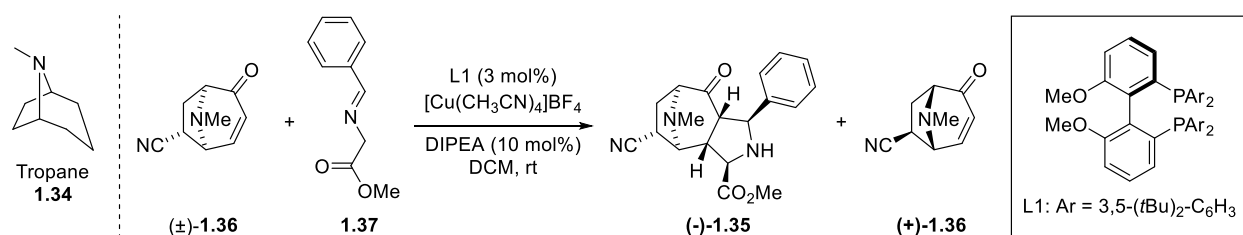
Figure 1.6 BIOS based upon the withanolides. **a)** BIOS upon the C/D-ring *trans*-hydrindane scaffold (in bold) to afford new modulators of hedgehog signalling. **b)** BIOS using pregnenolone as a core scaffold to afford new inhibitors of Wnt signalling.

The major disadvantage of the BIOS approach stems from the use of known NPs as the basis of library synthesis. Not only is the chemical space covered by known NP scaffolds smaller than all possible permutations of NP-like chemical space, the ability of BIOS-derived compounds to explore biological space can be confined by retention of the parent NPs bioactivity. In order to overcome these limitations, fragment based approaches drawing inspiration from the principles of fragment-based drug discovery (FBDD) were explored.⁴²

1.3.4 Natural product fragment-based approaches

FBDD is an approach that has seen extensive use by medicinal chemists as a powerful method to develop new drug candidates.⁴³ In FBDD, small fragments (typical molecular weight < 250 Da) are screened against a target of interest and “hit” fragments grown via connection to other fragments in a structure-guided manner. Whilst FBDD can in principle explore a large degree of chemical space, this often goes unrealised owing to the fact that most fragment collections are derived from known drugs and are dominated by sp² rich aromatic molecules.^{44–46}

Drawing inspiration from the ability of small molecular fragments to efficiently probe chemical space, a cheminformatics analysis of 180,000 NP structures was performed, identifying 2000 suitable NP-fragments.⁴² Compared to commercial fragment collections, these NP-fragments were rich in structural complexity, diversity, and Fsp³, similar to the NPs they were derived from. As these fragments were markedly different from commercial collections, it was expected that any compounds resulting from use of these fragments would better probe uncharted chemical space whilst retaining greater biological relevance. This fragment based approach was exemplified with the identification of suitable NP-fragments that could serve as new chemotypes of inhibitors against kinases and phosphatases.⁴² One specific example of a NP-fragment is the tropane fragment **1.34**, found in over 600 diverse alkaloid NPs, and which has seen use in the synthesis of several NP-fragment derived libraries.^{47,48} A small library of tropane-pyrrolidine fusions **1.35** was synthesised in an enantioselective one-pot copper(I)-catalysed [3+2] cycloaddition between tropane-derived fragment **1.36** and the azomethine ylide precursor **1.37** (Scheme 1.2).⁴⁸



Scheme 1.2 Enantioselective synthesis of tropane-pyrrolidine fused compounds **1.35** via a copper(I)-catalysed [3+2] cycloaddition and racemic tropane-derived fragment **1.36** and azomethine ylide precursor **1.37**.

1.3.5 Pseudo-natural products

In an logical evolution of the NP-fragment based approach, the concept of pseudo-NPs was born.⁴⁹ Combining the use of biologically pre-validated scaffolds from BIOS and the use of NP-fragments, it was hypothesised that the recombination of NP-fragments in ways not observed in NPs should give rise to compound collections inaccessible by biosynthetic pathways.⁵⁰ These compounds, termed pseudo-NPs, should therefore allow exploration of chemical space that is uncovered by known NPs as well as identifying compounds with new bioactivities. To achieve these unprecedented scaffold fusions, the natural product fragments can be recombined in one of four ways: via a monopodal connection, spiro connection, fused connection, or bridged connection with 0, 1, 2, and 3 shared atoms respectively (Figure 1.7).

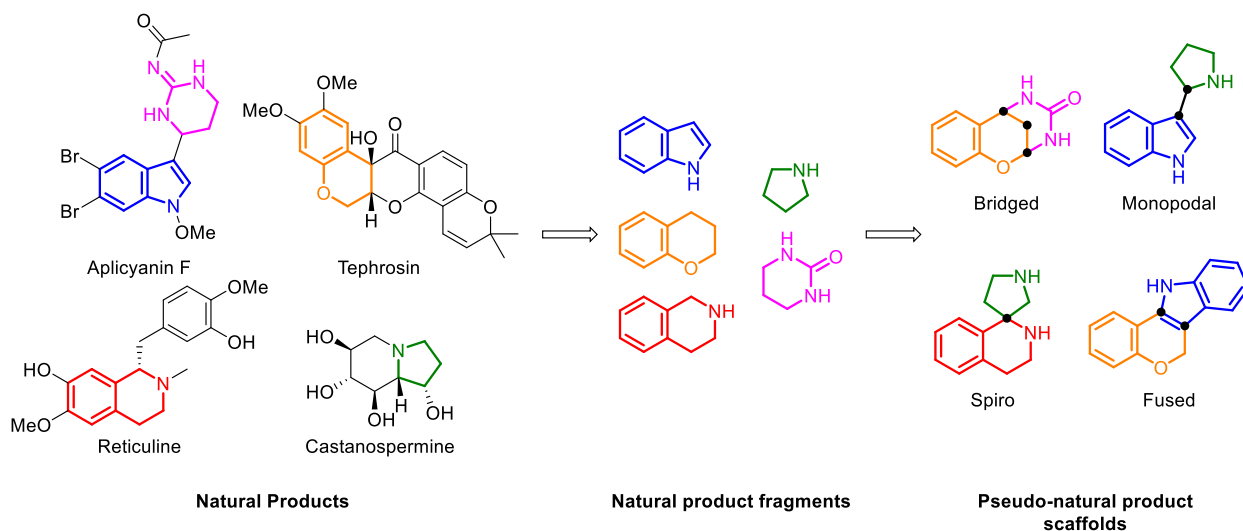


Figure 1.7 General principle of the pseudo-natural product approach. Natural products are simplified into their core natural product fragments, and then recombined either by bridged, monopodal, spiro, or fused connections to afford pseudo-natural product scaffolds. Figure redrawn and modified from reference.⁵¹

The type of connectivity of a fragment recombination is not the only factor to consider when synthesising pseudo-NP libraries. The regiochemistry of a given recombination has also proved to be an important influence on the bioactivity of pseudo-NPs. A 155-member library of tetrahydroquinoline-pyrrolidine pseudo-NPs was synthesised featuring 8 different patterns of fragment recombination and regiochemistry, and subjected to morphological profiling in a cell-painting assay to suggest possible bioactivities. Three different classes of regioisomeric edge-fused analogues were found to display remarkably different clustering in the assay and therefore are likely to possess different bioactivities..⁵² Whilst the concept of

pseudo-NPs is recent, they can be readily identified in modern screening collections.⁵³ Cheminformatics analysis of biologically relevant compounds in the ChEMBL database suggest that approximately 23% of these compounds can be defined as pseudo-NPs and that pseudo-NPs have thus been synthesised for over 45 years before their recent definition.

Despite the fact that the pseudo-NP approach was only described in 2018, it has been well-validated as being capable of consistently affording novel bioactive compounds (Figure 1.8).⁴⁹ The recombination of chromane and tetrahydropyrimidone NP-fragments in a bridging bipodal manner afforded a library of 44 chromopynone pseudo-NPs, with compound **1.38** identified as a potent and selective inhibitor of the glucose transporters Class 1 glucose transporters (GLUT) 1 and 3.⁵⁰ The pyrano-furo-pyridone class of pseudo-NPs was synthesised by recombination of dihydropyran and pyridone fragments. The most potent analogue **1.39** of this class was found to be an inducer of reactive oxygen species (ROS) via inhibition of mitochondrial complex 1.⁵⁴ A class of macrocyclic pseudo-NPs **1.40** derived from cinchona-alkaloid and pyrrolidine fragments were synthesised and characterised as potent inducers of microtubule associated protein I light chain 3 (LC3) lipidation, an important protein in the degradative process of autophagy.⁵⁵

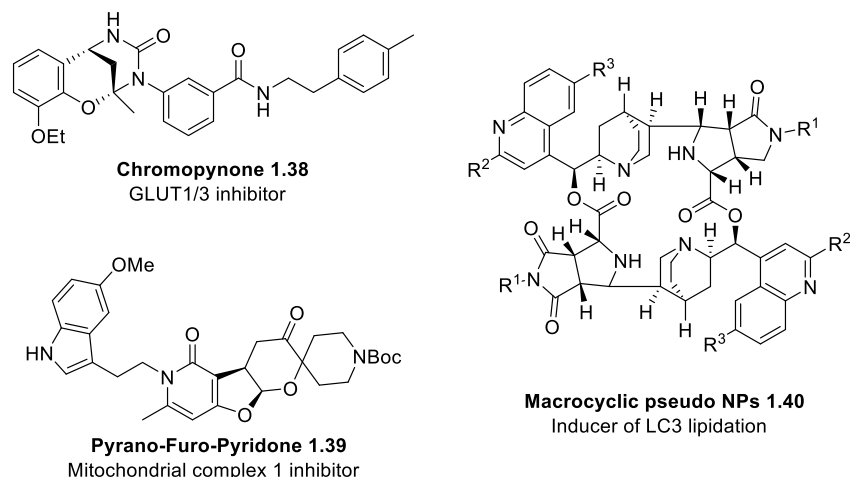
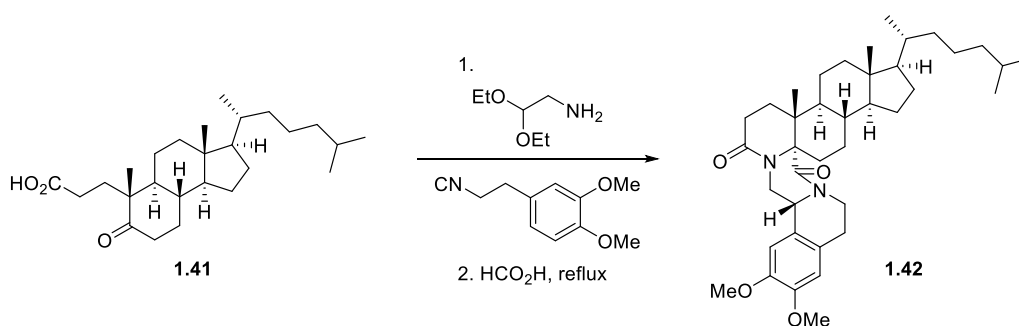


Figure 1.8 Select examples of bioactive pseudo-NPs with a diverse range of bioactivities.

The pseudo-NP approach has also seen use in combination with other library synthesis techniques and expansions to the approach have been suggested. A library of over 90 sesquiterpenoid alkaloid pseudo-NPs was synthesised in a fusion of the pseudo-NP approach and the ring distortion strategy encountered in CtD.⁵⁶ Three sesquiterpene lactones were used for the basis of the ring distortion step, wherein 9 stereochemically diverse intermediates were fused to pyrrolidine fragments. Biological evaluation of this pseudo-NP library revealed a range of bioactivities, including inhibition of osteoblast differentiation that was dependent upon the Hedgehog-signalling pathway. In an attempt to further the chemical space explored by pseudo-NPs it has been proposed that fusing NP fragments with non-NP fragments, namely those found in pharmaceutical compounds, should facilitate a more efficient exploration of non-NP chemical space. This has been exemplified by fusing a steroid backbone with the unnatural pyrazinoisoquinoline fragment (Scheme 1.3).⁵⁷ Reaction of a steroid-derived acid **1.41** with 2,2-diethoxyethylamine and various isocyanides in an Ugi reaction and subsequent Pictet-Spengler afforded a small collection of steroid-pyrazinoisoquinoline fusions. Biological evaluation of these analogues identified one compound **1.42** with moderate antiproliferative activity against the cancer cell line HepG2, acting in a caspase-independent mechanism.



Scheme 1.3 Recombination of the steroid and pyrazinoisoquinoline fragments via a tandem Ugi/Pictet-Spengler reaction to afford antiproliferative pseudo-NPs.

1.4 Sterols and sterol homeostasis

The observed diversity in biological effects of steroids and steroidal compounds is inherently linked to the key functions of endogenous sterols in cells. Cholesterol, the most abundant mammalian sterol, plays several critical functions in mammalian cells including providing structure and stability to plasma membranes (PM) and other organelle membranes, wherein it constitutes approximately 30% of membrane lipid content alongside other phospho- and sphingolipids.⁵⁸ Cholesterol also serves as the starting point for the biosynthesis of other steroid hormones in steroidogenic tissues, including cortisol, estradiol, and testosterone.⁵⁹ Cholesterol itself also possesses diverse bioactivity, having important regulatory roles in processes such as hedgehog signalling and Wnt signalling.^{60,61} Cholesterol, in addition to its oxidised metabolites known as oxysterols, are also implied in numerous diseases including atherosclerosis, multiple sclerosis, and Niemann-Pick disease.^{62,63}

The range of cellular functions as well as associations of abnormal levels of sterols in a number of diseases necessitate the existence of systems to tightly control and regulate levels of cholesterol within the cell. To this end, cells have developed processes to maintain cholesterol homeostasis, working to balance its biosynthesis, uptake from exogenous sources, and efflux.⁶⁴

1.4.1 Cholesterol biosynthesis

De novo biosynthesis of cholesterol is a highly complex process, involving the concerted action of numerous enzymes over multiple individual steps and serves as the major source of cellular cholesterol (Figure 1.9).⁶⁵ Biosynthesis commences via the conversion of acetate in the form of acetyl-coenzyme A (acetyl-CoA) to mevalonate, including the rate-limiting reduction of 3-hydroxy-3-methylglutaryl-CoA (HMG-CoA) to mevalonate by the endoplasmic reticulum (ER)-resident HMG-CoA reductase (HMGCoR).⁶⁶ Through conversion of mevalonate to activated isoprene building blocks and subsequent condensations, the 30-carbon terpenoid squalene is synthesised. Oxidation of squalene by squalene monooxygenase (SM) to 2,3-oxidosqualene represents the second major rate-limiting reaction of the sequence.⁶⁷ 2,3-Oxidosqualene undergoes cyclisation to yield lanosterol, which through a series of reductions affords cholesterol and closes the biosynthetic pathway.⁶⁵

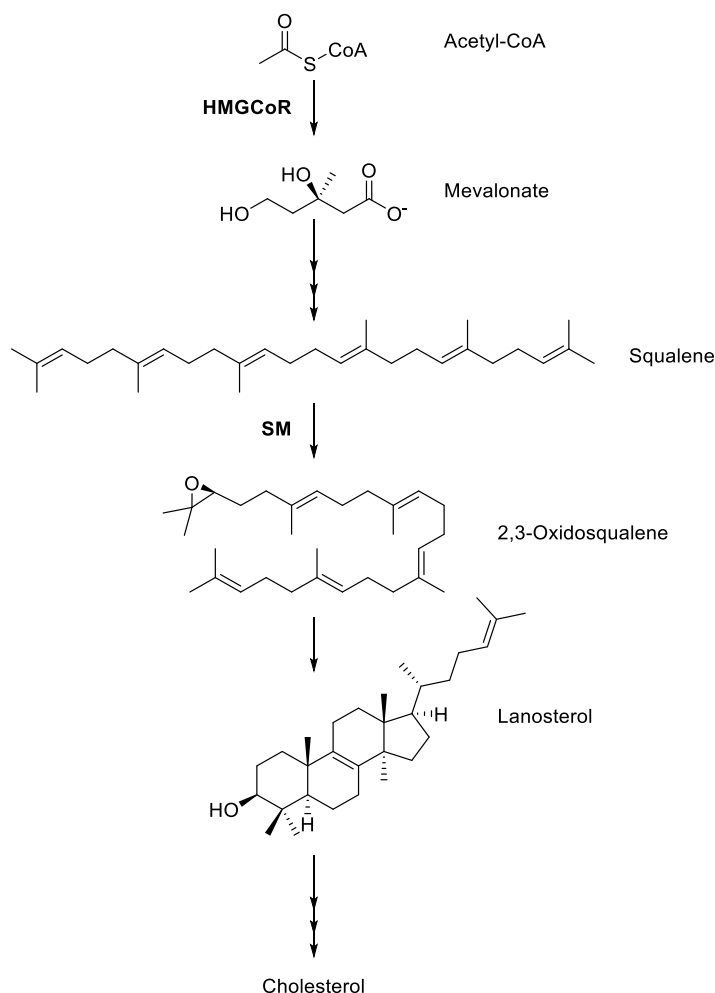


Figure 1.9 A simplified representation of cholesterol biosynthesis highlighting key intermediates in the biosynthesis and the two rate-limiting enzymes, HMGCoR and SM. HMGCoR = HMG-CoA Reductase, SM = Squalene monooxygenase

1.4.2 Cholesterol uptake

Cellular uptake of dietary cholesterol occurs by two major processes, either by the Niemann-Pick type C1-like 1 (NPC1L1) protein in enterocytes or by the low-density lipoprotein (LDL) receptor (LDLR) from the blood, both of which occur in a clathrin-dependent manner (Figure 1.10).⁶⁴ Under low levels of cellular cholesterol, NPC1L1 translocates to the plasma membrane of intestinal cells and binds to unesterified cholesterol.⁶⁸ Endocytosis of NPC1L1-bound cholesterol delivers the receptor and cholesterol to the endocytic recycling compartment (ERC), from which cholesterol can be transported to the ER via currently unknown mechanisms.⁶⁹

The LDLR is a PM bound protein, which binds to LDL-particles containing cholesterol esters (CEs) through its extracellular ligand binding domain. Once bound, the receptor undergoes endocytosis – releasing its cargo of LDL upon undergoing a conformational change in the acidic endosomes.⁷⁰ The LDL derived CEs are ultimately hydrolysed by lysosomal acid lipases, releasing free cholesterol into the lysosomal lumen.⁷¹ Cholesterol is then transported from lysosomes, typically to the ER, by the Niemann-Pick type C1 (NPC1), Niemann-Pick type C2 (NPC2), and lysosome-associated membrane protein-2 (LAMP2) proteins.⁷²

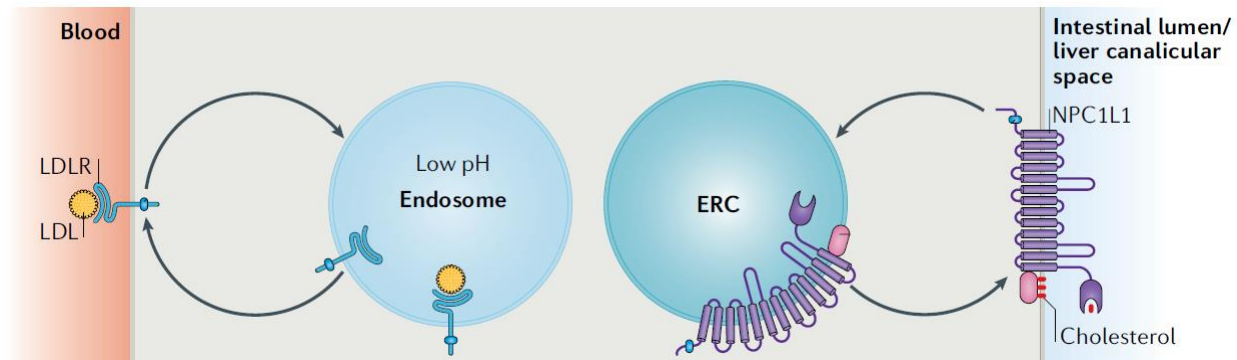


Figure 1.10 LDLR and NPC1L1-mediated uptake of cholesterol. Figure reproduced and modified with permission from reference.⁶⁴ Copyright (2019) Springer Nature.

1.4.3 Regulation of cholesterol homeostasis

In order to maintain correct cholesterol homeostasis, the interplay of cholesterol biosynthesis and uptake must be tightly regulated. A number of mechanisms are present to achieve this, of which the ER-bound sterol regulatory element-binding protein 2 (SREBP2) plays a significant role in regulating cholesterol biosynthesis genes as well as influencing LDLR-mediated uptake.⁷³ When cellular cholesterol levels are high, cholesterol binds to the SREBP-cleavage activating protein (SCAP) which in-turn results in binding to insulin-induced gene (INSIG) proteins 1 and 2, blocking its export from the ER and preventing subsequent upregulation of the transcription of cholesterol biosynthesis genes (Figure 1.11b).^{74,75} Oxysterols that can form when ER cholesterol levels are high are also known to promote the retention of SREBP2 by direct binding to INSIG, enhancing its binding to SCAP.⁷⁶

When ER cholesterol levels are low (Figure 1.11a), SCAP adopts an alternative conformation that allows binding to COPII vesicles and dissociation from INSIG, allowing translocation of the SCAP-SREBP2 complex to the Golgi apparatus.⁷⁷ At the Golgi, proteolytic cleavage of SREBP2 by site-1 and site-2 proteases (S1P/S2P) releases nuclear SREBP2 (nSREBP2), which is subsequently translocated to the nucleus.⁷⁸ In the nucleus, nSREBP2 binds to sterol-regulatory elements (SREs) of genes involved in cholesterol biosynthesis and uptake including HMGCoR, SM, LDLR, as well as the SREBP2 gene itself; resulting in an upregulation of their transcription.⁷⁹

In addition to the SREBP2/SCAP regulatory axis, additional transcriptional regulation occurs to properly maintain cholesterol homeostasis.^{64,80} Uptake of cholesterol by NPC1L1 can, for example, be both positively and negatively regulated by the proliferator-activated receptor α – retinoid X receptor α (PPAR α -RXR α) complex and the cyclic adenosine monophosphate (cAMP)-responsive element-binding protein H (CREBH) protein respectively.^{81,82} LDLR-mediated uptake of LDL is also further regulated by the E3 ubiquitin ligase inducible degrader of LDL-receptor (IDOL). IDOL and NPC1L1 expression are also both regulated by liver X receptors.⁸³

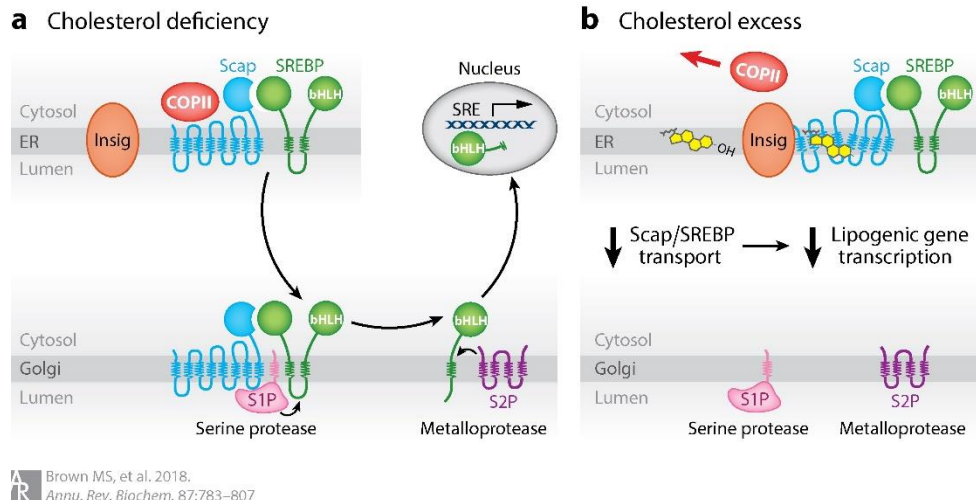


Figure 1.11 SREBP processing under low levels of cholesterol (**a**) and high levels of cholesterol (**b**). (**a**) under low levels of cholesterol, the SREBP-SCAP complex translocated to the golgi, wherein it is cleaved to release nSREBP, leading to upregulation of cholesterol biosynthesis gene transcription. (**b**) under high levels of cholesterol, INSIG binds to SCAP, leading to the retention of SREBP in the ER, preventing the upregulation of cholesterol biosynthesis gene transcription. Figure reproduced with permission from reference.⁸⁴ Copyright (2017) Annual Reviews.

When levels of cellular cholesterol are too high, cholesterol can either be removed from the cell via efflux or processed for storage.⁸⁵ A significant source of cholesterol efflux occurs via the ATP-binding cassette (ABC) family of transport proteins, particularly the protein ABCA1. ABCA1 can transport cholesterol to apolipoprotein A1 (ApoA-1) which subsequently forms high-density lipoproteins (HDL) which are transported back to the liver in a process known as reverse cholesterol transport.⁸⁶ Excess cellular cholesterol can also be esterified by the ER-resident enzymes acyl-CoA cholesterol acyltransferase (ACAT) 1 and 2, and the resulting CEs stored in organelles known as lipid droplets (LDs). LDs consist of a core of CEs and triacylglycerols (formed by esterification of fatty acids by the enzymes diacylglycerol O-acyltransferase (DGAT)1/2) surrounded by a phospholipid monolayer, in which multiple proteins involved a number of processes including LD biogenesis and regulation of contact sites are present.^{87,88} Lipids stored in LDs can be utilised as needed by either lipophagy or lipolysis.⁸⁷

1.5 Sterol transport proteins

In contrast to the more general regulation of cholesterol homeostasis by transcriptional methods, a finer level of regulation of cholesterol homeostasis is achieved by a combination of vesicular and non-vesicular transport mediated by families of sterol transport proteins (STPs). Vesicular transport of cholesterol by STPs occurs via the proteins NPC1 and NPC2. NPC1 and NPC2 work in tandem to transport LDL-derived cholesterol from lysosomes, derived from hydrolysis of CEs, to the PM where it is subsequently transported to the ER.^{89,90} Non-vesicular transport of cholesterol is achieved by three major families of STPs: the oxysterol-binding protein (OSBP)-related proteins (ORPs), the steroidogenic acute regulatory protein (StAR)-related lipid transfer (START)-related domain (STARD) proteins, and the Aster/GRAMD1 proteins.⁹¹ These three families of STPs are responsible for the transfer of cholesterol between the membranes of different organelles, typically to-and-from the ER (Figure 1.12), binding to and transporting cholesterol in their hydrophobic sterol-binding domains (SBDs).

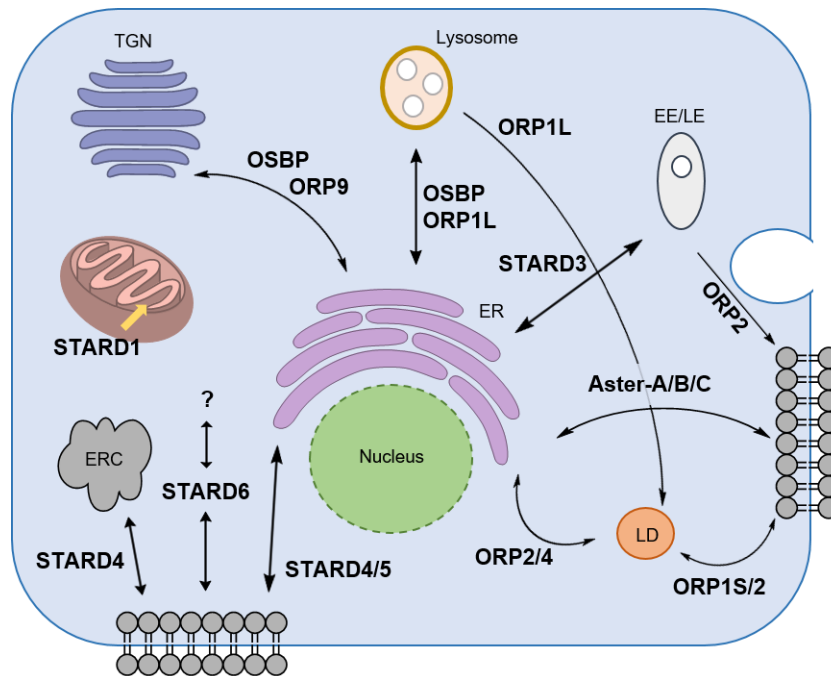


Figure 1.12 Intracellular non-vesicular cholesterol transport by sterol transport proteins. EE: early endosome, ER = endoplasmic reticulum, ERC = endocytic recycling compartment, LD = lipid droplet, LE = late endosome, TGN = trans-Golgi network. Figure reproduced from reference.⁹¹

1.5.1 Aster proteins

The Aster proteins are the smallest and most recently described family of STPs involved in non-vesicular cholesterol transport. The Aster family is comprised of 3-cholesterol binding proteins Aster-A, Aster-B, and Aster-C (also known as GRAMD1A, GRAMD1B, and GRAMD1C) in addition to 2 members lacking a SBD – GRAMD2A and GRAMD2B (previously referred to as GRAMD3).^{92,93} The Asters are a family of ER-resident proteins that facilitate the transport of LDL-derived cholesterol between the PM and ER.⁹⁴ Asters-A, -B, and -C are composed of three main domains - an N-terminal GRAM domain, C-terminal transmembrane (TM) domain, and a core central StART-like domain (Figure 1.13).⁹²

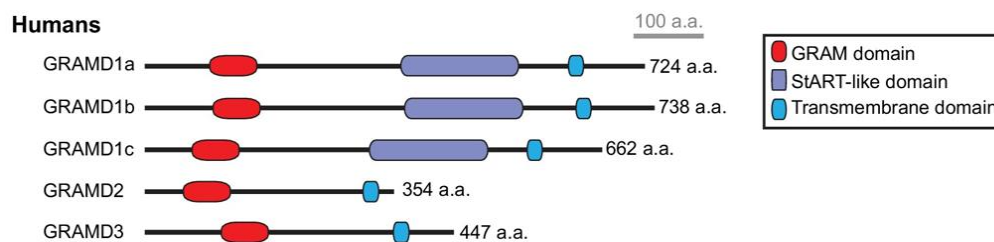


Figure 1.13 Schematic representations of the Aster/GRAMD1/2 proteins. Figure reproduced from reference.⁹⁵

The GRAM domain of Asters-A, -B, and -C has been shown to act as a coincidence detector for PM cholesterol, responsible for the recruitment of the Asters to the PM under high levels of cholesterol. This binding and recruitment only occurs when cholesterol, unsequestered by sphingomyelin, is in close-proximity of anionic lipids such as phosphatidylserine (PS), allowing for a fine control of its extraction and transport to the ER.^{95,96} The TM domain is responsible for anchoring the protein to the ER, but also has

roles in forming homo- and heteromeric dimers, a process critical for the recruitment of the Asters to ER-PM contact sites.⁹⁵ The central START-like SBD of the Asters, named the ASTER domain, has little sequence similarity to SBDs of other known STPs, and readily binds to cholesterol and side-chain oxidised oxysterols in a hydrophobic pocket.⁹² X-ray crystal structures of murine Aster-A revealed that despite their low sequence similarity, the 3D structure of the ASTER domain broadly resembles that of the START domain. Slight differences in the ASTER domain result in a sterol-binding mode different to that of other SBDs, in which the ligand is rotated by 120 °C along its axis (Figure 1.14).⁹² Additionally, the binding pocket features a volume unoccupied by sterol ligands which could serve to accommodate larger ligands – with recent studies revealing the ability of Aster-A and -B to bind and mediate transport of carotenoids.⁹⁷

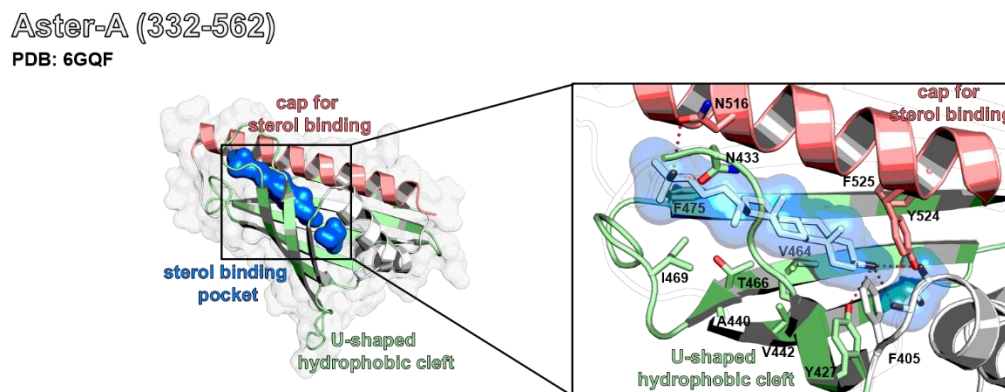


Figure 1.14 Co-crystal structure of murine Aster-A and 25-hydroxycholesterol. Figure reproduced from reference.⁹¹

1.5.2 Functions of the Aster proteins

In light of their recent description, the individual physiological functions of the Aster proteins has begun to be investigated. The differential patterns of tissue expression observed for the Asters suggest that each should possess distinct functions from one another, with Aster-A having highest expression in the brain, Aster-B in adrenal tissues, and Aster-C in the testes and liver.⁹²

The role of Aster-A in autophagy was elucidated through identification of the small molecule inhibitor Autogramin-2, which inhibits Aster-A mediated cholesterol transfer between the ER and forming phagophore.⁹⁸ On the other hand, Aster-B has been identified as a key regulator of HDL-derived cholesterol transport to the ER in steroidogenic tissues, acting downstream of the known scavenger receptor class B type 1 (SR-BI) receptor.⁹² Aster-B has additionally been identified as a regulator of ER – mitochondria cholesterol transport and the uptake of CE-derived fatty acids, further supporting its role as a regulator of steroidogenesis.⁹⁹ Mutations in the GRAM domain of Aster-B have also been associated with intellectual disability, arising from defective cholesterol sensing.⁹⁶ Studies of Aster-C have identified it as a negative regulator of mammalian target of rapamycin complex 1 (mTORC1) signalling under conditions of nutrient starvation.¹⁰⁰ Similarly to Aster-A, a putative role of Aster-C as a negative regulator of starvation induced autophagy has been suggested, as well as regulating mitochondrial bioenergetics by mediating mitochondria – ER cholesterol transfer.¹⁰¹ Expression levels of the Aster proteins has also been associated with differential pathogenesis and prognoses in cancers including renal carcinoma and breast cancer, highlighting how small-molecule modulation of the Asters could prove to have therapeutic relevance.^{100,102,103}

1.5.3 Small molecule inhibitors of sterol transport proteins

Despite the critical importance of STPs in a range of cellular processes, their modulation by small molecules has remained challenging, with few inhibitors of these proteins having been identified. A series of structurally unrelated NPs were found to share a common fingerprint of cytotoxicity against the National Cancer Institute 60 cancer cell lines (NCI-60), with all compounds inhibiting cell growth at nanomolar potencies.¹⁰⁴ These NPs, including Cephalostatin 1, Ritterazine B, Schweinfürthin A, and OSW-1 were found to bind to and inhibit the STPs OSBP and ORP4L, with the group of compounds subsequently named the ORPphilins (Figure 1.15).

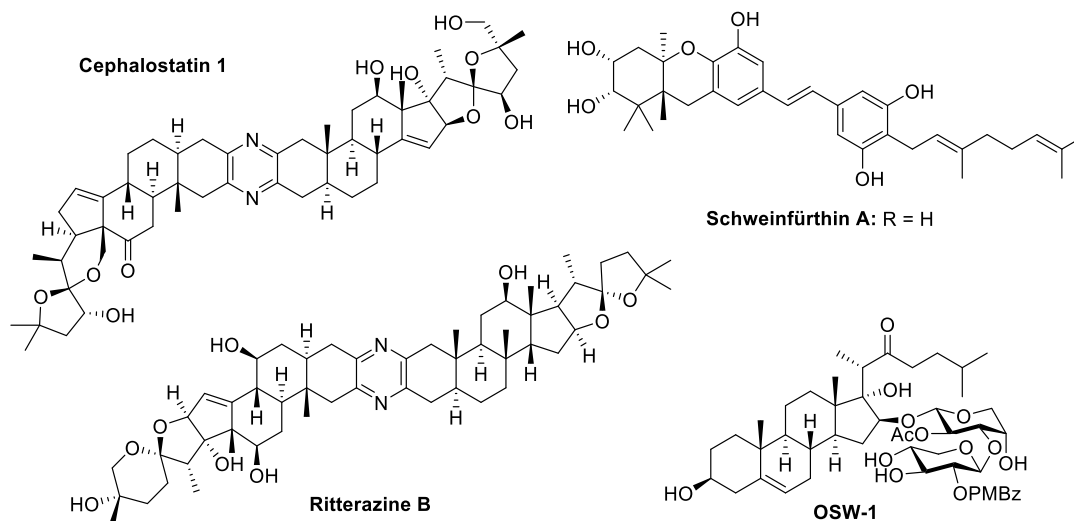


Figure 1.15 Structures of the ORPphilins, inhibitors of OSBP and ORP4L.

Further work has identified ORP inhibitors with improved selectivity profiles over the ORPphilins (Figure 1.16). Schweinfürthin G, a member of the Schweinfürthin family of NPs, was identified and utilised as an inherently fluorescent probe to further study the dynamics of OSBP/ORP4L-associated cytotoxicity arising from their inhibition.¹⁰⁵ Similarly to Schweinfürthin A, Schweinfürthin G displays increased selectivity for OSBP over ORP4L. Complementing the OSBP-selectivity of the Schweinfürthins, a synthetic analogue of OSW-1, LYZ-81, was identified as a selective inhibitor of ORP4L.¹⁰⁶ LYZ-81 potently binds to ORP4L and inhibits the transfer of phosphatidylinositol 4,5-bisphosphate (PIP₂) from the PM, interfering with downstream calcium-dependent bioenergetics, and inducing death in leukemia stem cells. From a phenotypic screen designed to identify inducers of ABCA1, a series of nicotinamides were identified as hits, with subsequent target identification efforts revealing ORP7 as their target. The optimised compound G was found to upregulate apoA-I-mediated efflux of cholesterol as well as increasing levels of ABCA1 at the PM, identifying ORP7 as a possible regulator of ABCA1.¹⁰⁷

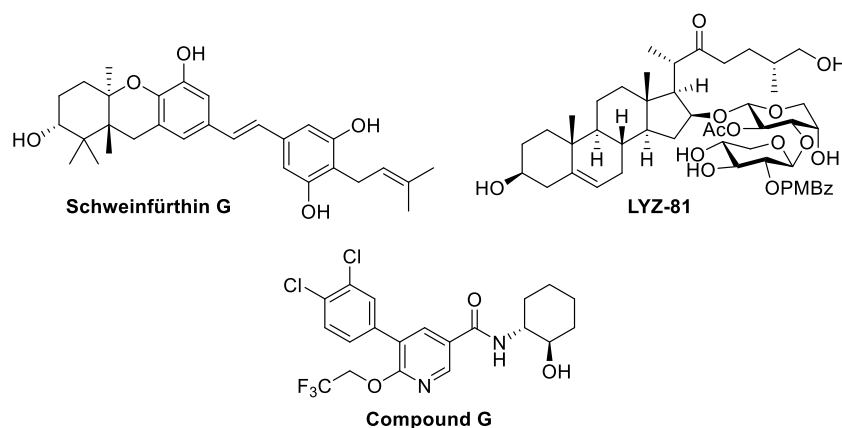


Figure 1.16 Structures of OSBP/ORP4L selective compounds Schweinfürthin G and LYZ-81, and the ORP7 inhibitor Compound G

The approved antifungal drug itraconazole that has multiple off-target effects including anticancer and hedgehog inhibitory activity was identified as a broad-spectrum antiviral agent, with effects mainly seen against enteroviruses (Figure 1.17).¹⁰⁸ Target identification revealed that the antiviral activity of this compound was dependent upon inhibition of OSBP, and that likewise, OSW-1 shares its antiviral profile. Efforts to decouple the antifungal activity of itraconazole from its OSBP-related antiviral activity have also been performed, revealing the importance of the core ring scaffold and dispensable nature of the triazole ring for antiviral activity – suggesting that it could be possible to identify synthetic OSBP inhibitors with increased selectivity.¹⁰⁹

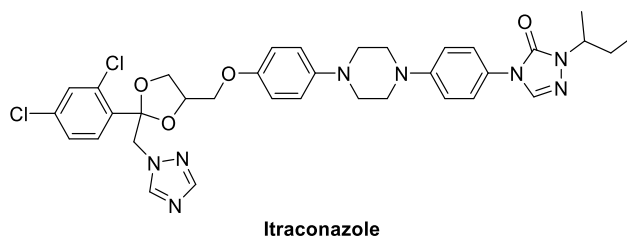


Figure 1.17 Structure of the antiviral OSBP inhibitor itraconazole

A number of compounds inhibiting the Aster proteins have been identified with varying degrees of selectivity (Figure 1.18). From a phenotypic screen for autophagy inhibition, Autogramin-2 was identified as a potent inhibitor of starvation and rapamycin-induced autophagy, exerting its effects through inhibition of Aster-A.⁹⁸ Autogramin-2 was also found to be highly selective over both Aster-B and -C, as well as over other STPs such as STARD1 and STARD3. Inhibitors targeting Aster-B and Aster-C have been identified, including AI-3d and AI-11, derived from the pan-STP inhibitor U18666A and the endogenous oxysterol 20 α -hydroxycholesterol respectively.¹¹⁰ Whilst these compounds inhibit the Aster proteins, their selectivity over the other Asters is poor, warranting the identification of alternative inhibitors of Aster-B and -C with improved selectivity profiles.

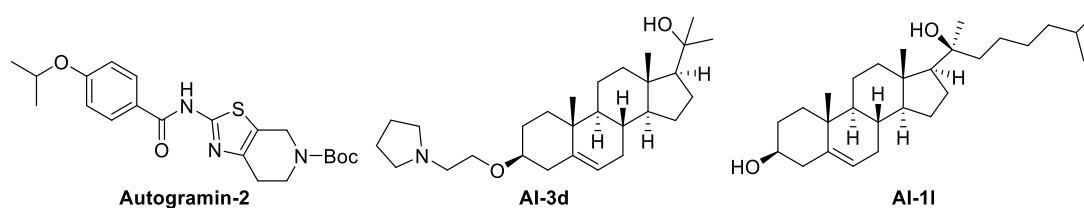


Figure 1.18. Structures of the Aster inhibitors Autogramin-2, AI-3d, and AI-11.

In contrast to the ORPs and Asters, only one potential inhibitor has been identified targeting the STARDs. A virtual screen against STARD3 identified a pyrimidone-derived inhibitor, although the identified compound possesses poor potency for STARD3 and would therefore require significant optimisation and further profiling to find use as a STARD3 inhibitor.¹¹¹ As other known STARD inhibitors target STARD2 and STARD11 (referred to as phosphatidylcholine transfer protein (PCTP) and ceramide transport protein (CERT) respectively), proteins responsible for the transfer of phosphatidylcholine and ceramide respectively, the STARDs represent a significant gap in the field of STP inhibitors.^{112,113}

Part II - Synthesis of a sterol-inspired compound collection

2.1 Project Aims and Outline

In response to the lack of potent and selective STP inhibitors, an approach to synthesise a sterol-inspired compound collection was designed – incorporating elements of proven techniques including DOS, BIOS, and the pseudo-NP approach. It was anticipated that fusion of a primary steroidal scaffold to a series of secondary heterocyclic scaffolds would afford a biased collection of sterol-inspired compounds enriched in hits against STPs (Figure 2.1), providing a rational approach to identify new STP inhibitors in contrast to the mainly serendipitous discoveries seen thus far. To evaluate the performance of the sterol-inspired compound collection, it would be screened against the Aster family of STPs serving as a model STP family, using complementary biochemical assays. Hit compounds identified from initial screening would be subjected to further validation, and after subsequent optimisation the resulting compounds would be further profiled using a combination of biochemical and cell biology techniques.

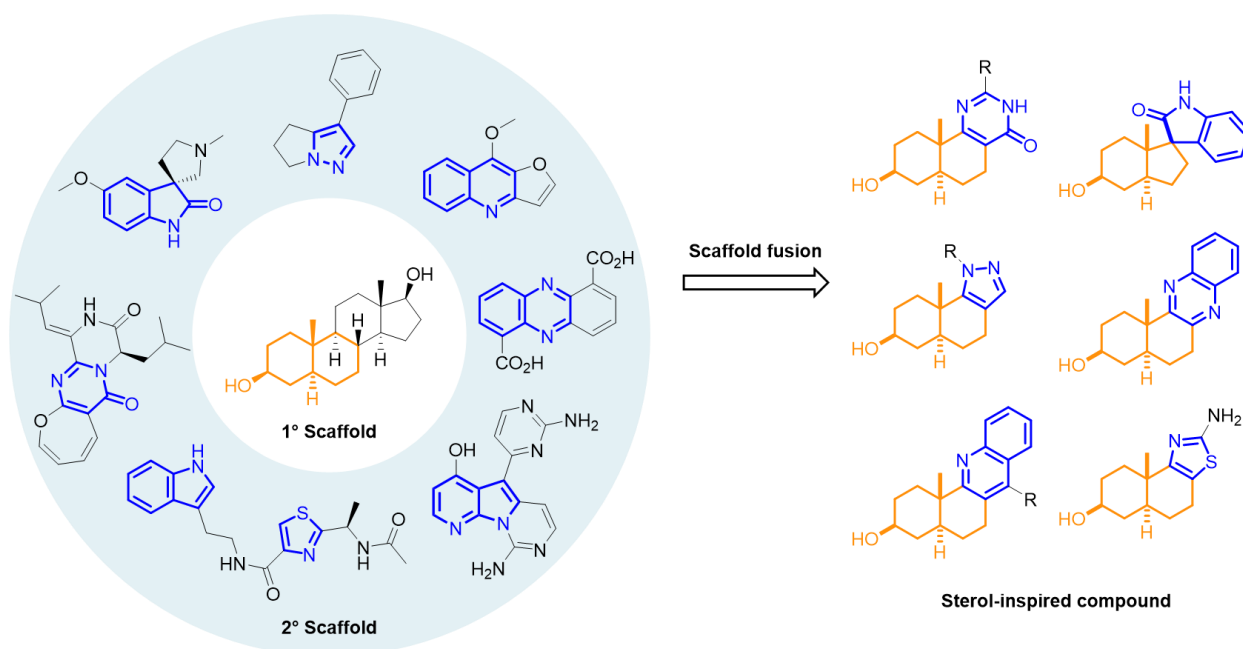


Figure 2.1 Concept for the synthesis of a sterol-inspired compound collection. Fusion of a primary sterol scaffold to a series of secondary heterocyclic scaffolds afford a collection of sterol-inspired compounds. Figure reproduced with permission from reference.¹¹⁴ Copyright (2021) John Wiley and Sons.

In the following sections, this process will be described as follows: part II concerns the design and synthesis of the sterol-inspired compound collection, including the optimisation of building block and analogue synthesis. Part III covers the process of assay optimisation and biochemical screening of the sterol-inspired compound collection against the Aster proteins, including the identification of the active enantiomer of the Aster-A and Aster-C hit compounds, concluded by optimisation of the Aster-C inhibitor series. Lastly, part IV covers the preliminary biological evaluation of these Aster-A and Aster-C inhibitors in the context of cholesterol homeostasis and autophagy, utilising a combination of biochemical techniques and confocal microscopy.

2.2: Designing a sterol-inspired compound collection

To design an approach to synthesising a sterol-inspired compound collection, it was decided to incorporate elements of several validated approaches to synthesise bioactive compound collections. The pseudo-NP approach provided significant inspiration to the overall design philosophy. It was anticipated that fusion of a core sterol fragment to heterocyclic scaffolds encountered in other NPs would afford sterol-inspired compounds capable of binding to STPs, with the heterocyclic scaffolds imparting selectivity between different STPs. Application of the pseudo-NP approach typically involves the fusion of a limited number of NP-fragments with one another, therefore, to further scaffold diversity in the sterol-inspired collection, different classes of heterocycles would be targeted rather than focussing on one or two classes of heterocycle fusions. Additionally, non-natural fragments would be included for fusion to the steroidal fragment, expanding the chemical and biological space probed by the compound collection.

The two main requirements of a suitable steroidal fragment for synthesis was that it should be representative of multiple classes of sterols and thus promote favourable interactions with sterol-binding proteins, and secondly it should facilitate the fusion of heterocyclic scaffolds in a limited number of synthetic steps. To this end, it was decided that the sterol fragment should represent the sterol AB-ring system and contain the C3-hydroxyl and axial methyl group, as these regions are critical in the binding of sterols to their protein targets - typically being buried in the hydrophobic binding site.¹¹⁵ Use of a truncated sterol fragment compared to the complete tetracyclic sterol core would also limit problems typically associated with use of the latter, decreasing off-target interactions associated with the complete sterol backbone.

To facilitate a range of diverse scaffold fusions, it was decided to incorporate a ketone into the chosen sterol fragment, as the reactivity of the ketone functional group makes it well-suited for the synthesis of NP-inspired compound collections.¹¹⁶ In order to limit potential reagent incompatibilities and limit side-reactions, it was also decided to use a fully saturated AB-ring fragment missing the alkene seen in the B-ring of cholesterol. A study to perform a proteome-wide mapping of cholesterol-interacting proteins utilised a trans-fused photoreactive sterol probe, successfully identifying over 250 cholesterol-binding proteins.¹¹⁷ Favourable mapping was shown compared to both a cis-fused (*Cis*-sterol) and epimeric probe (*Epi*-sterol), with the trans-fused probe (*Trans*-sterol) found to most closely resemble the three-dimensional structure of cholesterol (Figure 2.2).

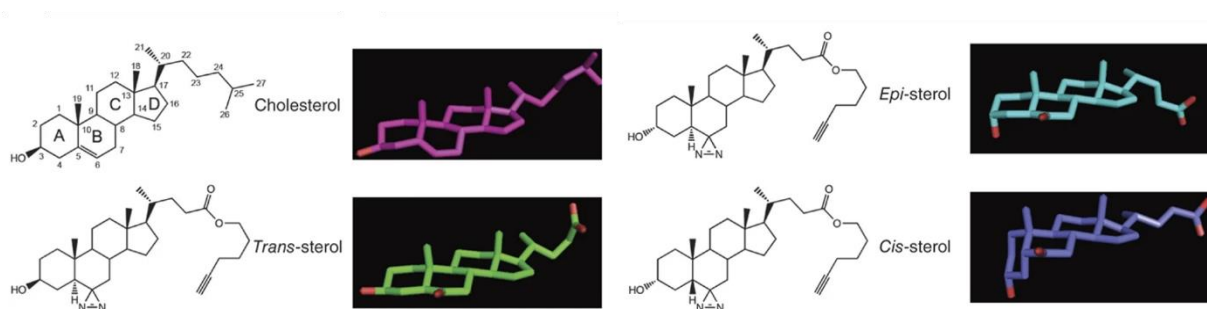


Figure 2.2 Chemical structures and X-ray structures of cholesterol and *trans*-, *epi*-, and *cis*-sterol photoaffinity probes used in a proteome-wide mapping of cholesterol-interacting proteins. Figure reproduced and modified with permission from reference.¹¹⁷ Copyright (2013) Springer Nature.

Taking these individual factors into consideration, the trans-fused decalone **2.01** was chosen as the building block for construction of the sterol-inspired compound collection (Figure 2.3). Decalone **2.01** can be synthesised via the well-known Wieland-Miescher ketone (WMK) **2.02**, a bicyclic ketone that itself can be readily accessed from commercially available starting materials and is often used in the total synthesis of

steroidal and terpene NPs.¹¹⁸ Two similar synthetic routes to trans-fused decalone **2.01** have been published to date, however some experimental details are lacking and the spectral characterisation limited by instrumentation available at the time. The synthetic routes towards decalone **2.01** therefore offer an opportunity for significant optimisation.^{119,120}

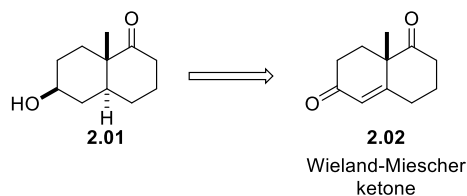


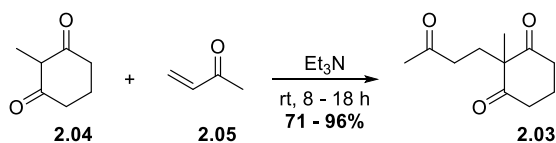
Figure 2.3 Sterol-inspired building block **2.01** and the Wieland-Miescher ketone **2.02**

Before commencing synthesis of the sterol-inspired compound collection, further guidelines were established to focus synthetic efforts. Firstly, the library building blocks and therefore all analogues would be synthesised as racemates. In doing so, the size of the screening collection is effectively doubled by testing both enantiomers of a given compound. Whilst this approach would ultimately require additional work to identify active enantiomers of any hit compounds emerging from screening, it is not possible to state with absolute certainty that the natural stereochemistry represents the preferred binding configuration for all STPs. Secondly, analogues should be accessible in no more than four synthetic steps from the decalone building block **2.01** or closely related intermediates. Lastly, between three and five analogues featuring different patterns of substituents with varied electronic properties should be synthesised per scaffold fusion. This would allow preliminary SAR information to be obtained for screening hits at an early stage.

2.2.1 Synthesis of a sterol-inspired building block

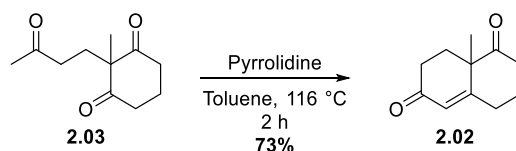
Synthesis of the sterol-inspired building block **2.01** commenced by synthesising triketone **2.03** (Table 2.1). Triketone **2.03** was synthesised in a solvent-free procedure, reacting diketone **2.04** and methyl vinyl ketone **2.05** in the presence of triethylamine.¹²¹ This procedure was used to consistently yield the desired product in excellent yield and purity (entries 1 - 3) and was also successfully scaled up to 0.25 mole of diketone **2.04** with no decrease in yield (entry 4).¹²²

Table 2.1 Synthesis of triketone **2.03**



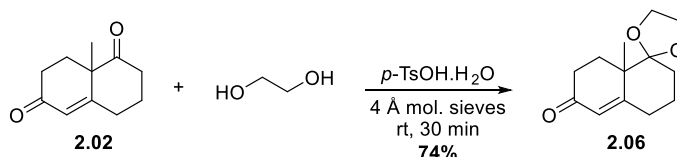
Entry	2.04 (equiv.)	2.05 (equiv.)	Et ₃ N (equiv.)	Yield (%)	Comments
1	1	1.1	0.1	93	5 g 2.04 , 18 h at rt
2	1	1.1	0.1	95	10 g 2.04 , 18 h at rt
3	1	1.1	0.1	90	15 g 2.04 , 18 h at rt
4	1	1.2	0.01	96	50 g 2.04 , 8 h at rt, 2.05 not purified before use, reaction mixture stirred with activated charcoal and filtered through a silica plug

Heating triketone **2.03** under Dean-Stark conditions in the presence of pyrrolidine afforded the WMK **2.02** in good yields (Scheme 2.1). Purification of the crude product was achieved by either flash chromatography or filtration through a silica plug, affording the product as an oil that readily solidified upon standing.



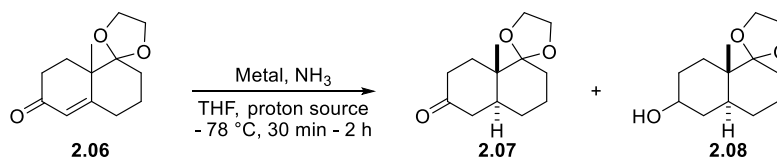
Scheme 2.1 Synthesis of the Wieland-Miescher ketone **2.02**

In order to install the desired AB-ring stereochemistry of the sterol-inspired building block, it was necessary to selectively protect the ketone carbonyl as the ethylene ketal. Initial attempts to protect the ketone as the ethylene ketal following the published protocols towards ketone **2.01** proved unsuccessful – with the harsh refluxing conditions affording mixtures of ketal protected enone, unreacted ketone, as well as the bis-ketal product.¹¹⁹ Employing conditions reported by Ciceri and Demnitz allowed for the rapid chemoselective synthesis of ketal **2.06** by reaction with an excess of ethylene glycol, stoichiometric *p*-toluenesulfonic acid monohydrate (*p*-TsOH.H₂O), and 4 Å molecular sieves (Scheme 2.2).¹²³



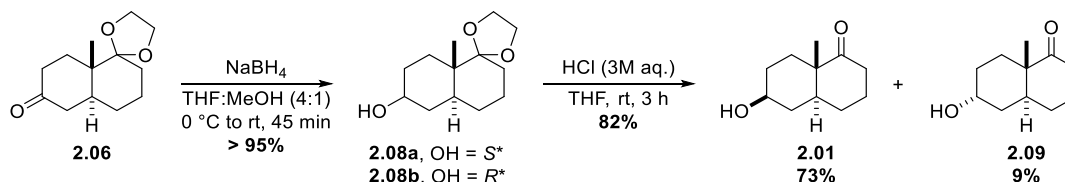
Scheme 2.2 Synthesis of the ethylene ketal **2.06**

The desired *trans* stereochemistry at the ring-junction atoms was achieved by a dissolving metal reduction of the enone double bond (Table 2.2). At first, the reduction was performed by dissolving sodium in ammonia, with ethanol as the chosen proton source (entry 1).¹¹⁹ The reaction proceeded with complete diastereoselectivity for the *trans*-fused ketone **2.07**, however isolated yields were poor. These conditions suffered from poor reproducibility (entry 2), often proceeding with over reduction of the enone to yield mixtures of the desired ketone **2.07** and alcohol **2.08**. Changing the metal from sodium to lithium (entry 3) appeared promising, however formation of alcohol **2.08** was still observed. Hypothesising that the over reduction could arise from use of ethanol as the proton source, *tert*-butanol was chosen as a proton source with lower acidity. Use of *tert*-butanol improved conversion and further decreased the observed over reduction (entries 4 and 5). Through further minor modifications including quenching excess lithium with isoprene, conditions were identified that reproducibly yielded the desired *trans*-fused ketone **2.07** on a multi-gram scale (entry 6).

Table 2.2 Synthesis of ketone **2.07** by dissolving metal reduction

Entry	Metal (equiv.)	Proton source (equiv.)	Time (min)	Quenching reagent	Yield (%)	Comment
1	Na (2.7)	EtOH (1.5)	120	NH ₄ Cl	26	-
2	Na (2.7)	EtOH (1.2)	30	NH ₄ Cl	-	Over reduction to 2.08
3	Li (2.3)	EtOH (1.0)	30	NH ₄ Cl	-	Over reduction to 2.08
4	Li (2.3)	<i>t</i> -BuOH (1.0)	30	NH ₄ Cl	55	Over reduction to 2.08 , yield after purification
5	Li (2.3)	<i>t</i> -BuOH (1.0)	60	NH ₄ Cl	62	2.06 in crude reaction, yield after purification
6	Li (4.0)	<i>t</i> -BuOH (2.0)	30	Isoprene	87	No column

With future SAR efforts in mind, it was decided that the reduction of the carbonyl of ketone **2.07** would not be optimised for complete diastereoselectivity, so that sufficient quantities of the diastereoisomeric ketone **2.09** could be isolated alongside the desired ketone **2.01** after deprotection of the ketal. Ketone **2.07** was cleanly reduced in quantitative yield with sodium borohydride in a mixed solvent system of THF:methanol (4:1), yielding an inseparable mixture of diastereoisomeric alcohols in a ratio of 86:14 **2.08a:2.08b**.¹²⁴ The diastereoisomeric mixture of alcohols was deprotected with aqueous hydrochloric acid in THF, and the sterol-inspired ketone **2.01** and its diastereoisomer **2.09** were isolated after separation by flash chromatography (Scheme 2.3).

**Scheme 2.3** Synthesis of sterol-inspired ketone **2.01** and diastereoisomeric ketone **2.09** from trans-fused ketone **2.06** by hydride reduction and ketal deprotection

2.2.2 Synthesis of intermediate building blocks

In order to further increase the scaffold diversity of the sterol-inspired compound collection, it was necessary to synthesise a number of additional building blocks derived from ketone **2.01** (Figure 2.4). Directly from ketone **2.01** the α -bromoketone **2.10** and hydroxymethylene **2.11** were targeted. Anticipating chemistry using strongly basic or acidic conditions, it was decided to synthesise an intermediate **2.12** in which the C3-OH group was protected as the methoxyethoxymethyl (MEM) ether owing to its favourable chemical stability under a range of conditions.¹²⁵ From MEM-ketone **2.12** a MEM-protected hydroxymethylene **2.13** and β -ketoester **2.14** would also be synthesised.

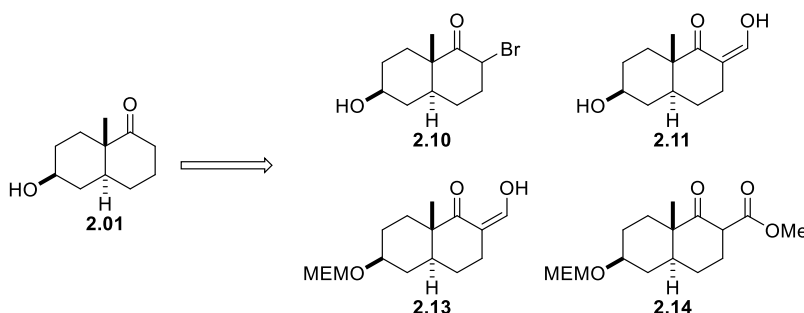
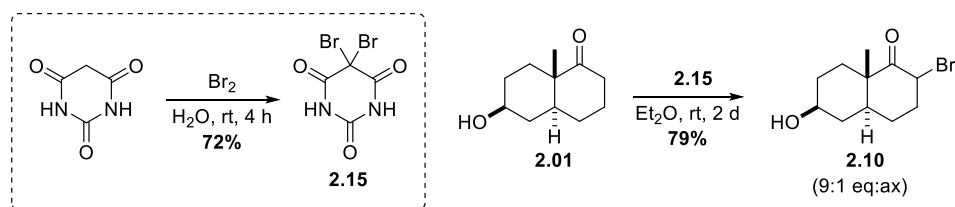


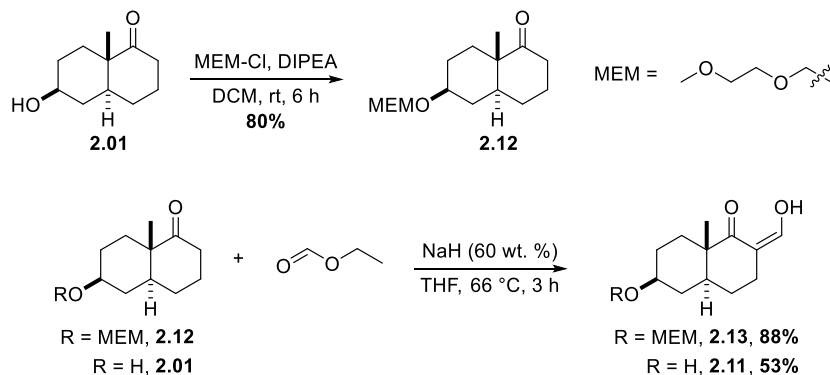
Figure 2.4 Key intermediate building blocks targeted from sterol-inspired ketone **2.01**

Selective mono- α -bromination of ketone **2.01** was achieved using 5,5-dibromobarbituric acid **2.15**. Synthesis began by bromination of barbituric acid with an excess of bromine, affording 5,5-dibromobarbituric acid **2.15** as a white powder after isolation. Reaction of ketone **2.01** with sub-stoichiometric amounts of 5,5-dibromobarbituric acid (0.6 equiv.) yielded the desired α -bromoketone **2.10** after two days at room temperature (Scheme 2.4). The α -bromoketone **2.10** was isolated after workup as an inconsequential 9:1 mixture of equatorial:axial isomers, as determined by analysis of coupling constants of the carbonyl α proton.



Scheme 2.4 Synthesis of 5,5-dibromobarbituric acid **2.15** and α -bromoketone **2.10**

Protection of the C3-OH of ketone **2.01** as the MEM-ether was achieved in high yield by reacting with MEM-Cl in the presence of *N,N*-diisopropylethylamine (DIPEA), affording the MEM-ketone **2.12** as a yellow oil (Scheme 2.5). From protected ketone **2.12**, MEM-hydroxymethylene **2.13** was synthesised by a Claisen condensation with ethyl formate in the presence of sodium hydride, with the product isolated as the enol-tautomer, stabilised by an intramolecular hydrogen bond. Additionally, the unprotected hydroxymethylene **2.11** was synthesised from ketone **2.01** in an analogous procedure, albeit it in poorer yields and without further purification owing to instability of the compound on silica gel (Scheme 2.5).



Scheme 2.5 Synthesis of MEM-ketone **2.12**, and hydroxymethylenes **2.11** and **2.13** from ketones **2.01** and **2.12**.

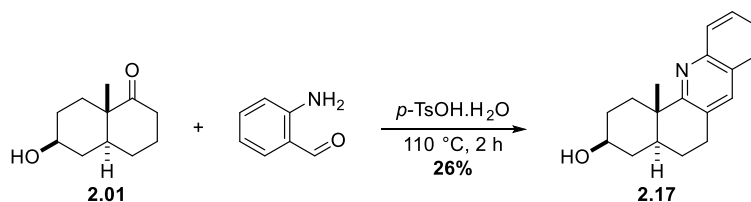
The final intermediate targeted before commencing analogue synthesis was β -ketoester **2.14** (Table 2.3). Synthesis of β -ketoester **2.14** was initially attempted by reaction of methyl cyanofomate with the *in situ* generated lithium enolate of MEM-ketone **2.12** (entry 1), however only minor traces of C-acylated product were identified, with the suspected O-acylated product **2.16** identified as the major product. The C-acylation of ketones using methyl cyanofomate has been reported to be sensitive to the choice of solvent, and thus the reaction was attempted using diethyl ether instead of THF (entry 2)¹²⁶. Increasing quantities of the β -ketoester **2.14** were formed, however the suspected O-acylated product **2.16** was still detected. Changing the base from lithium bis(trimethylsilyl)amide (LiHMDS) to lithium diisopropylamide (LDA) (entry 3) was observed to further increase formation of the desired β -ketoester **2.14**, however significant amounts of side-products were still forming. Ultimately, changing the acylating agent to methyl carbonate and the base to sodium hydride allowed for the synthesis of β -ketoester **2.14** in high yields and with no formation of the suspected O-acylated product **2.16** (entry 4).

Table 2.3 Synthesis of β -ketoester **2.14** from MEM-ketone **2.12**.

Entry	Acylating agent (equiv.)	Base (equiv.)	Solvent	Temperature (°C)	Time (h)	Yield (%)	Comments
1	(1.25)	LiHMDS (1 M, THF) (1.25)	THF	- 78	1	-	Formation of 2.16 observed
2	(2.0)	LiHMDS (1 M, THF) (2)	Et ₂ O	- 78	2	-	Formation of 2.16 observed
3	(1.5)	LDA (1.1)	Et ₂ O	- 78	2	-	Formation of 2.16 observed
4	(10)	NaH (60 wt. %) (10)	THF	66	6	78	Exclusive formation of 2.14 ,

2.2.3 Analogue synthesis from the sterol inspired ketone

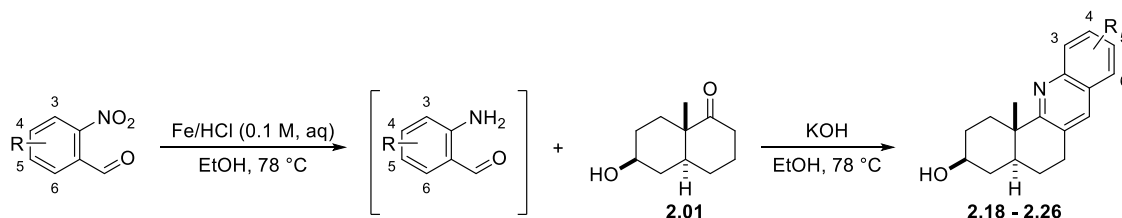
Synthesis of the sterol-inspired compound collection began directly from the sterol-inspired ketone **2.01**. The first class of heterocycle fusions to be targeted were analogues fused to quinoline. Ketone **2.01** was initially reacted with 2-aminobenzaldehyde and *p*-TsOH.H₂O under solvent-free conditions (Scheme 2.6) in a classical Friedländer quinoline synthesis, affording the unsubstituted quinoline-fused analogue **2.17** in acceptable yield.



Scheme 2.6 Synthesis of quinoline-fused analogue **2.17** via classical Friedländer conditions

Owing to the inherent instability of 2-aminobenzaldehydes and their prohibitive pricing from commercial suppliers, alternative methods to synthesise quinoline-fused analogues were sought. Reductive procedures wherein the 2-aminobenzaldehyde could be prepared in situ from the corresponding 2-nitrobenzaldehyde and cyclised with ketone **2.01** without isolation of the 2-aminobenzaldehyde offered a viable route to the quinoline-fused analogues. A one-pot procedure was identified in which the 2-nitrobenzaldehyde was reduced to the 2-aminobenzaldehyde using iron and catalytic hydrochloric acid under reflux in ethanol, followed by a potassium hydroxide mediated cyclisation with ketone **2.01**.¹²⁷ Following these conditions, eight additional quinoline-fused analogues **2.18** – **2.26** were successfully synthesised in moderate yields (Table 2.4).

Table 2.4 Synthesis of quinoline fused analogues **2.18** – **2.27** via a one-pot reductive Friedländer synthesis



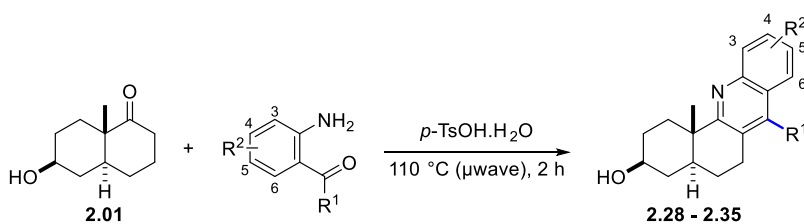
Entry	Compound	R	Reduction time (h)	Cyclisation time (h)	Yield (%)	Comments
1	2.18	5-Cl	0.75	4	49	
2	2.19	4,5-OMe	3.5	48	23	formate salt
3	2.20	4-Cl	1	6	56	
4	2.21	6-Cl	1	5	50	
5	2.22	5-F	1	20	27	impure S _N Ar product isolated
6	2.23	5-Br	1.5	2	37	
7	2.24	4-F	1	4	24	
8	2.25	4-OMe	4	20	31	
9	2.26	5-NMe ₂	6	48	30	impure
10	2.27	5-OH	-	-	-	dimerisation of aminobenzaldehyde

The quinoline-fused analogues were generally isolated in high purity after purification. For the 5-F substituted analogue **2.22** (entry 5), the prolonged cyclisation time resulted in formation of the S_NAr product in which the fluorine group was substituted by an ethoxy group. Therefore, cyclisation of the 4-F substituted analogue **2.24** (entry 7) was stopped when formation of the S_NAr product was detected. The 5-NMe₂ analogue **2.26** (entry 9) was successfully synthesised, however it was isolated in 70% purity. This analogue

was excluded from use in screening due to the low purity, as well as its high fluorescence emission at wavelengths commonly used in biochemical assays. The reduction of 2-nitro-5-hydroxybenzaldehyde (entry 10) was successful, though the corresponding 2-aminobenzaldehyde was seen to rapidly dimerise and the reaction therefore not subjected to cyclisation with ketone **2.01**.

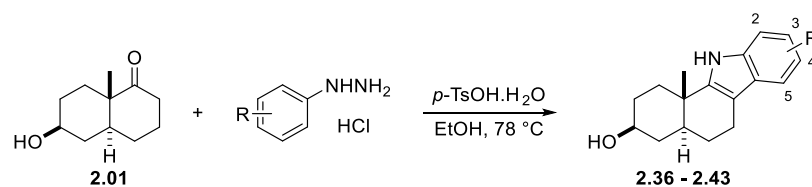
In a related Friedländer synthesis, a series of quinoline-fused analogues bearing additional alkyl and aryl substitution were synthesised. Ketone **2.01** was reacted with either a 2-aminoacetophenone or 2-aminobenzophenone with stoichiometric *p*-TsOH.H₂O under microwave irradiation and solvent free conditions, affording eight additional analogues **2.28** – **2.35** in good yields (Table 2.5). Quinolines in which R¹ = 2-fluorophenyl were isolated as inseparable mixtures of conformational isomers due to restricted rotation around the C-Ar bond (Table 2.5, highlighted bond).

Table 2.5 Synthesis of quinoline-fused analogues **2.28** – **2.35** via a microwave assisted Friedländer synthesis



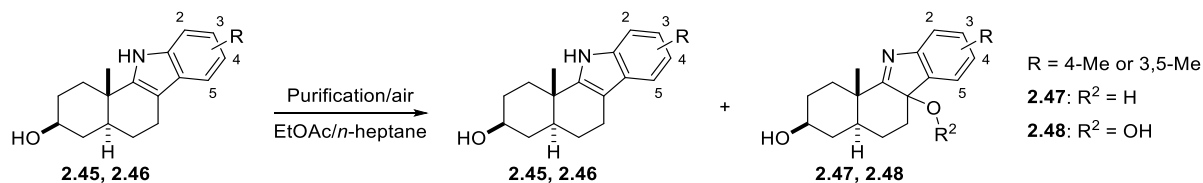
Entry	Compound	R ¹	R ²	Yield (%)	Comments
1	2.28	Ph	H	68	-
2	2.29	Ph	5-Cl	73	-
3	2.30		5-Cl	79	conformational isomerism
4	2.31		5-NO ₂	41	conformational isomerism
5	2.32	Me	5-Cl	53	aminoacetophenone synthesised by reduction of nitroacetophenone (PtO ₂ /C/H ₂)
6	2.33	Me	H	67	-
7	2.34		H	59	-
8	2.35		H	59	-

The second series of analogues synthesised directly from sterol-inspired ketone **2.01** were the indole-fused analogues. Indole-fused analogues were successfully synthesised employing classical Fischer indole synthesis conditions in which sterol-inspired ketone **2.01** was reacted with different phenylhydrazines under acidic conditions, with *p*-TsOH.H₂O identified as the optimal choice of acid (Table 2.6).

Table 2.6 Synthesis of indole-fused analogues **2.36** – **2.43**

Entry	Compound	R	Reaction time (h)	Yield (%)	Comments
1	2.36	H	4	52	phenylhydrazine free base used
2	2.37	4-Br	20	67	-
3	2.38	4-F	2.5	50	-
4	2.39	4-OMe	24	72	-
5	2.40	3,5-Cl	48	35	-
6	2.41	2-F	3	39	-
7	2.42	4-Cl	2.5	37	-
8	2.43	3-Br	5.5	49	isolated as mixture of regioisomers (3/5-Br)
9	2.44	4-NO ₂	-	-	no cyclisation of hydrazone
10	2.45	4-Me	-	-	oxidation of indole
11	2.46	3,5-Me	-	-	oxidation of indole

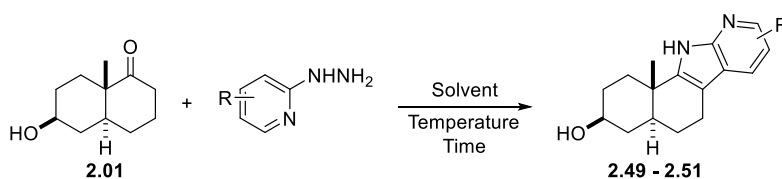
Indole analogues were generally accessed in moderate to high yields, with no deviations from the standard procedure. Indoles bearing two electron-withdrawing groups (entry 5) suffered from prolonged reaction times owing to the inability of the electron-poor hydrazone to cyclise. Likewise, the nitro-substituted hydrazone (entry 9) failed to cyclise at all with no traces of product identified. Use of unsymmetrical hydrazines gave rise to inseparable mixtures of regioisomers (entry 8) and were therefore deprioritised for synthesis. Attempts to synthesise methyl substituted indoles **2.45** and **2.46** (entries 10 and 11) were successful in forming the desired indole products, however decomposition was observed after workup and purification. Analysis of purified products by nuclear magnetic resonance (NMR) spectroscopy did not support the formation of any distinct products, however analysis by LCMS suggested formation of oxidised products **2.47** and **2.48** (Scheme 2.7). Spontaneous oxidation of tetrahydrocarbazoles in air has been reported, however, further attempts to either fully oxidise the indole or prevent their oxidation proved unsuccessful.^{128,129}

**Scheme 2.7** Spontaneous oxidation of methyl-substituted indoles during purification of crude reaction mixtures

Following the successful synthesis of the indole-fused analogues, a series of complementary azaindole-fused analogues were targeted. Preliminary attempts sought to utilise palladium-catalysed syntheses to overcome the inherent limitations of the Fischer indole synthesis and instead utilise haloaminopyridines. Unfortunately, either no conversion of the sterol-inspired ketone **2.01** was observed or only minor (5 –

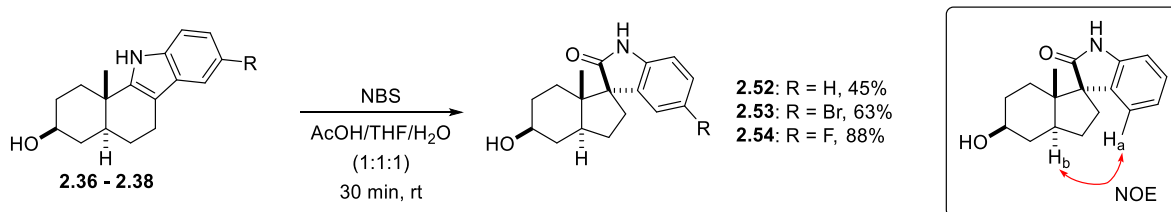
10%) formation of the desired azaindole was observed. As such, subsequent attempts returned to classical Fischer indole synthesis conditions (Table 2.7). First attempts reacted ketone **2.01** with 2-hydrazinopyridines in 4% aqueous sulfuric acid at 160 °C under microwave irradiation (entries 1 and 2). Under such conditions, the hydrazone formed rapidly, however cyclisation to the desired 7-azaindole was slow due to protonation of the pyridine ring. Switching to reacting ketone **2.01** with 2-hydrazinopyridines in diethylene glycol (DEG) at 250 °C under microwave irradiation proved to be necessary to cyclise the intermediate hydrazones, yielding the desired 7-azaindoles **2.49** – **2.51** (entries 3 – 5) in variable yields.¹³⁰ These conditions were applied to both 3- and 4-hydrazinopyridines, however no traces of hydrazone or azaindole were detected (entries 6 and 7), likely due to the electron-deficient nature of the intermediate hydrazone.¹³¹

Table 2.7. Synthesis of azaindole-fused analogues **2.49** – **2.51**



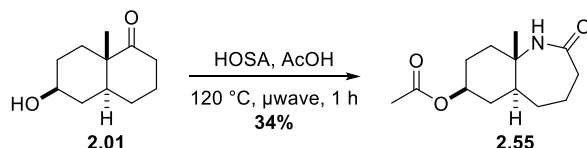
Entry	Compound	Hydrazine	Solvent	Temperature (° C)	Time (h)	Yield (%)	Comments
1	-		4% aq. H ₂ SO ₄	160	1	-	-
2	-		4% aq. H ₂ SO ₄	160	1	-	-
3	2.49		DEG	250	3	39	-
4	2.50		DEG	250	3	10	-
5	2.51		DEG	250	3	25	-
6	-		DEG	250	3	-	No conversion
7	-		DEG	250	3	-	No conversion

A series of spirocyclic oxindole analogues **2.52** – **2.54** were synthesised from the corresponding indole-fused analogues. The number of spirocyclic analogues synthesised was however limited, anticipating that the increased three-dimensionality may not be as relevant in engaging STPs as the sterol-binding domain is typically flat in nature, despite their often favourable properties as screening compounds. Spiro-oxindoles **2.52** – **2.54** were synthesised in high yields by an oxidative rearrangement, wherein the indoles analogues were brominated using *N*-bromosuccinimide (NBS) in a mixed solvent system of acetic acid/THF/water, rearranging in an acid promoted semi-pinacol rearrangement to yield the desired products **2.52** – **2.54** (Scheme 2.8), with oxindole **2.52** isolated alongside ~10% of brominated product **2.53**. The identity of the isolated diastereoisomer was assigned by the presence of an NOE correlation between a proton of the oxindole phenyl ring (H_a) and the axial ring junction proton (H_b) (Scheme 2.8).



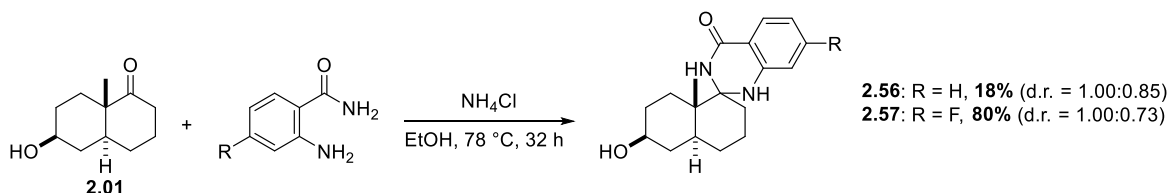
Scheme 2.8 Synthesis of spirooxindole analogues **2.52** – **2.54** and NOE correlation used to identify the isolated diastereoisomer

Ketone **2.01** was subjected to a Beckmann rearrangement in order to synthesise the ring-expanded lactam analogue **2.55**. Reaction of ketone **2.01** with hydroxylamine-*O*-sulfonic acid (HOSA) in glacial acetic acid and heating at 120 °C via microwave irradiation yielded the ring-expanded analogue **2.55** as one regioisomer via the intermediate oxime-*O*-sulfonic acid (Scheme 2.9). The reaction also proceeded with acetyl protection of the C3-OH, with retention of the hydroxyl group stereochemistry.



Scheme 2.9 Synthesis of ring-expanded lactam analogue **2.55**

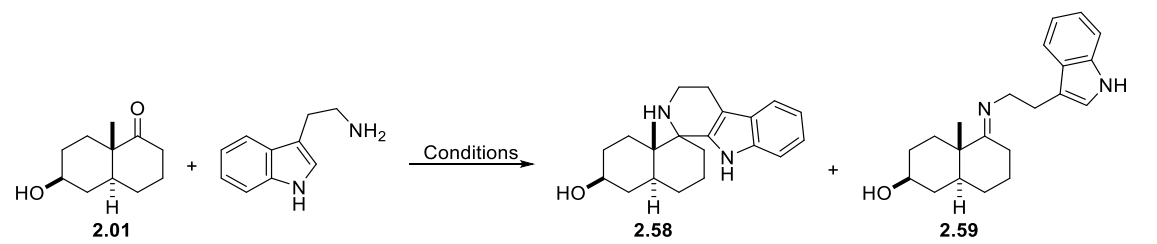
Additional spirocyclic analogues were synthesised from the sterol-inspired ketone **2.01**. Ketone **2.01** was reacted with the appropriate 2-aminobenzamide with stoichiometric ammonium chloride, heating at reflux until reaction completion, yielding dihydroquinazolinone analogues **2.56** and **2.57** as inseparable mixtures of diastereoisomers (Scheme 2.10).



Scheme 2.10 Synthesis of spirocyclic dihydroquinazolinone analogues **2.56** and **2.57**.

Synthesis of spirocyclic tetrahydroisoquinoline (THIQ) analogues from ketone **2.01** was attempted via a Pictet-Spengler reaction (Table 2.8). Initial attempts to react ketone **2.01** with tryptamine under acidic or Dean-Stark conditions gave no conversion to the desired product (entries 1 and 2).^{132,133} Iodine was identified as a promising catalyst for the Pictet-Spengler reaction of ketone **2.01** and tryptamine (entry 3).¹³⁴ Further increasing the equivalents of iodine appeared to accelerate the reaction (entry 4), however monitoring of the reaction by NMR analysis showed formation of both the THIQ product **2.58** and uncyclised ketimine **2.59**, the identity of which were supported by the presence of ¹³C signals arising from the new spirocyclic centre and the ketimine carbon respectively. Performing the reaction using microwave-assisted heating (entry 5) or using dry acetonitrile (entry 6) did not improve conversion. Conversion above that seen in entry 4 was unable to be achieved, even with application of alternative reaction conditions (entry 7). The poor conversion could be explained by a combination of electronic and steric effects, with the parent ketone **2.01** and derived ketimine **2.59** having low electrophilicity, as well as the steric influence of the nearby axial methyl group – rendering formation of the quaternary spirocyclic centre difficult.

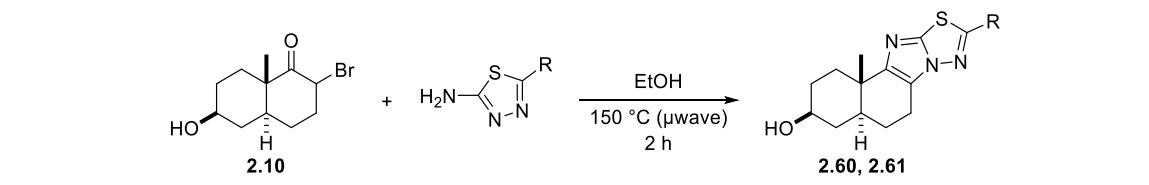
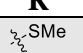
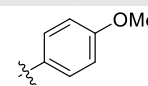
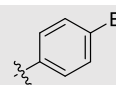
Table 2.8 Attempted synthesis of spirocyclic THIQ analogue **2.58** via a Pictet-Spengler reaction

				
Entry	Conditions	Time (h)	2.01:2.58/2.59	Comments
1	DCE, TFA, Na ₂ SO ₄ , 40 °C	18	-	No conversion
2	Toluene (Dean-Stark), then CHCl ₃ , TFA, rt	18	-	No conversion
3	I ₂ (0.1 eq.), MeCN, 82 °C	48	1:0.25	-
4	I ₂ (0.2 eq.), MeCN, 82 °C	24	1:0.40	-
5	I ₂ (0.2 eq.), MeCN, 100 °C	2.5	1:0.15	Microwave heating
6	I ₂ (0.2 eq.), MeCN, 82 °C	48	1:0.05	Dry MeCN
7	TMS-Cl, pyridine, 100 °C	5	-	Sealed tube, minor traces of product

2.2.4 Analogue synthesis from the sterol-inspired α -bromoketone

Starting from the α -bromoketone intermediate **2.10** a number of ring-fused analogues were successfully synthesised. Reaction of α -bromoketone **2.10** with aminothiadiazoles under microwave irradiation provided access to two imidazothiadiazole-fused analogues **2.60** and **2.61** (Table 2.9) (entry 1 and 2). Though the imidazothiadiazole scaffold is not found in NPs, it is instead found in many drugs.¹³⁵ The scope of the reaction was limited partially by available aminothiadiazoles reagents, but also the reaction conditions. The forcing reaction conditions often resulted in a partial reductive-dehalogenation of the α -bromoketone **2.10** to ketone **2.01**. Attempts to synthesise the *p*-bromophenyl substituted analogue **2.62** (entry 3) was also found to result in reductive-dehalogenation of the aminothiadiazoles reagent and product, giving inseparable mixtures of the 4-bromophenyl and phenyl-substituted analogues.

Table 2.9 Synthesis of imidazothiadiazole-fused analogues **2.60** and **2.61**.

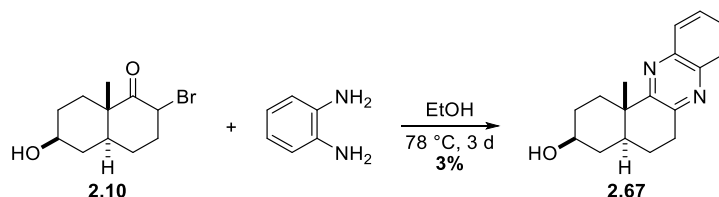
				
Entry	Compound	R	Yield (%)	Comment
1	2.60		36	-
2	2.61		39	-
3	2.62		-	Dehalogenation of aminothiadiazoles

In a related procedure, a series of thiazole-fused analogues **2.63** – **2.65** were synthesised by reaction of α -bromoketone **2.10** with thioamides in refluxing ethanol (Table 2.10) (Entries 1 – 3). Reacting with thiourea instead of a thioamide provided access to the aminothiazole-fused analogue **2.66** in good yield after an aqueous workup (entry 4).

Table 2.10 Synthesis of thiazole-fused analogues **2.63** – **2.66**.

Entry	Compound	R	Time (h)	Yield (%)
1	2.63		3	26
2	2.64		48	61
3	2.65		48	43
4	2.66		4	67

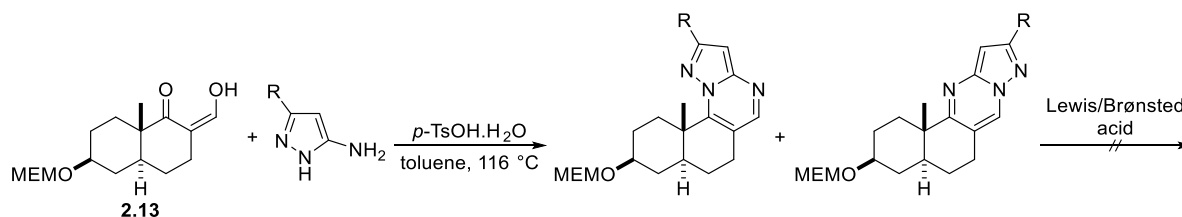
Reaction of α -bromoketone **2.10** with *o*-phenylenediamine in refluxing ethanol afforded the single quinoxaline-fused analogue **2.67** in poor yield (Scheme 2.11). Conversion to the desired quinoxaline **2.67** was poor and purification by both flash chromatography on silica gel and preparative-HPLC was required to isolate the compound in acceptable purity and remove the unreacted *o*-phenylenediamine reagent. The scope of the reaction was also limited, as use of substituted *o*-phenylenediamines would result in mixtures of regioisomeric products. As such, no further quinoxaline-fused analogues were synthesised.



Scheme 2.11 Synthesis of quinoxaline-fused analogue **2.67**.

2.2.5 Analogue synthesis from the sterol-inspired hydroxymethylenes

The first series of analogues targeted from the hydroxymethylene building blocks were pyrazolo[1,5-*a*]pyrimidine-fused analogues. The MEM-protected HM **2.13** was reacted with several 2-aminopyrazoles, refluxing under Dean-stark conditions with catalytic *p*-TsOH.H₂O, cleanly yielding mixtures of regioisomeric angular and linear regioisomers (Scheme 2.12). Deprotection of the MEM protecting group was attempted using both Brønsted acids (TFA in DCM, 6 M aq. HCl) and Lewis acids (Cerium(III) chloride), however no deprotection was observed. Analysis of reaction mixtures confirmed that the MEM group was retained, alongside decomposition of the mixture, with LCMS analysis suggesting that dimerisation to the methylene acetal had occurred.¹³⁶ It was thus decided to synthesise the pyrazolopyrimidine-fused analogues directly from the unprotected HM **2.11**.



Scheme 2.12 Attempted synthesis of pyrazolopyrimidine-fused analogues from MEM-protected hydroxymethylene **2.13**.

Under the same conditions the MEM-protected pyrazolopyrimidines were synthesised, the corresponding pyrazolopyrimidines **2.68a** – **2.72a** and **2.68l** – **2.72l** were successfully synthesised from HM **2.11** (Table 2.11). Analogues were accessed as regioisomeric pairs, with the angular isomer being the major product (entries 1 -3, 5) for all analogues bar one (entry 4). Separation of the regioisomers was achieved by preparative HPLC, affording the pyrazolopyrimidine-fused analogues in low yields, likely due to their poor solubility in the aqueous mobile phase as yields of the crude reaction mixture were acceptable.

Table 2.11 Synthesis of pyrazolopyrimidine-fused analogues **2.68a** – **2.72a** and **2.68l** – **2.72l**.

Entry	Compound	R	Crude ratio (a:b)	Angular yield (%)	Linear yield (%)
1	2.68		2.3:1.0	19	7
2	2.69		2.3:1.0	22	5
3	2.70		2.0:1.0	22	3
4	2.71		1.0:1.0	13	8
5	2.72		2.5:1.0	17	5

The MEM-protected HM **2.13** could be reacted with substituted hydrazines to afford pyrazole-fused analogues. Similar to the pyrazolopyrimidine-fused analogues, the pyrazole-fused compounds could form as both angular and linear regioisomers (Table 2.12). Reaction of the HM **2.13** with substituted hydrazines in either glacial acetic acid (entry 1) or a mixed solvent system of methanol:acetic acid (entries 2 – 6) yielded the desired pyrazole-fused analogues, with the angular regioisomer forming as the major product. For the reaction performed in glacial acetic acid, complete deprotection of the MEM ether was observed, however in the mixed solvent system of methanol:acetic acid only partial deprotection was observed. The mixtures of partially deprotected products were fully deprotected before purification using 6 M aqueous HCl in THF. Separation of regioisomers was achieved by preparative HPLC, affording the pyrazole-fused analogues **2.73a** – **2.78a** and **2.73l**, **2.75l**, and **2.78l** in moderate yields.

Table 2.12 Synthesis of angular pyrazole-fused analogues **2.73a** – **2.78a** and linear pyrazole-fused analogues **2.73l**, **2.75l**, and **2.78l**.

Entry	Compound	R	Conditions	Angular yield (%)	Linear yield (%)
1	2.73		A	12	5
2	2.74		B	27	-
3	2.75		B	8	6
4	2.76		B	47	-
5	2.77		B	27	-
6	2.78		B	30	18

The 2-fluorophenyl substituted pyrazole **2.77** (entry 5) was isolated as a mixture of conformational isomers, owing to restricted rotation around the pyrazole-phenyl C-N bond imparted by a steric clash of the 2-fluoro substituent and the axial methyl group. Variable temperature NMR (VT-NMR) of pyrazole **2.77** showed a coalescence of the methyl signals upon heating at 70 °C (343 K), suggesting an intermediate energy barrier for the interconversion of the two conformations (Figure 2.5).

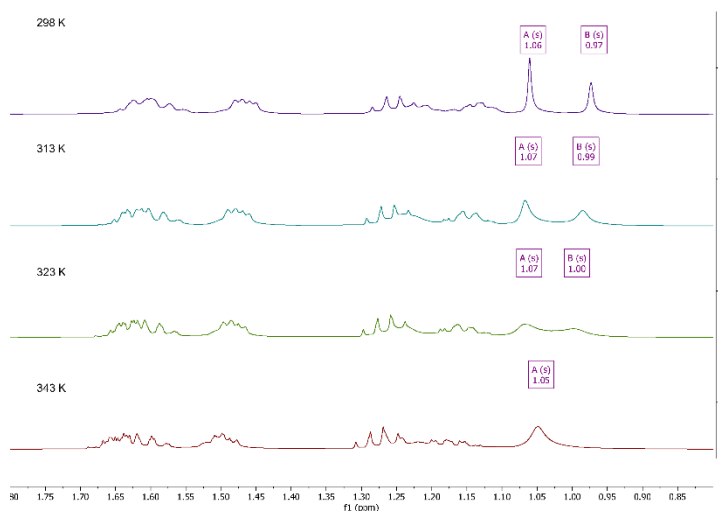
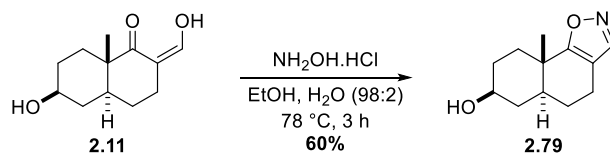


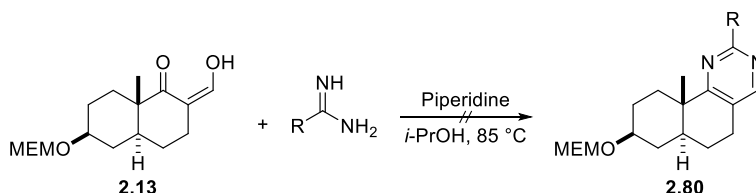
Figure 2.5 VT-NMR of pyrazole **2.77**, with the signals of the axial methyl group highlighted, showing coalescence of signals at higher temperatures.

The isoxazole-fused analogue **2.79** was successfully synthesised by reaction of the unprotected HM **2.11** with hydroxylamine hydrochloride in an ethanol:water (98:2) mixture, affording the product in moderate yield after purification (Scheme 2.13).



Scheme 2.13 Synthesis of isoxazole-fused analogue **2.79**.

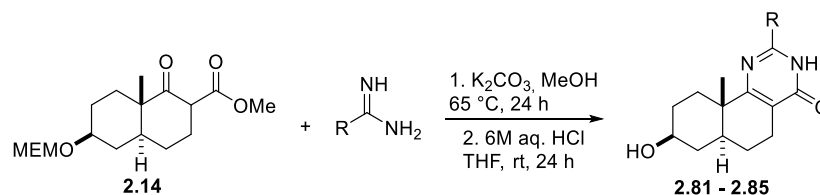
The last family of analogues targeted from the HM intermediates were pyrimidine fused-analogues **2.80**. The synthesis of structurally related WMK-derived pyrimidine fusions was reported in the patent literature, wherein a HM was reacted with a series of substituted amidines (alkyl, aryl, heteroaryl) by refluxing in isopropanol and piperidine.¹³⁷ Application of these conditions to the MEM-protected HM **2.13** were unsuccessful in affording the desired pyrimidine-fused analogues **2.80** (Scheme 2.14). Despite attempts to further optimise the reaction, only traces of product or complex reaction mixtures formed. As such, an alternative approach to pyrimidine-fused analogues was desired.



Scheme 2.14 Attempted synthesis of pyrimidine-fused analogues **2.80**

2.2.6 Analogue synthesis from the sterol-inspired β -ketoester

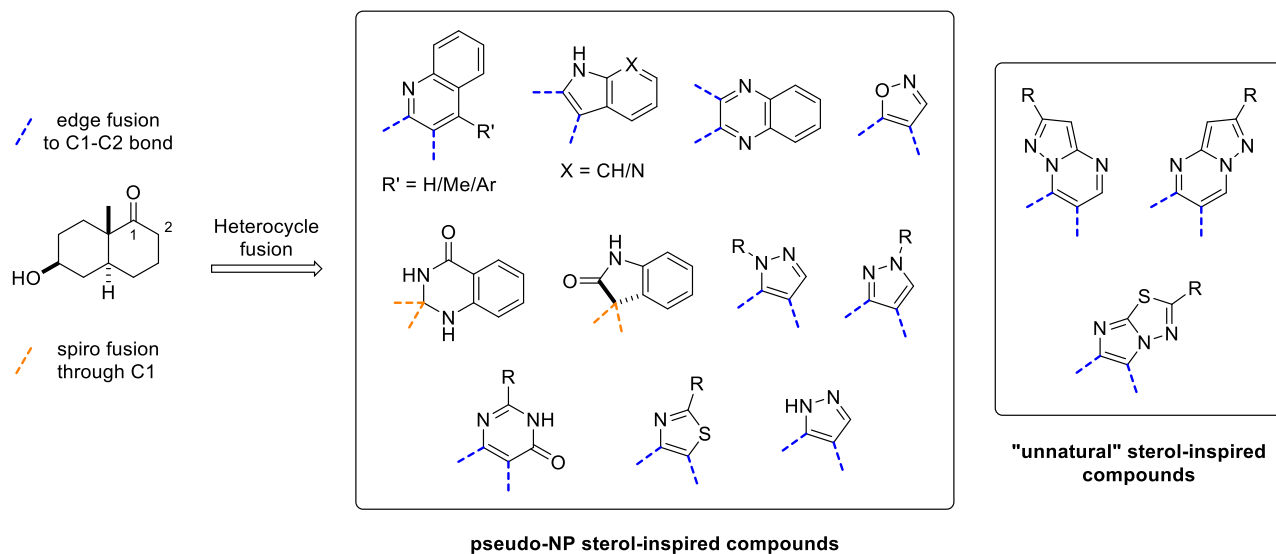
It was found that pyrimidone-fused analogues could be synthesised from the sterol-inspired β -ketoester **2.14**, allowing access to a series of analogues complementary to the previously targeted pyrimidine-fused analogues. The β -ketoester **2.14** was initially reacted with a substituted amidine, refluxing in methanol in the presence of potassium carbonate (Table 2.13) (entry 1), affording a 1:1 mixture of the MEM-protected pyrimidone and MEM-ketone **2.12** arising from decarboxylation.¹³⁸ Ensuring that the methanol was adequately dried facilitated the synthesis of MEM-protected pyrimidones in good yields with no decarboxylation of β -ketoester **2.14**. The desired pyrimidone-fused analogues **2.81** – **2.85** were synthesised following acidic deprotection of the MEM-ether (entries 2 – 6). The aminopyrimidone **2.86** accessed from reaction of β -ketoester **2.14** with guanidine was successfully synthesised, however deprotection of the MEM group under a range of conditions proved unsuccessful, resulting in the formation of unidentified products (entry 7).

Table 2.13 Synthesis of pyrimidone-fused analogues **2.81** – **2.85** from β -ketoester **2.14**.

Entry	Compound	R	Yield (%)	Comments
1	-		-	Decarboxylation of 2.14 , solvent not dried
2	2.81		42	-
3	2.82		76	-
4	2.83		54	-
5	2.84		69	-
6	2.85		62	-
7	2.86		-	Deprotection of MEM unsuccessful

2.3 Sterol-inspired compound collection summary

In total, the final sterol-inspired compound collection was composed of 65 sterol-inspired compounds (Figure 2.6). These 65 compounds comprised 14 different heterocyclic scaffolds, 11 of which can be considered as pseudo-NPs with the other 3 scaffold fusions featuring “unnatural” heterocycles. A majority of analogues were accessed in high purity (> 95%) and none of the compounds exhibited significant fluorescence at wavelengths utilised in typical biochemical assays, and the collection thus deemed appropriate for use in screening against STPs.

**Figure 2.6** Summary of heterocycle-fusions present in the sterol-inspired compound collection.

The sterol-inspired compound collection was analysed using cheminformatics approaches to allow comparison to known pseudo-NP screening collections. The NP-likeness score was calculated for the sterol-inspired compound collection, the DrugBank approved drugs, the National Cancer Institute NP-V set (a representative set of NPs), and a curated library of steroids.^{139–141} The NP-likeness score was implemented as a metric to assess the structural similarity of compounds compared to NPs and synthetic molecules, with negative values associated with synthetic molecules and positive values with NPs.¹³⁹ The NP-likeness scores determined for the sterol-inspired compounds have good overlap with both the set of approved drugs and NP-V, suggesting the compound collection has retained some degree of biological relevance (Figure 2.7). It should be noted that the sterol-inspired compounds and steroid set show very little overlap, highlighting that the sterol-inspired compounds, despite containing a conserved sterol AB-ring fragment, occupy an area of chemical space different to naturally occurring steroids.

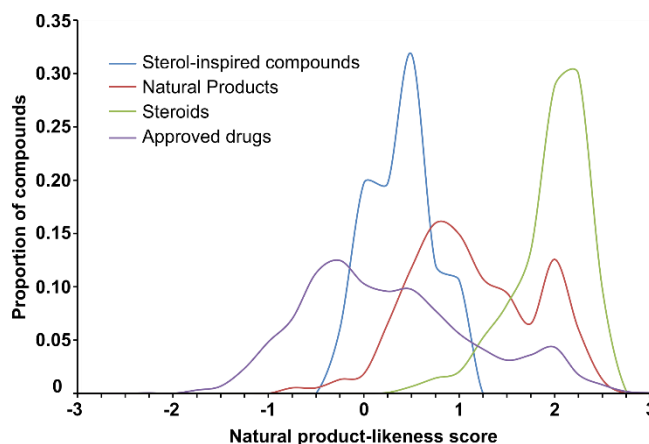


Figure 2.7 NP-likeness scores of the sterol-inspired collection (green), NCI NP-V set (red), library of steroids (purple), and DrugBank approved drugs (cyan). Details of preparation and information of the library of steroids are described in the experimental procedures.

The three-dimensionality of the sterol-inspired compounds was assessed using a principal moment of inertia (PMI) ternary plot.¹⁴² The sterol-inspired compounds mainly occupied the rod-like/disc-like axis, due to the fusion of largely flat and aromatic fragments, similar to the library of steroids (Figure 2.8). The spirocyclic and angular pyrazole-fused analogues displayed a more spherical shape, moving away from the planar nature of the other sterol-inspired compounds. This demonstrates that the sterol-inspired compound collection should be capable of engaging the sterol-binding domains of various STPs due to the mainly planar nature, but might find use in target agnostic phenotypic screens.

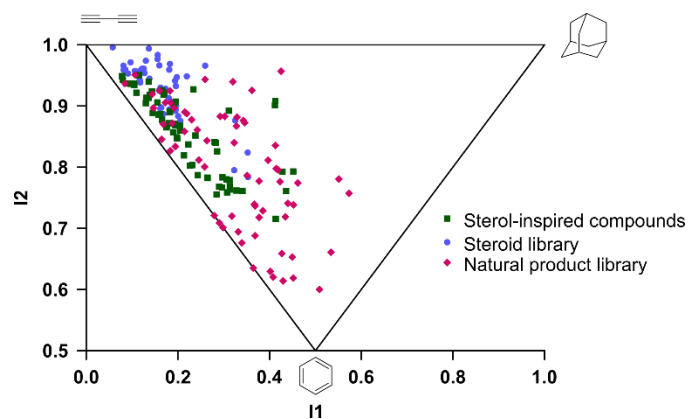


Figure 2.8 PMI plot of sterol-inspired compounds (green squares), the curated library of steroids (blue circles), and a random subset of NPs (pink diamonds). Details of preparation and information of the NP subset are described in the experimentals section. PMI values of compounds were calculated using LLAMA.¹⁴²

Part III: Biochemical screening and optimisation of STP inhibitors

3.1 Aster proteins as a screening target

To evaluate the suitability of the sterol-inspired compound collection in producing hit compounds against STPs, the Aster proteins were chosen as a model family of STPs. The Aster family represents the smallest family of STPs, with just three cholesterol-binding members (Aster-A, Aster-B, and Aster-C) compared to 16 proteins in the ORP family, of which an unknown number bind sterols, and 5 sterol binding STARDs. It was therefore anticipated that screening against the Asters would provide a better idea on whether the sterol-inspired collection could afford selective hit compounds.⁹¹ The previous development of the Aster-A inhibitor Autogramin-2 also provided evidence that it was possible to achieve selective inhibition within this protein family.⁹⁸

Current methods to study STPs including the Asters mainly rely upon genetic perturbations of individual proteins, however these approaches are often met by functional redundancies wherein another often unknown STP can compensate for the loss of another STP.^{98,101} Additionally, silencing of protein expression compared to inhibition of the activity of an individual domain can give rise to different phenotypes and biological effects, particularly if the protein in question has additional scaffolding effects not mediated by a ligand-binding domain.¹⁴³ The identification of potent and selective inhibitors of Aster-B and Aster-C would therefore allow individual probing of all three proteins over shorter time periods, and facilitate the elucidation of their biological roles in a manner complementary to genetic methods. Additionally, discovery of new Aster-A inhibitor chemotypes would serve to validate the biology elucidated around Aster-A from Autogramin-2.

Screening of the sterol-inspired compound collection was performed using a differential scanning fluorimetry (DSF) assay, with hit compounds validated via fluorescence polarisation (FP), and subsequent confirmation of sterol-transfer inhibition using a liposomal-based fluorescence resonance energy transfer (FRET) assay. All assays were performed using purified recombinant human ASTER domains for Aster-A, Aster-B, and Aster-C, expressed and purified according to published protocols by a laboratory technician and a project student in the Laraia group.⁹⁸

3.2 Differential scanning fluorimetry

Differential scanning fluorimetry (DSF) is a biophysical technique routinely used to screen small-molecule compound libraries, based upon a compounds ability to stabilise (or destabilise) a protein of interest (POI) towards thermal denaturation.¹⁴⁴ A POI exists in an equilibrium of conformational states, that when simplified, can be viewed as either the native folded state or an unfolded state, with increased temperatures pushing the equilibrium towards the unfolded state.¹⁴⁵ Small molecules can bind to the POI binding site and confer stability to the protein against thermal denaturation, increasing its melting temperature (T_m) compared to vehicle treated protein.

The thermal denaturation of proteins can be monitored through use of fluorescent dyes. The most commonly used dye, Sypro Orange, has a fluorescent profile that is sensitive to its local environment. In aqueous solutions its fluorescence is quenched, whereas in hydrophobic surroundings its fluorescence increases.¹⁴⁶ Thus, when the POI is in its native state low values of fluorescence will be measured, and fluorescence will increase as the temperature increases and protein unfolds (Figure 3.1). Eventually, proteins begin to aggregate and a decrease in fluorescence is observed. Plotting fluorescence intensity against temperature

produces sigmoidal curves in which the inflection point represents the measured T_m , the temperature at which 50% of the protein is in its unfolded state.^{144,145}

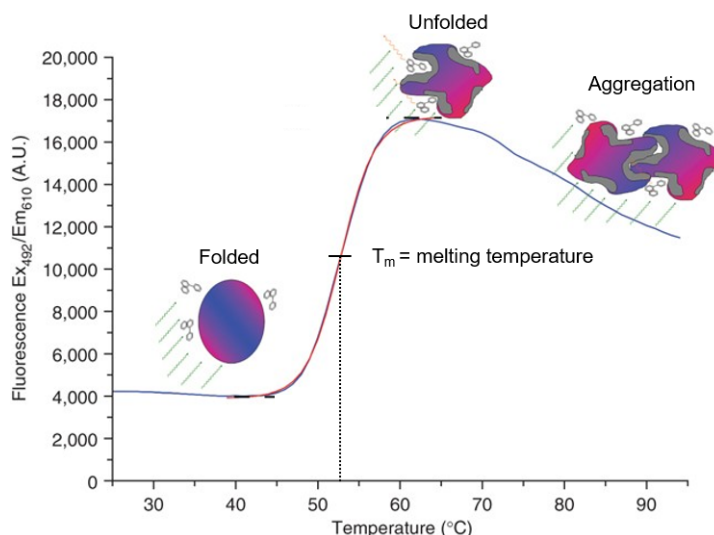


Figure 3.1 Graph of absolute fluorescence against temperature (°C) exemplifying a typical DSF experiment using Sypro Orange. The inflection point represents the melting temperature (T_m) of the protein. Figure reproduced and modified with permission from reference.¹⁴⁴ Copyright (2007) Springer Nature.

3.2.1 Preliminary screening of the sterol-inspired collection by DSF

The sterol-inspired compound collection was screened by DSF against the ASTER domains of Aster-A, -B-, and -C by a project student in the Laraia group. Purified ASTER domains at a concentration of 0.5 mg/mL were incubated for 30 minutes in the presence of compounds to be tested at a concentration of 50 μ M or dimethyl sulfoxide (DMSO) as a negative control, before running the assay following a modified literature protocol.⁹⁸ Melting temperatures were calculated with the Roche TSA analysis programme and expressed as the difference compared to DMSO-treated samples (ΔT_m). The upper and lower cutoffs for hit selection were set at ± 2 standard deviations from the mean melting temperature of the library ($\mu T_m \text{ library} \pm 2\sigma T_m \text{ library}$) (figure 3.2a – 3.2c).

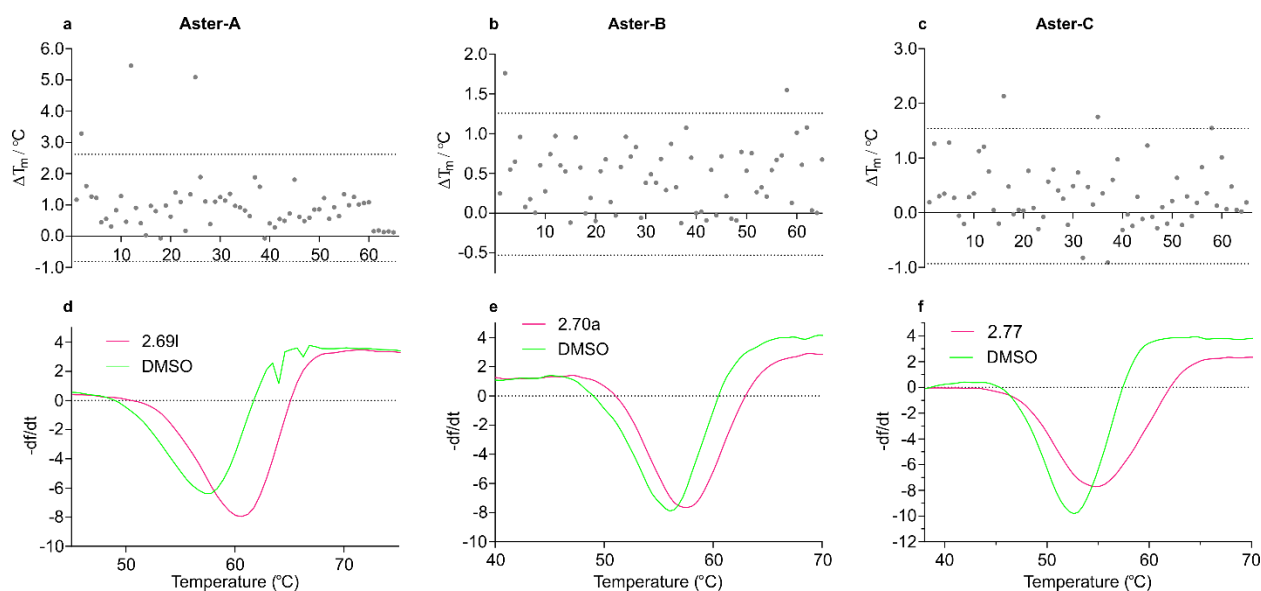


Figure 3.2 DSF screening data for the sterol-inspired compound collection against Aster-A, -B, and -C ASTER domains. **a – c:** ΔT_m values for individual compounds, with dotted lines marking hit cut-off at μT_m library $\pm 2\sigma T_m$ library. **d – f:** melting curves of select hit compounds and DMSO controls for Aster-A, -B, and -C ASTER domains. Data shown are from one representative experiment of three independent replicates.

Using these cut-offs, a total of six compounds were identified as putative hits capable of stabilising their respective ASTER domain towards thermal denaturation (Figure 3.3), representing a hit rate of 9% for the sterol-inspired compound collection. Of these six compounds, only two (**2.68I** and **2.70a**) were seen to be unselective binders that bound to Aster-B in addition to either Aster-A or -C – suggesting that the compound collection was able to yield selective compounds against the Aster proteins. The thermal stabilisation of the ASTER domains is clearly visualised by the melting curves for each protein, comparing vehicle treatment with a representative hit compound (Figure 3.2d – 3.2f). Two linear pyrazolopyrimidine-fused analogues **2.68I** and **2.69I** were identified as hits against Aster-A alongside one imidazothiadiazole fused analogue **2.61**, and two angular pyrazole-fused analogues **2.76a** and **2.77a** identified as hits against Aster-C. The identification of different chemotypes with activity against two separate Aster proteins strengthened the likeliness the compounds were true-positives, and prompted their validation in a second biochemical assay.

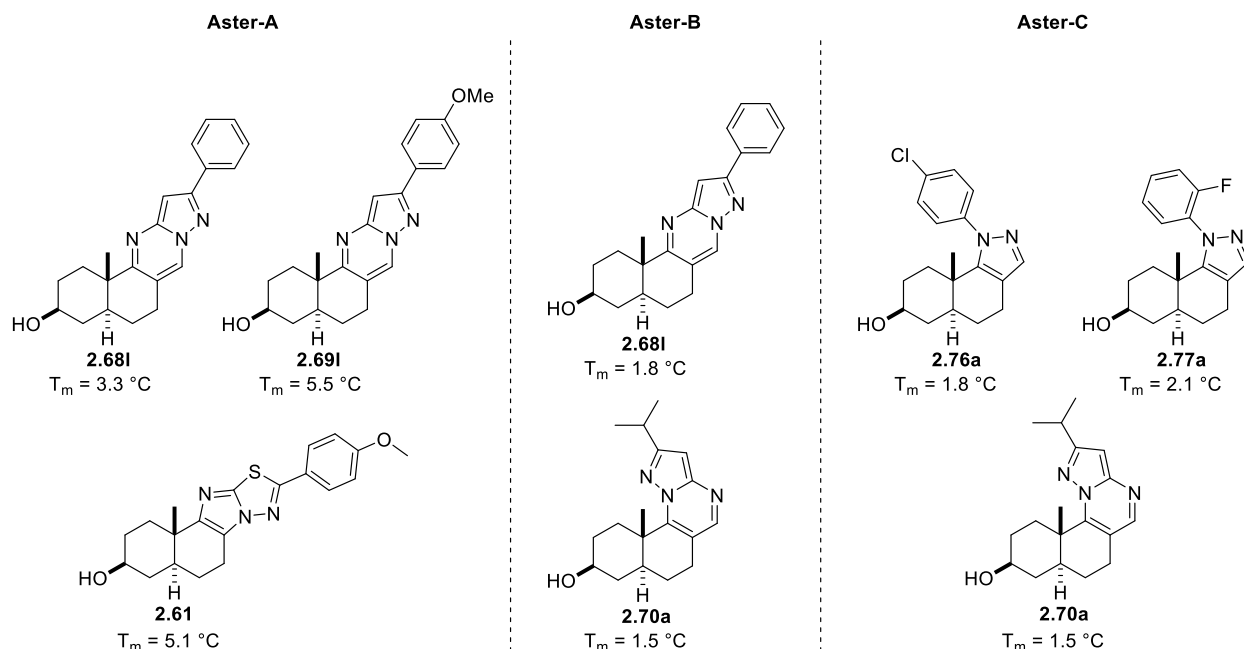


Figure 3.3. Structures of hits arising from DSF screening of the sterol-inspired compound collection against Aster protein ASTER domains.

3.3 Fluorescence polarisation

Fluorescence polarisation (FP) is a biochemical assay that allows interrogation of molecular binding interactions and rapid determination of half maximal inhibitory concentration (IC₅₀) values, and since its widespread adoption in HTS, has been applied to identify small molecule binders to numerous protein classes.¹⁴⁷ FP is an assay based upon the physical phenomena that a fluorescent molecule excited with plane-polarised light will emit light that is largely depolarised due to rapid rotation of the molecule over its fluorescence lifetime. FP is inversely proportional to the fluorophores rotation, which is itself dependent upon molecular size. Therefore, changes in molecular size arising from binding of the fluorescent molecule to a larger protein receptor will cause changes in FP.^{147,148} As such, an unbound fluorescent probe rotates rapidly in solution and emitted light will remain largely depolarised, whereas a probe bound to a much larger protein will tumble less rapidly and a larger proportion of incident light will remain polarised (Figure 3.4)

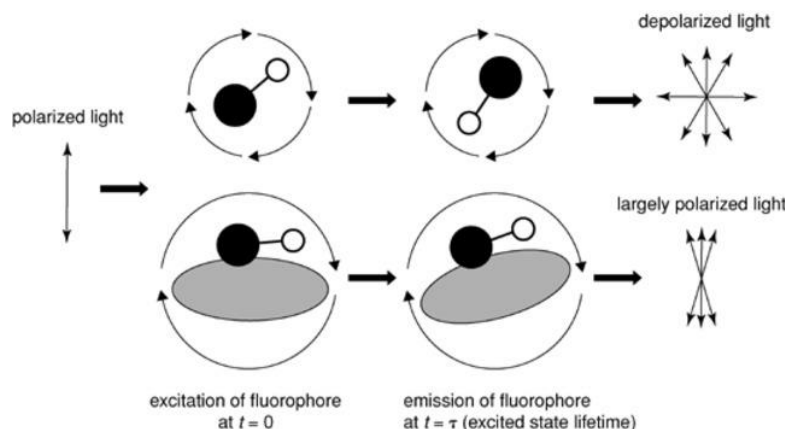


Figure 3.4 Representation of fluorescence polarisation. A fluorophore will rapidly rotate in solution and incident polarised light will rapidly depolarise (top). When the fluorescent complex increases in size (i.e. binding to a protein), incident polarised light remains largely polarised as the larger complex rotates at a slower rate (bottom). Figure reproduced from reference.¹⁴⁹

Experimentally, FP is measured by exciting an assay sample with polarised light, and measuring the intensity of emitted light parallel (I_{\parallel}) and perpendicular (I_{\perp}) to that of the excitation light, such that FP can be calculated as the normalised difference between the parallel and perpendicular emitted light (Equation 1.).¹⁴⁵

$$\text{Equation 1.} \quad \text{FP} = \frac{I_{\parallel} - I_{\perp}}{I_{\parallel} + I_{\perp}}$$

In practice, FP assays are often run in a competition mode in which a fixed concentration of fluorescent probe known to bind to the chosen target is incubated with varying concentrations of the compound to be tested. Under these conditions, the polarisation of the system is proportional to the amount of unlabelled compound bound to the receptor, allowing for the determination of IC_{50} values.¹⁴⁹

3.3.1 Hit validation by fluorescence polarisation

Validation of hit compounds from the prior DSF screens was performed by an FP assay adapted from a literature procedure.⁹⁸ FP experiments were performed in competition mode using 22-*N*-(7-nitrobenz-2-oxa-1,3-diazol-4-yl)amino-cholesterol (22-NBD-Chol) which is known to bind to the Asters with high affinity (average dissociation constant (K_d) for all Asters less than 100 nM).⁹² Before testing the hit compounds in dose response, each ASTER domain was titrated (4,000 – 8 nM) against a fixed concentration of 22-NBD-Chol (20 nM) to determine the optimum protein concentration for use in the assay. Protein concentrations were chosen by selecting the concentration that gave an 80% change in the assay window (polarisation in units of mP) – offering a sufficient assay window and minimising protein consumption. The optimum protein concentration was determined to be 1.0 μM for Aster-A and Aster-B, whereas for Aster-C the 80% change was between 0.5 – 1.0 μM . Initial hit validation used a protein concentration of 1.0 μM before later lowering to 0.5 μM . (Figure 3.5). Hit compounds were screened in dose response, initially against their hit-protein, and subsequently against the remaining two Aster proteins to determine selectivity. FP data was normalised, setting 100% inhibition as the average mP value from fluorophore-only controls and 0% inhibition as the average mP value from fluorophore-ASTER controls. Curves were fitted to the normalised data via non-linear regression, allowing for the determination of IC_{50} values for the compounds.

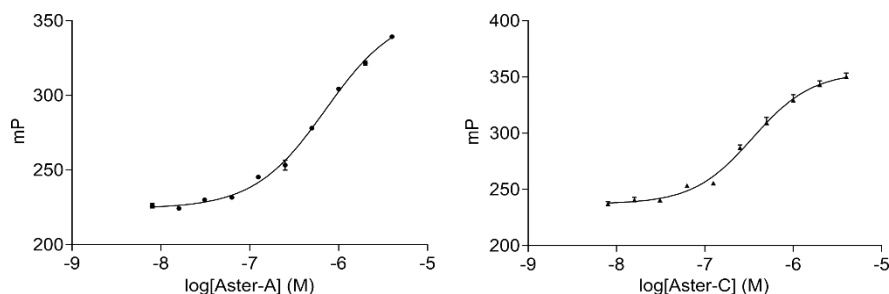


Figure 3.5 Titration of Aster protein ASTER domains of Aster-A and Aster-C (4,000 – 8 nM) against a fixed concentration of 22-NBD-Chol (20 nM)

From the six hits identified in the primary DSF screens, five were successfully validated, showing a dose-dependent inhibition of 22-NBD-Chol binding to their respective ASTER domain. This additionally shows that the compounds are likely to be directly binding to the ASTER domains in their cholesterol-binding pocket and outcompeting the fluorescent probe. Neither hit compound against Aster-B validated in the FP assay, however the linear pyrazolopyrimidine **2.68l** which was identified as a hit against both Aster-A and –B was successfully validated as inhibiting Aster-A, alongside analogue **2.69l**. It was observed that the assay window was smaller for Aster-B (35 mP) compared to both Aster-A and Aster-C (> 70 mP). To investigate whether the FP assay using Aster-B was an issue, or rather the initial hit compounds were binding non-specifically, the known pan-STP inhibitor U18666A which potently inhibits Aster-B was used as a positive control.¹¹⁰ U18666A was found to potently inhibit 22-NBD-Chol binding to Aster-B ($IC_{50} = 1.05 \pm 0.45 \mu M$) in a dose-responsive manner (Figure 3.6), suggesting that the original hits were false-positives and that functionalisation of the C3-hydroxyl could be a plausible strategy to develop Aster-B inhibitors from the sterol-inspired collection. After failing to validate angular pyrazolopyrimidine **2.70a** as an Aster-B hit, it was subsequently invalidated as a hit against Aster-C.

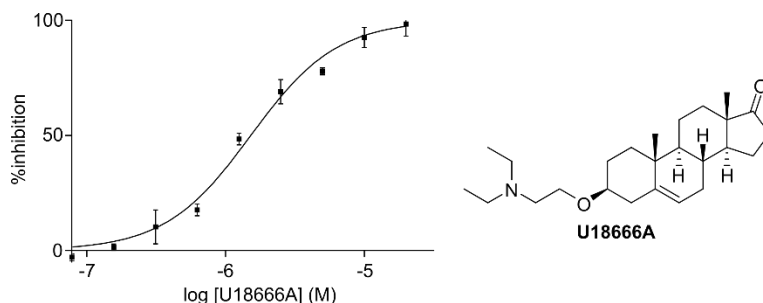


Figure 3.6 Dose response curve for U18666A against Aster-B ASTER domain. Data shown from one representative experiment of three independent replicates.

The linear pyrazolopyrimidines **2.68l** and **2.69l** both inhibited Aster-A, with the *para*-methoxy substituted analogue **2.69l** being the more potent of the two (**2.68l** $IC_{50} = 6.59 \pm 0.35 \mu M$ and **2.69l** $IC_{50} = 1.23 \pm 0.23 \mu M$) (Figure 3.7). Further profiling their selectivity against Aster-B and –C revealed no significant inhibition until a concentration of 20 μM , however, their solubility in the aqueous assay conditions limited an accurate determination of IC_{50} values. The imidazothiadiazole analogue **2.61** also potently inhibited Aster-A ($IC_{50} = 1.62 \pm 0.25 \mu M$) though with a poorer selectivity profile – inhibiting Aster-C with similar potency ($IC_{50} = 3.69 \pm 0.91 \mu M$). A similar IC_{50} was determined for the known Aster-A inhibitor Autograin-2 ($IC_{50} = 1.93 \pm 1.06 \mu M$).

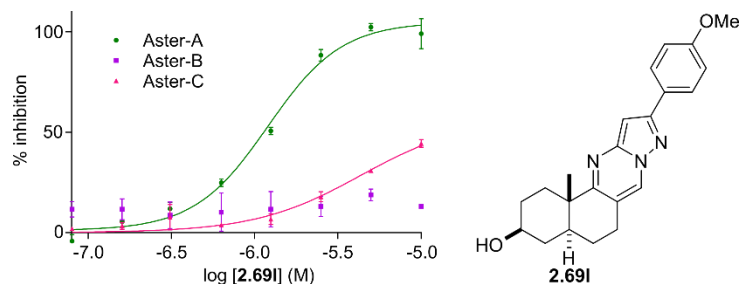


Figure 3.7 Dose response curves for pyrazolopyrimidine-fused **2.69I** against Aster-A, -B, and -C ASTER domains. Data shown from one representative experiment of three independent replicates.

The angular pyrazole-fused analogues **2.76a** and **2.77a** both inhibited Aster-C (**2.76a** $IC_{50} = 3.89 \pm 0.32 \mu M$ and **2.77a** $IC_{50} = 2.29 \pm 1.10 \mu M$) with good potency, with analogue **2.77a** (named (\pm)-Astercin 1) also having a promising selectivity over both Aster-A (15-fold, $IC_{50} = 42.3 \pm 1.14 \mu M$) and Aster-B (30-fold, $IC_{50} = 68.0 \pm 4.31 \mu M$) (Figure 3.8). The observed selectivity of these analogues prompted further investigation, with all of the angular pyrazoles and linear pyrazoles not identified as hits in the primary DSF screen screened against Aster-C in dose response by FP.

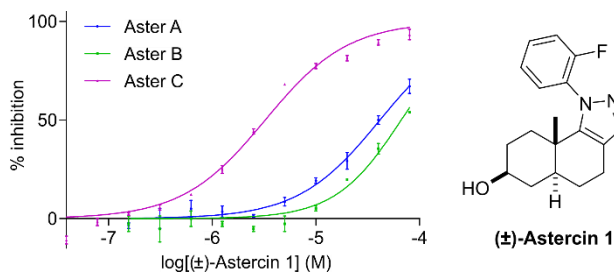


Figure 3.8 Dose response curves for (\pm)-Astercin 1 against Aster-A, -B, and -C ASTER domains. Data shown from one representative experiment of three independent replicates.

Screening of the pyrazole-fused series against Aster-C identified a clear trend in potency. Angular pyrazole-fused analogues (**2.73a**, **2.75a**, **2.76a**) featuring 4-substituted or unsubstituted phenyl rings were found to be moderately active, however 3,5-di substitution (**2.78a**) resulted in a complete loss of activity (Figure 3.9). The phenyl ring was also identified as being critical for Aster-C inhibition, with the unsubstituted analogue **2.74** showing no inhibition at the highest concentrations. Likewise, the linear pyrazole-fused analogues (**2.73l**, **2.75l**, and **2.78l**) were inactive against Aster-C. The observation of clear SAR validated one of the guiding principles outlined in designing the sterol-inspired compound collection; that synthesising analogues featuring different substitution patterns should serve to provide SAR at an early stage. A retrospective analysis of the screening results also suggests that for biased screening collections such as the sterol-inspired compound collection, the hit cut-off could be lowered to include more true positives in the primary screen.

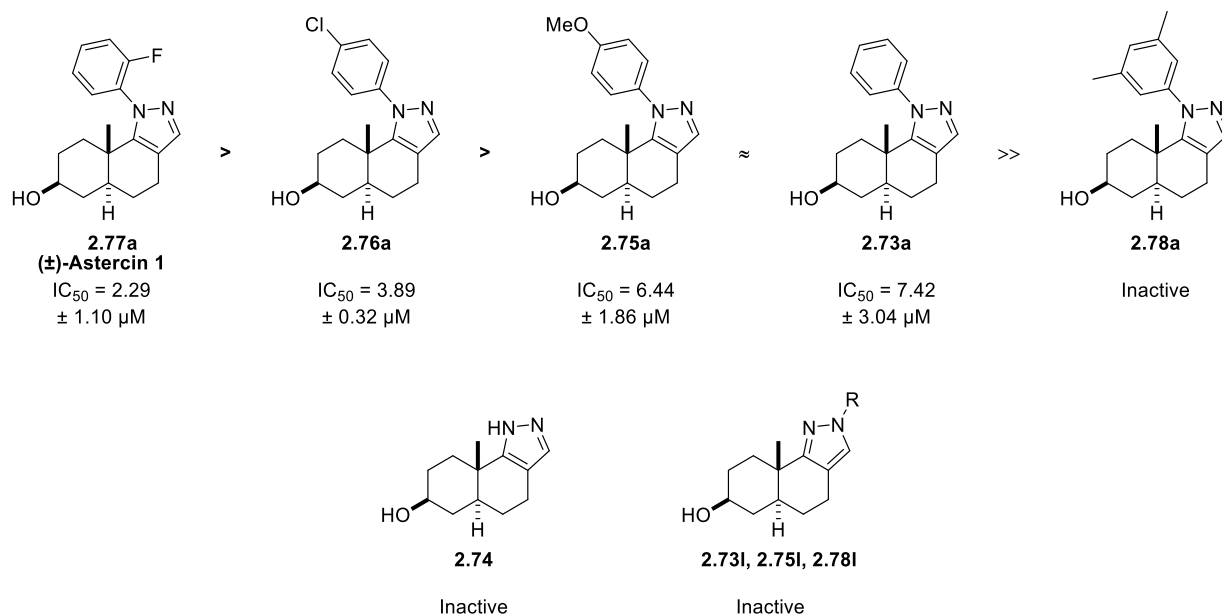


Figure 3.9 Structures and trend in Aster-C potency of the pyrazole-fused Aster-C inhibitors.

With validated hit compounds against both Aster-A and Aster-C, it was decided to prioritise the Astercin series for identification of the active enantiomer and for confirmation of their sterol-transfer inhibitory activity. This decision was influenced by the informative SAR obtained from FP screening of the Astercin series, as well as the lack of suitable Aster-C selective tool compounds. Whilst the oxysterol-derived AI-11 was recently reported as a selective inhibitor of Aster-C, its selectivity profile has not been sufficiently reported against Aster-A or Aster-B.¹¹⁰ Additionally, AI-11 was a comparatively poor inhibitor of Aster-C when tested alongside (±)-Astercin, with inhibition plateauing at ~60%, potentially arising due to poor compound solubility, aggregation, or sequence differences between human and murine Aster-C ASTER domain (Figure 3.10).

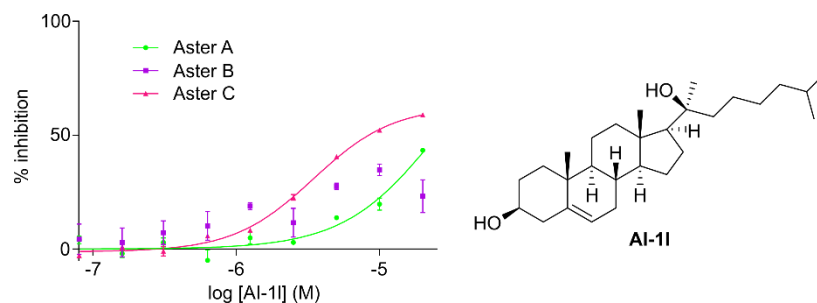


Figure 3.10 Dose response curves for AI-11 against Aster-A, -B, and -C ASTER domains. Data shown from one representative experiment of three independent replicates.

3.4 Identification of the active enantiomer of (±)-Astercin

3.4.1 Synthesis of (*S*)- and (*R*)-Wieland-Miescher Ketone

In order to access both enantiomers of (±)-Astercin-1 and identify the active enantiomer, it was necessary to modify the synthetic route to be enantioselective, rather than diastereoselective. To do so, the two enantiomers of the WMK, (*S*)-WMK ((*S*)-**2.02**) and (*R*)-WMK ((*R*)-**2.02**) were synthesised utilising two different organocatalysts. To access the (*S*)-WMK it was initially decided to synthesise the prolinamide catalyst **3.01** and to access the (*R*)-WMK the binaphthyl-prolinamide **3.02** was selected (Figure 3.11).^{121,150} The former catalyst was initially chosen owing to its structural simplicity and commonly available starting materials, and the latter for lower catalyst loadings and reaction scalability.

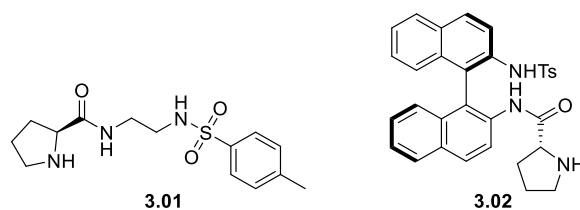
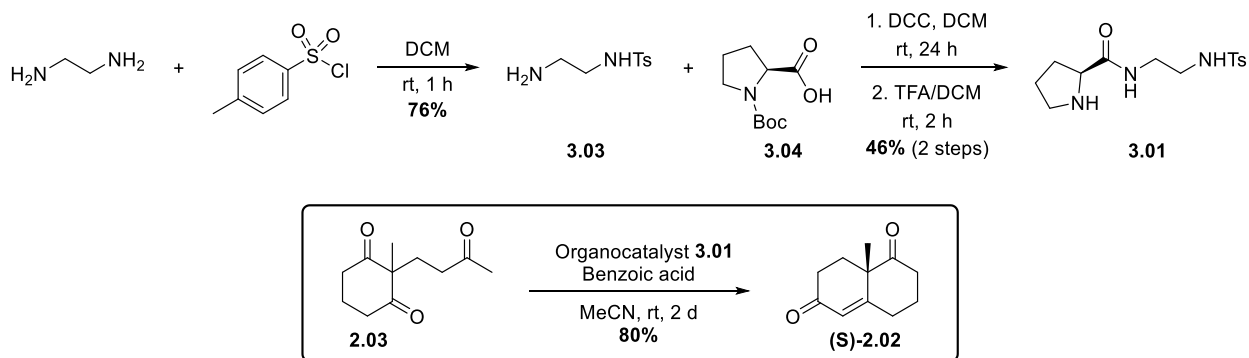


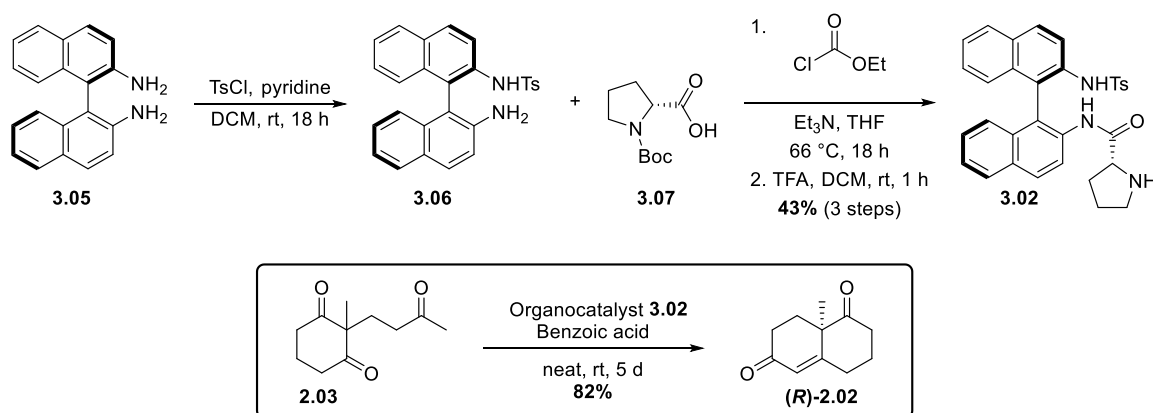
Figure 3.11 Structures of the prolinamide organocatalysts used to synthesise (*S*)-WMK and (*R*)-WMK.

Organocatalyst **3.01** was synthesised according to the procedure of Pedrosa *et al.*¹⁵⁰ Ethylenediamine was monotosylated by treatment with *p*-Toluenesulfonyl chloride (Tosyl chloride) in good yield. The resulting monotosylated amine **3.03** was coupled to (*tert*-butoxycarbonyl)-L-proline (Boc-L-proline) **3.04** in a *N,N*-Dicyclohexylcarbodiimide (DCC) mediated amide coupling, which following deprotection of the Boc group with TFA afforded the desired organocatalyst **3.01** in 46% yield over two steps. The organocatalytic WMK synthesis utilising organocatalyst **3.01** with a benzoic acid co-catalyst afforded the desired (*S*)-WMK in high yield over 2 days (Scheme 3.1).



Scheme 3.1 Synthesis of prolinamide organocatalyst **3.01** and (*S*)-WMK (**S**)-**2.02**

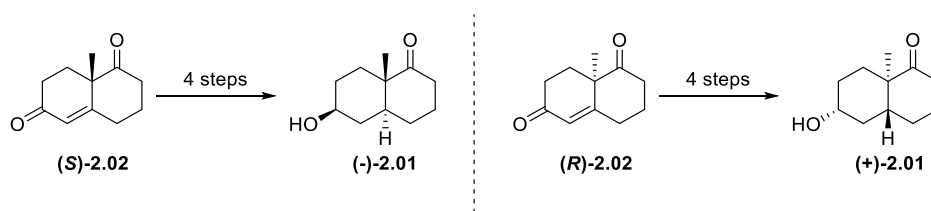
The BINAM-prolinamide organocatalyst **3.02** was synthesised according to the procedure of Vióñez et al.¹²² Enantiopure (*R*)-(+)-1,1'-Binaphthyl-2,2'-diamine **3.05** was tosylated using tosyl chloride and pyridine, and the crude mixture of bis- and mono-tosylated product **3.06** coupled to Boc-D-Proline **3.07**, via activation of the proline carboxylic acid with ethyl chloroformate. TFA deprotection of the Boc-protected amine afforded the organocatalyst **3.02** in 43% yield over three steps. In combination with a benzoic acid co-catalyst, organocatalyst **3.02** was used in a multi-gram scale synthesis of the (*R*)-WMK (**R**)-**2.02**, with the reaction proceeding in high yields and a low catalyst loading of 1% (Scheme 3.2).¹²¹



Scheme 3.2 Synthesis of binaphthyl-prolinamide organocatalyst **3.02** and (*R*)-WMK (*R*)-**2.02**.

3.4.2 Synthesis of (+)- and (-)-Astercin 1

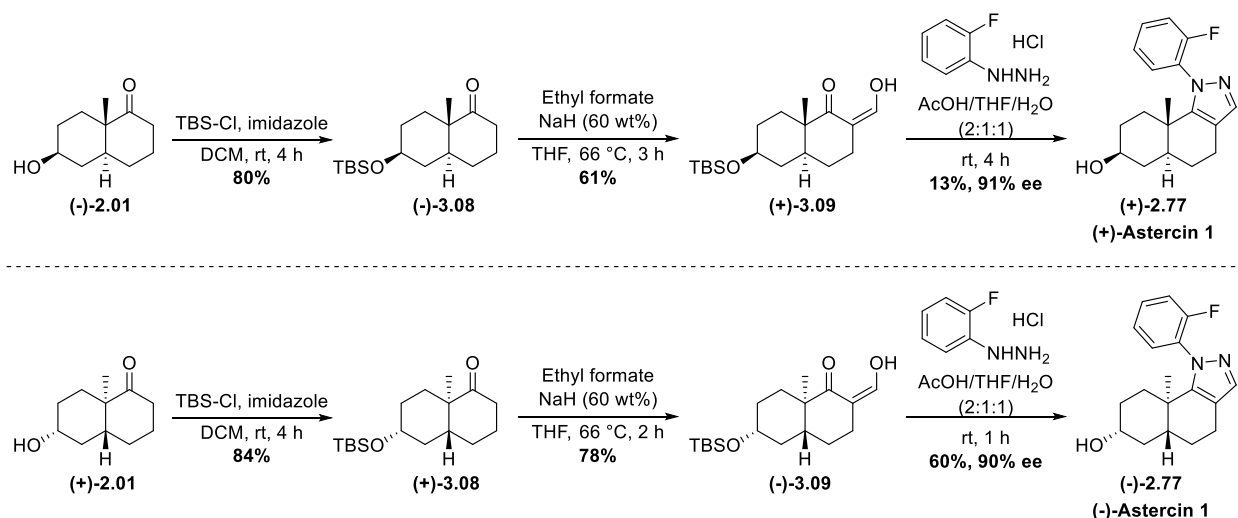
Each enantiomer of decalone **2.01** was synthesised in four steps from the corresponding enantioenriched WMK, according to the procedures used to synthesise (\pm)-**2.01**. From (*S*)-**2.02**, decalone (-)-**2.01** was synthesised and decalone (+)-**2.01** from the (*R*)-**2.02** (Scheme 3.3).



Scheme 3.3 Synthesis of (-)-**2.01** and (+)-**2.01** from (*S*)-WMK **2.02** and (*R*)-WMK **2.02**.

In synthesising (+)- and (-)-Astercin 1, synthesis of the pyrazole-fused analogues was subjected to further optimisation with future SAR studies in mind. To simplify the protection and deprotection steps, the MEM-ether was changed to a silyl-ether, and alternative conditions to improve regioselectivity identified to simplify purification.

The C3-hydroxyl was cleanly protected as the *tert*-butyldimethylsilyl (TBS) ether by reaction with TBS-Cl and imidazole, affording TBS-ketones (-)-**3.08** and (+)-**3.08** as white solids – in contrast to MEM-ketone **2.12** which was isolated as an oil. TBS-protected hydroxymethylenes (+)-**3.09** and (-)-**3.09** were synthesised in a procedure analogous to MEM-protected hydroxymethylene **2.13**. In conditions inspired by An et al, TBS-protected hydroxymethylenes (+)-**3.09** and (-)-**3.09** were reacted with 2-fluorophenyl hydrazine in a mixed solvent system of acetic acid/THF/water, affording the desired angular-fused pyrazoles in high regioselectivity.¹⁵¹ The acidic conditions were also sufficient to fully deprotect the TBS-ether, removing one synthetic step compared to the original synthesis. The individual enantiomers (+)-Astercin 1 (+)-**2.77** and (-)-Astercin 1 (-)-**2.77** were successfully isolated after purification by preparative-HPLC and flash chromatography respectively, with each isolated in 90% enantiomeric excess (ee) (Scheme 3.4).



Scheme 3.4 Synthesis of (+)-Astercin 1 (+)-2.77 and (-)-Astercin 1 (-)-2.77 from decalones (-)-2.01 and (+)-2.01.

3.4.3 Screening of Astercin 1 enantiomers by fluorescence polarisation

The two enantiomers of (\pm)-Astercin 1 were screened in dose response against the three Aster proteins, revealing that (-)-Astercin 1 was the more active enantiomer of the racemate (Figure 3.12) (Table 3.1). (-)-Astercin 1 inhibits Aster-C with a low micromolar potency, with 30-fold selectivity over Aster-B and greater than 50-fold selectivity over Aster-A. (+)-Astercin 1 was over 10-fold less potent against Aster-C, however it was over 4-fold more potent against Aster-A. This results suggests that the Asters have differential binding preferences dependent upon ligand stereochemistry, with Aster-A preferentially binding ligands with “natural” stereochemistry (i.e. identical to cholesterol) whereas Aster-B and -C preferentially bind ligands with “unnatural” stereochemistry (i.e. identical to *ent*-cholesterol). This finding not only offers insight into how sterol-like ligands bind to the Asters, but could also be used to gain selectivity within different classes of sterol-inspired inhibitors against different families of STPs. Additionally, this finding validates synthesising focussed compound collections such as the sterol-inspired collection as racemates, as by synthesising the collection with “natural” stereochemistry under the assumption it would be preferred, would have prevented the identification of the Astercin series.

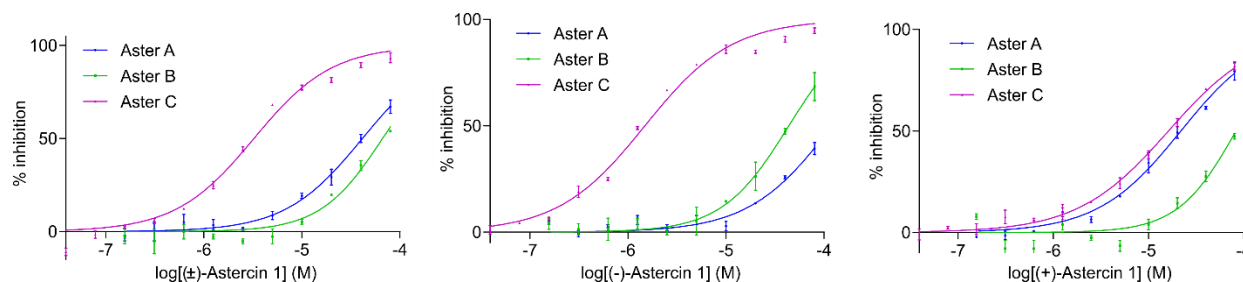


Figure 3.12 Dose response curves for (\pm)-Astercin 1, (-)-Astercin 1, and (+)-Astercin 1 against ASTER domains of Asters-A, -B, and -C. Data shown from one representative experiment of three independent replicates. Figure reproduced with permission from reference.¹¹⁴ Copyright (2021) John Wiley and Sons.

Table 3.1 IC₅₀ values determined from FP experiments of (±)-Astercin 1, (-)-Astercin 1, and (+)-Astercin 1 against ASTER domains of Asters-A, -B, and -C

Compound	Aster-A IC ₅₀ (μM) ^[a]	Aster-B IC ₅₀ (μM) ^[a]	Aster-C IC ₅₀ (μM) ^[a]
(±)-Astercin 1	42.3 ± 1.14	68.0 ± 4.31	2.29 ± 1.10
(-)-Astercin 1	> 80	46.8 ± 5.78	1.51 ± 0.56
(+)-Astercin 1	23.0 ± 1.16	78.0 ± 4.26	16.9 ± 5.41

[a] IC₅₀ values are reported as the mean ± s.d. of three individual experiments run in triplicate.

3.5 Inhibition of Aster-mediated sterol transfer by (-)-Astercin

3.5.1 Liposomal FRET assays

To validate the ability of (-)-Astercin 1 to inhibit Aster-C mediated cholesterol transfer, a liposomal cholesterol transfer assay based upon FRET was adapted and optimised to a microplate-based format.^{98,113} FRET is a physical phenomenon in which an excited donor fluorophore can transfer energy to an acceptor fluorophore by non-radiative mechanisms, resulting in fluorescence of the acceptor fluorophore at a wavelength separated from the donor fluorophore.¹⁵² FRET efficiency is inversely dependent upon the sixth power of the distance between the donor and acceptor fluorophore, making the technique highly sensitive to the distance between the two. As such, FRET is routinely used to study proximity-based events in biological screening.¹⁵³

In this context, the assay uses liposomes as a model plasma membrane, and monitors the disruption of a FRET pair of a fluorescent cholesterol derivative 23-BODIPY-Cholesterol (BODIPY-Chol) and the fluorescent lipid rhodamine 1,2-dihexadecanoyl-sn-glycero-3-phosphoethanolamine (N-Rh-DHPE) (Figure 3.13). Aster-mediated transfer of BODIPY-Chol from donor liposomes containing the FRET pair to acceptor liposomes prepared with no fluorescent lipids is monitored by observance of a decrease in FRET-emission over time. Treatment with an Aster-inhibitor would therefore inhibit the transfer of BODIPY-Chol from donor to acceptor liposomes, and the decrease in FRET signal over time would be expected to be lower than vehicle treatment.

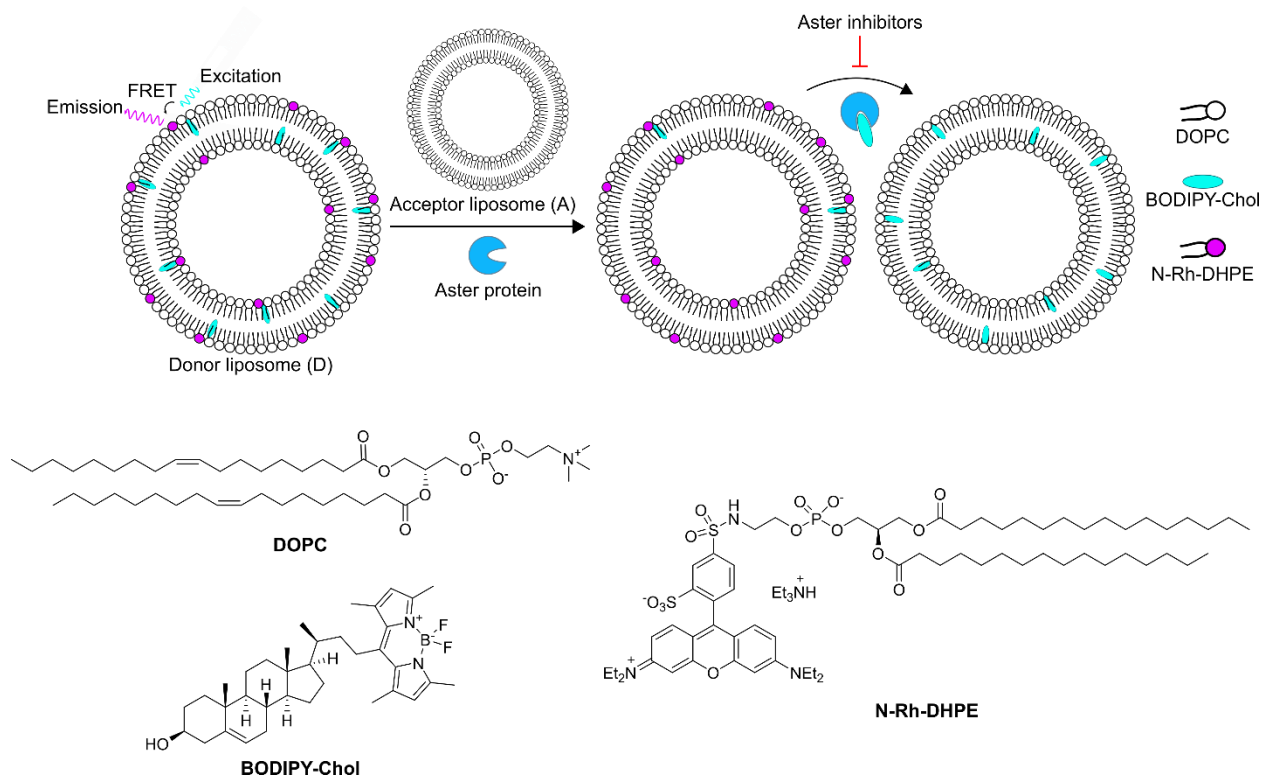


Figure 3.13 Schematic for the liposomal FRET sterol-transfer assay and chemical structures of liposome components. Aster proteins transfer BODIPY-Chol from donor (D) to acceptor (A) liposomes, disrupting the FRET pair with a corresponding decrease in FRET-emission intensity. Inhibition of Aster-mediated transfer of BODIPY-Chol from donor to acceptor liposomes gives a slower decrease in FRET-emission intensity over time. Figure reproduced and modified with permission from reference.¹¹⁴ Copyright (2021) John Wiley and Sons.

3.5.2 Liposomal FRET assay optimisation

Following the protocol of Laraia *et al*, liposomes were prepared from the phospholipid 1,2-dioleoyl-sn-glycero-3-phosphocholine (DOPC).⁹⁸ Lipid films were prepared by mixing the three lipids in chloroform in a 99:0.5:0.5 ratio of DOPC:BODIPY-Chol:N-Rh-DHPE for donor (D) liposomes, 100:0:0 for acceptor (A) liposomes, 99.5:0.5:0 for donor-cholesterol (D-Chol) liposomes, and 99.5:0:0.5 for acceptor-DHPE (A-DHPE) liposomes, and subsequently evaporating the solvent under a stream of nitrogen. Rehydration of the lipid films in assay buffer was achieved after extensive vortexing and sonication. Rehydrated lipid films were subjected to five freeze-thaw cycles, affording multilamellar vesicles. Extrusion 21 times through a 100 nM polycarbonate membrane at 40 °C afforded homogenous unilamellar liposomes that were stored at 4 °C and used on the same day of preparation.

The sterol-transfer assay was initially optimised using Aster-C. Donor and acceptor liposomes were mixed in a 1:1 ratio (final concentration of 16 μ M of each liposome) in the presence of Aster-C (1 μ M) and the fluorescence intensity measured at 10 second intervals over a period of 10 minutes, exciting at 488 nm and monitoring emission at 590 nm. Two systems were initially tested, the first in which BODIPY-Chol would be transported away from N-Rh-DHPE into acceptor liposomes (D \rightarrow A) resulting in a decrease in fluorescence intensity over time, and the second in which BODIPY-Chol would be transported into

liposomes containing N-Rh-DHPE (D-Chol \rightarrow A-DHPE) resulting in an increase in fluorescence intensity over time.

In both liposome configurations, the fluorescence signals for the assay controls were as expected. In the first configuration, acceptor liposomes (A) had fluorescence comparable to the background, whereas donor liposomes (D) and the combination of donor and acceptor liposomes (D + A) had high fluorescence values. In the second configuration, both D-Chol and A-DHPE liposomes were fluorescent, with the D-Chol + A-DHPE combination having an additive fluorescence value (Figure 3.14). Addition of Aster-C to the respective liposome mixtures gave rise to the expected decrease and increase in fluorescence intensity respectively. For further optimisation, it was decided to use the first configuration of liposomes owing to a greater assay window.

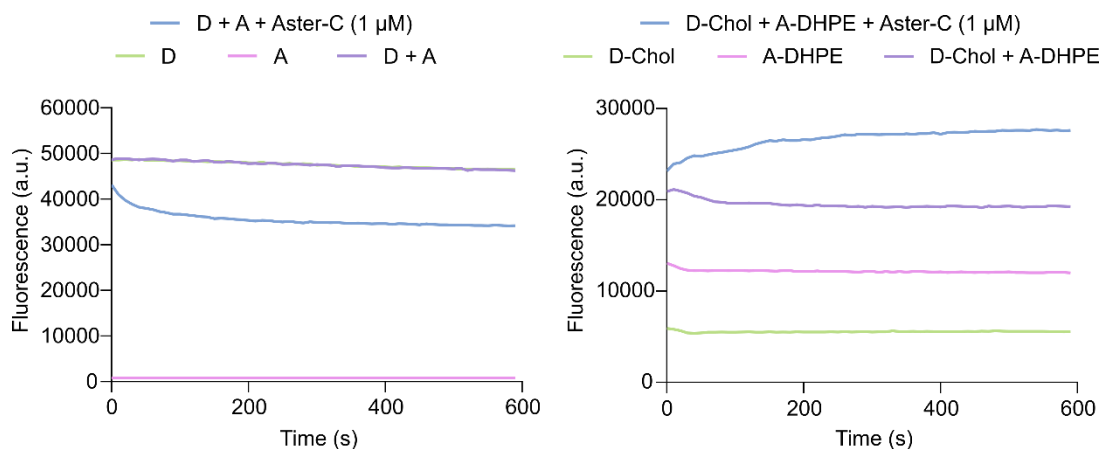


Figure 3.14 Fluorescence intensity over time for the liposomal FRET assay run in configuration 1 (D \rightarrow A transport) and configuration 2 (D-Chol \rightarrow A-DHPE transport).

3.5.3 Modulation of Aster-mediated cholesterol transfer by Astercin 1

Screening (\pm)-Astercin-1 against Asters-A and B demonstrated no significant inhibition of Aster-A or -B mediated cholesterol transfer at 10 μ M, with the normalised fluorescence values (I/I_0) overlapping with the vehicle control. Inhibition of Aster-A mediated cholesterol transfer was confirmed through use of Autogramin-2 as a positive control. For Aster-B, U18666A was selected as a positive control, however it was observed that normalised fluorescence values were greater than the donor + acceptor liposome control. This could have arose from disruption of liposome structure via insertion of the aminosteroid into the phospholipid membrane (Figure 3.15).

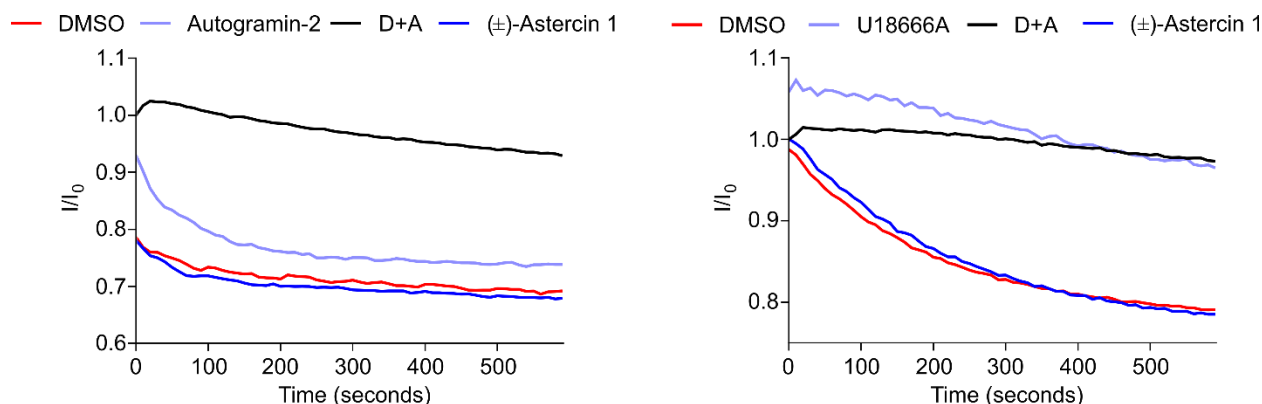


Figure 3.15 Modulation of Aster-A (left) and Aster-B (right) mediated cholesterol transfer between donor and acceptor liposomes by (±)-Astercin 1 and tool compounds. Protein concentration = 1 μ M. Data shown from one representative experiment of three independent replicates. Figure reproduced and modified with permission from reference.¹¹⁴ Copyright (2021) John Wiley and Sons.

Both enantiomers and the racemate of Astercin-1 were screened at 10 μ M against Aster-C in the sterol transfer assay. The trend in compound potency determined by FP was reflected in the ability of the Astercin 1 enantiomers to inhibit Aster-C mediated cholesterol transfer. Cholesterol transfer was significantly inhibited by (-)-Astercin-1 and moderately by (±)-Astercin-1 compared to the vehicle control and (+)-Astercin-1 (Figure 3.16). AI-11 was included as a positive control, however no inhibition of Aster-C mediated cholesterol transfer was observed, supporting its poor potency as determined by FP. The efficiency of cholesterol transfer by the individual ASTER domains was consistent with reported literature, with Aster-A having the most efficient transfer (vehicle I/I_0 starting at approx. 0.8) compared to Aster-B and Aster-C which transfer cholesterol with similar efficiencies (vehicle I/I_0 starting between 0.9 – 1.0).⁹⁵

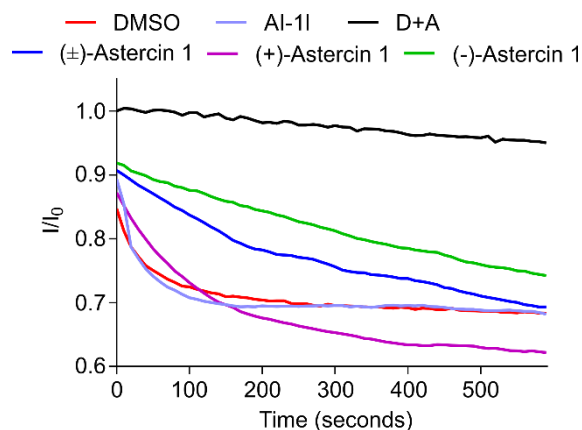


Figure 3.16 Modulation of Aster-C mediated cholesterol transfer between donor and acceptor liposomes by (±)-Astercin, (-)-Astercin 1, (+)-Astercin 1 and AI-11. Protein concentration = 1 μ M. Data shown from one representative experiment of three independent replicates. Figure reproduced and modified with permission from reference.¹¹⁴ Copyright (2021) John Wiley and Sons.

Screening of the sterol-inspired compound collection successfully validated the original hypothesis that fusion of a sterol-inspired fragment to a series of heterocyclic fragments should afford a collection enriched in hit compounds against STPs. From the synthesised collection of 65 sterol-inspired compounds, (-)-Astercin-1, the most potent and selective inhibitor of Aster-C was identified demonstrating the power of this approach to identify new STP inhibitors. Additionally, two novel chemotypes of Aster-A inhibitors were identified, providing complementary compounds that could be used alongside Autogramin-2 in investigating and validating Aster-A related biology. Before assessing whether (-)-Astercin-1 could be a suitable for use as a tool compound in cellular models, it was decided to further optimise the compound for potency and selectivity.

3.6 Optimisation of (-)-Astercin 1

Optimisation of (-)-Astercin-1 commenced by an analysis of its structure, revealing several sites that could be modified as part of an SAR study (Figure 3.17). Substitution on the pyrazole-phenyl ring could be readily changed, complementing the preliminary SAR obtained from the initial screening. The pyrazole ring could be modified using late-stage functionalisation or a handle for coupling chemistry installed at an earlier stage. Lastly, core modifications to the AB ring system could be made to explore the effects of additional oxidations, reductions, or hydroxyl functionalisation on compound potency.

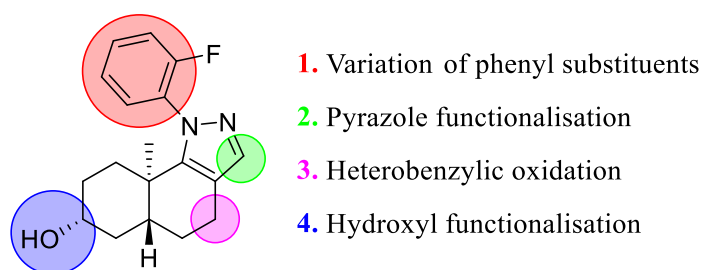
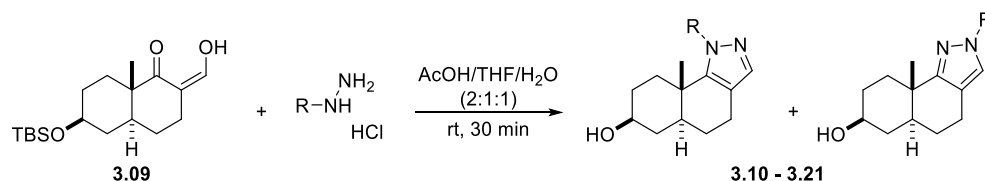


Figure 3.17 Key sites of modification for the SAR study of (-)-Astercin-1

3.6.1 Variation of phenyl substitution

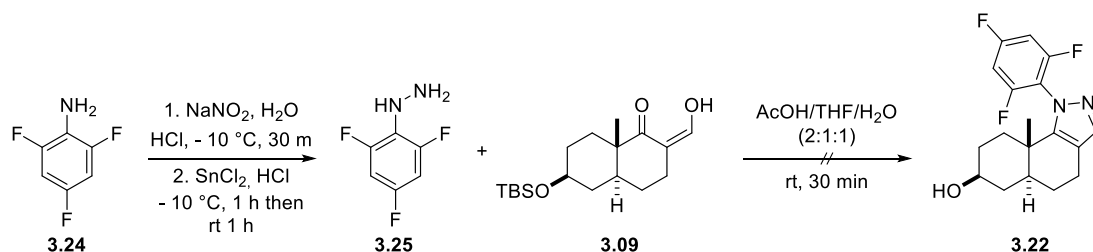
The design of Astercin-1 analogues with varied phenyl substitution was informed by the preliminary SAR obtained from the primary screening and subsequent validation of the Astercin series. A range of phenylhydrazines were chosen for reaction with hydroxymethylene **3.09** in order to address several key questions, namely what is the optimum size for the substituent at the 2-position, is the combination of 2- and 4-substitution additive in compound potency, and lastly whether 3- or 2,5- substitution would be tolerated. Pyrazole analogues were synthesised according to the optimised procedure, and all analogues were generally isolated in acceptable yields and purity (Table 3.2).

Table 3.2 Synthesis of pyrazole-fused analogues with varied phenyl-R substitution from HM **3.09**

Entry	Compound	R	Yield (%)	Comments
1	3.10	3-Fluorophenyl	56	-
2	3.11	2-fluoro-4-chlorophenyl	52	-
3	3.12	2,4-difluorophenyl	47	-
4	3.13	2-fluoro-5-chlorophenyl	29	-
5	3.14	2-methoxyphenyl	21	-
6	3.15	2,6-difluorophenyl	17	-
7	3.16	2,5-difluorophenyl	57	-
8	3.17	2-fluoro-6-bromophenyl	22	Atropisomers showing minor separation by LCMS
9	3.18	2-chlorophenyl	58	
10	3.19	cyclohexyl	51	-
11	3.20a	4- <i>tert</i> -butylphenyl	13	-
12	3.20l		22	-
13	3.21a	4-fluorophenyl	22	-
14	3.21l		16	-
15	3.22	2,4,6-trifluorophenyl	< 1	Product + hydrazone isolated, free base of hydrazine used
16	3.23	2,6-dichlorophenyl	-	

Similar to (-)-Astercin-1, all pyrazoles bearing 2-substitution on the phenyl ring were isolated as mixtures of conformational isomers. Analogues with larger substituents in the 2-position (entries 5, 8, 9) showed greater spacing of the ^1H NMR signals arising from the axial methyl group, suggesting increasing energy barriers for interconversion between the conformational isomers, and possibly the formation of separable atropisomers. However, only the 2-fluoro-6-bromophenyl **3.17** (entry 8) pyrazole began to show separation by either LCMS or TLC. Symmetrisation of the phenyl ring in the 2,6-difluoro substituted analogue **3.15** (entry 6) allowed for isolation of a single conformational isomer. Additionally, two analogues provided isolable quantities of the linear 4-substituted phenyl pyrazoles **3.20l** and **3.21l** (entries 12 and 14).

The synthesis of the 2,4,6-trifluoro substituted pyrazole **3.22** was attempted (entry 15) starting from 2,4,6-trifluoroaniline **3.24** (Scheme 3.5). Diazotization of 2,4,6-trifluoroaniline **3.24** with sodium nitrite in aqueous hydrochloric acid and reduction of the in-situ generated diazonium species with tin (II) chloride afforded the desired phenylhydrazine **3.25**. Upon reaction with hydroxymethylene **3.09**, only minor amounts of pyrazole **3.22** could be isolated alongside the uncyclised hydrazone intermediate. Likewise, reaction of hydroxymethylene **3.09** with 2,6-dichlorophenyl hydrazine afforded a mixture of diastereoisomeric hydrazones, likely arising due to the inability of the electron-deficient hydrazone to undergo cyclisation under the mild reaction conditions.



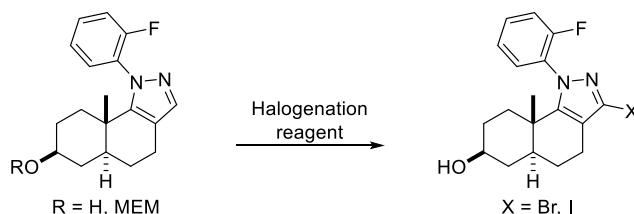
Scheme 3.5 Synthesis of 2,4,6-trifluorophenyl hydrazine **3.25** from 2,4,6-trifluoroaniline **3.24**, and the unsuccessful synthesis of pyrazole analogue **3.22**

3.6.2 Modifications to the pyrazole ring and sterol A/B ring

Crystal structures of 25-HC derived AI-11 bound to murine Aster-C show that the C3-OH group is buried deep in the hydrophobic cholesterol binding pocket of the protein.¹¹⁰ Under the assumption that (-)-Astercin-1 could bind in a similar manner to other steroidal ligands, it was thought that substitution on the pyrazole ring could favourably contribute to compound binding, occupying space that is typically occupied by sterol C/D-rings and the alkyl side chain. It was anticipated that analogues bearing substituents on the pyrazole ring could be accessed either via a halogenated intermediate with subsequent metal-catalysed cross couplings, or by direct functionalisation with radical chemistry.

Initial efforts focussed on identifying conditions for halogenating the pyrazole ring (Table 3.3). Following conditions reported in a patent working with structurally related WMK-derived pyrazoles, (\pm)-Astercin was reacted with bromine in the presence of sodium carbonate (entry 1).¹³⁷ Unfortunately, despite the literature precedence, only decomposition of the starting material was observed. Halogenation using either NBS or *N*-iodosuccinimide (NIS) was also attempted (entries 2 - 5). Use of NBS in DMF at either room temperature or $60\text{ }^\circ\text{C}$ gave no conversion. Changing to NIS resulted in minor iodination, however oxidation of the C3-OH to the ketone was observed, likely occurring through the formation of an intermediate hypoiodite species.¹⁵⁴ Iodination was attempted on the MEM-protected Astercin **3.26**, as it was expected that NIS would deprotect a TBS-protected Astercin, however deprotection was also observed upon attempted iodination of MEM-astercin **3.26** (entry 6).¹⁵⁵ Use of alternative brominating agents including 1,3-Dibromo-5,5-dimethylhydantoin (DBDMH), 5,5-dibromobarbituric acid, or iodine/silver acetate gave no conversion to the desired product (entries 7 - 9).¹⁵⁶

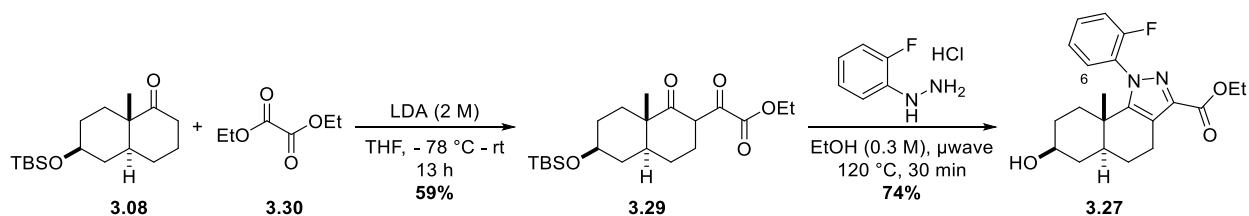
Table 3.3 Conditions attempted to synthesise halogenated (\pm)-Astercin from (\pm)-Astercin and MEM-Astercin



Entry	R	Reagents	Conditions	Observations
1	OH	Br ₂ /Na ₂ CO ₃	DCM, - 10 °C	Decomposition
2	OH	NBS	DMF, rt	No conversion
3	OH	NBS	DMF, 60 °C	Oxidation of OH
4	OH	NIS	DMF, rt	Minor iodination
5	OH	NIS	DMF, 60 °C	Minor iodination and oxidation of OH
6	OMEM	NIS	DMF, rt – 60 °C	Deprotection of MEM ether
7	OMEM	DBDMH 	DCM, rt	No conversion
8	OH	Dibromobarbituric acid	DCM, rt	No conversion
9	OH	I ₂ /AgOAc	MeCN, rt	No conversion

The lack of conversion of (\pm)-Astercin **1** to the halogenated derivative was attributed to the inherent reactivity of the pyrazole system, as the free position of the pyrazole ring is too electron deficient and thus unreactive towards electrophilic reagents. As expected, attempts to functionalise this position of the pyrazole ring with radical methods, including both classical and borono-minisci reactions proved ineffective.^{157,158} It was therefore decided to target an alternative intermediate for functionalisation to overcome the poor reactivity of the pyrazole ring. One plausible intermediate was the pyrazole ester **3.27**, which would offer an alternative point of functionalisation for analogue synthesis and further SAR by providing access to the corresponding carboxylic acid **3.28**.

In order to synthesise the pyrazole ester **3.27**, the intermediate diketoester **3.29** was synthesised (Scheme 3.6). The TBS-protected ketone **3.08** was deprotonated with LDA to generate the lithium enolate, which was reacted with diethyl oxalate **3.30**, yielding the desired diketoester **3.29** in acceptable yields after purification. Pyrazole ester **3.27** was successfully synthesised in a microwave assisted Knorr pyrazole synthesis, reacting the intermediate diketoester **3.29** with 2-fluorophenylhydrazine hydrochloride, proceeding alongside deprotection of the TBS-ether.



Scheme 3.6 Synthesis of intermediate diketoester **3.29** and Astercin ester **3.27** from TBS-ketone **3.08**

The structure of the isolated regioisomer was assigned by analysis of 1D and 2D NMR data. The structure of the major conformation was supported by existence of a strong NOE correlation between the protons of the methyl group and the aromatic proton in the 6-position of the phenyl ring (Figure 3.18, major conformation, see appendix for NOESY spectra). The methyl signal arising from the minor conformation was observed to couple to the aromatic fluorine substituent ($^7J(\text{F},\text{H}) = 1.3 \text{ Hz}$, $^6J(\text{F},\text{C}) = 3.9 \text{ Hz}$) by a through-space coupling (Figure 3.18, minor conformation).¹⁵⁹

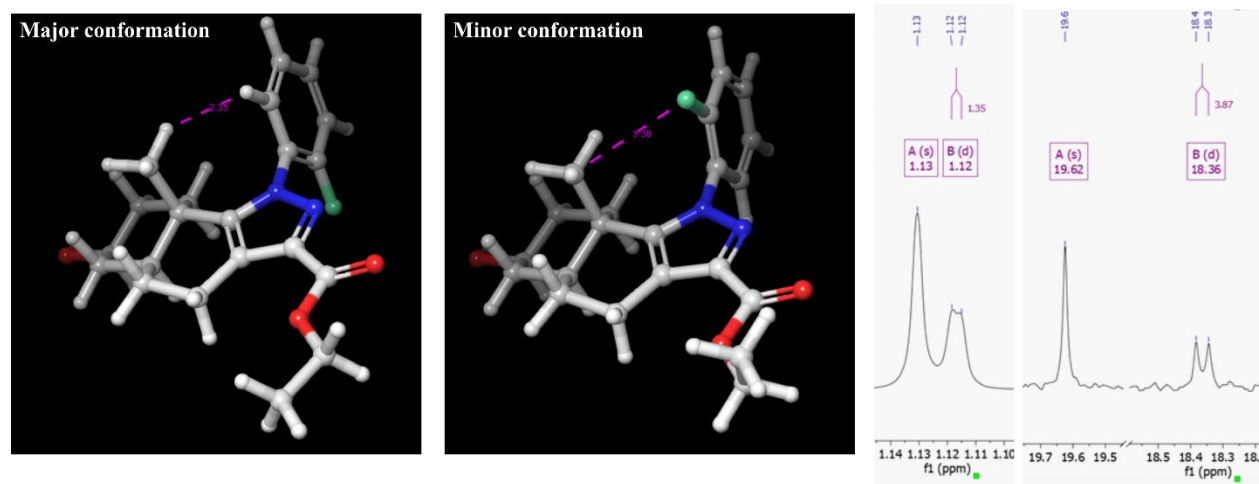
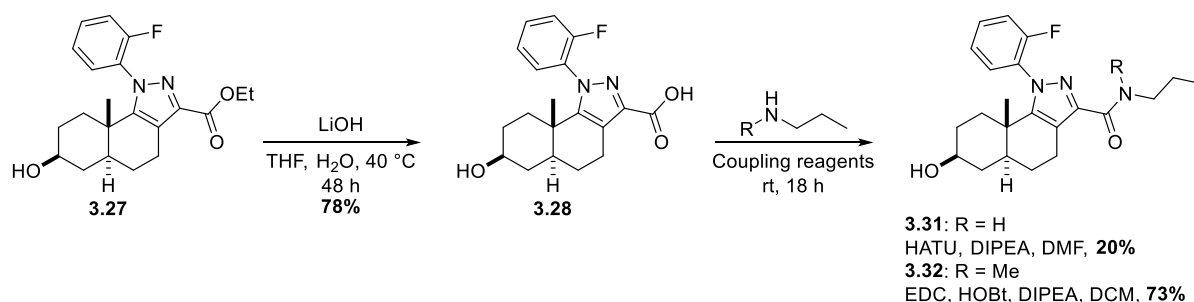


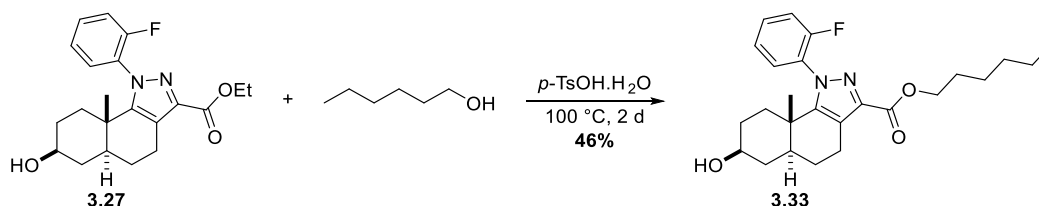
Figure 3.18 Structures of the major and minor conformations of astercin ester **3.27**, with distances (in Ångström) between coupled atoms of key correlations drawn in purple. ^1H and ^{13}C NMR of the axial methyl signal showing through-space coupling only for the minor conformation. Structures and conformations generated in Maestro.

The pyrazole carboxylic acid **3.28** was synthesised in a base-mediated hydrolysis of astercin ester **3.27**, utilising lithium hydroxide in a THF/ H_2O solvent system and yielding the desired acid **3.28** in good yield after workup (Scheme 3.7). From this carboxylic acid intermediate, two amide analogues were synthesised. Coupling of carboxylic acid **3.28** with propylamine using the coupling agent 1-[Bis(dimethylamino)methylene]-1H-1,2,3-triazolo[4,5-b]pyridinium-3-oxide hexafluorophosphate (HATU) afforded propylamide analogue **3.31** in low yield after purification by preparative HPLC (Scheme x). Coupling of *N*-methylpropylamine using the coupling agent EDC/HOBt yielded the *N*-methylpropylamide analogue **3.32** in good yield after purification (Scheme 3.7).



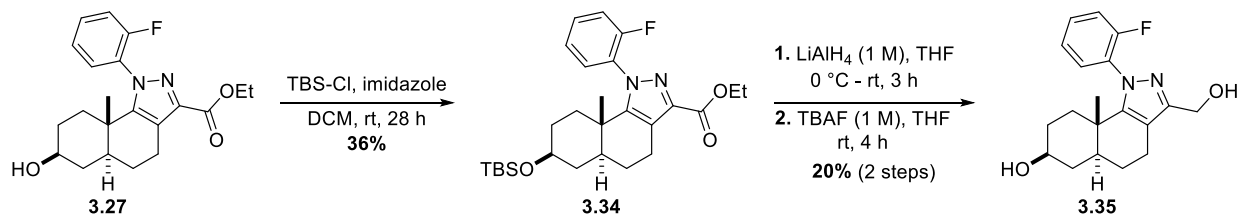
Scheme 3.7 Synthesis of carboxylic acid **3.28** and amide analogues **3.31** and **3.32**

A number of different analogues were prepared directly from Astercin ester **3.27**. The Astercin ester **3.27** was subjected to a transesterification with 1-hexanol, anticipating that a long alkyl chain projected from the pyrazole ring could extend into an unoccupied region of the ASTER domain binding pocket of Aster-C. Heating ester **3.27** at 100 °C in an excess of 1-hexanol with *p*-TsOH.H₂O yielded the hexyl-ester **3.33** in moderate yields after two days (Scheme 3.8).



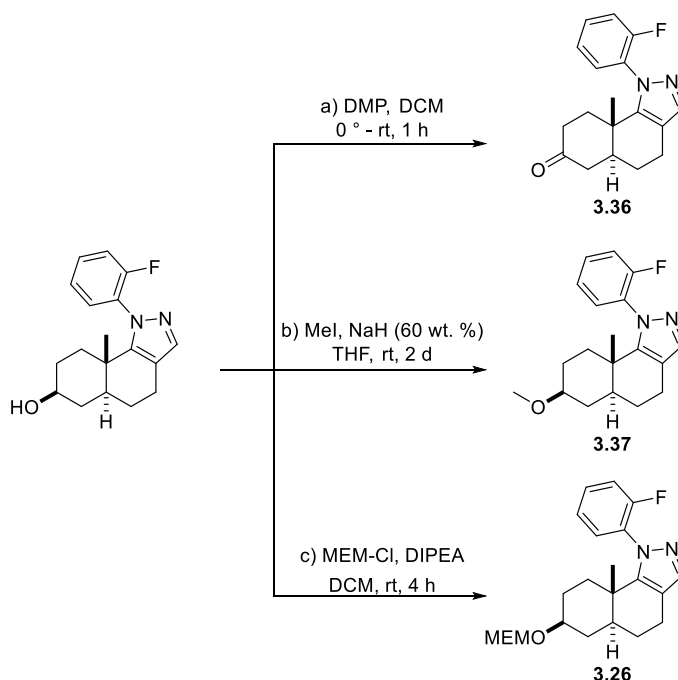
Scheme 3.8 Synthesis of hexyl-ester **3.33** by an acid-promoted transesterification of astercin ester **3.27**

To offer an additional point of functionalisation for the synthesis of Astercin analogues, the ester was reduced directly to the corresponding primary alcohol (Scheme 3.9). Before reducing the ester, the A-ring C3-OH was protected as the TBS-ether to allow for chemoselective alkylation of the primary alcohol if required. The C3-OH was protected using standard conditions, yielding TBS-protected astercin ester **3.34** in moderate yields. The ester was reduced directly to the primary alcohol using lithium aluminium hydride and the TBS-ether deprotected using TBAF, affording the desired astercin analogue **3.35** bearing a primary alcohol on the pyrazole-ring.



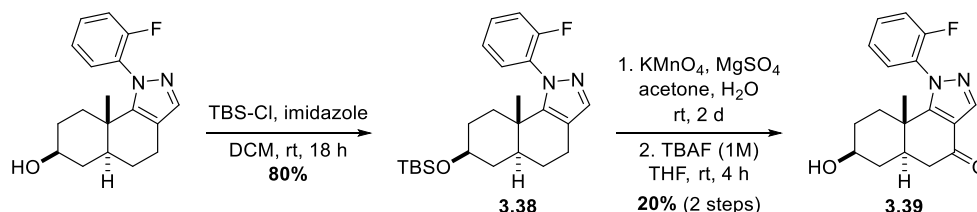
Scheme 3.9 Synthesis of TBS-protected astercin ester **3.34**, reduction of the ester to primary alcohol, and TBS-deprotection to primary alcohol **3.35**.

The C3-OH of Astercin was oxidised to the C3-ketone analogue **3.36** in high yield using Dess-Martin periodinane (DMP) (Scheme 3.10). Methylation of the C3-OH was achieved using methyl iodide and sodium hydride, yielding the desired methoxy-astercin analogue **3.37** (Scheme 3.10). During the attempted halogenation of the astercin pyrazole ring, MEM-protected astercin **3.26** was prepared employing standard MEM-protection conditions (Scheme 3.10).



Scheme 3.10 Synthesis of C3-OH modified analogues from Astercin-1 a) DMP oxidation of C3-OH to ketone **3.36** b) Methylation of C3-OH to yield C3-methoxy analogue **3.37** c) MEM-protection of C3-OH to yield MEM-astercin-1 **3.26**.

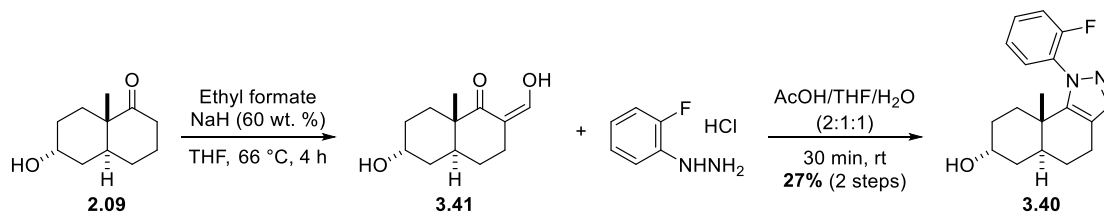
It was decided to protect the C3-OH of Astercin 1 as the TBS-ether before attempting a heterobenzylic oxidation of the Astercin B-ring, following similar rationale to the synthesis of TBS-protected astercin ester **3.34**. Employing the standard conditions of TBS-protection, TBS-protected astercin **3.38** was isolated in high yields (Scheme 3.11). The heterobenzylic oxidation was achieved using potassium permanganate in a mixed solvent system of acetone/H₂O, which after TBAF deprotection of the TBS-ether yielded the B-ring ketone analogue **3.39** in a two-step sequence (Scheme 3.11).



Scheme 3.11 Synthesis of B-ring ketone analogue **3.39** via TBS-protected astercin **3.38**

The final analogue to be targeted was the astercin diastereoisomer **3.40**, in which the C3-OH occupies the axial position rather than the equatorial position. Initial attempts to synthesise diastereoisomer **3.40** via standard methods were unsuccessful. These attempts were met with two main difficulties, firstly the TBS-protection of the axial alcohol proved challenging and secondly deprotection of the TBS-ether was not achieved during the pyrazole synthesis. In order to overcome these challenges, it was decided to synthesise the diastereoisomer **3.40** directly from ketone **2.09** in a telescoped procedure (Scheme 3.12). Reaction of ketone **2.09** with ethyl formate and sodium hydride in THF afforded the hydroxymethylene **3.41**, which after a solvent swap to the AcOH/THF/H₂O solvent system for the pyrazole synthesis was reacted

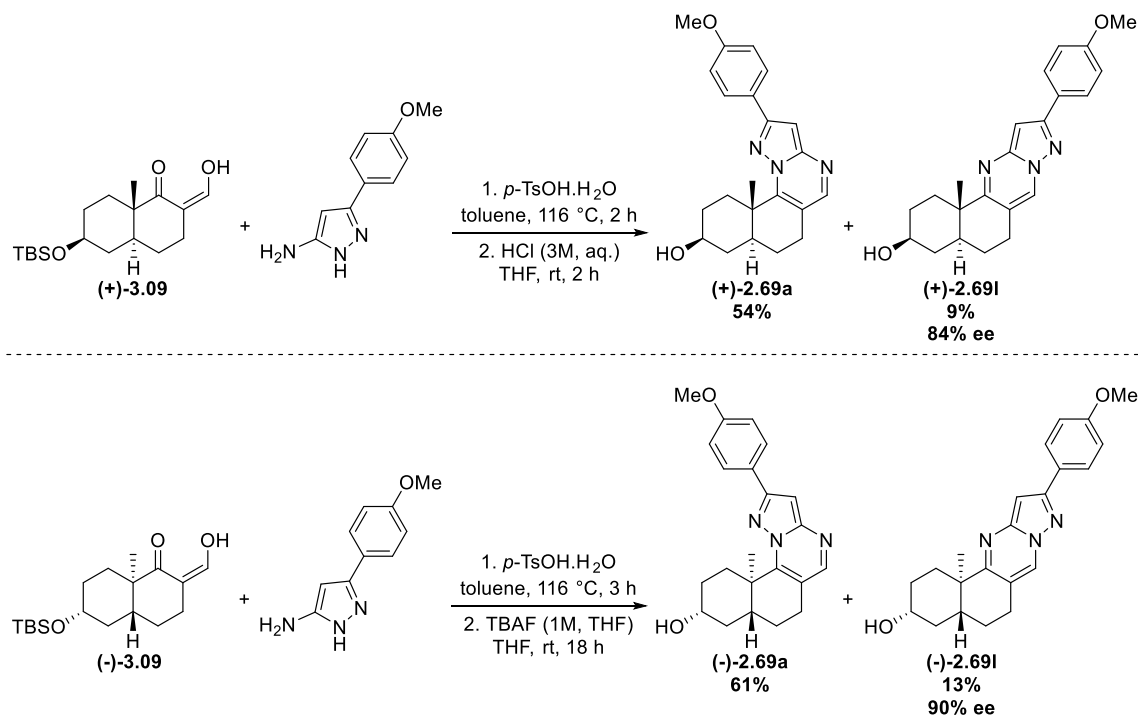
immediately with 2-fluorophenylhydrazine, yielding the desired diastereoisomer **3.40** in 27% yield over 2 steps.



Scheme 3.12. Telescoped synthesis of astercin diastereoisomer **3.40** from the ketone diastereoisomer **2.09**

3.6.3 Synthesis of pyrazolopyrimidine Aster-A inhibitor enantiomers

Alongside the optimisation of (-)-Astercin 1, the two enantiomers of the pyrazolopyrimidine Aster-A inhibitor (\pm)-**2.69** were synthesised by another PhD student in the Laraia group (Scheme 3.13). The pyrazolopyrimidines were synthesised in a modified protocol from the TBS-protected hydroxymethylenes (+)-**3.09** and (-)-**3.09** instead of the unprotected hydroxymethylene **2.11**. Reaction with the appropriate aminopyrazole afforded regioisomeric mixtures of TBS-protected pyrazolopyrimidines. Deprotection of the TBS group with either aqueous hydrochloric acid in THF ((+)-**2.69a** and (+)-**2.69l**) or tetra-*n*-butylammonium fluoride (TBAF) in THF ((-)-**2.69a** and (-)-**2.69l**) and separation of regioisomers by flash chromatography afforded the desired “linear” regioisomers as minor products and the “angular” regioisomers as the major products and in acceptable enantiomeric excess.



Scheme 3.13 Synthesis of pyrazolopyrimidine Aster-A inhibitor enantiomers (+)-**2.69l** and (-)-**2.69l**.

3.7 Biochemical analysis of (±)-Astercin-1 SAR compounds

With the collection of 23 (±)-Astercin-1 analogues synthesised, all analogues were screened against Aster-C in 12-point 1:2 dose response, starting from a top concentration of 80 μ M and a protein concentration of 0.5 μ M. Compounds seen to inhibit 22-NBD-Chol binding comparably with (-)-Astercin 1 were subsequently tested in dose response against both Aster-A and Aster-B (Table 3.4). As newer batches of purified proteins were utilised in these assays, (-)-Astercin-1 was also retested in dose response. As expected, (-)-Astercin-1 was found to bind both Aster-A and Aster-B with higher potency, reflecting the higher quality of purified protein (entry 13), though the window of selectivity was still comparable to initial findings.

Table 3.4 IC₅₀ values determined from FP experiments of (±)-Astercin 1 phenyl-ring SAR analogues against the ASTER domain of Asters-A, -B, and -C

Entry	Compound	R	Aster-A IC ₅₀ (μ M) ^[a]	Aster-B IC ₅₀ (μ M) ^[a]	Aster-C IC ₅₀ (μ M) ^[a]
1	3.10	3-Fluorophenyl	nd	nd	19.3 ^[b]
2	3.11	2-fluoro-4-chlorophenyl	> 80 ^[c]	> 80 ^[c]	1.92 \pm 0.19
3	3.12	2,4-difluorophenyl	66.5 \pm 3.59	65.8 \pm 2.64	1.66 \pm 0.41
4	3.13	2-fluoro-5-chlorophenyl	nd	nd	38.9 ^[b]
5	3.14	2-methoxyphenyl	nd	nd	> 80 ^[c]
6	3.15	2,6-difluorophenyl	23.9 \pm 8.34	15.9 \pm 0.70	1.12 \pm 0.21
7	3.16	2,5-difluorophenyl	nd	nd	10.9 \pm 2.65
8	3.17	2-fluoro-6-bromophenyl	nd	nd	5.58 \pm 1.91
9	3.18	2-chlorophenyl	nd	25.6 \pm 10.6	1.80 \pm 0.48
10	3.19	Cyclohexyl	nd	nd	> 80 ^[c]
11	3.20	4- <i>tert</i> -butylphenyl	nd	nd	> 80 ^[c]
12	3.21	4-fluorophenyl	nd	nd	5.02 \pm 1.44
13	(-)-Astercin 1	2-Fluorophenyl	57.0 ^[b]	20.4 \pm 1.13	1.27 \pm 0.22

[a] IC₅₀ values are reported as mean \pm s.d. of three individual experiments run in either duplicate or triplicate. [b] experiment run in singlicate or duplicate [c] inhibition at 80 μ M was lower than 50%. nd = not determined

The collection of 12 (-)-Astercin 1 analogues bearing different phenyl substituents provided key SAR information. The optimal substituent in the 2- position was confirmed to be the fluoro substituent seen in (-)-Astercin-1, with the 2-methoxy analogue **3.14** (entry 5) completely losing affinity for Aster-C whereas the 2-chloro analogue **3.18** (entry 9) had comparable binding to Aster-C, but worse selectivity over Aster-B. Substitution in the 3-position alone was mildly tolerated, with the 3-fluoro analogue **3.10** (entry 1) still binding to Aster-C with moderate potency. Substitution at the 4-position was well tolerated with small substituents, in line with findings from the preliminary SAR obtained from library synthesis, with the 4-fluoro analogue **3.21** (entry 12) binding with comparable potency to the 4-chloro analogue **2.76**. The cyclohexyl analogue **3.19** and 4-*tert*-butyl substituted analogue **3.20** (entries 10 and 11) were found not to bind Aster-C, supporting the conclusion that only smaller substituents are well tolerated on the phenyl ring, and that the phenyl ring is crucial for retaining compound potency.

Analogues bearing 2,5-disubstitution were seen to retain some affinity for Aster-C (entries 4 and 7), but were weaker binders compared to (-)-Astercin-1. The 2,6-difluoro analogue **3.15** exhibited excellent binding to Aster-C, equalling that of (-)-Astercin-1, however its selectivity profile against both Aster-B and Aster-C were poorer (entry 6). Changing the 6-substituent from fluorine to bromine yielded an analogue **3.17** with worse binding compared to **3.15** (entry 8). Ultimately, combination of 2- and 4-substitution afforded the most promising analogues, with the 2-fluoro-4-chloro analogue **3.11** and 2,4-difluoro analogue **3.12** potently binding to Aster-C with improved selectivity compared to (-)-Astercin 1 (entries 2 and 3).

Subsequently, analogues featuring modifications to the sterol A/B ring system or the pyrazole ring were screened in dose response against Aster-C (Table 3.5). Analogues bearing modifications to the pyrazole ring generally resulted in decreased binding to Aster-C (entries 2 – 4, 6), with the hexyl ester analogue **3.33** (entry 5) precipitating during the assay. Surprisingly the Astercin ester **3.27** had comparable Aster-C binding to (-)-Astercin-1, however its selectivity over Aster-A was decreased (entry 1). Modifications to the sterol A/B-ring system consistently decreased Aster-C potency (entries 7 – 11), highlighting the important contribution of this scaffold, presence of the C3-hydroxyl, and its relative orientation for Astercin binding. These observations reflected the differential ability of oxysterols to bind to the Aster proteins.⁹²

Table 3.5 IC₅₀ values determined from FP experiments of (±)-Astercin 1 A-ring/B-ring/pyrazole ring SAR analogues against the ASTER domain of Asters-A, -B, and -C

Entry	Compound	Aster-A IC ₅₀ (μM) ^[a]	Aster-B IC ₅₀ (μM) ^[a]	Aster-C IC ₅₀ (μM) ^[a]
1	3.27	14.4 ± 3.68	> 80 ^[c]	2.67 ± 0.78
2	3.28	nd	nd	> 40 ^[c]
3	3.31	nd	nd	14.9 ^[b]
4	3.32	nd	nd	18.4 ^[b]
5	3.33	nd	nd	nd ^[d]
6	3.35	> 80 ^[c]	> 80 ^[c]	8.25 ± 2.61
7	3.36	nd	nd	11.7 ± 0.83
8	3.37	nd	nd	7.28 ^[b]
9	3.26	nd	nd	>> 40 ^[c]
10	3.39	nd	nd	23.9 ± 4.84
11	3.40	nd	> 80 ^[c]	20.5 ^[b]

[a] IC₅₀ values are reported as mean ± s.d. of three individual experiments run in either duplicate or triplicate. [b] experiment run in duplicate [c] inhibition at indicated concentration was lower than 50% [d] compound insoluble in assay conditions, precipitate observed. nd = not determined

In general, modifications to the core A/B-ring structure of (-)-Astercin 1 did not favourably contribute to Aster-C binding, with changes typically decreasing potency tenfold (Figure 3.19). Substituents attached directly to the pyrazole ring were tolerated to a greater extent, with the ester analogue **3.27** being equipotent to (±)-Astercin-1. This finding suggests that exploration from this ester handle could provide a viable attachment point for an alkyl or polyethylene glycol linker for development of bifunctional degraders, fluorescently tagged Astercin analogues, or reactive probes for additional biological studies. Consistent with previous findings with the Astercin series, 2-substitution with a small halogen (fluoro or chloro) was critical for binding to Aster-C, with larger substituents rendering analogues less active. Pleasingly, the combination of the substitution pattern of the two most potent hits from the original screening (2-fluoro, 4-chloro/fluoro) gave rise to the analogues **3.11** and **3.12** with good Aster-C potency and selectivity over Aster-A and Aster-B. As modifications to the core structure of (-)-Astercin 1 did not favourably contribute to potency or selectivity, the SAR study was concluded and the individual enantiomers of **3.11** and **3.12** synthesised.

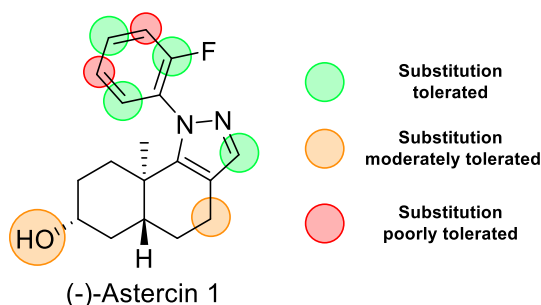
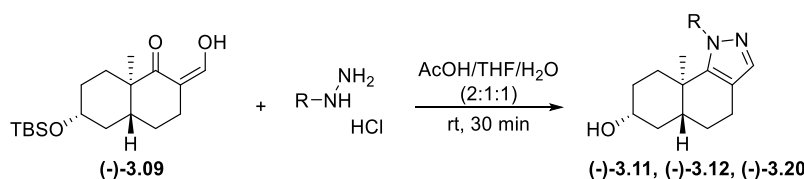


Figure 3.19 Summary of substituent tolerance at modified positions in (-)-Astercin 1

Following the optimised protocol for the synthesis of Astercin analogues, the two analogues (-)-**3.11** and (-)-**3.12** were synthesised in high yields and purity from HM (-)-**3.09**, with no linear products being isolated (Table 3.6, entries 1 and 2). In addition to these two analogues, the 4-*tert*-butyl substituted analogue **3.20** was synthesised (entry 3) to possibly serve as a negative control in future cellular experiments.

Table 3.6 Synthesis of pyrazole-fused analogue single enantiomers for full selectivity profiling



Entry	Compound	R	Yield (%)	Comments
1	(-)- 3.11	2-fluoro-4-chloro	64	-
2	(-)- 3.12	2-fluoro-4-fluoro	65	-
3	(-)- 3.20	4- <i>tert</i> -butyl	48	Isolated alongside linear pyrazole (23%)

The two enantiomers (-)-**3.11** and (-)-**3.12** were screened against the three Asters, alongside the proposed negative control (-)-**3.20** and the pyrazolopyrimidine-fused Aster-A inhibitor (+)-**2.691** (Table 3.7). Both (-)-**3.11** and (-)-**3.12** potently bound to Aster-C with comparable levels of selectivity over both Aster-A and Aster-B. As expected, the 4-*tert*-butyl substituted analogue (-)-**3.20** showed poor binding to all Asters at concentrations up to 80 μM . Finally, the single enantiomer of pyrazolopyrimidine (+)-**2.691** (named Asterpyrin-1) was observed to potently bind to Aster-A with a sufficient window of selectivity over Aster-B and Aster-C. Owing to its slightly higher Aster-C potency, compound (-)-**3.11** (named Astercin-2) was chosen for characterisation in the sterol-transfer assay and for use in subsequent cellular studies.

Table 3.7 IC₅₀ values determined from FP experiments of optimised (-)-Astercin 1 analogues (-)-**3.11**, (-)-**3.12**, proposed negative control (-)-**3.20**, and pyrazolopyrimidine Aster-A inhibitor (+)-**2.691** against ASTER domains of Asters-A, -B, and -C

Compound	Aster-A IC ₅₀ (μM) ^[a]	Aster-B IC ₅₀ (μM) ^[a]	Aster-C IC ₅₀ (μM) ^[a]
(-)- 3.11 (Astercin-2)	> 80	45.2 \pm 7.80	0.93 \pm 0.32
(-)- 3.12	> 80	41.4 \pm 14.3	1.68 \pm 0.01
(-)- 3.20	> 80	> 80	> 80
(+)- 2.691 (Asterpyrin-1)	1.96 \pm 0.3	> 80	28.9 \pm 3.7

Before screening Astercin-2 and Asterpyrin-1 in the sterol transfer assay, further optimisation of protein concentration for Aster-A and Aster-C was performed. The assay was run without addition of inhibitors, at four different concentrations for Aster-C (Figure 3.20a) and two different concentrations for Aster-A (Figure 3.20b). Use of either 0.25 or 0.13 μM of Aster-C resulted in normalised fluorescence values consistently starting at 0.95, thus for subsequent experiments a protein concentration of 0.25 μM was chosen. For Aster-A, where cholesterol transport is known to be the most efficient, a protein concentration of 0.13 μM was necessary to produce normalised fluorescence values starting at 0.90. With protein concentrations optimised, Astercin-2 and Asterpyrin-1 were screened for their ability to inhibit Aster-mediated cholesterol transport.

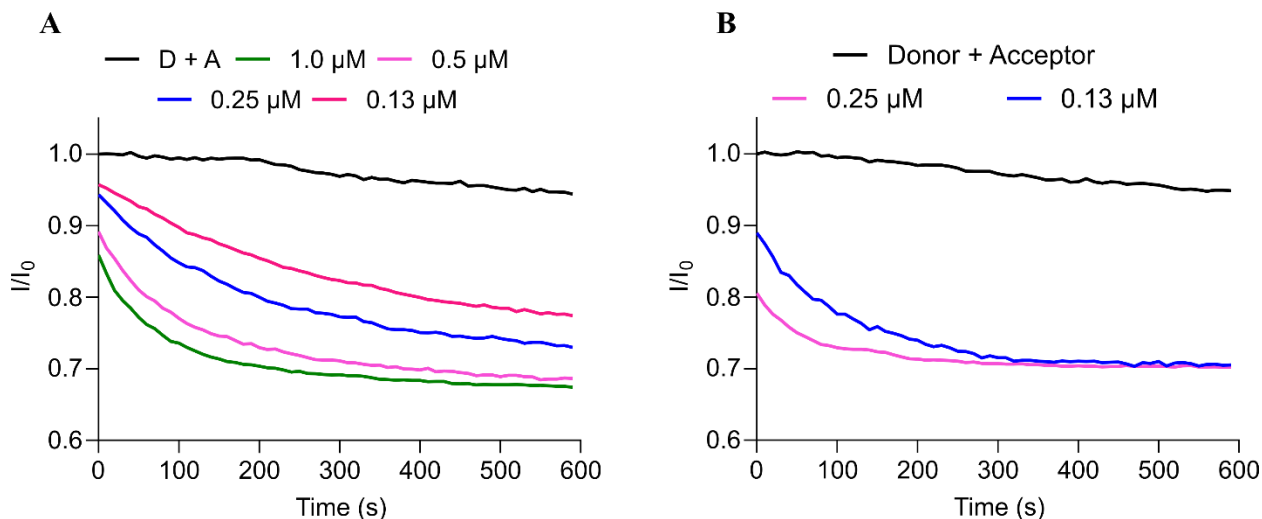


Figure 3.20 Optimisation of protein concentration in the sterol transfer assay using Aster-C (A) and Aster-A (B).

With lower protein concentrations being used compared to the initial screening of (-)-Astercin-1, compound concentrations were also decreased accordingly. Astercin-2 did not to modulate Aster-A or Aster-B mediated cholesterol transfer at a 1 μM and 10 μM respectively, whereas Aster-C mediated cholesterol transfer was significantly inhibited compared to the vehicle control at 1 μM (Figure 3.21a - c). Additionally, Asterpyrin-1 significantly inhibited Aster-A mediated cholesterol transfer at 1 μM compared to Astercin-2 (Figure 3.21a).

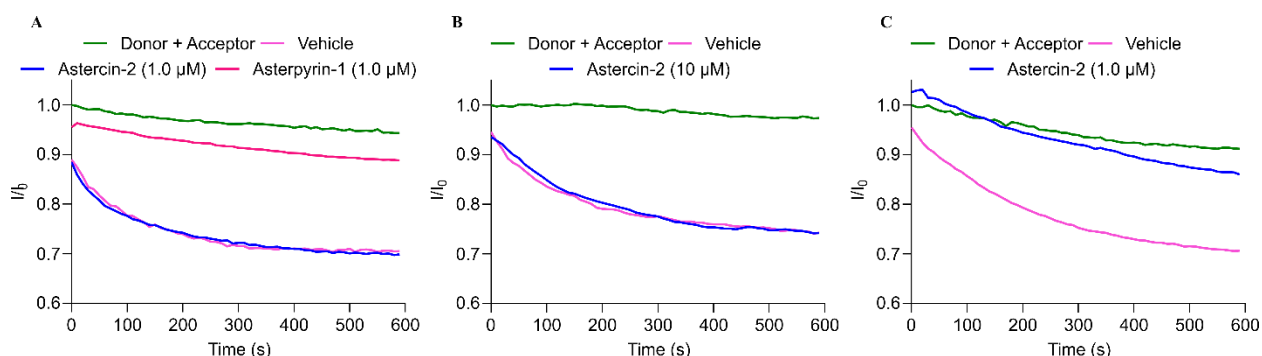


Figure 3.21 Modulation of Aster-mediated cholesterol transfer between donor and acceptor liposomes by Astercin-2 and Asterpyrin-1. **A)** Modulation of Aster-A mediated cholesterol transfer (protein concentration = 0.13 μM). **B)** Modulation of Aster-B mediated cholesterol transfer (protein concentration = 1.0 μM). **C)** Modulation of Aster-C mediated cholesterol transfer (protein concentration = 0.25 μM).

Following the optimisation of Astercin-1 to afford Astercin-2 and the identification of Asterpyrin-1, both compounds were deemed appropriate for use in the planned cellular studies. Both compounds potently inhibited their main target protein with low micromolar potency, with greater than 10-fold selectivity over the other Aster proteins.

Part IV. Biological characterisation of sterol-inspired Aster-inhibitors

4.1 Inhibition of autophagy by Asterpyrin-1

To begin the cellular evaluation of Asterpyrin-1 and Astercin-2, their effects on autophagy were studied, as several publications have linked the activity of Aster-A and Aster-C to autophagosome biogenesis.^{98,101} Autophagy is a conserved cellular pathway responsible for degradation of a range of different cargo.¹⁶⁰ Three general types of autophagy have been reported including microautophagy, chaperone-mediated autophagy, and macroautophagy.^{161,162} The most commonly studied form of autophagy is macroautophagy, which will subsequently be referred to as autophagy. Autophagy proceeds via the formation of the double-membraned organelle known as a phagophore, following initiation signals from mTORC1 and AMP-activated protein kinase (AMPK) and activation of the two protein complexes Unc51-like kinase 1 (ULK1) complex and the phosphoinositide 3-kinase (PI3K) class III complex I (Figure 4.1).¹⁶³ One integral protein in autophagy is LC3, which is necessary for the maturation of the phagophore to autophagosome. The cytosolic form of LC3 (referred to as LC3-I) is conjugated to the phospholipid phosphatidylethanolamine (PE) giving rise to its lipidated form, LC3-II. LC3-II can then be anchored into the phagophore membrane, recruiting other proteins necessary for maturation.¹⁶⁴ During the folding process, cargo are sequestered in the autophagosome for degradation. The autophagosome subsequently fuses with lysosomes, forming autolysosomes, and degrading the engulfed cargo through action of hydrolytic enzymes.¹⁶⁵

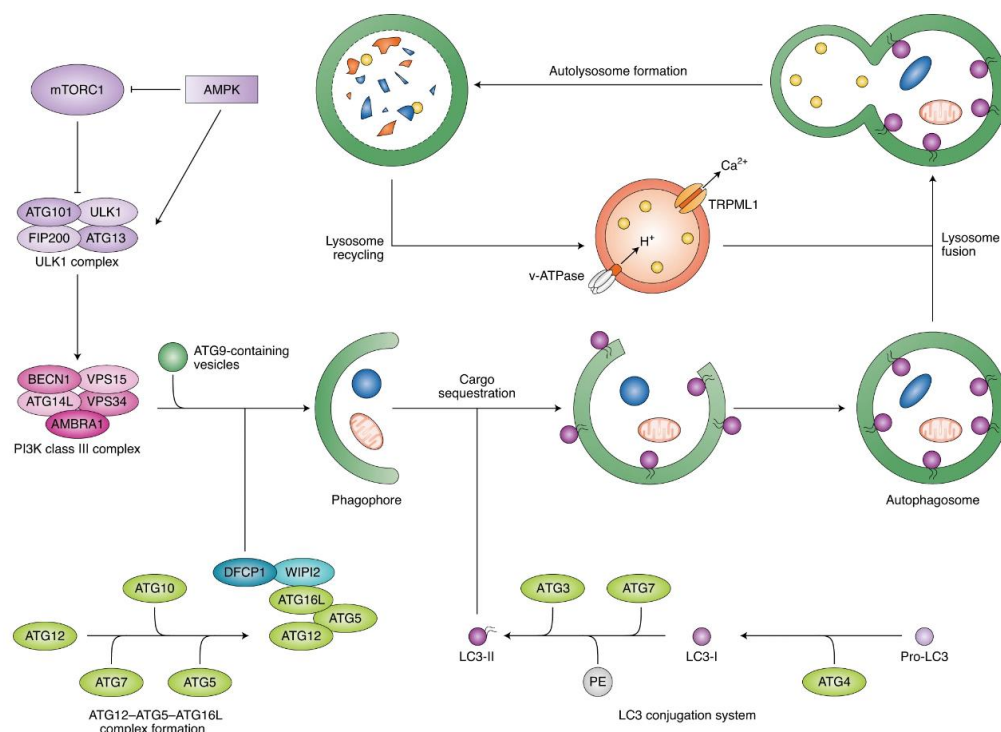


Figure 4.1. A general overview of the autophagy pathway. Figure reproduced from reference.¹⁶⁰

Small molecule modulators of autophagy are typically identified by probing levels of LC3-I/LC3-II.¹⁶⁶ One assay that is frequently used in high content phenotypic screening to identify autophagy modulators utilises a green fluorescent protein (GFP)-LC3 reporter cell line. Cells are imaged after compound treatment under

fed conditions or autophagy induction, and autophagosomes quantified as green puncta. Changes in LC3 levels observed in this assay required further biochemical characterisation to elucidate whether LC3 levels are changing in response to autophagy induction, early or late stage inhibition, or by blocking fusion of lysosomes to autophagosomes. The most common approach to achieve this is assessing levels of LC3-I and LC3-II by western blot.

As inhibition of Aster-A is known to inhibit starvation-induced autophagy, Asterpyrin-1 was tested to investigate whether it was able inhibit starvation-induced autophagy similarly to Autogramin-2.⁹⁸ U2OS cells were treated for 3 hours with Asterpyrin-1 (AP1) or Autogramin-2 (AG2), and levels of LC3-I and LC3-II probed by western blot with an anti-LC3 antibody (Figure 4.2). Compound treatments were performed under fed conditions in complete media or under amino acid starvation by performing compound treatments in Earle's balanced salt solution (EBSS), both in the presence of the lysosomotropic agent chloroquine (CQ) which acts to block fusion of the autophagosome and lysosome, leading to accumulation of LC3-II.¹⁶⁰ Asterpyrin-1 inhibited starvation-induced autophagy (lane 7) similar to Autogramin-2 (lane 5), with both compound treatments resulting in lower levels of LC3-II compared to the vehicle control (lane 3). In line with this data, (\pm)-Asterpyrin-1 was able to inhibit starvation-induced autophagy in a phenotypic screen in the reporter cell line MCF7-eGFP-LC3. In combination, these observations provides further support that the observed autophagy inhibition is the result of inhibition Aster-A, as this phenotype is induced by two different chemotypes that both biochemically inhibit the Aster-A ASTER domain.

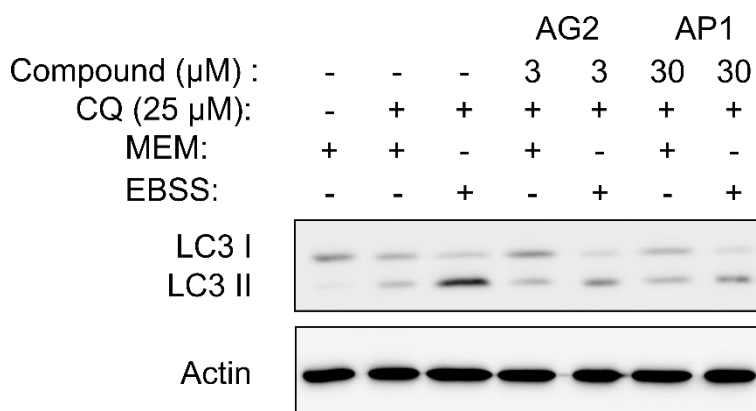


Figure 4.2. Inhibition of LC3 lipidation in U2OS cells following treatment with either Autogramin-2 or Asterpyrin-1 for 3 hours under fed and starved conditions.

The concentration of Asterpyrin-1 required to inhibit LC3-I lipidation comparably to Autogramin-2 are tenfold higher, suggesting differences in membrane permeability between the two compounds (Figure 4.2). This observation was further supported by the differences in cellular IC_{50} values for autophagy inhibition whilst the two compounds were found to have similar biochemical potencies by FP (Figure 4.3). These findings suggest that introduction of an assay measuring membrane permeability would be a beneficial assay to perform as part of tool compound characterisation, and explain the observed differences in biochemical and cellular potencies.

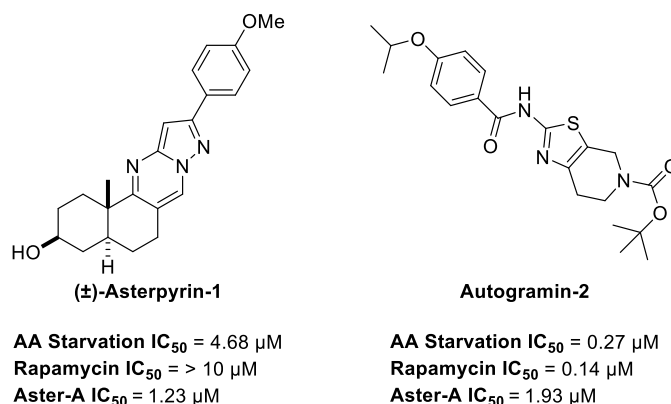


Figure 4.3. Comparison of cellular inhibition of amino acid starvation and rapamycin-induced autophagy and biochemical binding to Aster-A ASTER domain for (±)-Asterpyrin-1 and Autogramin-2

4.3 Relevance of Aster-C in autophagy

Whilst limited research has been performed specifically around Aster-C two independent reports have suggested a potential role in autophagy, however, the data presented conflict one another.^{100,101} One report suggests that Aster-C is a negative regulator of starvation-induced autophagy, with Aster-C depletion by genetic knockdown inducing autophagy similar to the affects arising from cholesterol depletion.¹⁰¹ On the other hand, Aster-C knockout (KO) was shown to result in significant accumulation of LC3-II under amino acid starvation associated with its role as a regulator of mTORC1 signalling, however autophagic flux was not investigated alongside levels of LC3.¹⁰⁰ Given the ambiguous role of Aster-C in autophagy, Astercin-2 was utilised to investigate whether either phenotype could be reproduced via small molecule inhibition of the Aster-C cholesterol binding domain rather than genetic knockout or knockdown.

U2OS cells were treated with Astercin-2 (10 μM) at three different time points under starvation conditions either with or without CQ to block lysosomal fusion, and LC3 levels probed by western blot (Figure 4.4a). No changes in LC3 levels were observed from short term treatment, thus cells were pre-treated with Astercin-2 (10 μM) before amino acid starvation and CQ treatment, allowing for prolonged inhibition of Aster-C. U2OS cells were pre-treated with Astercin-2 for 24 hours before treatments with Astercin-2 under both starvation and fed conditions, with and without CQ, and LC3 levels probed by western blot (Figure 4.4b, 4.4c). Under starvation conditions (Figure 4.4b), no significant changes in LC3 lipidation were observed with Astercin-2 pre-treatment. A minor decrease in LC3-II was observed in cells pre-treated with Astercin-2 in the absence of CQ (lanes 4 - 6) compared to vehicle treated cells (lanes 1 - 3), suggesting a possible degradation of LC3-II associated with autophagy induction. The experiment was repeated under fed conditions in the presence of CQ to investigate whether the observed changes could be due to autophagy induction (Figure 4.4c). Pre-treatment with Astercin-2 was observed to give minor increases in LC3-II levels (lanes 6 - 8) relative to cells without pre-treatment (lanes 1, 4-5). These findings are consistent with the report of Aster-C as a negative regulator of starvation-induced autophagy. Likewise, the significance of the observed changes in LC3 lipidation were minor. As such, no further experiments were performed on the role of Aster-C in autophagy.

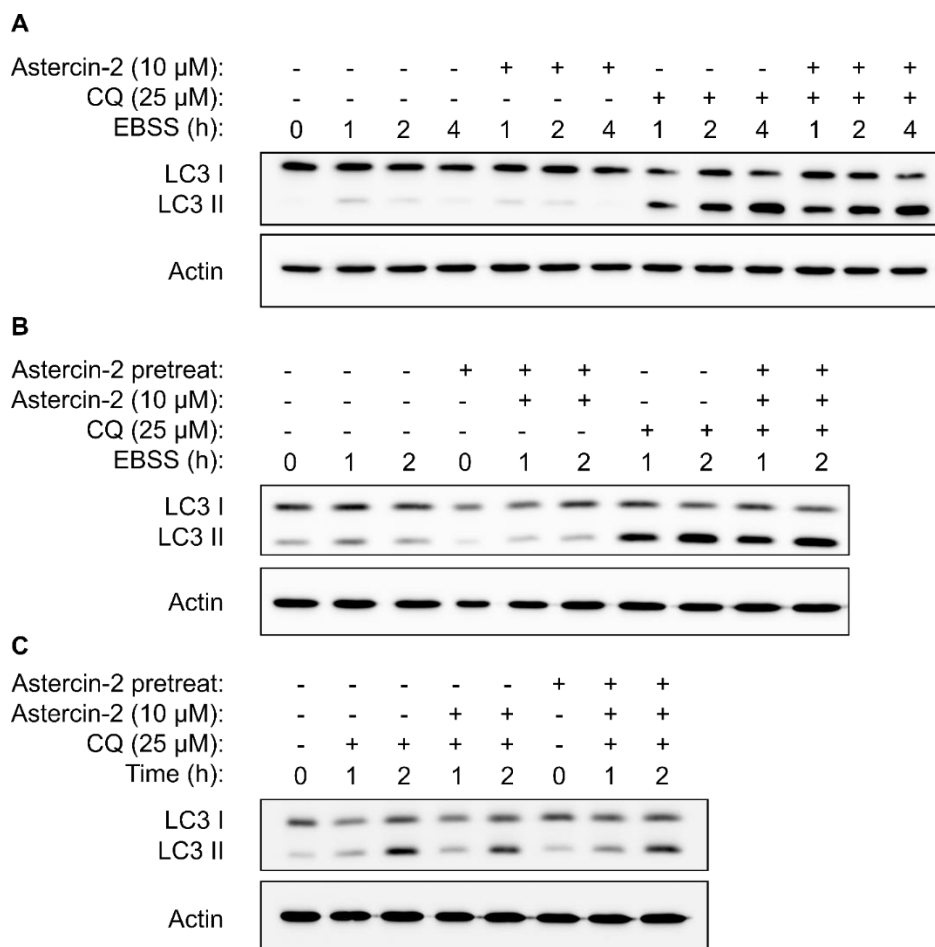


Figure 4.4 LC3 levels in Astercin-2 treated U2OS cells under starvation-induced autophagy and fed conditions. **A)** Astercin-2 treatments under starvation conditions with or without chloroquine **B)** Astercin-2 treatments under starvation conditions with or without chloroquine, and a 24 hour pre-treatment with Astercin-2 (10 μ M) **C)** Astercin-2 treatments in fed cells with chloroquine, and a 24 hour pre-treatment with Astercin-2 (10 μ M).

4.4 Cellular localisation of Aster-A and Aster-C

With Asterpyrin-1 and Astercin-2 demonstrating activity in a cellular context, the localisation of both Aster-A and Aster-C in U2OS cells was investigated. To investigate their localisation, U2OS cells were transiently transfected with plasmids encoding for fluorescent Aster constructs. A plasmid encoding mCherry-Aster-A was available in the group of Prof. Yaowen Wu and a plasmid encoding eGFP-Aster-C was constructed, cloning human Aster-C into an eGFP vector. U2OS and HeLa cells were transfected with equal quantities of mCherry-Aster-A/eGFP-Aster-C DNA overnight and imaged by live-cell confocal microscopy. The mCherry-Aster-A construct was efficiently expressed in both cell lines, however the expression of eGFP-Aster-C was poor in both cell lines (Figure 4.5). Sequencing of the eGFP-Aster-C plasmid revealed a leucine to proline point mutation in the Aster-C coding sequence, with such a mutation likely expecting to be disruptive to protein structure and thus contributing to the poor expression of the plasmid.

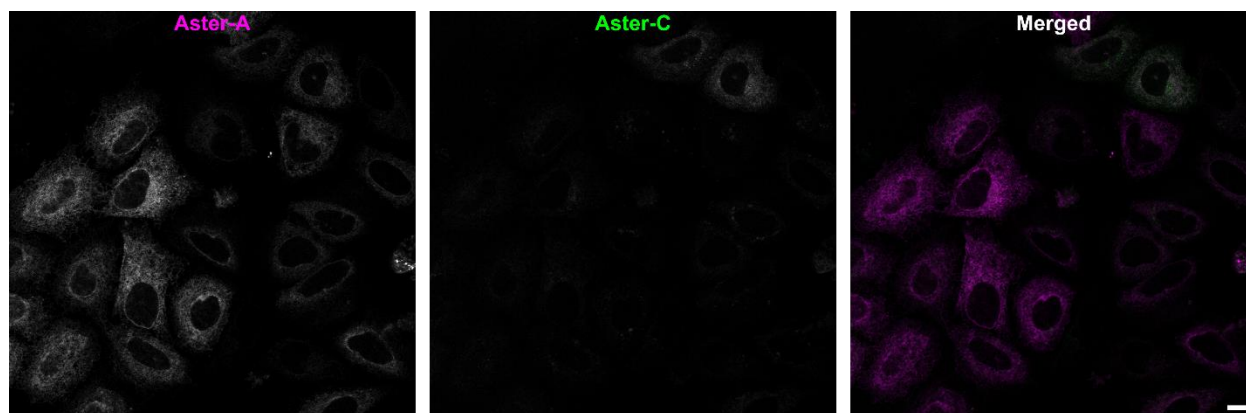


Figure 4.5 Differential expression of mCherry-Aster-A (magenta) and eGFP-Aster-C (green) in live HeLa cells. Scale bar = 10 μ m.

Correction of the Aster-C point mutation by PCR mutagenesis yielded an eGFP-Aster-C plasmid showing improved expression levels and the expected reticular expression pattern. U2OS cells were transfected with a 1:3 ratio of mCherry-Aster-A/eGFP-Aster-C DNA overnight, cells fixed with paraformaldehyde (PFA), and after permeabilization the mCherry and eGFP signals amplified by labelling with anti-mCherry and anti-eGFP antibodies and subsequently with fluorescent secondary antibodies (Figure 4.6). Imaging confirmed the reticular expression pattern expected for ER-resident proteins was conserved for both Aster proteins, but that Aster-A was more uniformly expressed through the ER. Aster-C was generally expressed in a uniform manner, but regions of relative enrichment over Aster-A were observed, which might suggest that the two proteins are not likely to be redundant and as such may possess unique biological functions.

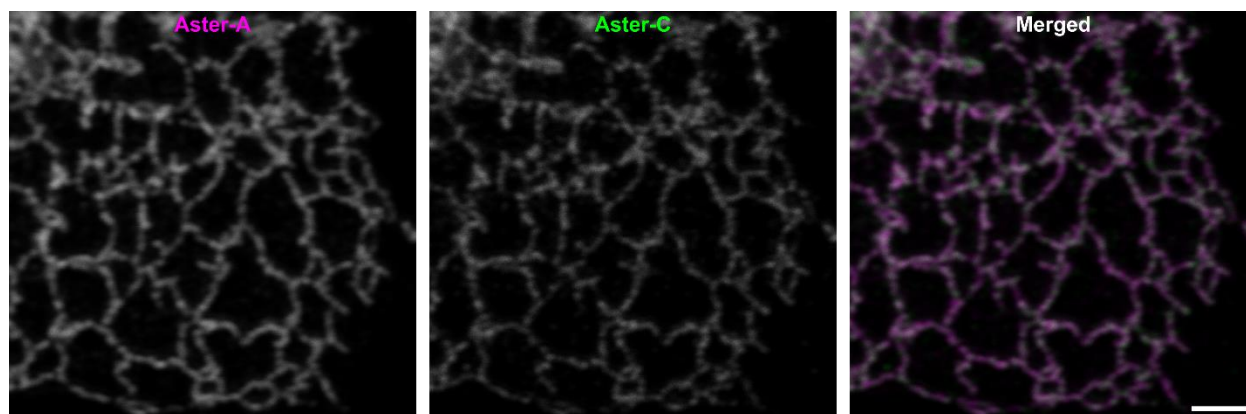


Figure 4.6 Expression and localisation of Aster-A (magenta) and Aster-C (green) in fixed U2OS cells. Immunofluorescence images of U2OS cells transfected with mCherry-Aster-A (magenta) and eGFP-Aster-C (green). mCherry and eGFP signals were enhanced with anti-mCherry and anti-eGFP antibodies respectively. Scale bar = 2 μ m.

4.5 Cellular cholesterol

Cellular cholesterol is found in two main forms, either in its free form sequestered in plasma membranes and organelle membranes or as CEs after esterification by the ER-resident ACAT1/2 (Figure 4.7). The main objective of the cellular studies with Astercin-2 and Asterpyrin-1 was to investigate whether selective inhibition of Asters gave rise to differential changes in the localisation and levels of cholesterol and CEs in cells.

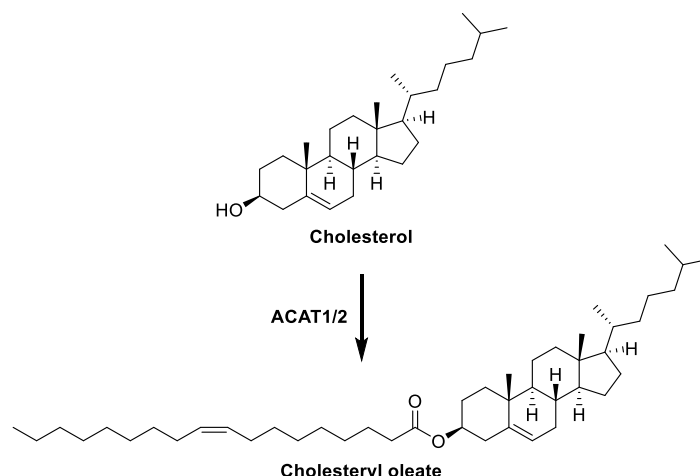


Figure 4.7 Esterification of cholesterol to a cholesterol ester by the ER-resident enzymes ACAT1 and ACAT2. Cholesteryl oleate is presented as a representative cholesterol ester.

Numerous probes have been reported that efficiently label free cholesterol in cells (Figure 4.8).¹⁶⁷ The most commonly used chemical stain for cholesterol is the polyene antibiotic filipin which readily crosses cellular membranes and binds cholesterol, after which cholesterol can be visualised by the inherent fluorescence of filipin.¹⁶⁸ Another important class of cholesterol binding probes are the cholesterol-dependent cytolysins (CDCs) which are families of pore-forming protein toxins secreted by bacteria, with commonly used examples including Perfringolysin O (PFO), Anthrolysin O (ALO), and Ostreolysin A (Oly A).¹⁶⁹ CDCs bind to cholesterol located in the PM with different binding properties, with engineered variants of natural CDCs probes capable of binding to differing concentrations of cholesterol as well as opposing leaflets of the PM.¹⁶⁷

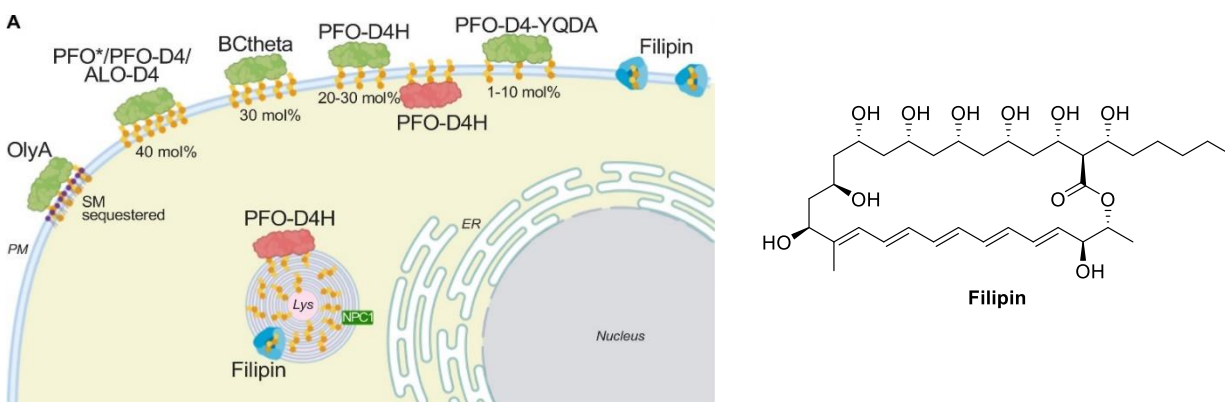


Figure 4.8 Examples of commonly used cholesterol labelling probes including Filipin in addition to PFO, ALO, and OlyA derived probes. Figure reproduced with permission from reference.¹⁶⁷ Copyright (2021) Elsevier.

Labelling and visualisation of CEs can be performed by either direct chemical stains, or indirectly using immunofluorescence (IF) methods to label LD-associated proteins. Chemical methods to label LDs utilise hydrophobic small molecule fluorophores that accumulate and fluoresce in the hydrophobic core of the LD.¹⁷⁰ Commonly used LD dyes include Oil Red O, Nile Red, and BODIPY 493/503, however limitations of poor solubility, issues of selectivity, and high fluorescent backgrounds often favour the use of IF methods (Figure 4.9).¹⁷⁰ Perilipin 2 (PLIN2) is a widely expressed LD-associated protein, residing in the

phospholipid monolayer surrounding the core of neutral lipids, and therefore is routinely used as a target for IF visualisation of LDs.¹⁷¹

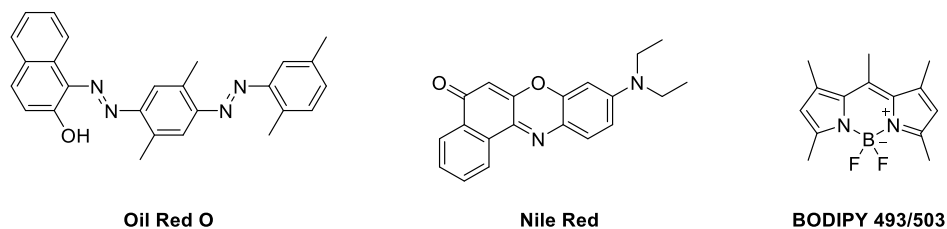


Figure 4.9 Chemical structures of representative small molecule stains for lipid droplets.

4.6 Modulation of free cholesterol by Asterpyrin-1 and Astercin-2

The Aster proteins are known to facilitate the transport of free cholesterol between the PM and ER, therefore investigating the effects of Asterpyrin-1 and Astercin-2 on free cholesterol was prioritised. U2OS cells were treated with either Asterpyrin-1, Autogramin-2 or Astercin-2 at 10 μ M for 20 hours. After PFA fixation, free cholesterol was stained with filipin, the nuclei counterstained using DRAQ5, and the samples immediately imaged by confocal microscopy (Figure 4.10). Treatment with both Aster-A inhibitors resulted in the formation of numerous bright puncta, occurring as early as the 4 hour treatment time, representing a significant accumulation of cholesterol compared to vehicle treated cells. The magnitude of the accumulation was consistent with the relative cellular potency of Asterpyrin-1 and Autogramin-2 in inhibiting autophagy. Treatment of Autogramin-2 at 10 μ M for longer than 24 hours was found to cause cell death, likely due to cholesterol-associated lipotoxicity. Treatment with Astercin-2, however, did not affect levels or the localisation of free cholesterol, with the observed phenotype matching the vehicle treatment and being consistent with data reported for the Aster-C inhibitor AI-11.¹¹⁰

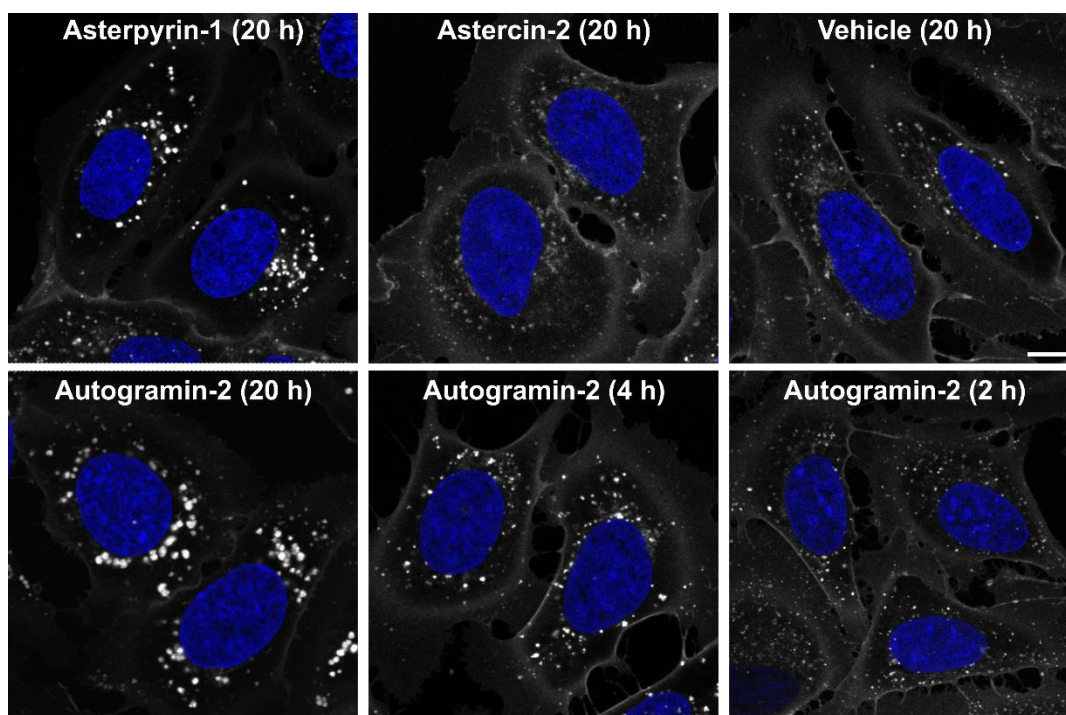


Figure 4.10 Cholesterol staining in U2OS cells following compound treatment at 10 μ M. Nuclei stained with DRAQ5 (blue) and cholesterol stained with filipin (grey). Scale bar = 10 μ m.

The accumulation of free cholesterol arising from prolonged inhibition of Aster-A was visually similar to the phenotype observed in Niemann-Pick disease type C, in which cholesterol accumulates in lysosomes due to mutations in the lysosomal cholesterol transporters NPC1 or NPC2.⁶³ In order to determine whether cholesterol accumulation induced by Aster-A inhibition was occurring in a specific organelle, immunofluorescence was utilised to visualise components of the endolysosomal pathway. For initial investigations Autogramin-2 was chosen owing to the greater magnitude of cholesterol accumulation relative to Asterpyrin-1. U2OS cells were treated with 10 μ M Autogramin-2 for 24 hours and cells fixed by PFA upon completion of treatment. Free cholesterol was stained using Filipin, nuclei counterstained with DRAQ5, and early endosomes visualised with an anti-early endosome antigen 1 (EEA1) antibody (Figure 4.11). In Autogramin-2 treated cells an increased amount of EEA1 staining was observed relative to the vehicle control, however co-localisation with the filipin staining was not observed. The increased number of EEA1 puncta was indicative of an upregulation of the endolysosomal pathway, therefore it was investigated whether cholesterol was instead accumulating in lysosomes.

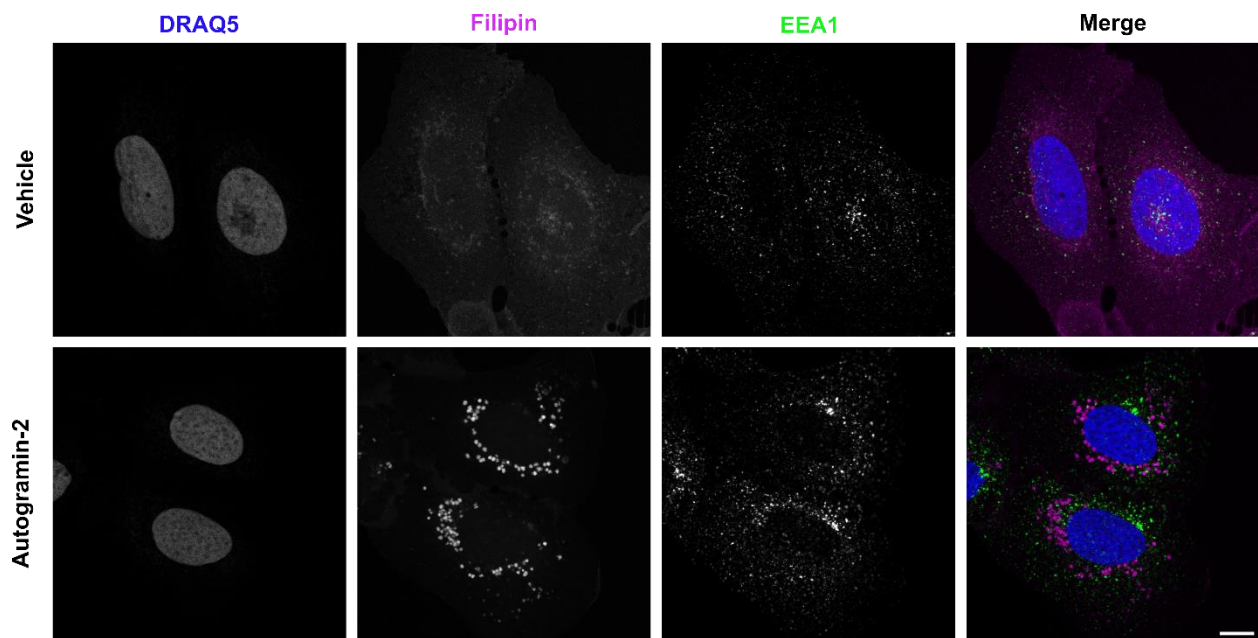


Figure 4.11 Cholesterol accumulation arising from prolonged Aster-A inhibition is not occurring in early endosomes. Immunofluorescence images of U2OS cells treated with autogramin-2 (10 μ M) or vehicle (0.1% DMSO) for 24 hours. Early endosomes were visualised with an anti-EEA1 antibody (green), nuclei were stained with DRAQ5 (blue), and cholesterol stained with filipin (magenta). Scale bar = 10 μ m.

Samples were stained using an anti-lysosomal associated membrane protein 1 (LAMP1) antibody to visualise whether cholesterol was accumulating in lysosomes, similarly to Niemann-Pick disease type C (Figure 4.12). In vehicle treated cells the LAMP1 staining was punctate in nature, reflecting a normal distribution of lysosomes. Upon prolonged treatment with Autogramin-2, the size of the LAMP1 positive structures was increased compared to the vehicle control, and also enveloped the filipin-stained cholesterol, indicating that the cholesterol was accumulating in lysosomes.

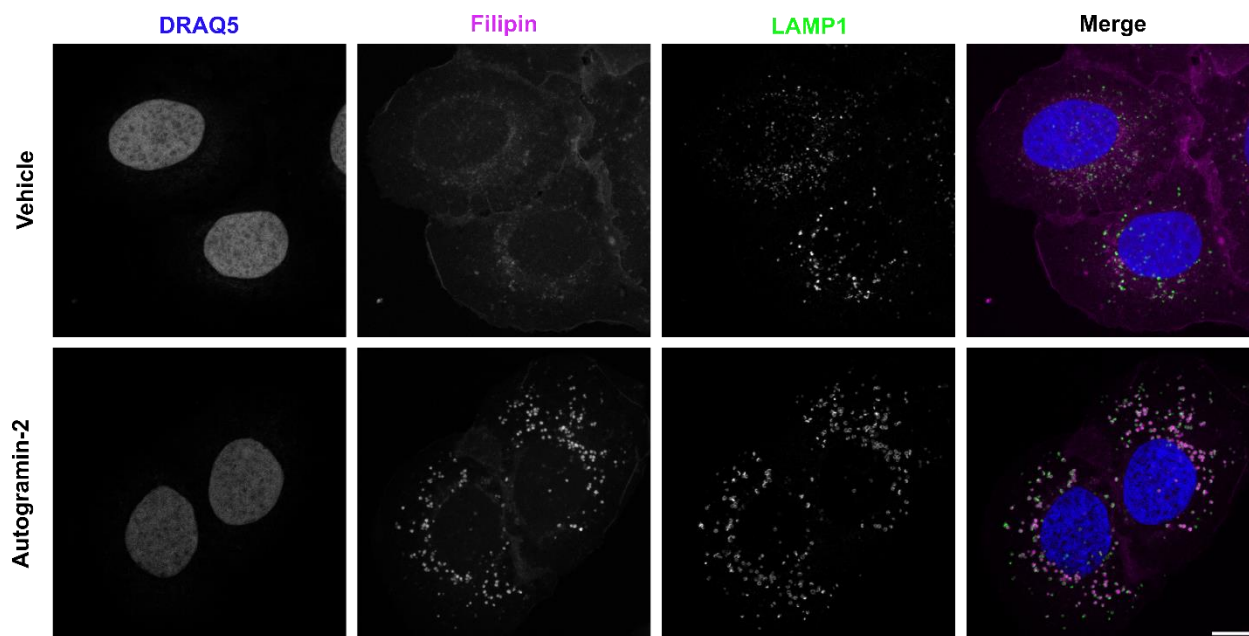


Figure 4.12 Prolonged Aster-A inhibition induces accumulation of cholesterol in lysosomes. Immunofluorescence images of U2OS cells treated with autograinin-2 (10 μ M) or vehicle (0.1% DMSO) for 24 hours. Lysosomes were visualised with an anti-LAMP1 antibody (green), nuclei were stained with DRAQ5 (blue), and cholesterol stained with filipin (magenta). Scale bar = 10 μ m.

With confirmation that cholesterol was accumulating in lysosomes, lysosomes were assessed for markers of membrane damage. Galectin-3 (Gal3) is a cytosolic carbohydrate-binding lectin that binds to β -galactosides that can be used as a marker of lysosomal damage.¹⁷² Upon lysosomal damage, β -galactosides present in the glycocalyx of the lysosome become accessible and Gal3 is rapidly recruited to the site of damage, after which it recruits endosomal sorting complexes require for transport (ESCRT) components and induces autophagy for lysosomal repair and removal respectively.¹⁷³ Visualising Gal3 using an anti-Gal3 antibody (Figure 4.13) under vehicle treatment showed a faint and diffuse cytosolic distribution of Gal3, consistent with the low expression of Gal3 in U2OS cells.¹⁷² Though Autograinin-2 treatment resulted in a nuclear localisation of Gal3, no formation of Gal3 puncta nor co-localisation of with the filipin staining was observed, indicating that cholesterol was not accumulating in damaged lysosomes.

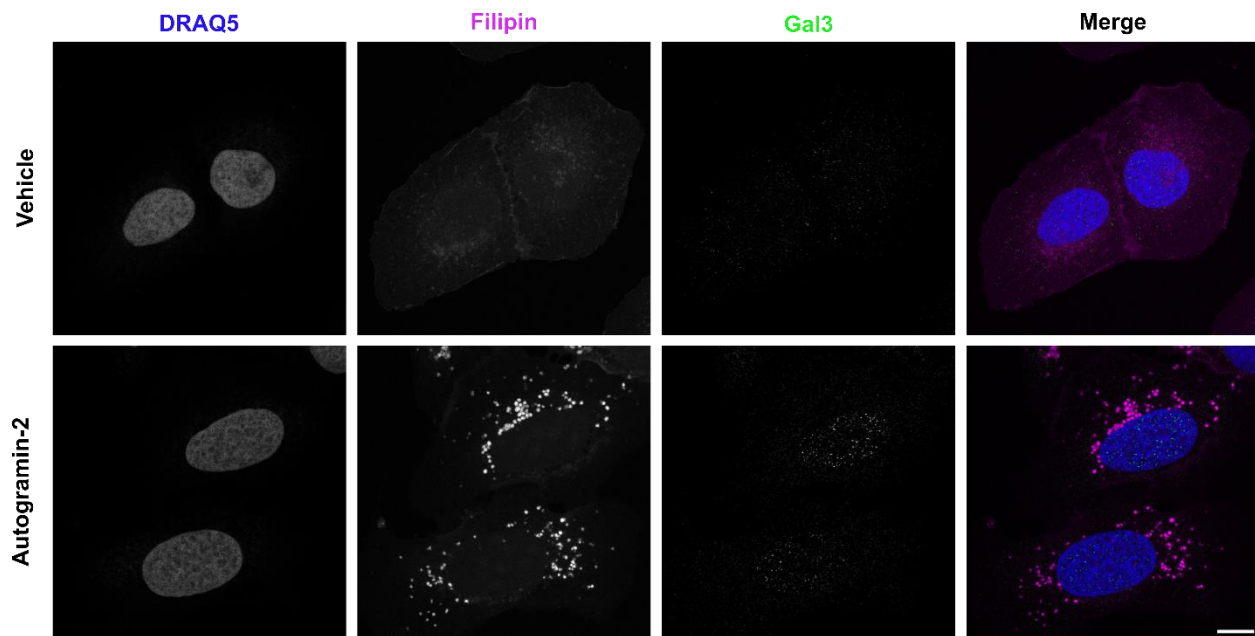


Figure 4.13 Cholesterol accumulation arising from prolonged Aster-A inhibition is not occurring in damaged lysosomes. Immunofluorescence images of U2OS cells treated with autograin-2 (10 μ M) or vehicle (0.1% DMSO) for 24 hours. Galectin 3 was visualised with an anti-Gal3 antibody (green), nuclei were stained with DRAQ5 (blue), and cholesterol stained with filipin (magenta). Scale bar = 10 μ m.

To better visualise the cholesterol accumulation induced by prolonged Aster-A inhibition, a Z-stack was taken of a an individual U2OS cell after treatment with Autograin-2 (10 μ M) for 24 hours and rendered in 3D (Figure 4.14). From the reconstruction it was evident that the cholesterol accumulation (magenta) was spherical in nature and enclosed in a LAMP1 positive structure (green), further supporting the conclusion that cholesterol was accumulating in lysosomes.

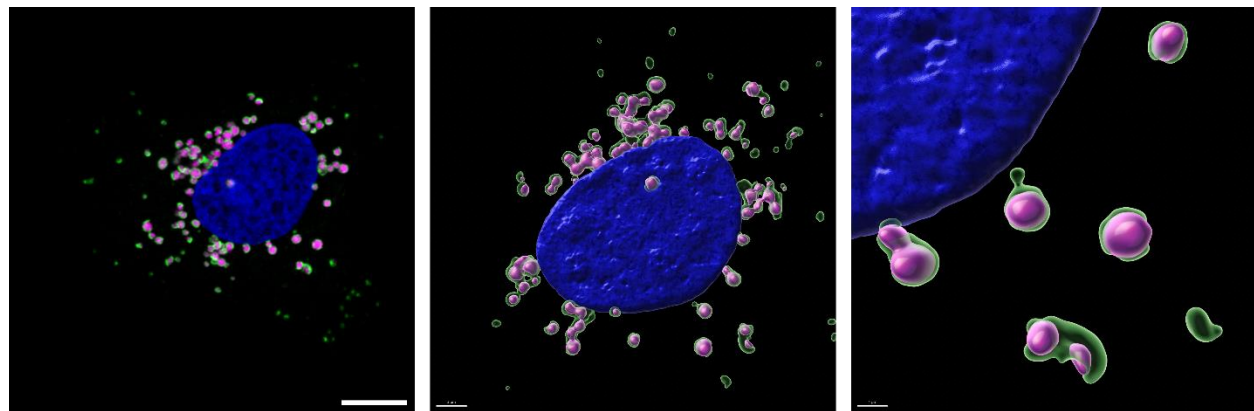


Figure 4.14 3D rendering of lysosomal cholesterol accumulation in U2OS cells treated with autograin-2 (10 μ M) for 24 hours. Left: Single plane of Z-stack image (scale bar = 10 μ m). Middle + right: 3D reconstruction of Z-stack image (scale bars = 3 μ m and 1 μ m respectively). Lysosomes were visualised with an anti-LAMP1 antibody (green), nuclei were stained with DRAQ5 (blue), and cholesterol stained with filipin (magenta). 3D rendering was performed in Imaris.

The accumulation of lysosomal cholesterol in cells derived from NPC1 patients is associated with impaired autophagy and decreased degradation of autophagosomes and accordingly, increased levels of LC3-II.¹⁷⁴ This prompted the investigation on whether lysosomal cholesterol accumulation arising from Aster-A inhibition also resulted in accumulation of LC3. U2OS cells were treated with 10 μ M Asterpyrin-1 for 24 hours and cells fixed by PFA upon completion of treatment. Free cholesterol was stained using Filipin, LC3 visualised with an anti-LC3 antibody, and lysosomes with an anti-LAMP1 antibody (Figure 4.14A). Under vehicle treatment LC3 has a diffuse cytosolic distribution with few punctate structures, consistent with a basal level of autophagy. Upon treatment with Asterpyrin-1, an increase in LC3 staining was observed, with a mixture of larger puncta and ring-shaped structures present, localising to and enveloping the filipin/LAMP1 positive structures (Figure 4.14B). This data indicates that LC3 is being recruited directly to the lysosomal membrane, in response to the accumulation of lysosomal cholesterol.

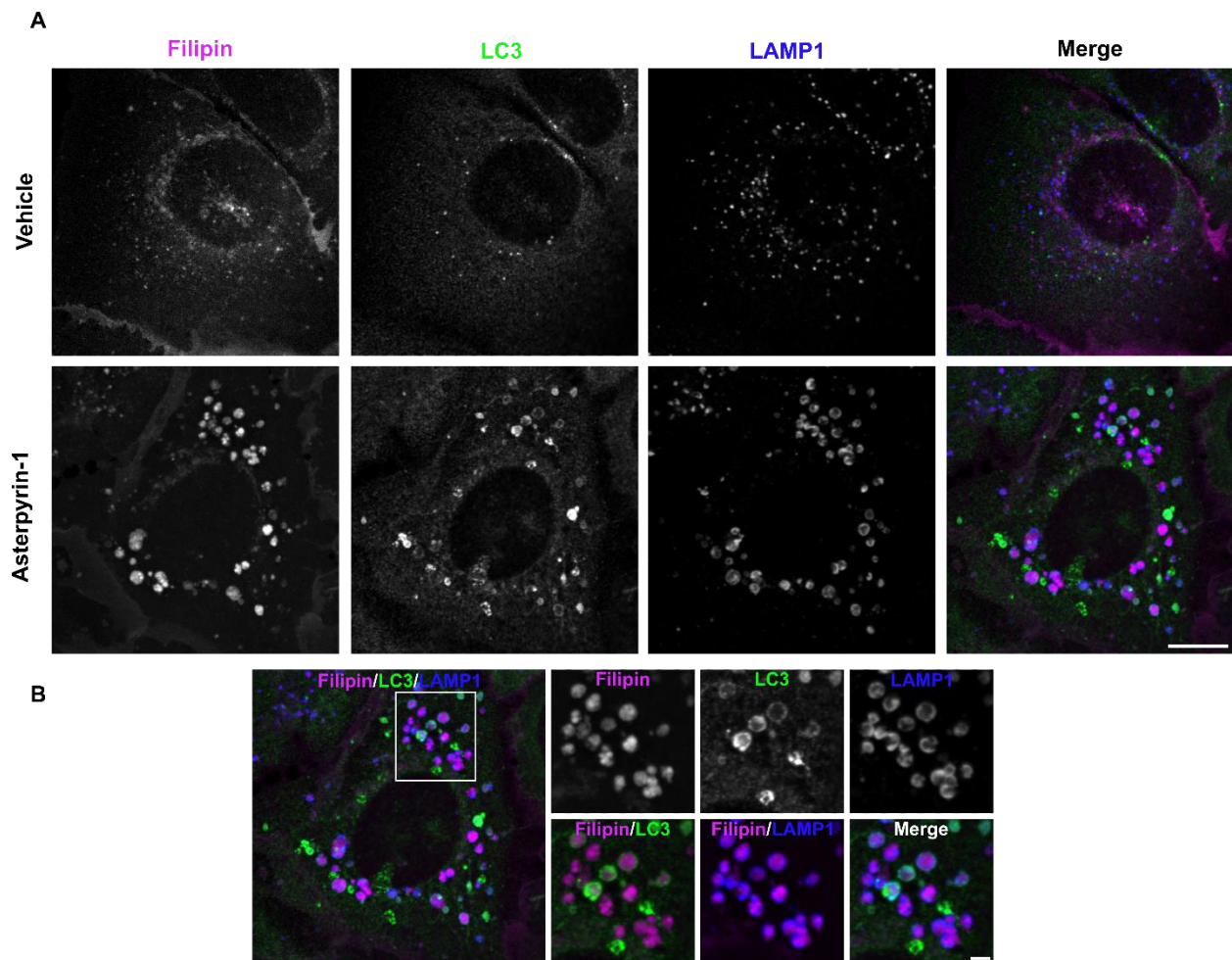


Figure 4.14 Prolonged inhibition of Aster-A by Asterpyrin-1 causes LC3 recruitment to cholesterol-laden lysosomes. **A)** Immunofluorescence images of U2OS cells treated with Asterpyrin-1 (10 μ M) or vehicle (0.1% DMSO) for 24 hours. LC3 and lysosomes were visualised with an anti-LC3 antibody (green) and anti-LAMP1 antibody (blue) and cholesterol stained with filipin (magenta). Scale bar = 10 μ m **B)** Inset of Asterpyrin-1 treated cells from panel A. Scale bar = 2 μ m.

Levels of LC3-II were probed by western blot in HeLa Kyoto cells after treatment with either Autogramin-2 or Asterpyrin-1 for 24 hours (Figure 4.15). Increases in LC3 were observed with both compound treatments, directly supporting the immunofluorescence imaging. LC3 lipidation occurred in a dose-dependent manner for both compounds, with 5 μ M of Autogramin-2 producing a maximal level of lipidation, and higher concentrations resulting in either senescence (10 μ M) or cell death (20 μ M). Asterpyrin-1 gave rise to the greatest level of LC3 lipidation at 20 μ M with no significant cytotoxicity observed. Additionally, levels of LC3-II were analysed in a series of HeLa Kyoto KO cell lines deficient for key autophagy components including FIP200, ATG7, and ATG16L (Figure 4.15). Canonical lipidation of LC3 cannot occur in these KO cell lines, therefore increases in LC3-II relative to vehicle controls would indicate lipidation is occurring through non-canonical mechanisms. No increases in LC3 lipidation were observed in any KO cell line, indicating that the observed increase in LC3 lipidation in the WT cells was canonical in nature and occurring via the normal autophagy pathway.

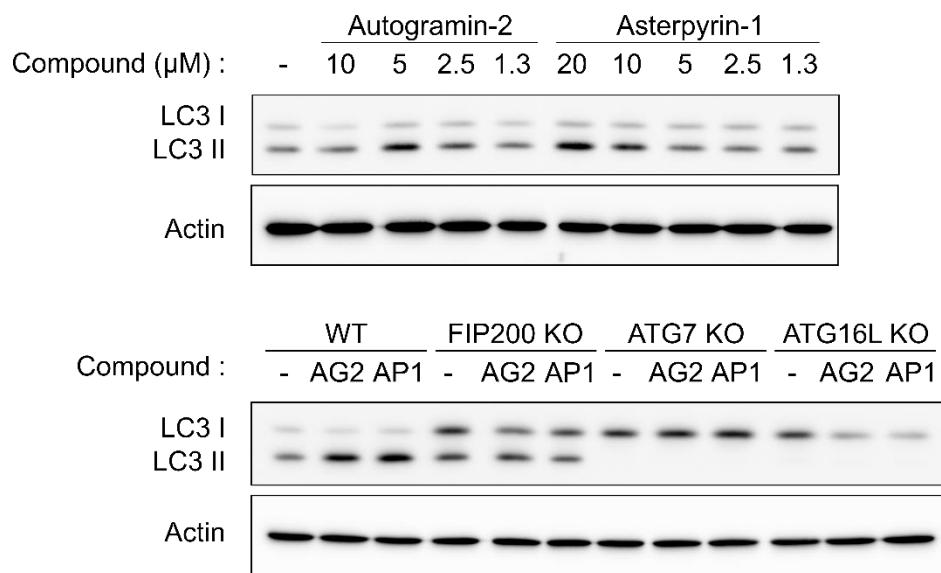


Figure 4.15 Changes in LC3 lipidation in HeLa Kyoto and HeLa Kyoto knockout cell lines arising from Autogramin-2 (AG2) or Asterpyrin-1 (AP1) treatment for 24 hours. Top: Dose response of LC3 lipidation induction in HeLa Kyoto WT. Bottom: LC3 levels in HeLa Kyoto cell lines treated with Autogramin-2 treated cells (5 μ M) and Asterpyrin-1 (20 μ M) for 24 hours.

4.7 Modulation of lipid droplets by Asterpyrin-1 and Astercin-2

As Astercin-2 treatment did not induce changes in free cholesterol staining, its effects on cholesterol esters were investigated. Staining of neutral lipids was achieved using the dye HCS LipidTOX Red, chosen for its simple staining protocol and higher specificity over dyes such as Oil Red O and Nile Red. U2OS cells were treated with Asterpyrin-1 and Astercin-2 at 10 μ M for 24 hours, alongside Autogramin-2. After PFA fixation, neutral lipids were stained with HCS LipidTOX Red, nuclei counterstained with Hoechst 33342, and cells imaged by confocal microscopy (Figure 4.16). Neutral lipid staining revealed that under basal conditions, U2OS cells maintain a constant albeit low population of LDs, evidenced by the small number of bright puncta. No increase in puncta was observed in cells treated with either Aster-A inhibitor, with both samples having comparable numbers of LDs to vehicle treated cells. However, spherical voids in neutral lipid staining were observed which would coincide with the observed accumulation of lysosomal cholesterol. Treatment of cells with Astercin-2 resulted in significant accumulation of lipid droplets, with a near uniform increase in the number of bright puncta across all cells in the sample.

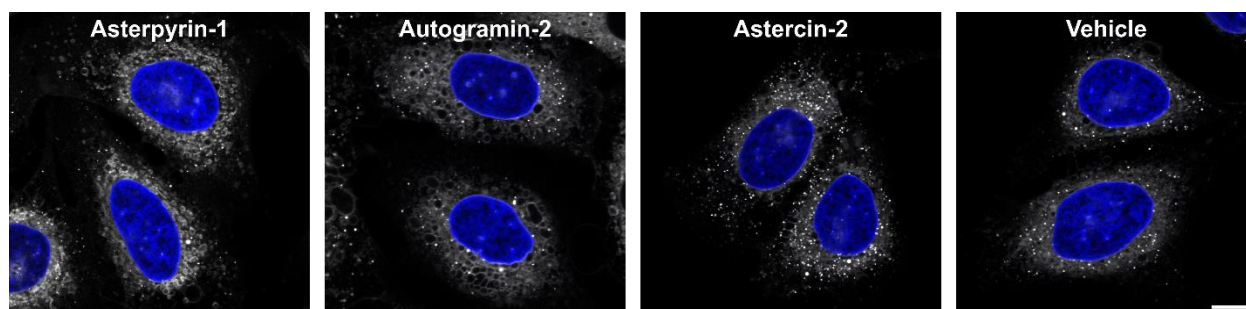


Figure 4.16 Lipid droplet staining in U2OS cells following 24 hour compound treatment at 10 μ M. Lipid droplets/neutral lipids stained with HCS LipidTOX Red (grey) and nuclei stained with Hoechst 33342 (blue). Scale bar = 10 μ m.

Consistent with what is known, LD populations were seen to be variable with a heterogeneous distribution within the same sample.^{175,176} To overcome this inherent variability, LD accumulation in Astercin-2 and vehicle treated cells was quantified by analysing the LD content of 50 individual cells in biological triplicate, using two different parameters of the cell-normalised area occupied by LDs and number of LDs per cell. The difference in normalised LD area per cell and number of LDs counted per cell were both significantly different between Astercin-2 and vehicle treated cells, with an almost four-fold and two-fold increase respectively (Figure 4.17A). Astercin-2 was also able to induce LD formation in a dose-dependent manner at concentrations as low as 1.3 μ M, however for future experiments a concentration of 10 μ M was used owing to the largest induction of LD formation (Figure 4.17B).

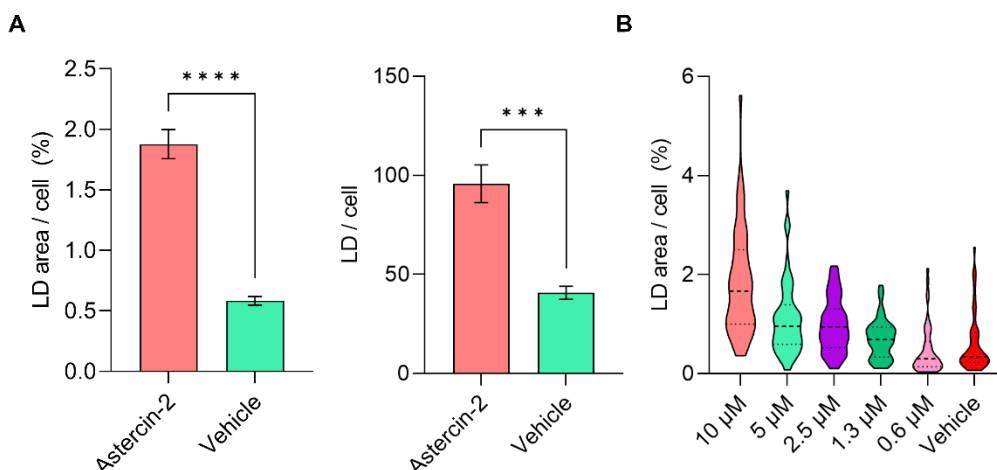


Figure 4.17. Quantification of lipid droplets in Astercin-2 treated U2OS cells. A) Quantification of LD area per cell and LD number per cell, data collected from 3 biological replicates, with each replicate analysing lipid droplets from 50 individual cells. Statistical significance determined by a Student's t-test. *** $P < 0.0007$, **** $P < 0.0001$ B) Violin plots of LD area per cell from a dose-response of Astercin-2 in U2OS cells.

Genetic knockout of Aster-C has been reported to result in accumulation of LDs in C2C12 cells under amino acid starvation.¹⁰⁰ In light of this finding, the accumulation of LDs in U2OS cells during amino acid starvation with Astercin-2 treatment was investigated. U2OS cells were subjected to amino acid starvation by incubation in EBSS at three different time points in the presence of Astercin-2 (10 μ M) or vehicle, and LDs stained with HCS LipidTOX as per prior experiments (Figure 4.18). Contradictory to the data reported in C2C12 cells, nutrient starvation alone was able to induce an accumulation of large numbers of LDs at

both 2 and 4 hour time points compared to fed cells cultured in complete media, independent of Astercin-2 treatment and consistent with the role of LDs as a buffer against lipotoxicity towards mitochondria.^{100,177} Likewise, Astercin-2 treatment resulted in an increase accumulation of LDs above that of vehicle treated cells under nutrient starvation. Prolonged starvation for 24 hours was sufficient to deplete LD stores in both Astercin-2 and vehicle treated cells, as lipids were utilised by a form of selective autophagy known as lipophagy.¹⁷⁸ The discrepancies between data obtained from knockout of Aster-C and small molecule inhibition highlights the functional consequence of loss of the whole protein, as well as the variable populations of LDs across different cell lines. Additionally, the resolution of LD imaging in the original publication was limited, and as such the accurate detection of small LDs potentially limited.

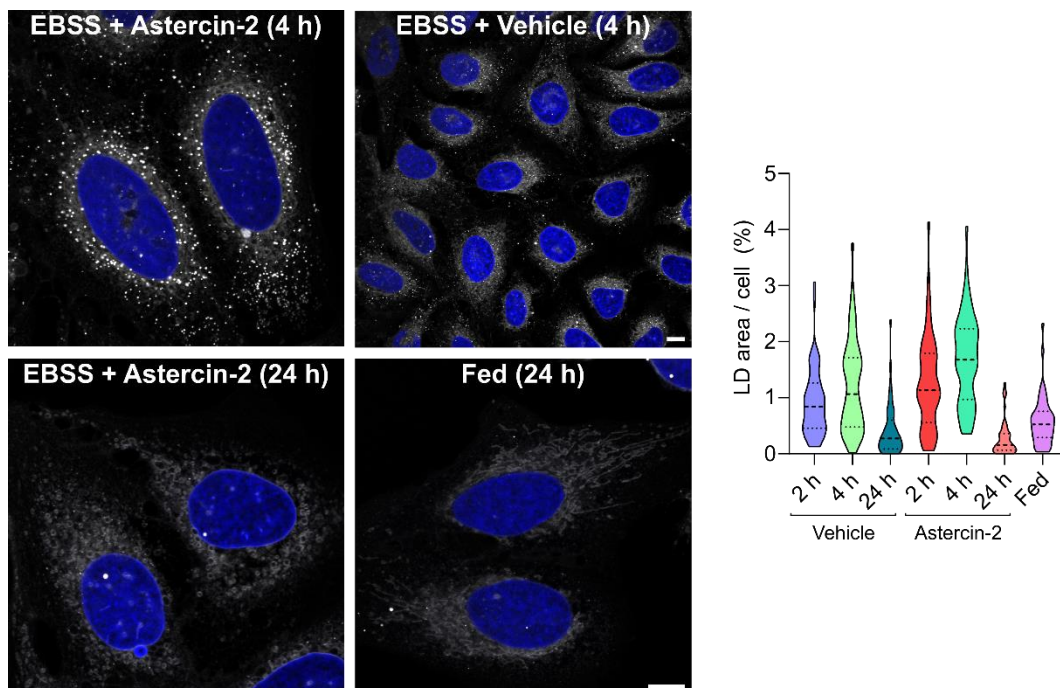


Figure 4.18 Lipid droplet staining in U2OS cells following either vehicle or Astercin-2 treatment under starved and fed conditions. Lipid droplets/neutral lipids stained with HCS LipidTOX Red (grey) and nuclei stained with Hoechst 33342 (blue). Scale bars = 10 μ m. Violin plots of lipid droplet area per cell from one biological replicate in which 50 individual cells were analysed per treatment.

In order to further probe the nature of the LD accumulation induced by Astercin-2 further experiments blocking key enzymes involved in LD biogenesis were performed. The ACAT inhibitor ATR-101 was chosen as a nanomolar inhibitor of both ACAT1 and ACAT2, anticipating that co-treatment with Astercin-2 would prevent LD accumulation if Astercin-2 treatment was causing an accumulation of ER cholesterol and thus cholesterol ester rich LDs.¹⁷⁹ U2OS cells were treated with ATR-101 (1 or 10 μ M) and Astercin-2 (10 μ M) with ATR-101 (1 or 10 μ M) for 24 hours, and lipid droplets stained with HCS LipidTOX (Figure 4.19). Treatment with ATR-101 alone gave minor decreases in the number of LDs compared to vehicle treatment, demonstrating the minor role of cholesterol esters in LDs compared to triacylglycerols in non-steroidogenic cell types.¹⁸⁰ In the presence of ATR-101 (1 μ M), Astercin-2 was unable to induce an accumulation of LDs, further supporting that the LDs accumulating in response to Astercin-2 treatment are enriched in cholesterol esters. When ATR-101 and Astercin-2 were used in combination at 10 μ M, excessive cytotoxicity was observed and cells could not be imaged. ATR-101 has been shown to be cytotoxic in an adrenocortical carcinoma cell line when co-administered with exogenous cholesterol.¹⁷⁹ The

observed toxicity in the 10 μM co-treatment could therefore be explained by Astercin-2 potentially causing an accumulation of free cholesterol at the ER that cannot be esterified due to ACAT inhibition, thus potentiating the cytotoxicity of ATR-101.

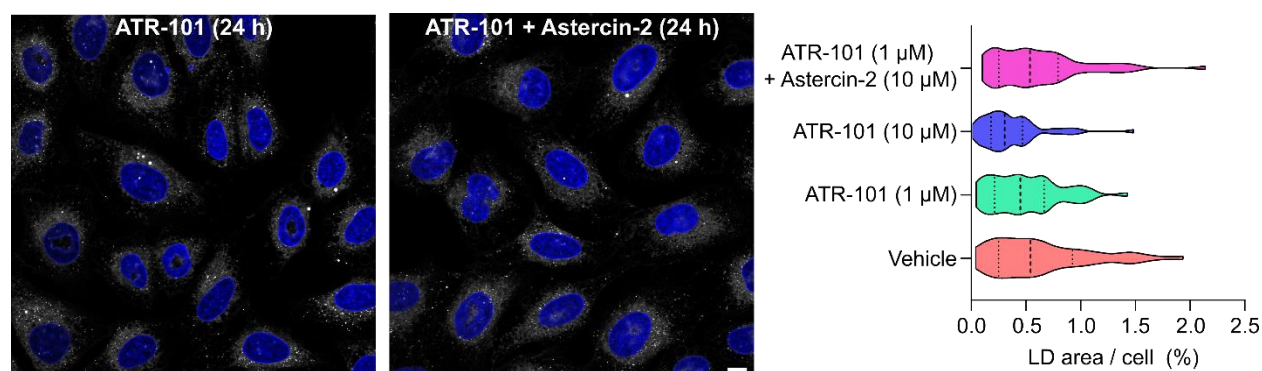


Figure 4.19 Lipid droplet staining in U2OS cells treated with ATR-101 (1 μM) and Astercin-2 (10 μM). Lipid droplets/neutral lipids stained with HCS LipidTOX Red (grey) and nuclei stained with Hoechst 33342 (blue). Scale bar = 10 μm . Violin plots of lipid droplet area per cell in U2OS cells treated with ATR-101/Astercin-2/vehicle. One biological replicate in which 50 individual cells were analysed per treatment.

In addition to studying the effect of ACAT inhibition on Astercin-2 induced LD accumulation, the effect of inhibiting DGAT1 and 2 was investigated. The DGAT enzymes are responsible for the esterification of fatty acids to produce triacylglycerols, thus DGAT inhibition should inhibit the formation of LDs. To fully inhibit both DGAT enzymes, a combination of the DGAT1 inhibitor T863 (DGATi1) and DGAT2 inhibitor PF-06424439 (DGATi2) were used.¹⁷⁷ U2OS cells were treated with both DGAT inhibitors (10 μM) and Astercin-2 (10 μM) for 24 hours, and lipid droplets stained with HCS LipidTOX (Figure 4.20). Treatment with both DGAT inhibitors completely inhibited LD formation, consistent with the critical role of triacylglycerols in LD structure, and consequently Astercin-2 was unable to cause accumulation of LDs when DGAT1/2 were inhibited.

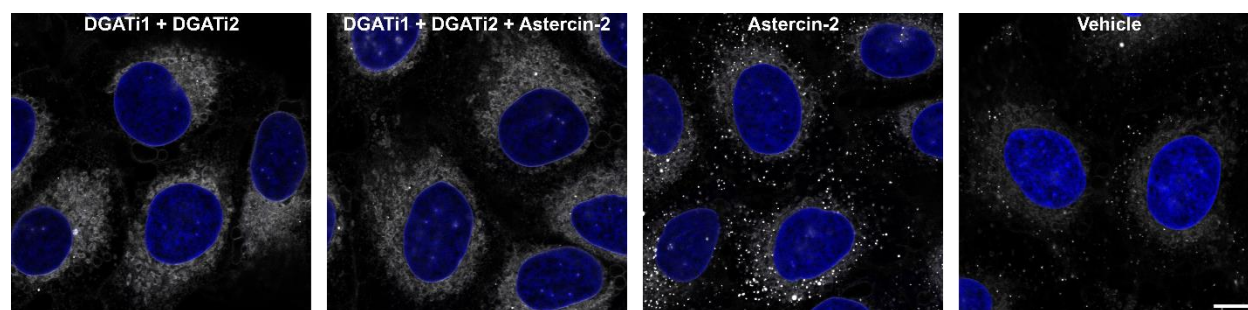


Figure 4.20 Lipid droplet staining in U2OS cells treated with DGAT inhibitors (10 μM each) and Astercin-2 (10 μM) for 24 hours. Lipid droplets/neutral lipids stained with HCS LipidTOX Red (grey) and nuclei stained with Hoechst 33342 (blue). Scale bar = 10 μm .

Aster-C has been suggested to facilitate the transport of cholesterol from mitochondria to the ER, therefore it was decided to determine whether the LD accumulation caused by Astercin-2 treatment was associated with the purported role of Aster-C in mitochondrial cholesterol transport.¹⁰¹ Initially, the localisation of Aster-C with mitochondria and lysosomes in U2OS cells was investigated under basal conditions by immunofluorescence. U2OS cells were transfected with the eGFP-Aster-C plasmid and a mCherry-ActA plasmid to visualise Aster-C and the mitochondria, with the latter plasmid consisting of a mitochondria-

targeting signal derived from the ActA protein of *Listeria monocytogens*.¹⁸¹ Signals from eGFP and mCherry were amplified using anti-eGFP and anti-mCherry antibodies respectively, and lysosomes visualised with an anti-LAMP1 (LAMP1) antibody (Figure 4.21). Under basal conditions, no clear localisation of Aster-C to either organelle was observed, with Aster-C residing mainly where the ER would be expected to occupy, mitochondria forming a filamentous network, and lysosomes appearing as puncta.

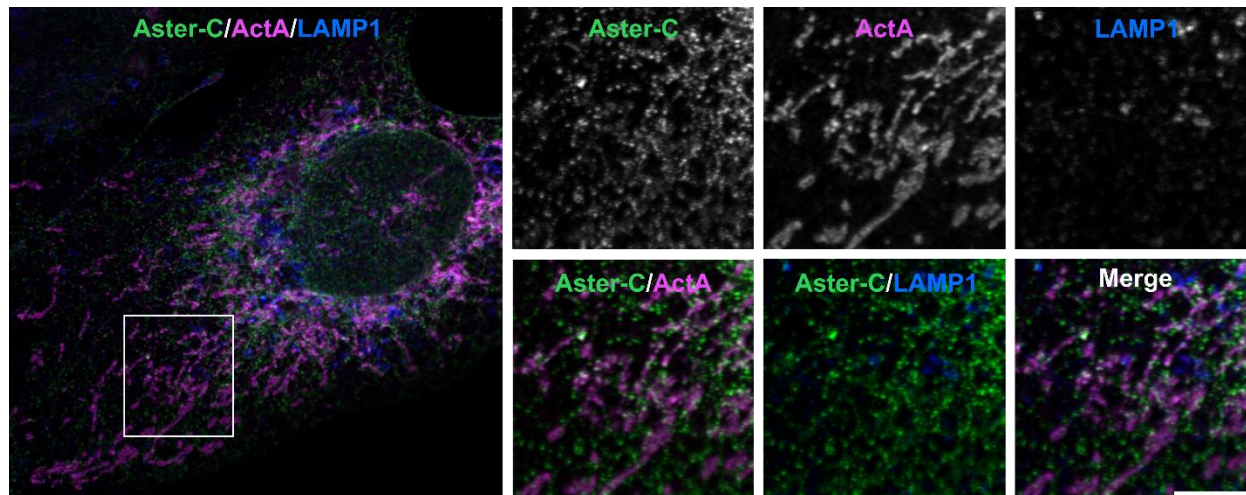


Figure 4.21 Localisation of Aster-C, mitochondria, and lysosomes in vehicle treated U2OS cells. Immunofluorescence images of U2OS cells transfected with eGFP-Aster-C (green) and mCherry-ActA (magenta, mitochondria), and lysosomes visualised with an anti-LAMP1 antibody (blue). eGFP and mCherry signals were enhanced with anti-eGFP and anti-mCherry antibodies respectively. Scale bar = 2 μ m.

The experiment was repeated in U2OS cells treated with Astercin-2 (10 μ M) for 24 hours to determine whether Aster-C inhibition would result in any changes to subcellular localisation (Figure 4.22). No significant changes in localisation were observed in response to compound treatment, though unfortunately problems in sample preparation limited the number of fully transfected cells that could be imaged. Live cell imaging could have offered a better method to investigate whether Aster-C localised with either mitochondria or lysosomes, as dynamic interactions and formation of membrane-contact sites would be more easily identified, however the low expression of the eGFP-Aster-C construct hindered this approach.

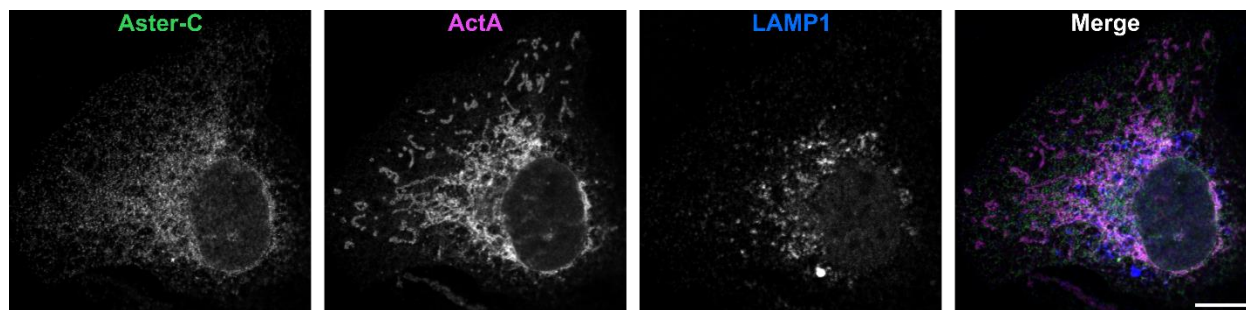


Figure 4.22 Localisation of Aster-C, mitochondria, and lysosomes in Astercin-2 treated U2OS cells. Immunofluorescence images of U2OS treated with Astercin-2 (10 μ M for 24 hours) and transfected with eGFP-Aster-C (green) and mCherry-ActA (magenta, mitochondria), and lysosomes visualised with an anti-LAMP1 antibody (blue). eGFP and mCherry signals were enhanced with anti-eGFP and anti-mCherry antibodies respectively. Scale bar = 10 μ m.

The combination of LD staining and immunofluorescence to investigate whether LDs were associated with mitochondria also proved unsuccessful, with the mounting media significantly decreasing the LipidTOX signal. Accordingly, alternative methods to visualise the localisation of mitochondria and LDs were pursued. Mitochondria in live U2OS were efficiently labelled using either CellLight™ Mitochondria-GFP or MitoTracker Deep red, therefore fixation with PFA and LD staining with HCS LipidTOX was attempted with both methods. Unfortunately, both approaches were observed to result in disruption of normal mitochondrial morphology (Figure 4.23), with the mitochondria displaying spherical and globular morphology rather than the expected filamentous distribution and smaller size (observed in IF imaging, figures 4.21 and 4.22). The disruption of normal mitochondrial morphology could be explained by minor differences in the fixation procedure between LipidTOX and immunofluorescence samples, or due to LipidTOX itself, though further experiments would be required for verification. These problems could be averted by use of live cell imaging using a live cell compatible LD dye such as BODIPY 493/503 or IF visualisation of LDs.

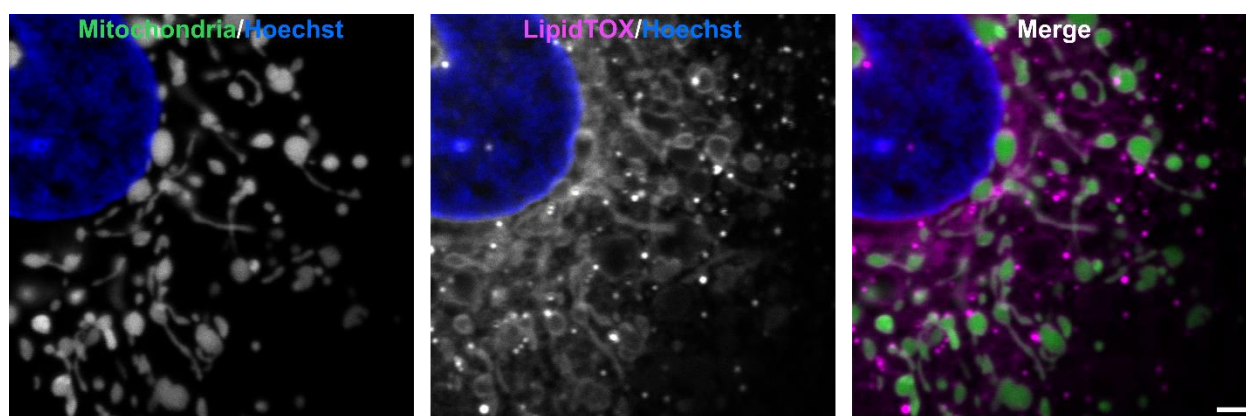


Figure 4.23 Co-staining of nuclei (Hoechst 33342, blue), mitochondria (CellLight™ Mitochondria-GFP, green), and lipid droplets/neutral lipids (HCS LipidTOX red, magenta) in fixed U2OS cells. Scale bar = 2 μ m.

4.8 Discussion of Aster inhibitor biology

The biological characterisation of Asterpyrin-1 and Astercin-2 in cellular models revealed the induction of two distinctly different phenotypes, arising from inhibition of two closely related proteins. Inhibition of Aster-A by Asterpyrin-1 inhibited starvation-induced autophagy over short time periods, as per the known Aster-A inhibitor Autogramin-2, with treatments over extended time periods causing an accumulation of cholesterol in lysosomes as well as recruitment of LC3-II. Conversely, inhibition of Aster-C by Astercin-2 induced no changes in free cholesterol but instead resulted in a significant accumulation of cholesterol ester rich lipid droplets with minor changes in levels of LC3-II. Whilst little research into the effects of genetic or small molecule manipulation of Aster-A or Aster-C has been performed specifically focussing on free cholesterol and cholesterol esters, the findings from Asterpyrin-1 and Astercin-2 have been largely consistent with what has been reported.

Inhibition of autophagy has been reported to induce accumulation of both free cholesterol as well as LDs using both KO cell lines and small molecule autophagy inhibitors.^{174,178} Similar phenotypes are also observed in cells featuring NPC1 mutations, in which accumulation of cholesterol and lipids occur in late endosomes and lysosomes along with large accumulations of LC3-II due to impaired autophagic degradation.¹⁷⁴ Prolonged treatments with either Asterpyrin-1 or Autogramin-2 replicate the lysosomal accumulation of cholesterol arising from NPC1 mutations and autophagy inhibition, however no associated

accumulation of LDs was observed. Together, this suggests a function of Aster-A independent of its role in regulating autophagosome biogenesis. As cholesterol is accumulating in lysosomes it would be logical to investigate whether Aster-A also plays a role in lysosomal cholesterol trafficking. Aster-B has been reported to play a key role in lysosomal cholesterol trafficking, interacting with NPC1 to tether ER-endosomal membrane contact sites in a cholesterol-dependent manner, mediating transport of cholesterol from the lysosome.¹⁸² Accordingly, knockdown of Aster-B also resulted in a minor increase in staining of free cholesterol by filipin, albeit to a lesser extent than in NPC-depleted cells. A similar function could be plausible for Aster-A, however this was not identified in the highlighted study. Chemical inhibition of Aster-B produced no increase in filipin staining, supporting the identified scaffolding effect of Aster-B in lysosomal cholesterol transport, suggesting that Aster-A might instead have a more direct role in lysosomal cholesterol trafficking, though it should be noted that the Aster-B inhibitor used had known off-target effects.^{110,182} Additionally, the elevated levels of LC3 lipidation arising from inhibition of Aster-A requires further investigation to determine whether it corresponds to an induction of autophagy and how this is occurring throughout prolonged autophagy inhibition.

Similar to the report that Aster-C KO resulted in LD accumulation during amino acid starvation due to defective lipophagy, inhibition of Aster-C by Astercin-2 was able to induce an accumulation of LDs during amino acid starvation, but this effect was also observed under fed conditions.¹⁰⁰ These findings were presented in the context that the effects were independent of the role of Aster-C in cholesterol trafficking, indicating the inhibition of the cholesterol transport activity of Aster-C results in LD accumulation by a separate mechanism. Inhibition of ACAT1/2 was sufficient to prevent LD accumulation induced by Astercin-2 treatment, suggesting that Aster-C inhibition is causing an accumulation of free cholesterol at the ER. Attempts to further study the mechanism of this LD accumulation proved unsuccessful, but further work would help elucidate whether Aster-C could be serving as an ER-LD tethering protein.⁸⁷

Whether Aster-C is responsible for transporting LD-derived cholesterol to an unknown organelle, or for transporting cholesterol between the ER and another organelle remains unclear. Loss of the STP STARD1, responsible for transporting cholesterol from the outer mitochondrial membrane to inner mitochondrial membrane, produces a similar phenotype of accumulation of CEs in LDs.¹⁸³ Considered alongside data suggesting Aster-C has a key role in cholesterol transport between mitochondria and the ER, preliminary experiments were performed to study the localisation of Aster-C with mitochondria in the presence of Astercin-2 treatment, however these proved unsuccessful due to several factors.¹⁰¹ In spite of this, the involvement of mitochondria in the observed LD accumulation remains the most promising route for future investigation.

Summary and conclusions

In order to address the poor availability of tool compounds targeting sterol transport proteins, a design strategy to access a screening collection enriched in hits against sterol transport proteins was developed. By fusing a primary steroidal scaffold to a series of heterocyclic scaffolds, 65 sterol-inspired compounds were synthesised for use in screening against STPs. Screening the compound collection against the Aster proteins as model STPs in DSF, FP, and FRET based assays gave a hit rate of 9% for the sterol-inspired compounds. This resulted in the identification and validation of two new chemotypes of Aster-A inhibitors in addition to the most potent and selective inhibitor of Aster-C to date, (-)-Astercin-1. Subsequent SAR studies around the Astercin series yielded the optimised analogue Astercin-2, demonstrating improved potency against Aster-C and an improved window of selectivity over both Aster-A and Aster-B. The individual enantiomers of the pyrazolopyrimidine-fused chemotype of Aster-A inhibitors were synthesised, from which the potent Aster-A inhibitor Asterpyrin-1 was identified.

Finally, the suitability of Asterpyrin-1 and Astercin-2 as potential tool compounds to study Aster-related biology was studied. Both compounds were utilised to investigate their effects on the levels and localisation of free cholesterol and cholesterol esters, as well as their ability to modulate autophagy and levels LC3 lipidation. In doing so, two distinct but opposing phenotypes were observed to arise from the selective inhibition of Aster-A and Aster-C. Inhibition of Aster-A by Asterpyrin-1 produced significant accumulation of cholesterol in lysosomes and direct recruitment of LC3 to the lysosomal membrane. On the other hand, Aster-C inhibition by Astercin-2 resulted in a large accumulation of LDs enriched in esterified cholesterol (Figure 5).

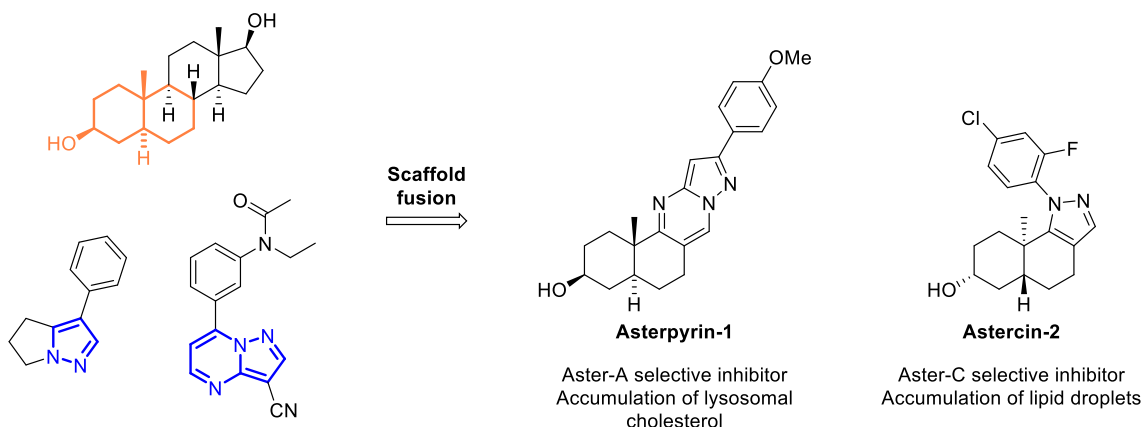


Figure 5 Identification of Aster-A and Aster-C selective inhibitors, Asterpyrin-1 and Astercin-2, by fusion of a primary sterol-inspired scaffold to secondary heterocyclic scaffolds and their main cellular phenotypes.

Future work

The success of the sterol-inspired compound collection in affording new inhibitors of Aster-A and Aster-C, in addition to demonstrating the use of these compounds in cellular contexts to assist in elucidating Aster related biology, warrants the expansion of this technique by incorporating other steroidal primary fragments for fusion to both heterocyclic and spirocyclic secondary fragments. Accordingly, work in the group has begun on synthesising sterol-inspired compounds featuring testosterone, estrogen, and bile acid inspired steroidal primary fragments (Figure 6A). Additionally, sterol building blocks featuring additional oxidation could be synthesised and incorporated into the compound collections or analogues functionalised at a late stage, representing a subset of oxysterol-inspired compounds (Figure 6B). SAR of Astercin-1 revealed a possible attachment site for linkers which could allow for the development of bifunctional degraders of Aster-C. Preliminary work has commenced, aiming to synthesise proteolysis targeting chimeras (PROTACs) of Astercin-1 which would allow for the side-by-side comparison of Aster-C inhibition and degradation in biological studies (Figure 6C)

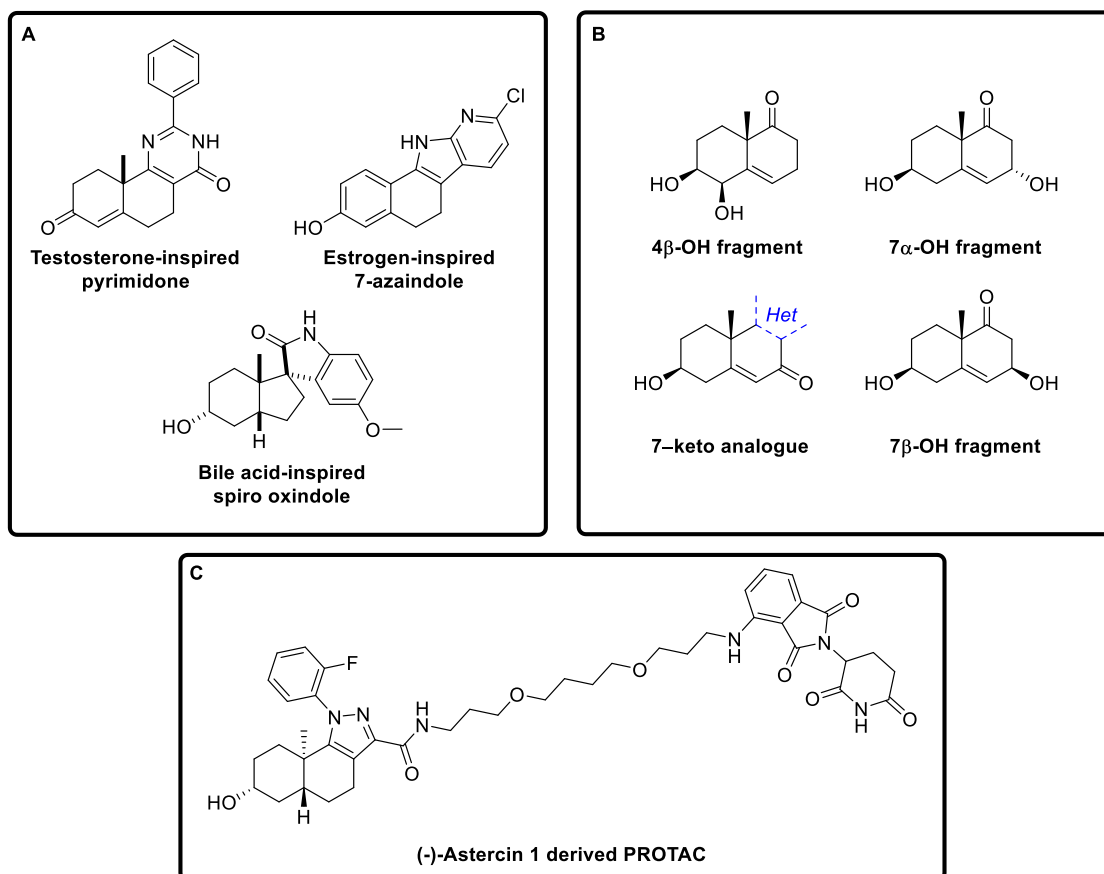


Figure 6 Future synthetic work related to the sterol-inspired compound collection. **A)** Sterol inspired compounds derived from testosterone, estrogen, and bile acid inspired fragments synthesised in the Laraia lab. **B)** Oxysterol-inspired primary steroidal fragments and oxidised analogues accessed by late-stage functionalisation. **C)** Representative structure of an (-)-Astercin-1 derived PROTAC synthesised in the Laraia lab.

Work in the lab has also begun on expressing, purifying, and assay development for a number of other STPs from the ORP and STARD families. Screening of the sterol-inspired compound collection against these proteins will occur in due course, with the anticipation that selective inhibitors can be identified, particularly against STPs with no currently known ligands. This will additionally allow a more complete picture of inter-family STP selectivity to be determined for reported STP inhibitors and further gauge their suitability as tool compounds. In addition to the remaining non-vesicular STPs, it would also be of interest to develop assays screening against NPC1 and NPC2 given the known association of vesicular and non-vesicular sterol trafficking. The implementation of additional assays directly focussing on cholesterol localisation, such as an assay utilising filipin staining, would also assist in identifying both steroidal and non-steroidal hits capable of modulating cholesterol homeostasis.

Further experiments involving Asterpyrin-1 and Astercin-2 after investigation of their wider STP selectivity would be of great interest. Assessing lysosomal proteolytic degradation in the presence of both compounds would immediately assist in elucidating whether the observed cholesterol/cholesterol ester accumulations are occurring due to impaired lysosomal function. This could be monitored using assays such as the DQ-red-BSA assay which utilises a fluorescent bovine serum albumin (BSA) construct that will only fluoresce when hydrolysed by proteolytic enzymes.¹⁰⁰ Determining whether either compound directly interferes with SREBP processing, and therefore cholesterol homeostasis, would be paramount and could be achieved through western blotting to detect SREBP2 cleavage or through a specific reporter-gene assay. Investigating mitochondrial function in the presence of Astercin-2 would further support its role in transporting cholesterol between the ER and mitochondria. Mitochondrial oxygen consumption can be monitored using a Seahorse analyser, and implementing an experiment in Astercin-2 treated cells would be simple to perform. Though not presented in this thesis, preliminary experiments into cell viability of Astercin-2 treated cells utilising the alamarBlue assay has been performed. These experiments suggested that Astercin-2 was interfering with the reduction of the resazurin-based dye, further supporting a role of Aster-C in correct mitochondrial function and supporting continued research in this area.

Experimentals

Biology Procedures

Differential scanning fluorimetry

Differential scanning fluorimetry experiments were performed in a buffer composed of 20 mM HEPES pH 7.5, 300 mM NaCl, and 2 mM DTT in Milli-Q water.

Aster-A, Aster-B and Aster-C ASTER domains were incubated (protein concentration of 0.5 mg/mL) for 30 minutes at room temperature in the presence of compounds to be tested (50 μ M concentration). Subsequently, SYPRO orange (Thermo Fisher) was added for a final concentration of 5x SYPRO orange and the solutions were transferred to a 384-well plate (LightCycler® 480 Multiwell Plate 384, white) with a final volume of 10 μ L. The fluorescence intensity was measured in a Roche LightCycler 480 II with an initial incubation at 25 °C for 5 minutes followed by acquisition steps of 0.2 °C up to 95 °C, incubating for 5 seconds at each step. Melting temperatures were calculated with the Roche TSA analysis program.

Fluorescence polarisation

Fluorescence polarization experiments were performed at room temperature in a buffer composed of 20 mM HEPES pH 7.5, 300 mM NaCl, 0.01% (vol/vol) Tween-20, 0.5% glycerol and 2 mM DTT in a final volume of 30 μ L in black, flat-bottom, non-binding 384-well plates (Corning). For competition experiments, 20 nM 22-NBD-cholesterol was mixed with 1 μ M of Aster-A, -B or 0.5 μ M Aster-C ASTER domains and incubated with desired concentrations of screening compounds for 20 minutes. The fluorescence polarization signal was measured using a Spark Cyto multimode microplate reader (Tecan) with filters set at 460 ± 10 nm for excitation and at 535 ± 10 nm for emission. The data was analysed using GraphPad Prism 9.4.1. Measured mP values were normalized setting 100% inhibition as the averaged FP signal from the protein + fluorophore control well and 0% as the averaged FP signal from the fluorophore control well. Curves were fitted to the normalized data via non-linear regression to allow the determination of IC₅₀ values.

Vesicle preparation for sterol transfer assay

Stock solutions were prepared of the required lipids. A stock solution of DOPC in chloroform (10 mg mL⁻¹) was prepared from a 25 mg mL⁻¹ solution (Avanti Polar Lipids, #850375C). Stock solutions of 23-(dipyrrometheneboron difluoride)-24-norcholesterol (TopFluor cholesterol, Avanti Polar Lipids, #810255) and *N*-(lissamine rhodamine B sulfonyl)-1,2-dihexadecanoyl-*sn*-glycero-3-phosphoethanolamine (ammonium salt) (*N*-Rh-DHPE, Invitrogen, #L1392) were prepared in methanol to a final concentration of 100 μ M. Stock solutions were mixed in a molar ratio of 99:0.5:0.5 of DOPC:TF-Chol:Rh-DHPE for the donor vesicles or DOPC alone for the acceptor vesicles, to a final volume of 1 mL. Evaporation of the solvent under a stream of nitrogen, followed by drying under vacuum overnight afforded the dried lipid films. The lipid films were hydrated in a buffer of 20 mM Hepes pH 7.5, 300 mM NaCl, and 2 mM DTT to a final concentration of 60 μ M. Solutions of the lipid films were vortexed extensively until full hydration was observed and sonicated for 5 minutes in a 40 °C water bath, followed by five freeze-thaw cycles (-196 °C → 40 °C). Homogenous unilamellar vesicles were obtained by extrusion 21 times through a polycarbonate membrane (0.1 μ m pore size, Avanti Polar Lipids) at 40 °C. Solutions were kept on ice and used on the same day as preparation.

Microplate-based cholesterol transfer assay

In a non-binding clear-bottom 96-well plate (Greiner Bio-one, cat# 655906), wells were prepared as follows.

For compound-containing wells, the compound and desired ASTER domain were incubated at room temperature for 30 minutes at an intermediate concentration twice that of the desired assay concentration (i.e. 20 μ M compound and 2.0 μ M protein). After incubation, acceptor liposomes were added and the well contents mixed via pipette. Subsequently, an equal volume of donor liposomes were added (final concentration of 16 μ M donor and acceptor liposomes) and the well contents mixed rapidly via pipette before measuring the FRET signal of the well. Control wells included: acceptor liposomes alone, donor liposomes alone, donor + acceptor liposomes, donor + acceptor liposomes + protein + vehicle.

Fluorescence intensity measurements were performed in a Tecan Spark Cyto plate reader at 25 °C, measuring from the bottom at 10 second intervals over a period of 10 minutes. The excitation filter was set at 488 \pm 20 nm and the emission filter set at 590 \pm 20 nm. Data was normalized to I_0 of the donor + acceptor control and plotted in GraphPad Prism 5.

Cell culture and transfection

U2OS cells and HeLa Kyoto cells were cultured in DMEM (Sigma) supplemented with 10% v/v FBS, 1% non-essential amino acids, and 1% penicillin streptomycin at a temperature of 37 °C and 5% CO₂. Transfection of DNA constructs was performed using X-tremeGENE HP DNA transfection reagent according to manufacturer's instructions. *In short: DNA and the transfection reagent were mixed in the desired ratio in Opti-MEM, incubated at room temperature for 15 minutes, then added to cells and incubated at 37 °C and 5% CO₂ for approx. 18 hours.* Transient transfection with CellLight Mitochondria-GFP, BacMam 2.0 was performed according to manufacturer's instructions, using 20 particles per cell.

Small molecule inhibitors

Small molecule tool compounds were either purchased from commercial suppliers or synthesised when possible. Autograin-2 and AI-11 were synthesised according to literature procedures.^{98,110} ATR-101 was purchased from Axon Medchem (cat. no. 2960), PF-06424439 was purchased from MedChemExpress (cat. no. HY-108341A), T863 was purchased from MedChemExpress (cat. no. HY-31119), U18666A was purchased from Cayman Chemicals (cat. no. 10009085)

Antibodies

Mouse anti- β -actin: WB – 1:10,000 (Sigma, A2228)

Rabbit anti-LC3B: WB – 1:1000 (Cell Signalling Technology, #2775)

Rabbit anti-Aster-C: WB – 1:1000 (Novus Biologicals, NBP1-90559)

Goat anti-Rabbit IgG (H+L), HRP: WB – 1:10,000 (Thermo Fisher, 31460)

Goat anti-Mouse IgG (H+L), HRP: WB – 1:10,000 (Thermo Fisher, 31430)

Mouse anti-LAMP1: IF – 1:100 (Cell Signalling Technology, #15665)

Rabbit anti-GAL3: IF – 1:200 (Cell Signalling Technology, #87985)

Rabbit anti-EEA1: IF – 1:50 (Cell Signalling Technology, #87985)

Rabbit anti-LC3: IF – 1:50 (MBL, PM036)

Rabbit anti-mCherry: IF – 1:200 (Thermo Fisher, PA5-34974)

Chicken anti-GFP: IF – 1:500 (Thermo Fisher, A10262)

Goat anti-Rabbit IgG (H+L), CY3: IF – 1:200 (Jackson ImmunoResearch, 111-165-003)

Goat anti-Mouse IgG (H+L), Alexa Fluor 568: IF – 1:200 (Thermo Fisher, A-11004)

Goat anti-Chicken IgY (H+L), Alexa Fluor 488: IF – 1:200 (Thermo Fisher, A-11039)

Goat anti-Mouse IgG (H+L), Alexa Fluor 647: IF – 1:200 (Thermo Fisher, A21235)

Immunoblotting

U2OS or HeLa cells were seeded into 6-well plates at a density 200,000 cells in 2 mL of complete media and the plates incubated at 37 °C and 5% CO₂ overnight. The following day, media was aspirated and replaced by media (complete media for fed conditions, EBSS for starvation conditions) containing the desired compounds and left for the desired treatment time. Cells were lysed with ice-cold lysis buffer (20 mM Tris-HCl pH 8, 300 mM KCl, 10% glycerol, 0.25% Nonidet P-40, 0.5 mM EDTA, 1 mM PMSF and 1x cOmplete protease inhibitor (Roche)) and passed through a needle 6 times, and cleared by centrifugation. Lysate protein concentration was determined using Bio-Rad Protein Reagent (Bio-Rad) and normalised. Samples were mixed with 4X sample buffer (containing 2-mercaptoethanol) and heated at 95 °C for 10 minutes. Proteins were separated by SDS-PAGE on a polyacrylamide gel (4% stacking gel, 15% resolving gel), running at 100 V until proteins had entered the resolving gel and then at 120 V until completion. Proteins were transferred to a 0.2 µm nitrocellulose membrane using the Trans-Blot Turbo transfer system (Bio-Rad) at 2.5 A/25 V for 7 minutes, transfer efficiency checked via ponceau staining, and membranes blocked with 5% milk in TBST. Membranes were washed with TBST (3 x 5 minutes) and then incubated with solutions of primary antibody in 5% BSA at 4 °C overnight or at room temperature for 1 hour (β-actin). After washing with TBST (3 x 5 minutes), membranes were incubated with the secondary antibody in 5% milk in TBST for 1 hour at room temperature, after which membranes were visualised using chemiluminescence and imaged on a ChemiDoc MP imaging system.

Fluorescence microscopy

Immunofluorescence imaging was performed on a Leica SP8 FALCON inverted confocal system (Leica Microsystems) equipped with a HC PL APO 63x/1.40 oil immersion lens and a temperature-controlled hood maintained at 37 °C and 5% CO₂. Filipin/Hoechst were excited using a 405 nm Diode laser, and eGFP/Alexa488, mCherry/Alexa568/Cy3/LipidTOX, and Alexa647/DRAQ5 fluorescence were excited using a tuned white light laser. Scanning was performed in line-by-line sequential mode.

Filipin Staining

Note: filipin staining were performed in the dark, protecting samples from light throughout experiments

8-well chamber slides were seeded with 2×10^4 U2OS cells and incubated at 37 °C and 5% CO₂ overnight. The following day, cells were incubated with the compounds or vehicle (0.1% DMSO) for the indicated time. Cells were fixed using 3% PFA in PBS for 30 minutes at room temperature, and then washed three times with PBS containing 1.5 mg/mL glycine. Cells were stained with filipin (0.05 mg/mL filipin in PBS + 10% FBS) for 30 minutes at 37 °C and then 90 minutes at room temperature. The cells were then washed three times with PBS for 5 minutes each, with the second wash containing DRAQ5 (1 µM from 5 mM stock) to stain the nuclei.

LipidTOX staining

8-well chamber slides were seeded with 1×10^4 U2OS cells and incubated at 37 °C and 5% CO₂ overnight. The following day, cells were incubated with the compounds or vehicle (DMSO) for 24 hours. Cells were fixed using 3% PFA in PBS for 20 minutes at room temperature, and then washed three times with PBS containing 1.5 mg/mL glycine. Cells were stained with LipidTOX neutral red (1:1000 dilution in PBS) for 30 minutes at room temperature. The cells were then washed three times with PBS for 5 minutes each, with the second wash containing Hoechst 33342 (1:2000 dilution) to stain the nuclei.

For each treatment condition, five images were taken per well allowing 50 cells to be selected and used for quantification of lipid droplets in ImageJ Fiji.

Immunofluorescence in combination with filipin staining:

U2OS cells were grown on glass coverslips in six-well plates, seeding 2×10^5 cells in 1.5 mL of media and incubated at 37 °C and 5% CO₂ overnight. The following day, any wells requiring transfection were transfected as per the outlined procedure (if transfection was not required, this step was skipped), and treated with the desired compound or vehicle the day after. Upon completion of compound treatments, cells were fixed with 3% PFA in PBS for 30 minutes at room temperature, and washed three times with PBS containing 1.5 mg/mL glycine. Cells were stained with filipin (0.05 mg/mL in PBS + 10% FBS) for 30 minutes at 37 °C, and then incubated with solutions of primary antibodies in the filipin solution for 2 hours at room temperature. The coverslips were washed three times with PBS before incubating with solutions of the fluorescent secondary antibodies for 30 minutes at room temperature. The coverslips were washed three times with PBS before mounting onto glass slides.

Immunofluorescence without filipin staining:

U2OS cells were grown on glass coverslips in six-well plates, seeding 2×10^5 cells in 1.5 mL of media and incubated at 37 °C and 5% CO₂ overnight. The following morning, any wells requiring transfection were transfected as per the outlined procedure (if transfection was not required, this step was skipped), and treated with the desired compound or vehicle either the same evening or the following day. Upon completion of compound treatments, cells were fixed with 4% PFA in PBS for 10 minutes, and washed three times with PBS containing 1.5 mg/mL glycine. Cells were permeabilised with 0.25% TX-100 in PBS for 5 minutes at room temperature, then washed three times with PBS for 5 minutes each. Cells were blocked by incubation in 5% donkey serum in PBS for 30 minutes at room temperature, and incubated with solutions of primary antibodies

in blocking buffer for 1 hour at room temperature. The coverslips were washed three times with PBS before incubation with solutions of the fluorescent secondary antibodies for 30 minutes at room temperature. The coverslips were washed three times with PBS before mounting onto glass slides.

Chemical modelling in Maestro

Modelling of the Astercin ester **3.27** and generation of the “major” and “minor” conformations was performed in the software Maestro. Ester **3.27** was drawn in 2D with set stereochemistry and 50 conformations were generated from the “Macromodel” programme by the “Conformational Search” application.

Cheminformatics library analysis

Cheminformatic analysis was performed on the 65-member sterol-inspired compound library in addition to a curated selection of steroids. Principle moment of inertia (PMI) analysis of compound libraries was performed using the open-access Lead Likeness and Molecular Analysis (LLAMA)^a web tool. PMI I1 and I2 coordinates calculated with LLAMA were used to generate PMI plots for the sterol-inspired, steroid, and natural product libraries, by plotting as a triangular graph using GraphPad Prism.

Natural product-likeness scores, as described by Ertl *et al*^b, were calculated for the sterol-inspired, steroid, natural product, and drug libraries using the Natural-Product-Likeness scoring system standalone java package.^c NP-likeness scores were extracted from the output .sdf files, binned into groups of 0.25 between -3 and +3, expressed as a percentage of total compounds, and plotted in Microsoft Excel.

SMILES of compounds were generated with Canvas (2018-2, Schrödinger).

Natural product library: The natural product compound library used for calculation of NP-likeness scores consisted of the National Cancer Institute “Natural Products Set V” compounds (<https://wiki.nci.nih.gov/display/NCIDTPdata/Compound+Sets>, accessed February 2021). For PMI analysis, a random selection of 20% of the compound set was performed using Canvas and exported as a separate .sdf file for use.

Steroid library: The steroid library used for calculation of NP-likeness scores consisted of compounds classified as “steroids” in the PubChem database^d. Before use in analysis, the 5927 compounds were subjected to quality control, which included removing duplicate entries, invalid SMILES strings, and non-steroidal compounds, resulting in a final collection of 4944 compounds.

Approved-drug library: The library of approved drugs used for calculation of NP-likeness scores was obtained from the DrugBank database.^e

Curated steroid library: For PMI analysis a smaller curated library of 46 representative steroidal compounds was created. This library encompasses a selection of endogenous mammalian, plant, marine, and fungal steroids in addition to a number of synthetic steroidal drugs. Compounds were randomly chosen from the KEGG PATHWAY Database^f, the modified PubChem steroid collection, and DrugBank.

Cheminformatics references

- a) Colomer, I.; Empson, C. J.; Craven, P.; Owen, Z.; Doveston, R. G.; Churcher, I.; Marsden, S. P.; Nelson, A. A Divergent Synthetic Approach to Diverse Molecular Scaffolds: Assessment of Lead-Likeness Using LLAMA, an Open-Access Computational Tool. *Chem. Commun.* **2016**, 52 (45), 7209–7212.
- b) Ertl, P.; Roggo, S.; Schuffenhauer, A. Natural Product-Likeness Score and Its Application for Prioritization of Compound Libraries. *J. Chem. Inf. Model.* **2008**, 48 (1), 68–74.
- c) Vanii Jayaseelan, K.; Moreno, P.; Truszkowski, A.; Ertl, P.; Steinbeck, C. Natural Product-Likeness Score Revisited: An Open-Source, Open-Data Implementation. *BMC Bioinformatics* **2012**, 13 (1), 106.
- d) Kim, S.; Chen, J.; Cheng, T.; Gindulyte, A.; He, J.; He, S.; Li, Q.; Shoemaker, B. A.; Thiessen, P. A.; Yu, B.; Zaslavsky, L.; Zhang, J.; Bolton, E. E. PubChem in 2021: New Data Content and Improved Web Interfaces. *Nucleic Acids Res.* **2021**, 49 (D1), D1388–D1395.
- e) Wishart, D. S.; Feunang, Y. D.; Guo, A. C.; Lo, E. J.; Marcu, A.; Grant, J. R.; Sajed, T.; Johnson, D.; Li, C.; Sayeeda, Z.; Assempour, N.; Iynkkaran, I.; Liu, Y.; Maciejewski, A.; Gale, N.; Wilson, A.; Chin, L.; Cummings, R.; Le, D.; Pon, A.; Knox, C.; Wilson, M. DrugBank 5.0: A Major Update to the DrugBank Database for 2018. *Nucleic Acids Res.* **2018**, 46 (D1), D1074–D1082.
- f) Kanehisa, M.; Furumichi, M.; Sato, Y.; Ishiguro-Watanabe, M.; Tanabe, M. KEGG: Integrating Viruses and Cellular Organisms. *Nucleic Acids Res.* **2021**, 49 (D1), D545–D551.
<https://doi.org/10.1093/nar/gkaa970>.

SMILES and NP-likeness scores of sterol-inspired compounds

Entry	SMILES	NP-likeness score
1	<chem>C1C[C@H](O)C[C@@H]([C@]12C)CCc3c2[nH]c4c3cccc4</chem>	0.8088
2	<chem>C1C[C@H](O)C[C@@H]([C@]12C)CCc3c2[nH]c4c3cc(cc4)OC</chem>	0.8176
3	<chem>C1C[C@H](O)C[C@@H]([C@]12C)CCc3c2[nH]c4c3cccc4F</chem>	0.4735
4	<chem>C1C[C@H](O)C[C@@H]([C@]12C)CCc3c2[nH]c4c3cc(Br)cc4</chem>	0.7709
5	<chem>C1C[C@H](O)C[C@@H]([C@]12C)CCc3c2[nH]c4c3cc(F)cc4</chem>	0.4708
6	<chem>C1C[C@H](O)C[C@@H]([C@]12C)CCc3c2[nH]c4c3c(Cl)cc(Cl)c4</chem>	0.4555
7	<chem>C1C[C@H](O)C[C@@H]([C@]12C)CCc3c2[nH]c4c3cc(Cl)cc4</chem>	0.6158
8	<chem>C1C[C@H](O)C[C@@H]([C@]12C)CCc3c2[nH]c4c3cc(Br)cn4</chem>	0.5252
9	<chem>C1C[C@H](O)C[C@@H]([C@]12C)CCc3c2[nH]c4c3cccn4</chem>	0.497
10	<chem>C1C[C@H](O)C[C@@H]([C@]12C)CCc3c2[nH]c4c3ccc(n4)Cl</chem>	0.3657
11	<chem>O=C(C)O[C@@H](CC1)C[C@@H]([C@]12C)CCCC(=O)N2</chem>	0.9949
12	<chem>C1C[C@H](O)C[C@@H]([C@]12C)CCc3c2nc4c(c3)cccc4</chem>	0.6512
13	<chem>C1C[C@H](O)C[C@@H]([C@]12C)CCc3c2nc4c(c3)cc(Cl)cc4</chem>	0.4749
14	<chem>C1C[C@H](O)C[C@@H]([C@]12C)CCc3c2nc4c(c3)cc(OC)c(c4)OC</chem>	0.7029
15	<chem>C1C[C@H](O)C[C@@H]([C@]12C)CCc3c2nc4c(c3)ccc(Cl)c4</chem>	0.4736
16	<chem>C1C[C@H](O)C[C@@H]([C@]12C)CCc3c2nc4c(c3)c(Cl)ccc4</chem>	0.4379
17	<chem>C1C[C@H](O)C[C@@H]([C@]12C)CCc3c2nc4c(c3C)cc(Cl)cc4</chem>	0.4703
18	<chem>C1C[C@H](O)C[C@@H]([C@]12C)CCc3c2nc4c(cc(Cl)cc4)c3-c5ccccc5F</chem>	0.0749
19	<chem>C1C[C@H](O)C[C@@H]([C@]12C)CCc3c2nc4c(c3)ccc(F)c4</chem>	0.3457
20	<chem>C1C[C@H](O)C[C@@H]([C@]12C)CCc3c2nc4c(cc(Cl)cc4)c3-c5ccccc5</chem>	0.3304
21	<chem>C1C[C@H](O)C[C@@H]([C@]12C)CCc3c2nc4c(cccc4)c3-c5ccccc5</chem>	0.4605
22	<chem>C1C[C@H](O)C[C@@H]([C@]12C)CCc3c2nc4c(c3)ccc(c4)OC</chem>	0.6595
23	<chem>C1C[C@H](O)C[C@@H]([C@]12C)CCc3c2nc4c(cccc4)c3-c5ccc(F)cc5</chem>	0.2154
24	<chem>C1C[C@H](O)C[C@@H]([C@]12C)CCc3c2nc4c(c3)cc(F)cc4</chem>	0.3369
25	<chem>C1C[C@H](O)C[C@@H]([C@]12C)CCc3c2nc4c(c3C)cccc4</chem>	0.6379
26	<chem>C1C[C@H](O)C[C@@H]([C@]12C)CCc3c2nc4c(cccc4)c3-c5ccc(Cl)cc5</chem>	0.3078
27	<chem>C1C[C@H](O)C[C@@H]([C@]12C)CCc3c2nc4c(c3)cc(Br)cc4</chem>	0.6226
28	<chem>C1C[C@H](O)C[C@@H]([C@]12C)CCc3c2nc4c(cc([N+](=O)[O-])cc4)c3-c5ccccc5F</chem>	0.3095
29	<chem>C1C[C@H](O)C[C@@H]([C@]12C)CCc3c2nc4n3nc(s4)-c5ccc(cc5)OC</chem>	0.0139
30	<chem>C1C[C@H](O)C[C@@H]([C@]12C)CCc3c2nc4n3nc(s4)SC</chem>	0.2231
31	<chem>C1C[C@H](O)C[C@@H]([C@]12C)CCc3c2nc(s3)N</chem>	0.412
32	<chem>C1C[C@H](O)C[C@@H]([C@]12C)CCc3c2nc(s3)-c4ccc(Cl)cc4</chem>	-0.1615
33	<chem>C1C[C@H](O)C[C@@H]([C@]12C)CCc3c2nc(s3)-c4ccc(cc4)OC</chem>	0.0628
34	<chem>C1C[C@H](O)C[C@@H]([C@]12C)CCc3c2nc(s3)-c4ccncc4</chem>	-0.0724
35	<chem>C1C[C@H](O)C[C@@H]([C@]12C)CCc3c2nc4c(n3)cccc4</chem>	0.4711
36	<chem>C1C[C@H](O)C[C@@H]([C@]12C)CCc3c2nc([nH]c3=O)-c4ccccc4</chem>	0.1567
37	<chem>C1C[C@H](O)C[C@@H]([C@]12C)CCc3c2nc([nH]c3=O)-c4ccc(cc4)OC</chem>	0.1976
38	<chem>C1C[C@H](O)C[C@@H]([C@]12C)CCc3c2nc([nH]c3=O)-c4ccc(Cl)cc4</chem>	-0.0024
39	<chem>C1C[C@H](O)C[C@@H]([C@]12C)CCc3c2nc([nH]c3=O)-c4ccncc4</chem>	0.0859
40	<chem>C1C[C@H](O)C[C@@H]([C@]12C)CCc3c2n(nc3)-c4ccccc4</chem>	-0.1583
41	<chem>C1C[C@H](O)C[C@@H]([C@]12C)CCc3c2n(nc3)-c4cc(C)cc(c4)C</chem>	-0.2397
42	<chem>C1C[C@H](O)C[C@@H]([C@]12C)CCc3c2n(nc3)-c4ccc(cc4)OC</chem>	-0.0864
43	<chem>C1C[C@H](O)C[C@@H]([C@]12C)CCc3c2n(nc3)-c4ccc(Cl)cc4</chem>	-0.3175
44	<chem>C1C[C@H](O)C[C@@H]([C@]12C)CCc3c2n(nc3)-c4c(F)cccc4</chem>	-0.3265
45	<chem>C1C[C@H](O)C[C@@H]([C@]12C)CCc3c2nn(c3)-c4ccccc4</chem>	-0.1248

46	C1C[C@H](O)C[C@@H]([C@]12C)CCc3c2nn(c3)-c4cc(C)cc(c4)C	-0.2092
47	C1C[C@H](O)C[C@@H]([C@]12C)CCc3c2nn(c3)-c4ccc(cc4)OC	-0.0558
48	C1C[C@H](O)C[C@@H]([C@]12C)CCc3c2[nH]nc3	0.3048
49	C1C[C@H](O)C[C@@H]([C@]12C)CCc3c2onc3	0.6839
50	C1C[C@H](O)C[C@@H]([C@]12C)CCc3c2n4c(nc3)ccn4	0.1007
51	C1C[C@H](O)C[C@@H]([C@]12C)CCc3c2nc4n(c3)ncc4	0.095
52	C1C[C@H](O)C[C@@H]([C@]12C)CCc3c2n4c(nc3)cc(n4)C(C)C	0.0145
53	C1C[C@H](O)C[C@@H]([C@]12C)CCc3c2nc4n(c3)nc(c4)C(C)C	0.0096
54	C1C[C@H](O)C[C@@H]([C@]12C)CCc3c2n4c(nc3)cc(n4)-c5ccccc5	-0.1477
55	C1C[C@H](O)C[C@@H]([C@]12C)CCc3c2nc4n(c3)nc(c4)-c5ccccc5	-0.152
56	C1C[C@H](O)C[C@@H]([C@]12C)CCc3c2n4c(nc3)cc(n4)-c5ccc(Cl)cc5	-0.2828
57	C1C[C@H](O)C[C@@H]([C@]12C)CCc3c2nc4n(c3)nc(c4)-c5ccc(Cl)cc5	-0.287
58	C1C[C@H](O)C[C@@H]([C@]12C)CCc3c2n4c(nc3)cc(n4)-c5ccc(cc5)OC	-0.0872
59	C1C[C@H](O)C[C@@H]([C@]12C)CCc3c2nc4n(c3)nc(c4)-c5ccc(cc5)OC	-0.0912
60	C1C[C@H](O)C[C@H](CC2)[C@@]1(C)[C@]23c4c(NC3=O)cccc4	0.7825
61	C1C[C@H](O)C[C@H](CC2)[C@@]1(C)[C@]23c4c(NC3=O)ccc(Br)c4	0.7696
62	C1C[C@H](O)C[C@H](CC2)[C@@]1(C)[C@]23c4c(NC3=O)ccc(F)c4	0.481
63	C1C[C@H](O)C[C@H](CCC2)[C@@]1(C)C23Nc4c(C(=O)N3)cccc4	0.4053
64	C1C[C@H](O)C[C@H](CCC2)[C@@]1(C)C23Nc4c(C(=O)N3)ccc(F)c4	0.1508
65	C1C[C@H](O)C[C@H](CCC2)[C@@]1(C)C23Nc4c(C(=O)N3)cc(Br)cc4	0.4099

SMILES of curated steroid library

Name	SMILES	Origin
Lanosterol	<chem>C[C@H](CCC=C(C)C)[C@H]1CC[C@]2(C)C1CCC3=C2CC[C@H]4C(C)(C)[C@@H](O)CC[C@]34C</chem>	Human
Zymosterol	<chem>O[C@H]4CC[C@]3(C)/C2=C(/[C@@H]1CC[C@H]([C@H](C)CC\C=C(/C)C)[C@@]1(C)CC2)CC[C@H]3C4)C</chem>	Human
5a-Cholesta-7,24-dien-3b-ol	<chem>C[C@H](CCC=C(C)C)[C@H]1CC[C@@H]2[C@@]1(CCC3C2=CC[C@@H]4[C@@]3(CC[C@@H](C4)O)C)C</chem>	Human
Desmosterol	<chem>C[C@H](CCC=C(C)C)[C@H]1CC[C@@H]2[C@@]1(CC[C@H]3[C@H]2CC=C4[C@@]3(CC[C@@H](C4)O)C)C</chem>	Human
Cholesterol	<chem>C[C@H](CCCC(C)C)[C@H]1CC[C@@H]2[C@@]1(CC[C@H]3[C@H]2CC=C4[C@@]3(CC[C@@H](C4)O)C)C</chem>	Human
22(S)-Hydroxycholesterol	<chem>C[C@@H]([C@H]1CC[C@@H]2[C@@]1(CC[C@H]3[C@H]2CC=C4[C@@]3(CC[C@@H](C4)O)C)C)[C@H](CCC(C)C)O</chem>	Human
20a, 22R-Dihydroxycholesterol	<chem>CC(C)CC[C@H]([C@@](C)([C@H]1CC[C@@H]2[C@@]1(CC[C@H]3[C@H]2CC=C4[C@@]3(CC[C@@H](C4)O)C)C)O)O</chem>	Human
20a-hydroxycholesterol	<chem>CC(C)CCC[C@](C)([C@H]1CC[C@@H]2[C@@]1(CC[C@H]3[C@H]2CC=C4[C@@]3(CC[C@@H](C4)O)C)C)O</chem>	Human
17a,20a-dihydroxycholesterol	<chem>CC(C)CCC[C@](C)([C@]1(CCC2[C@@]1(CCC3[C@H]2CC=C4[C@@]3(CC[C@@H](C4)O)C)C)O)O</chem>	Human
Pregnenolone	<chem>CC(=O)[C@H]1CC[C@@H]2[C@@]1(CC[C@H]3[C@H]2CC=C4[C@@]3(CC[C@@H](C4)O)C)C</chem>	Human
Corticosterone	<chem>C[C@]12CCC(=O)C=C1CC[C@@H]3[C@@H]2[C@H](C[C@]4([C@H]3CC[C@@H]4C(=O)CO)C)O</chem>	Human
Aldosterone	<chem>C[C@]12CCC(=O)C=C1CC[C@@H]3[C@@H]2[C@H](C[C@]4([C@H]3CC[C@@H]4C(=O)CO)C=O)O</chem>	Human
Pregnanediol	<chem>C[C@@H]([C@H]1CC[C@@H]2[C@@]1(CC[C@H]3[C@H]2CC[C@H]4[C@@]3(CC[C@H](C4)O)C)C)O</chem>	Human
Cortisone	<chem>C[C@]12CCC(=O)C=C1CC[C@@H]3[C@@H]2C(=O)C[C@]4([C@H]3CC[C@@]4(C(=O)CO)O)C</chem>	Human
Testosterone	<chem>C[C@]12CC[C@H]3[C@H]([C@@H]1CC[C@@H]2O)CCC4=CC(=O)CC[C@]34C</chem>	Human
Estriol	<chem>C[C@]12CC[C@H]3[C@H]([C@@H]1C[C@H]([C@@H]2O)O)CCC4=C3C=CC(=C4)O</chem>	Human
Estrone	<chem>C[C@]12CC[C@H]3[C@H]([C@@H]1CCC2=O)CCC4=C3C=CC(=C4)O</chem>	Human
3-Oxocholest-4-en-26-oic acid	<chem>C[C@H](CCCC(C)C(=O)OC)[C@H]1CC[C@@H]2[C@@]1(CC[C@H]3[C@H]2CCC4=CC(=O)CC[C@]34C)C</chem>	Human
Cholic acid	<chem>C[C@H](CCC(=O)O)[C@H]1CC[C@@H]2[C@@]1([C@H](C[C@H]3[C@H]2[C@@H]3[C@H]4[C@@]3(CC[C@H](C4)O)C)O)C</chem>	Human
7α-Hydroxy-4-cholesten-3-one	<chem>O=C\C=C2/[C@]([C@H]1CC[C@]3([C@H]([C@@H]1[C@H](O)C2)CC[C@@H]3[C@H](C)CCCC(C)C)C)CC4</chem>	Human
7a-hydroxy-3-oxo-4-cholestenoic acid	<chem>C[C@H](CCCC(C)C(=O)O)[C@H]1CC[C@@H]2[C@@]1(CC[C@H]3[C@H]2[C@@H]3(CC4=CC(=O)CC[C@]34C)O)C</chem>	Human
Progesterone	<chem>CC(=O)[C@H]1CC[C@@H]2[C@@]1(CC[C@H]3[C@H]2CCC4=CC(=O)CC[C@]34C)C</chem>	Human
Estradiol	<chem>C[C@]12CC[C@H]3[C@H]([C@@H]1CC[C@@H]2O)CCC4=C3C=CC(=C4)O</chem>	Human
27-hydroxycholesterol	<chem>C[C@H](CCC[C@@H](C)[C@H]1CC[C@@H]2[C@@]1(CC[C@H]3[C@H]2CC=C4[C@@]3(CC[C@@H](C4)O)C)CO</chem>	Human
25-hydroxycholesterol	<chem>C[C@H](CCCC(C)C)O[C@H]1CC[C@@H]2[C@@]1(CC[C@H]3[C@H]2CC=C4[C@@]3(CC[C@@H](C4)O)C)C</chem>	Human
7-Ketocholesterol	<chem>C[C@H](CCCC(C)C)[C@H]1CC[C@@H]2[C@@]1(CC[C@H]3[C@H]2C(=O)C=C4[C@@]3(CC[C@@H](C4)O)C)C</chem>	Human
Pentalinonsterol	<chem>CC(=CCCC(=C)[C@H]1CC[C@@H]2[C@@]1(CC[C@H]3[C@H]2CCC4=CC(=O)CC[C@]34C)C)C</chem>	Plant
Fomentarol C	<chem>CCO[C@@H]1C=C2[C@@H]3CC[C@@H]([C@]3(CC[C@@H]2[C@@]4([C@@]1(C[C@H](CC4)O)O)C)C)[C@H](C)/C=C/[C@H](C)C)C</chem>	Fungal
(2β,3β,5β,9ξ,20E)-2,3,14,25-Tetrahydroxycholesta-7,20(22)-dien-6-on	<chem>C/C=C\C(C)C(C)O/[C@H]1CC[C@@]2([C@@]1(CCC3C2=CC(=O)[C@H]4[C@@]3(C[C@@H]([C@@H](C4)O)O)C)O</chem>	Plant

Polyporoid C	<chem>CC(C)C(C)C[C@H]([C@@](C)([C@H]1[C@H](C[C@@]2[C@@]1(CC[C@H]3C2=CC(=O)[C@H]4[C@@]3[C[C@@H]([C@@H](C4)O)C)O)O)O</chem>	Fungal
Dihydrocholesterol	<chem>C[C@H](CCCC(C)C)[C@H]1CC[C@@H]2[C@@]1(CC[C@H]3[C@H]2CC[C@@H]4[C@@]3(CC[C@@H](C4)O)C)C</chem>	Human
Ganoderic acid B	<chem>C[C@H](CC(=O)CC(C)C(=O)O)[C@H]1CC(=O)[C@@]2([C@@]1(CC(=O)C3=C2[C@H](C[C@@H]4[C@@]3(CC[C@@H](C4)O)C)O)C)C</chem>	Fungal
Fusidic acid	<chem>C[C@H]1[C@@H]2CC[C@@]3([C@H]([C@]2(CC[C@H]1O)C)[C@@H](C[C@@H]4[C@@]3[C[C@@H](/C4=C/C(=O)C)C(=O)O)OC(=O)C)O)C</chem>	Fungal
Garcihombronane C	<chem>C[C@H](CC/C=C\C/C(=O)OC)O[C@@]1(CC=C2[C@@]1(CCC3=C2CC[C@@H]4[C@@]3(CC[C@H](C4(C)C)O)C)C)C</chem>	Plant
Diosgenin	<chem>C[C@@H]1CC[C@@]2([C@H]([C@H]3[C@@H](O2)C[C@@H]4[C@@]3(CC[C@H]5[C@H]4CC=C6[C@@]5(CC[C@@H](C6)O)C)C)OC1</chem>	Plant
E-Guggulsterone	<chem>O=C1C[C@@]2([H])[C@@]3([H])CCC4=CC(CC[C@@]4(C)[C@@]3([H])CC[C@@]2(C)/C1=C\C)=O</chem>	Plant
Cephalostatin 1	<chem>C[C@H]1[C@H]2CC=C3[C@]2(CO[C@]14[C@@H](CC(O4)(C)C)O)C(=O)C[C@H]5[C@H]3CC[C@@H]6[C@@]5(CC7=NC8=C(C[C@]9([C@H](C8)CC[C@@H]1[C@@H]9C[C@H]([C@]2(C1=C[C@H]1[C@@]2([C@@H]([C@@]2(O1)[C@@H](C[C@@](O2)(C)CO)C)O)C)O)C)N=C7C6)C</chem>	Marine
Protopanaxadiol	<chem>CC(=CCC[C@](C)([C@H]1CC[C@@]2([C@@H]1[C@@H](C[C@H]3[C@]2(CC[C@@H]4[C@@]3(CC[C@@H](C4(C)C)O)C)C)O)C)O)C</chem>	Plant
Lithocholic acid	<chem>C[C@H](CCC(=O)O)[C@H]1CC[C@@H]2[C@@]1(CC[C@H]3[C@H]2CC[C@@H]4[C@@]3(CC[C@H](C4)O)C)C</chem>	Human
Norethynodrel	<chem>O=C4CCC\1=C\CC[C@@H]2[C@@H]1CC[C@@]3([C@H]2CC[C@@]3(C#C)O)C)C4</chem>	Synthetic
Spironolactone	<chem>CC(=O)S[C@@H]1CC2=CC(=O)CC[C@@]2([C@@H]3[C@@H]1[C@@H]4CC[C@@]5([C@@]4(CC3)C)CCC(=O)O5)C</chem>	Synthetic
Fluocinonide	<chem>CC(=O)OCC(=O)[C@@]12[C@@H](C[C@@H]3[C@@]1(C[C@@H]([C@@]4([C@H]3[C@@H](C5=CC(=O)C=C[C@@]54C)F)F)O)C)OC(O2)(C)C</chem>	Synthetic
Finasteride	<chem>C[C@]12CC[C@H]3[C@H]([C@@H]1CC[C@@H]2C(=O)NC(C)(C)C)CC[C@@H]4[C@@]3(C=CC(=O)N4)C</chem>	Synthetic
Budesonide	<chem>CCCC1O[C@@H]2C[C@H]3[C@@H]4CCC5=CC(=O)C=C[C@@]5([C@H]4[C@H](C[C@@]3([C@@]2(O1)C(=O)CO)C)O)C</chem>	Synthetic
Eplerenone	<chem>C[C@]12CCC(=O)C=C1C[C@H]([C@@H]3[C@]24[C@H](O4)C[C@@]5([C@H]3CC[C@@]56CCC(=O)O6)C)C(=O)OC</chem>	Synthetic
Medrogestone	<chem>CC1=C[C@@H]2[C@H](CC[C@@]3([C@H]2CC[C@@]3(C)C(=O)C)C)[C@@]4(C1=CC(=O)CC4)C</chem>	Synthetic

General directions

All reactions were run under a N₂ atmosphere unless otherwise specified and were monitored by thin layer chromatography (TLC) and/or reversed-phase ultra-performance liquid chromatography mass spectrometry (RP-UPLC-MS). Commercially available reagents were purified according to standard procedures or were used as received from Alfa Aesar, Acros Organics, Combi-Blocks, Fisher Scientific, Merck, and Strem. All solvents used were of HPLC quality and dry solvents (DCM, Et₂O, THF, and Toluene) were obtained from a PureSolv system (Innovative Technology, Tronxy).

Analytical TLC was conducted on Merck aluminium sheets covered with silica (C60). The plates were either visualized under UV-light or stained by dipping in a developing agent followed by heating. KMnO₄ [KMnO₄ (3 g) in water (300 mL), K₂CO₃ (20 g) and 5% aqueous NaOH (5 mL)] was used as the developing agent. Flash column chromatography was performed using Merck Geduran® Si 60 (40-63 µm) silica gel using the specified eluent.

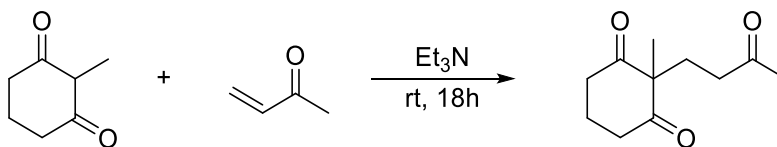
All new compounds were characterized by NMR, MS (ESI) and HRMS (ESI) (byproducts were not fully characterized). Structural assignments were made when possible for new compounds using COSY, HSQC, HMBC, H2BC, and NOESY spectra where appropriate. For the recording of ¹H NMR and ¹³C NMR a Bruker Ascend with a Prodigy cryoprobe (operating at 400 MHz for proton and 100 MHz for carbon) was used. The chemical shifts (δ) are reported in parts per million (ppm) and the coupling constants (J) in Hz. Spectra were referenced using the residual solvent peaks of the respective solvent; DMSO (δ 2.50 ppm for ¹H NMR and δ 39.52 ppm for ¹³C NMR), CDCl₃ (δ 7.26 ppm for ¹H NMR and δ 77.16 ppm for ¹³C NMR), CD₃OD (δ 3.31 ppm for ¹H NMR and δ 49.00 ppm for ¹³C NMR). The following abbreviations were used to report peak multiplicities: s = singlet, d = doublet, t = triplet, q = quartet, dd = doublet of doublets, sept = septet, m = multiplet, bs = broad singlet

Analytical RP-UPLC-MS (ESI) analysis was performed on a S2 Waters AQUITY RP-UPLC system equipped with a diode array detector using an Thermo Accucore C18 column (d 2.6 µm, 2.1 x 50 mm; column temp: 50 °C; flow: 1.0 mL/min). Eluents A (0.1% HCO₂H in H₂O) and B (0.1% HCO₂H in MeCN) were used in a linear gradient (5% B to 100% B) in 2.4 min and then held for 0.1 min at 100% B (total run time: 2.6 min). The LC system was coupled to a SQD mass spectrometer.

Preparative RP-HPLC was carried out on a Waters Alliance reversed-phase HPLC system consisting of a Waters 2545 Binary Gradient Module equipped with an xBridge BEH C18 OBD Prep Column (130 Å, 5 µm, 30 x 150 mm) operating at 20 °C and a flow rate of 20 mL/min, a Waters Photodiode Array Detector (detecting at 210-600 nm), a Waters UV Fraction Manager, and a Waters 2767 Sample Manager. Eluents A1 (0.1% HCO₂H in H₂O) and B1 (0.1% HCO₂H in MeCN) were used. Analytical LC-HRMS (ESI) analysis was performed on a Waters Alliance 2695 system. Samples were injected directly and the LC system was coupled to a Waters LCT Premier XE Micromass equipped with a Lock Mass probe operating in positive electrospray mode. Eluents A (0.1% HCO₂H in H₂O) and B (0.1% HCO₂H in MeCN) were used in a 1:1 ratio for a total run time of 2 min.

Chiral HPLC was run on a Waters 2695 Alliance Separations module with a Waters 2996 PhotoDiode Array detector, equipped with a ChiralPak AD-H column (5 µm, 250 x 4.6 mm).

2-methyl-2-(3-oxobutyl)cyclohexane-1,3-dione (2.03)



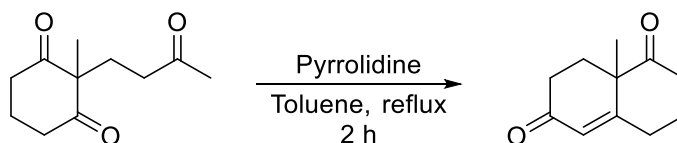
To a round bottom flask, 2-methyl-1,3-cyclohexanedione (10 g, 79.3 mmol), freshly distilled methyl vinyl ketone (7.20 mL, 87.2 mmol), and triethylamine (1.10 mL, 7.92 mmol) were added and the slurry stirred at room temperature for 18 hours. The brown oil was diluted with DCM, washed with 5% aqueous HCl (15 mL), water (15 mL), and the aqueous phases further extracted with DCM (3 x 15 mL). The combined organic phases were dried over anhydrous magnesium sulfate and the solvent removed under reduced pressure to afford the product as an amber oil (14.7 g, 75.1 mmol, 95% yield).

The ^1H and ^{13}C spectra are in agreement with those reported in the literature¹²¹

^1H NMR (400 MHz, CDCl_3) δ 2.76 – 2.58 (m, 4H), 2.34 (t, J = 7.5 Hz, 2H), 2.10 (s, 3H), 2.08 – 1.83 (m, 4H), 1.23 (s, 3H).

^{13}C NMR (101 MHz, CDCl_3) δ 210.1, 207.7, 64.5, 38.5, 37.9, 30.1, 29.7, 20.2, 17.7.

8a-methyl-3,4,8,8a-tetrahydronaphthalene-1,6(2H,7H)-dione (2.02)



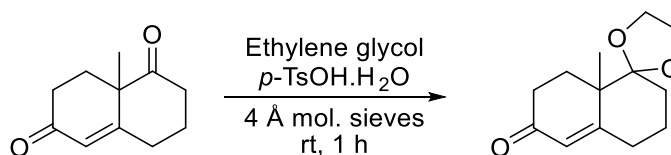
To a solution of 2-methyl-2-(3-oxobutyl)cyclohexane-1,3-dione (7.37 g, 37.5 mmol) in toluene (20 mL) was added pyrrolidine (0.31 mL, 3.75 mmol) before fitting the flask with a Dean-Stark trap. The reaction was heated at reflux for two hours, cooled to room temperature, and the solvent removed under reduced pressure. The crude oil was dissolved in DCM, washed with 5% aqueous HCl (15 mL), water (15 mL), and the combined aqueous phases extracted with DCM. The combined organic phases were then washed with brine (10 mL), dried over anhydrous magnesium sulfate, and the solvent removed to yield a crude brown oil. Purification of the crude oil by flash chromatography on silica gel (2:3 ethyl acetate/*n*-hexane) afforded the product as an amber oil that solidified to a solid upon storage at $-20\text{ }^\circ\text{C}$ (4.88 g, 27.4 mmol, 73% yield)

The ^1H and ^{13}C spectra are in agreement with those reported in the literature¹²¹

R_f = 0.194 (2:3 ethyl acetate/*n*-hexane);

^1H NMR (400 MHz, CDCl_3) δ 5.84 (d, J = 1.8 Hz, 1H), 2.76 – 2.65 (m, 2H), 2.53 – 2.41 (m, 4H), 2.19 – 2.07 (m, 3H), 1.76 – 1.63 (m, 1H), 1.44 (s, 3H).

^{13}C NMR (101 MHz, CDCl_3) δ 211.1, 198.4, 165.9, 126.0, 50.7, 37.8, 33.7, 31.9, 29.8, 23.4, 23.0.

8a-methyl-3,4,8,8a-tetrahydro-2H-spiro[naphthalene-1,2'-[1,3]dioxolan]-6(7H)-one (2.06)

To a flask containing ground 4 Å molecular sieves (2.50 g), 8a-methyl-3,4,8,8a-tetrahydronaphthalene-1,6(2H,7H)-dione (2.89 g, 16.2 mmol), *p*-TsOH.H₂O (3.08 g, 16.2 mmol), and anhydrous ethylene glycol (20 mL) were added and stirred at room temperature for 60 minutes. The reaction was poured into a mixture of ice-water: saturated NaHCO₃ (2:1, 50 mL) and the reaction mixture filtered under vacuum. The filtrate was extracted with ethyl acetate (4 x 50 mL) and the combined organic phases washed with brine (35 mL), dried over anhydrous magnesium sulfate, and the solvent removed under reduced pressure to yield a crude yellow oil. Purification of the crude oil by flash chromatography on silica gel (3:7 to 2:3 ethyl acetate/*n*-heptane) afforded the product as a colourless oil that solidified to a white solid upon storage at – 20 °C (2.66 g, 12.0 mmol, 74% yield)

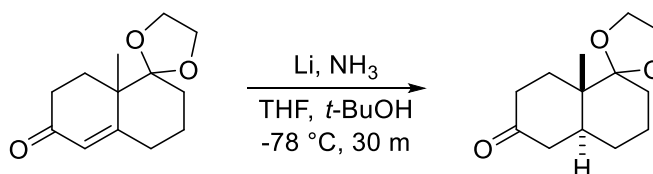
Note: on larger scales the purification of the Wieland-Miescher ketone ketal was performed via crystallisation from diisopropyl ether

The ¹H and ¹³C spectra are in agreement with those reported in the literature¹²³

*R*_f = 0.250 (2:3 ethyl acetate/*n*-hexane)

¹H NMR (400 MHz, CDCl₃) δ 5.81 (d, *J* = 2.0 Hz, 1H), 4.03 – 3.88 (m, 4H), 2.49 – 2.22 (m, 5H), 1.90 (td, *J* = 14.7, 13.9, 4.5 Hz, 1H), 1.83 – 1.60 (m, 4H), 1.35 (s, 3H)

¹³C NMR (101 MHz, CDCl₃) δ 199.4, 167.8, 125.8, 112.5, 65.5, 65.2, 45.2, 34.1, 31.6, 30.2, 27.0, 21.9, 20.7

(4a*S,8a*S**)-8a-methylhexahydro-2H-spiro[naphthalene-1,2'-[1,3]dioxolan]-6(5H)-one (2.07)**

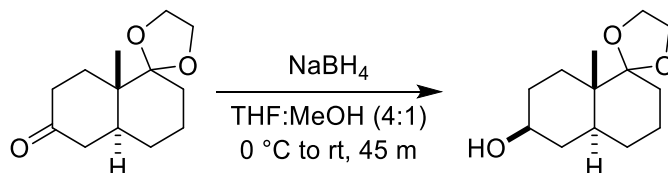
To an open flask containing ammonia (250 mL) at – 78 °C was added lithium (0.621 g, 90.0 mmol) which was dissolved with stirring over 30 minutes. A solution of ketone **2.06** (5.00 g, 22.5 mmol) and *tert*-butanol (4.31 mL, 45.0 mmol) in anhydrous THF (10 mL) was added dropwise to the deep-blue solution over 5 minutes, and the reaction left stirring for 30 minutes. The reaction was quenched via addition of isoprene until the blue colour had dissipated and the ammonia evaporated under a stream of nitrogen. The resulting crude yellow solid was partitioned between saturated aqueous NH₄Cl and Et₂O and the aqueous phase extracted twice with Et₂O. The combined organic phases were dried over anhydrous magnesium sulfate, and the solvent removed under reduced pressure to afford the product as a viscous yellow oil (4.40 g, 19.6 mmol, 87% yield)

$R_f = 0.422$ (1:1 ethyl acetate/*n*-heptane)

^1H NMR (400 MHz, CDCl_3) δ 4.01 – 3.78 (m, 4H), 2.43 – 2.26 (m, 2H), 2.25 – 2.09 (m, 2H), 2.08 – 1.97 (m, 1H), 1.91 (td, $J = 14.0, 13.5, 6.5$ Hz, 1H), 1.80 – 1.49 (m, 5H), 1.39 – 1.28 (m, 2H), 1.18 (s, 3H)

^{13}C NMR (101 MHz, CDCl_3) δ 211.6, 112.4, 65.3, 65.1, 44.3, 41.8, 41.5, 37.9, 30.5, 30.3, 28.2, 22.9, 13.1

(4a*S,8a*S**)-8a-methyloctahydro-2H-spiro[naphthalene-1,2'-[1,3]dioxolan]-6-ol (2.08)**



A solution of ketone **2.07** (2.03 g, 9.05 mmol) in a mixture of THF:MeOH (4:1) was cooled to 0 °C in an ice bath before addition of NaBH_4 (0.342 g, 9.05 mmol). The reaction was returned to room temperature and left to stir for 45 minutes, after which, water was added and the reaction left stirring for a further 15 minutes. The reaction was extracted with DCM three times, the combined organic phases dried over anhydrous magnesium sulfate, and the solvent removed under reduced pressure to afford the product as a colourless oil with a d.r. of 86:14 (*S**:*R**) (quantitative yield). The inseparable mixture of diastereoisomers was used in the subsequent step without any further purification.

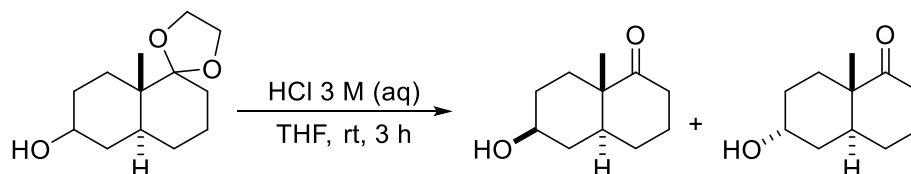
Note: Signals arising from the minor diastereoisomer are not presented

$R_f = 0.280$ (1:1 ethyl acetate/*n*-heptane)

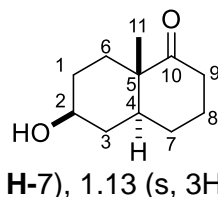
^1H NMR (400 MHz, CDCl_3) δ 3.98 – 3.83 (m, 4H), 3.66 – 3.50 (m, 1H), 1.89 – 1.77 (m, 1H), 1.77 – 1.12 (m, 13H), 0.99 (s, 3H)

^{13}C NMR (101 MHz, CDCl_3) δ 113.0, 71.1, 65.3, 65.1, 41.9, 39.7, 37.7, 31.2, 30.7, 28.7, 27.9, 23.2, 14.0.

(4a*S,6*S**,8a*S**)-6-hydroxy-8a-methyloctahydronaphthalen-1(2H)-one (2.01)**



To a solution of ketal **2.08** (2.15 g, 9.50 mmol) in THF (70 mL) was added aqueous 3M HCl (20 mL), and the reaction left stirring at room temperature for 3 hours. The reaction was neutralised by addition of saturated aqueous NaHCO_3 and extracted twice with dichloromethane. The combined organic phases were dried over anhydrous magnesium sulfate, and the solvent removed under reduced pressure to yield a crude oil. Purification of the crude oil by flash chromatography on silica gel (2:1 ethyl acetate/*n*-heptane) afforded the major diastereoisomer **2.01** (1.26 g, 6.91 mmol, 73% yield) and the minor diastereoisomer **2.09** (0.154 g, 0.84 mmol, 9% yield) as white solids.

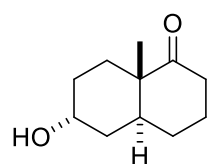


$R_f = 0.26$ (2:1 ethyl acetate/*n*-heptane)

$^1\text{H NMR}$ (400 MHz, CDCl_3) δ 3.64 – 3.53 (m, 1H, **H-2**), 2.70 – 2.58 (m, 1H, **H-9**), 2.28 – 2.15 (m, 1H, **H-9**), 2.06 – 1.98 (m, 1H, **H-8**), 1.94 – 1.86 (m, 1H, **H-6**), 1.79 – 1.61 (m, 4H, **H-3**, **H-6**, **H-7**, **H-8**), 1.54 – 1.35 (m, 5H, **H-1**, **H-3**, **H-4**, **H-7**), 1.13 (s, 3H, **H-11**);

$^{13}\text{C NMR}$ (101 MHz, CDCl_3) δ 215.8 (**C-10**), 70.6 (**C-2**), 47.8 (**C-5**), 43.9 (**C-4**), 37.6 (**C-9**), 37.0 (**C-3**), 31.0 (**C-6**), 30.9 (**C-1**), 27.6 (**C-7**), 26.4 (**C-8**), 15.9 (**C-11**)

HRMS (ESI+) m/z found 183.1377 $[\text{M}+\text{H}]^+$, $\text{C}_{11}\text{H}_{18}\text{O}_2$ calculated 183.1385 ($\Delta = -4.37$ ppm).

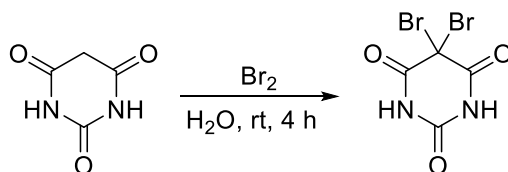


$R_f = 0.32$ (2:1 ethyl acetate/*n*-heptane)

$^1\text{H NMR}$ (400 MHz, CDCl_3) δ 4.04 (p, $J = 2.7$ Hz, 1H), 2.63 (td, $J = 14.1, 6.8$ Hz, 1H), 2.27 – 2.18 (m, 1H), 2.06 – 1.94 (m, 2H), 1.89 – 1.78 (m, 1H), 1.75 – 1.36 (m, 8H), 1.08 (s, 3H)

$^{13}\text{C NMR}$ (101 MHz, CDCl_3) δ 216.1, 65.9, 48.2, 38.3, 37.6, 34.8, 28.6, 27.3, 26.3, 26.2, 14.8.

5,5-dibromobarbituric acid (2.15)



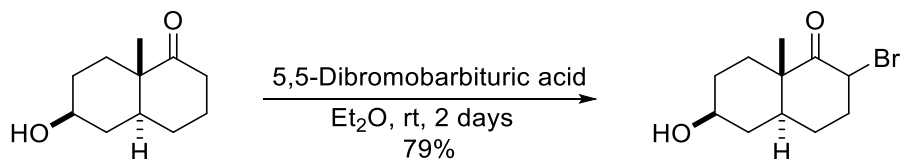
To a cooled (0 °C) suspension of barbituric acid (10 g, 78.1 mmol) in H_2O (30 mL), bromine was added dropwise until a yellow colour persisted in the mixture (approx. 2 equiv.). The reaction was left stirring for 4 hours and the white solid isolated by vacuum filtration. The wet 5,5-dibromobarbituric acid was dried at 40 °C under vacuum for 5 hours, affording the product as a white powdery solid. (16.1 g, 56.3 mmol, 72% yield).

$R_f = 0.60$ (1:1 ethyl acetate/*n*-pentane)

$^1\text{H NMR}$ (400 MHz, DMSO) δ 11.76

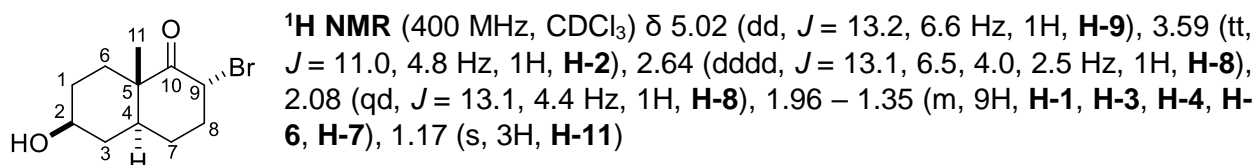
$^{13}\text{C NMR}$ (101 MHz, DMSO) δ 163.5, 149.0, 48.8.

(4a*S,6*S**,8a*S**)-2-bromo-6-hydroxy-8a-methyloctahydronaphthalen-1(2*H*)-one (2.10)**



To a solution of ketone **2.01** (0.350 g, 1.92 mmol) in anhydrous Et₂O (10 mL) was added 5,5-dibromobarbituric acid (0.329 g, 1.15 mmol) and the resulting solution stirred at room temperature for 2 days. The reaction mixture was partitioned between Et₂O and water, the organic phase washed with water, dried over anhydrous magnesium sulfate, and concentrated to yield the product as a viscous brown oil containing a mixture of the equatorial:axial α-bromoketone in a 9:1 ratio (0.396 g, 1.52 mmol, 79% yield).

Note: NMR data is presented for the major equatorial diastereoisomer only



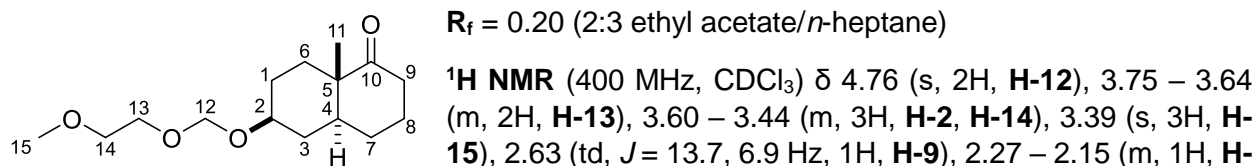
¹³C NMR (101 MHz, CDCl₃) δ 205.2 (**C-10**), 70.2 (**C-2**), 54.3 (**C-9**), 48.6 (**C-5**), 44.0 (**C-4**), 39.1 (**C-8**), 36.4 (**C-3**), 31.6 (**C-6**), 30.4 (**C-1**), 28.9 (**C-7**), 15.9 (**C-11**)

HRMS (ESI+) *m/z* found 261.0477 [M+H]⁺, C₁₁H₁₇BrO₂ calculated 261.0490 (Δ = -4.98 ppm)

(4a*S,6*S**,8a*S**)-6-((2-methoxyethoxy)methoxy)-8a-methyloctahydronaphthalen-1(2*H*)-one (2.12)**



A solution of ketone **2.01** (0.472 g, 2.59 mmol) and DIPEA (1.35 mL, 7.77 mmol) in anhydrous DCM (20 mL) was cooled to 0 °C in an ice bath before dropwise addition of 2-methoxyethoxymethyl chloride (0.591 mL, 5.18 mmol). The flask was returned to room temperature and left stirring at the same temperature for 6 hours. The reaction was neutralised via addition of saturated aqueous NH₄Cl and extracted twice with DCM. The combined organic phases were washed with water, brine, dried over anhydrous magnesium sulfate, and the solvent removed to yield the product as a crude amber oil. Purification of the crude oil via flash chromatography on silica gel (2:3 ethyl acetate/*n*-heptane) afforded the product as a colourless oil (0.556 g, 2.06 mmol, 80% yield)

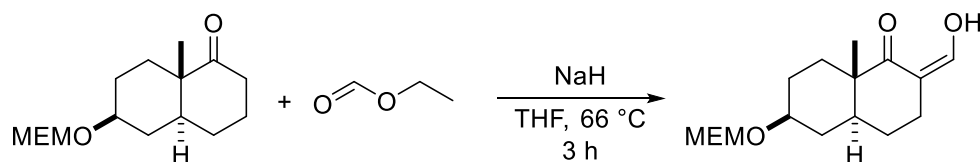


9), 2.07 – 1.89 (m, 2H, **H-1**, **H-7**), 1.86 – 1.77 (m, 1H, **H-3**), 1.78 – 1.35 (m, 8H, **H-1**, **H-3**, **H-4**, **H-6**, **H-7**, **H-8**), 1.12 (s, 3H, **H-11**)

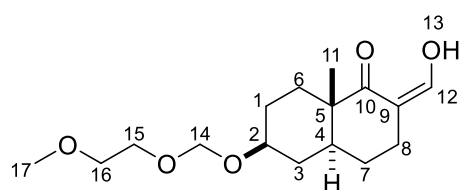
¹³C NMR (101 MHz, CDCl₃) δ 215.8 (**C-10**), 93.8 (**C-12**), 75.5 (**C-2**), 71.9 (**C-14**), 66.9 (**C-13**), 59.2 (**C-15**), 47.9 (**C-5**), 43.9 (**C-4**), 37.6 (**C-9**), 34.2 (**C-3**), 31.0 (**C-6**), 28.1 (**C-1**), 27.6 (**C-8**), 26.3 (**C-7**), 15.9 (**C-11**);

HRMS (ESI+) m/z found 271.1904 [M+H]⁺, C₁₅H₂₆O₄ calculated 271.1909 (Δ = -1.84 ppm).

(4aS*,6S*,8aS*)-2-(hydroxymethylene)-6-((2-methoxyethoxy)methoxy)-8a-methyloctahydronaphthalen-1(2H)-one (2.13)



A solution of ketone **2.12** (1.06 g, 3.92 mmol) and ethyl formate (3.17 mL, 39.2 mmol) in anhydrous THF (40 mL) was cooled to 0 °C in an ice bath before addition of NaH (60 wt% in mineral oil, 0.470 g, 11.8 mmol). The flask was returned to room temperature and heated at reflux for 3 hours. The reaction was then cooled to 0 °C in an ice bath and quenched via addition of aqueous NH₄Cl and the resulting mixture extracted with ethyl acetate. The organic phase was washed with water, brine, dried over anhydrous magnesium sulfate, and the solvent removed to afford the product as an amber oil (1.03 g, 3.45 mmol, 88% yield).



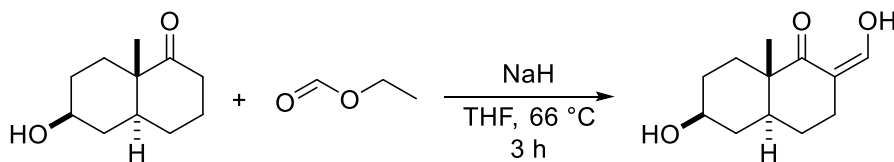
R_f = 0.36 (1:1 ethyl acetate/*n*-heptane)

¹H NMR (400 MHz, CDCl₃) δ 14.62 (d, *J* = 4.15 Hz, 1H, **H-13**), 8.48 (d, *J* = 4.15 Hz, 1H, **H-12**), 4.78 (s, 2H, **H-14**), 3.75 – 3.66 (m, 2H, **H-15**), 3.63 – 3.51 (m, 3H, **H-2**, **H-16**), 3.39 (s, 3H, **H-17**), 2.45 – 2.32 (m, 2H, **H-8**), 2.08 (dt, *J* = 13.5, 3.5 Hz, 1H, **H-6**), 2.02 – 1.93 (m, 1H, **H-1**), 1.86 – 1.78 (m, 1H, **H-3**), 1.58 – 1.31 (m, 6H, **H-1**, **H-3**, **H-4**, **H-6**, **H-7**), 1.13 (s, 3H, **H-11**)

¹³C NMR (101 MHz, CDCl₃) ¹³C NMR (101 MHz, CDCl₃) δ 193.2 (**C-10**), 186.0 (**C-12**), 106.1 (**C-9**), 93.9 (**C-14**), 75.7 (**C-2**), 71.9 (**C-16**), 66.9 (**C-15**), 59.2 (**C-17**), 40.7 (**C-5**), 39.3 (**C-4**), 34.2 (**C-3**), 31.5 (**C-6**), 28.1 (**C-1**), 24.9 (**C-7**), 23.1 (**C-8**), 17.6 (**C-11**)

HRMS (ESI+) m/z found 299.1857 [M+H]⁺, C₁₆H₂₆O₅ calculated 299.1858 (Δ = -0.33 ppm).

4aS*,6S*,8aS*,Z)-6-hydroxy-2-(hydroxymethylene)-8a-methyloctahydronaphthalen-1(2H)-one (2.11)



A solution of ketone **2.01** (0.250 g, 1.37 mmol) and ethyl formate (1.11 mL, 13.7 mmol) in anhydrous THF (10 mL) was cooled to 0 °C in an ice bath before addition of NaH (60 wt% in mineral oil, 0.164 g, 4.11 mmol). The flask was returned to room temperature and heated at reflux

for 3 hours. The reaction was then cooled to 0 °C in an ice bath and quenched via addition of aqueous NH₄Cl and the resulting mixture extracted with ethyl acetate. The organic phase was washed with water, brine, dried over anhydrous magnesium sulfate, and the solvent removed to afford the product as a yellow oil (0.153 g, 0.730 mmol, 53% yield)

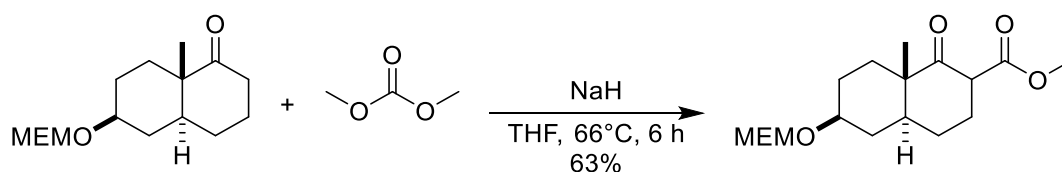
Note: mineral oil and solvent impurities seen in both ¹H and ¹³C NMR, only signals originating from the compound are presented, compound used immediately without purification

R_f = 0.3 (1:1 ethyl acetate/*n*-pentane)

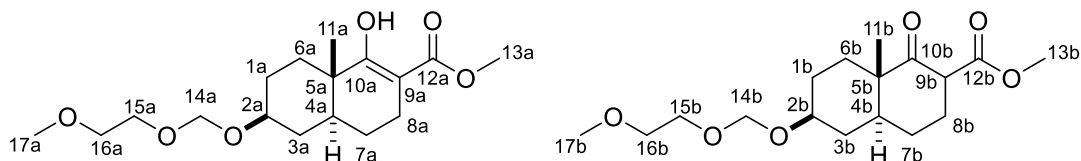
¹H NMR (400 MHz, CDCl₃) δ 8.48 (s, 1H), 3.71 – 3.58 (m, 1H), 2.43 – 2.37 (m, 2H), 2.09 (dt, *J* = 13.4, 3.4 Hz, 1H), 1.99 – 1.86 (m, 3H), 1.70 – 1.31 (m, 12H), 1.14 (s, 3H)

¹³C NMR (101 MHz, CDCl₃) δ = 193.8, 185.9, 106.1, 70.8, 39.3, 37.0, 31.5, 30.9, 24.8, 23.1, 17.7.

(4aS*,6S*,8aS*)-6-((2-methoxyethoxy)methoxy)-8a-methyl-1-oxodecahydronaphthalene-2-carboxylate (2.14)



To a solution of ketone **2.01** (0.556 g, 2.06 mmol) in anhydrous THF (30 mL) was added dimethyl carbonate (1.74 mL, 20.6 mmol) and NaH (60 wt. % dispersion in mineral oil, 0.823 g, 20.6 mmol) and the resulting suspension was heated at reflux for six hours. The reaction was cooled to 0 °C in an ice bath before quenching with saturated aqueous NH₄Cl and extracted twice with DCM. The combined organic phases were dried over anhydrous MgSO₄ and the solvent removed to afford a crude yellow oil. Purification of the crude oil by flash chromatography on silica gel (7:3 ethyl acetate/*n*-heptane) afforded the product as a pale-yellow oil comprised of the keto and enol tautomers (0.526 g, 1.60 mmol, 78% yield).



R_f = 0.33 (7:3 ethyl acetate/*n*-heptane)

¹H NMR (400 MHz, CDCl₃) δ 12.35 (s, 1H, OH), 4.76 (s, 2H, H-14a), 4.75 (s, 2H, H-14b), 3.73 (s, 3H, H-13b), 3.73 (s, 3H, H-13a), 3.71 – 3.66 (m, 5H, H-15a, H-15b, H-9b), 3.61 – 3.45 (m, 6H, H-2a, H-16a, H-2b, H-16b), 3.38 (s, 3H, H-17a), 3.38 (s, 3H, H-17b), 2.34 – 1.27 (m, 22H, H-1a, H-3a, H-4a, H-6a, H-7a, H-8a, H-1b, H-3b, H-4b, H-6b, H-7b, H-8b), 1.16 (s, 3H, H-11b), 1.12 (s, 3H, H-11a)

¹³C NMR (101 MHz, CDCl₃) δ 209.9 (C-10b), 178.8 (C-10a), 173.9 (C-12a), 171.0 (C-12b), 95.0 (C-9a), 93.8 (C-14a, C-14b), 75.8 (C-2a), 75.2 (C-2b), 71.92 (C-16a), 71.89 (C-16b), 66.94 (C-15b), 66.88 (C-15a), 59.17 (C-17b), 59.15 (C-17a), 53.0 (C-9b), 52.1 (C-13b), 51.6 (C-13a), 48.3 (C-5b), 44.1 (C-4b), 40.2 (C-4a), 38.4 (C-5a), 34.2 (C-3a), 34.0 (C-3b), 32.1 (C-6a), 30.8 (C-6b),

29.3 (**C-1b**), 28.1 (**C-1a**), 27.9 (**C-7b**), 26.5 (**C-8b**), 24.6 (**C-7a**), 22.7 (**C-8a**), 17.6 (**C-11a**), 15.6 (**C-11b**)

HRMS (ESI+) m/z found 329.1956 $[M+H]^+$, $C_{17}H_{28}O_6$ calculated 329.1964 ($\Delta = -2.43$ ppm).

General procedures for the synthesis of quinoline fused analogues

Method 1

Ketone **2.01** (70 mg, 0.384 mmol), *p*-TsOH.H₂O (73 mg, 0.384 mmol), and 2-aminobenzaldehyde (60.6 mg, 0.499 mmol) were added to a round bottom flask and the mixture heated at 110 °C for 2 hours. The reaction was cooled to room temperature, dissolved in DCM, washed with saturated aqueous NaHCO₃, brine, and dried over anhydrous sodium sulfate. The solvent was removed under reduced pressure to yield a crude brown solid which was purified via flash chromatography on silica gel (1:1 ethyl acetate/*n*-heptane), yielding the product as a red oil.

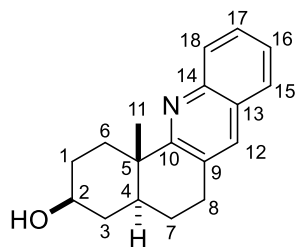
Method 2

To a solution of the substituted 2-nitrobenzaldehyde (0.274 mmol) in EtOH (1.5 mL) was added iron powder (61.2 mg, 1.10 mmol) and 0.1 M aqueous HCl (0.137 mL, 0.0137 mmol). The reaction was heated at reflux until full reduction of the 2-nitrobenzaldehyde was observed. To the solution of 2-aminobenzaldehyde was added potassium hydroxide (37 mg, 0.658 mmol) and ketone **2.01** (50 mg, 0.274 mmol) and the reaction heated at reflux until completion. The reaction mixture was cooled to room temperature, diluted with DCM, filtered through a pad of celite, and the organic phase washed with water. The aqueous phase was back extracted with DCM, the combined organic phases dried over anhydrous magnesium sulfate, and the solvent removed under reduced pressure to yield a crude oil. The crude compounds were purified via flash chromatography on silica gel or by preparative HPLC to yield the products as solids.

Method 3

To a 0.2 – 0.5 mL Biotage microwave vial was added ketone **2.01** (1.0 equiv.), the appropriate aceto- or benzophenone (1.3 equiv.), *p*-TsOH.H₂O (1.3 equiv.), and the contents mixed to combine the reagents. The vial was heated at 110 °C via microwave irradiation for 2 hours. The resulting solid was dissolved in DCM, washed with saturated aqueous Na₂CO₃, and then twice with water. The organic phase was dried over anhydrous magnesium sulfate and concentrated to yield a crude solid. The crude compounds were purified via flash chromatography on silica gel to yield the products as solids.

(**3S***,**4aS***,**12bS***)-12b-methyl-1,2,3,4,4a,5,6,12b-octahydrobenzo[*c*]acridin-3-ol



2.17, method 1 (26.5 mg, 0.0991 mmol, 26% yield, red oil)

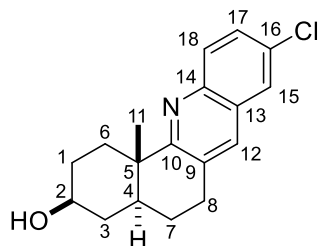
$R_f = 0.23$ (1:1 ethyl acetate/*n*-heptane)

¹H NMR (400 MHz, CDCl₃) δ 8.10 – 7.90 (m, 1H, **H-18**), 7.80 (s, 1H, **H-12**), 7.67 (d, $J = 8.1$ Hz, 1H, **H-15**), 7.59 (t, $J = 7.5$ Hz, 1H, **H-17**), 7.42 (t, $J = 7.4$ Hz, 1H, **H-16**), 3.78 – 3.65 (m, 1H, **H-2**), 3.12 – 3.03 (m, 2H, **H-8**), 2.85 (d, $J = 13.0$ Hz, 1H, **H-6**), 2.08 – 2.00 (m, 1H, **H-1**), 1.91 – 1.49 (m, 7H, **H-1**, **H-3**, **H-4**, **H-6**, **H-7**), 1.20 (s, 3H, **H-11**)

¹³C NMR (101 MHz, CDCl₃) δ 166.6 (**C-10**), 146.6 (**C-14**), 135.4 (**C-12**), 129.04 (**C-13**), 129.0 (**C-18**), 128.3 (**C-17**), 127.1 (**C-9**), 126.7 (**C-15**), 125.7 (**C-16**), 71.1 (**C-2**), 40.4 (**C-4**), 40.0 (**C-5**), 38.1 (**C-3**), 34.9 (**C-6**), 31.7 (**C-1**), 28.5 (**C-8**), 25.2 (**C-7**), 20.2 (**C-11**)

HRMS (ESI+) m/z found 268.1694 [M+H]⁺, C₁₈H₂₁NO calculated 268.1701 (Δ = -2.61 ppm).

(3S*,4aS*,12bS*)-9-chloro-12b-methyl-1,2,3,4,4a,5,6,12b-octahydrobenzo[c]acridin-3-ol



2.18, method 2, 45 minutes reduction, 4 hours cyclisation, purified via flash chromatography (40.1 mg, 0.133 mmol, 49% yield, pale-yellow solid)

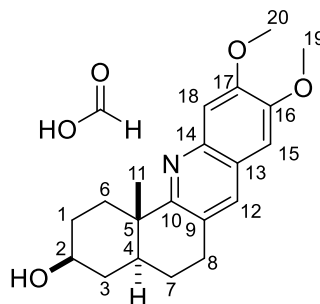
R_f = 0.26 (1:1 ethyl acetate/*n*-heptane)

¹H NMR (400 MHz, CDCl₃) δ = 7.91 (d, *J* = 8.9, 1H, **H-18**), 7.70 (s, 1H, **H-12**), 7.65 (d, *J* = 2.35 Hz, 1H, **H-15**), 7.52 (dd, *J* = 8.9, 2.35 Hz, 1H, **H-17**), 3.73 (tt, *J* = 15.8, 10.7, 4.8 Hz, 1H, **H-2**), 3.07 (m, 2H, **H-8**), 2.80 (m, 1H, **H-6**), 2.03 (m, 1H, **H-1**), 1.92 – 1.47 (m, 7H, **H-1**, **H-3**, **H-4**, **H-6**, **H-7**), 1.18 (s, 3H, **H-20**)

¹³C NMR (101 MHz, CDCl₃) δ = 167.0 (**C-10**), 144.8 (**C-14**), 134.4 (**C-12**), 131.3 (**C-16**), 130.7 (**C-18**), 130.2 (**C-9**), 129.2 (**C-17**), 127.7 (**C-13**), 125.4 (**C-15**), 71.1 (**C-2**), 40.3 (**C-4**), 40.0 (**C-5**), 38.1 (**C-3**), 34.8 (**C-6**), 31.7 (**C-1**), 28.5 (**C-8**), 25.0 (**C-7**), 20.1 (**C-11**)

HRMS (ESI+) m/z found 302.1304 [M+H]⁺, C₁₈H₂₀ClNO calculated 302.1311 (Δ = -2.32 ppm).

(3S*,4aS*,12bS*)-9,10-dimethoxy-12b-methyl-1,2,3,4,4a,5,6,12b-octahydrobenzo[c]acridin-3-ol



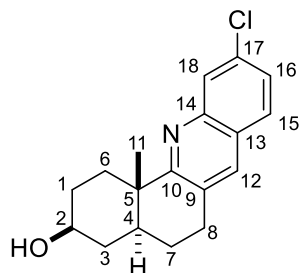
2.19, method 2, 3.5 hours reduction, 48 hours cyclisation, purified via preparative HPLC (24.0 mg, 0.062 mmol, 23% yield, pale-yellow solid)

¹H NMR (400 MHz, CDCl₃) δ = 7.81 (s, 1H, **H-12**), 7.64 (s, 1H, **H-18**), 6.95 (s, 1H, **H-15**), 4.03 (s, 3H, **H-20**), 3.98 (s, 3H, **H-19**), 3.72 (tt, *J* = 10.6, 4.8 Hz, 1H, **H-2**), 3.10 – 2.98 (m, 2H, **H-8**), 2.96 – 2.84 (m, 1H, **H-6**), 2.04 (m, 1H, **H-1**), 1.92 – 1.48 (m, 7H, **H-1**, **H-3**, **H-4**, **H-6**, **H-7**), 1.25 (s, 3H, **H-11**)

¹³C NMR (101 MHz, CDCl₃) δ = 162.8 (**C-10**), 153.1 (**C-17**), 150.1 (**C-16**), 141.3 (**C-14**), 136.7 (**C-12**), 127.4 (**C-9**), 122.9 (**C-13**), 105.5 (**C-18**), 104.2 (**C-15**), 70.9 (**C-2**), 56.6 (**C-20**), 56.2 (**C-19**), 40.6 (**C-4**), 39.5 (**C-5**), 37.7 (**C-3**), 34.6 (**C-6**), 31.5 (**C-1**), 28.4 (**C-8**), 25.0 (**C-7**), 20.0 (**C-11**)

HRMS (ESI+) m/z found 328.1910 [M+H]⁺, C₂₀H₂₅NO₃ calculated 328.1912 (Δ = -0.61 ppm).

(3S*,4aS*,12bS*)-10-chloro-12b-methyl-1,2,3,4,4a,5,6,12b-octahydrobenzo[c]acridin-3-ol



2.20, method 2, 1 hour reduction, 6 hours cyclisation, purified via flash chromatography (46.2 mg, 0.153 mmol, 56% yield, white solid)

R_f = 0.26 (2:3 ethyl acetate/*n*-pentane)

¹H NMR (400 MHz, DMSO) δ = 8.04 (s, 1H, **H-12**), 7.92 – 7.84 (m, 2H, **H-15**, **H-18**), 7.51 (dd, *J* = 8.7, 2.1 Hz, 1H, **H-16**), 3.53 – 3.40 (m, 1H, **H-**

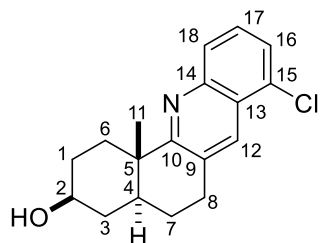
2), 3.03 (m, 2H, **H-8**), 2.65 – 2.56 (m, 1H, **H-6**), 1.84 (m, 1H, **H-1**), 1.77 – 1.31 (m, 7H, **H-1**, **H-3**, **H-4**, **H-6**, **H-7**), 1.07 (s, 3H, **H-11**)

¹³C NMR (101 MHz, DMSO) δ = 167.8 (**C-10**), 146.0 (**C-14**), 135.3 (**C-12**), 132.7 (**C-17**), 129.7 (**C-9**), 128.9 (**C-15**), 126.9 (**C-18**), 126.3 (**C-16**), 125.2 (**C-13**), 69.0 (**C-2**), 37.9 (**C-3**), 34.6 (**C-6**), 31.3 (**C-1**), 27.7 (**C-8**), 24.5 (**C-7**), 20.0 (**C-11**)

HRMS (ESI+) m/z found 302.1303 $[M+H]^+$, $C_{18}H_{20}ClNO$ calculated 302.1311 (Δ = -2.65 ppm).

Note: signals arising from C-4 and C-5 could not be seen on the 1D-¹³C spectrum but could be seen to appear within the residual solvent peak in the HMBC spectrum

(3S*,4aS*,12bS*)-8-chloro-12b-methyl-1,2,3,4,4a,5,6,12b-octahydrobenzo[c]acridin-3-ol



2.21, method 2, 1 hour reduction, 5 hours cyclisation, purified via flash chromatography (41.0mg, 0.136 mmol, 50% yield, white solid)

R_f = 0.32 (2:3 ethyl acetate/*n*-pentane)

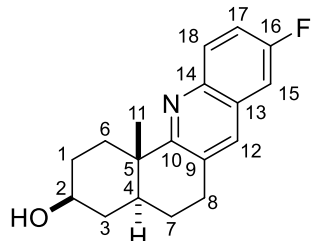
¹H NMR (400 MHz, DMSO) δ = 8.17 (s, 1H, **H-12**), 7.87 (d, J = 8.1 Hz, 1H, **H-16**), 7.68 – 7.56 (m, 2H, **H-17**, **H-18**), 4.59 (d, J = 4.6 Hz, 1H, **O-H**), 3.47 (tt, J = 10.0, 4.4 Hz, 1H, **H-2**), 3.20 – 3.01 (m, 2H, **H-8**), 2.66 – 2.57 (m, 1H, **H-6**), 1.89 – 1.80 (m, 1H, **H-1**), 1.80 – 1.32 (m, 7H, **H-1**, **H-3**, **H-4**, **H-6**, **H-7**), 1.08 (s, 3H, **H-11**)

¹³C NMR (101 MHz, DMSO) δ = 167.5 (**C-10**), 146.4 (**C-14**), 131.3 (**C-12**), 130.8 (**C-9**), 129.1 (**C-15**), 128.4 (**C-18**), 128.1 (**C-16**), 125.8 (**C-17**), 124.2 (**C-13**), 69.0 (**C-2**), 37.9 (**C-3**), 34.6 (**C-6**), 31.3 (**C-1**), 27.8 (**C-8**), 24.5 (**C-7**), 20.0 (**C-11**)

HRMS (ESI+) m/z found 302.1304 $[M+H]^+$, $C_{18}H_{20}ClNO$ calculated 302.1311 (Δ = -2.32 ppm).

Note: signals arising from C-4 and C-5 could not be seen on the 1D-¹³C spectrum but could be seen to appear within the residual solvent peak in the HMBC spectrum

(3S*,4aS*,12bS*)-9-fluoro-12b-methyl-1,2,3,4,4a,5,6,12b-octahydrobenzo[c]acridin-3-ol



2.22, method 2, 1 hour reduction, 20 hours cyclisation, purified via flash chromatography (21.4 mg, 0.0750 mmol, 27% yield, white solid)

R_f = 0.36 (2:3 ethyl acetate/*n*-pentane)

¹H NMR (400 MHz, $CDCl_3$) δ = 7.79 (s, 1H, **H-12**), 7.68 – 7.58 (m, 2H, **H-17**, **H-18**), 7.22 (td, J = 8.6, 2.6 Hz, 1H, **H-15**), 3.73 (tt, J = 10.7, 4.8 Hz, 1H, **H-2**), 3.05 (m, **H-8**), 2.81 (d, J = 13.3 Hz, 1H, **H-6**), 2.04 (m, 1H, **H-1**), 1.93 – 1.47 (m, 7H, **H-1**, **H-3**, **H-4**, **H-6**, **H-7**), 1.19 (s, 3H, **H-11**)

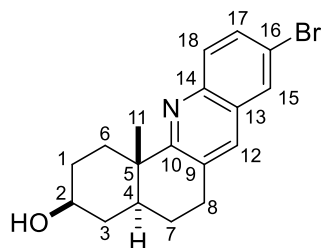
¹³C NMR (101 MHz, $CDCl_3$) δ = 167.7 (**C-10**), 162.6 (d, J = 250.7 Hz, **C-16**), 147.4 (**C-14**), 135.3 (**C-12**), 128.6 (d, J = 9.9 Hz, **C-18**), 128.4 (**C-9**), 124.1 (**C-13**), 116.2 (d, J = 24.8 Hz, **C-15**), 112.5 (d, J = 19.5 Hz, **C-17**), 71.1 (**C-2**), 40.4 (**C-4**), 40.1 (**C-5**), 38.1 (**C-3**), 34.8 (**C-6**), 31.7 (**C-1**), 28.4 (**C-8**), 25.1 (**C-7**), 20.2 (**C-11**)

¹⁹F NMR (377 MHz, $CDCl_3$) δ -112.1

HRMS (ESI+) m/z found 286.1604 $[M+H]^+$, $C_{18}H_{20}FNO$ calculated 286.1607 (Δ = -1.05 ppm).

Note: C-14 could not be seen on the 1D-¹³C spectrum but could be seen in the HMBC spectrum, compound isolated alongside impure S_NAr product

(3S*,4aS*,12bS*)-9-bromo-12b-methyl-1,2,3,4,4a,5,6,12b-octahydrobenzo[c]acridin-3-ol



2.23, 1.5 hours reduction, 2 hours cyclisation, purified via flash chromatography (35.0 mg, 0.101 mmol, 37% yield, white solid)

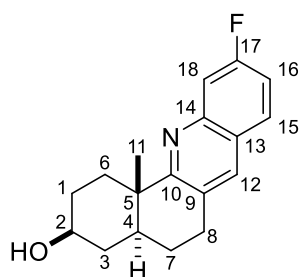
R_f = 0.30 (2:3 ethyl acetate/*n*-hexane)

¹H NMR (400 MHz, DMSO) δ = 8.12 – 8.06 (m, 1H, **H-15**), 7.97 (s, 1H, **H-12**), 7.80 (d, J = 9.1, 1.85 Hz, 1H, **H-18**), 7.71 (d, J = 9.1, 1.85 Hz, 1H, **H-17**), 4.58 (d, J = 4.7 Hz, 1H, **O-H**), 3.46 (tt, J = 10.1, 4.6 Hz, 1H, **H-2**), 3.07 – 3.02 (m, 2H, **H-8**), 2.67 – 2.56 (m, 1H, **H-6**), 1.88 – 1.79 (m, 1H, **H-1**), 1.77 – 1.28 (m, 7H, **H-1**, **H-3**, **H-4**, **H-6**, **H-7**), 1.07 (s, 3H, **H-11**)

¹³C NMR (101 MHz, DMSO) δ = 167.2 (**C-10**), 144.3 (**C-14**), 134.5 (**C-12**), 131.4 (**C-17**), 130.6 (**C-18**), 130.3 (**C-9**), 128.9 (**C-15**), 128.0 (**C-13**), 118.4 (**C-16**), 69.0 (**C-2**), 37.9 (**C-3**), 34.6 (**C-6**), 31.3 (**C-1**), 27.7 (**C-8**), 24.5 (**C-7**), 20.0 (**C-11**)

HRMS (ESI+) m/z found 346.0803 [$M+H$]⁺, C₁₈H₂₀BrNO calculated 346.0806 (Δ = -0.87 ppm).

(3S*,4aS*,12bS*)-10-fluoro-12b-methyl-1,2,3,4,4a,5,6,12b-octahydrobenzo[c]acridin-3-ol



2.24, 1 hour reduction, 4 hours cyclisation, purified via flash chromatography (19.0 mg, 0.0670 mmol, 24% yield, white solid)

R_f = 0.30 (1:1 ethyl acetate/*n*-pentane)

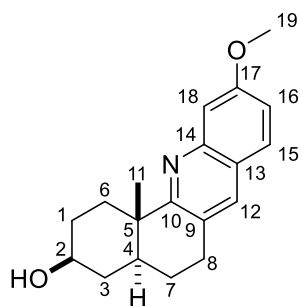
¹H NMR (400 MHz, CDCl₃) δ 7.78 (s, 1H, **H-12**), 7.72 – 7.54 (m, 2H, **H-15**, **H-18**), 7.26 – 7.17 (m, 1H, **H-16**), 3.72 (td, J = 10.9, 5.3 Hz, 1H, **H-2**), 3.13 – 2.97 (m, 2H, **H-8**), 2.81 (d, J = 13.3 Hz, 1H, **H-6**), 2.11 – 1.99 (m, 1H, **H-1**), 1.94 – 1.46 (m, 7H, **H-1**, **H-3**, **H-4**, **H-6**, **H-7**), 1.18 (s, 3H, **H-11**)

¹³C NMR (101 MHz, CDCl₃) δ 167.7 (**C-10**), 162.6 (d, J = 229.7 Hz, **C-17**), 147.5 (**C-14**), 135.3 (**C-12**), 128.6 (d, J = 10.1 Hz, **C-15**), 128.4 (**C-9**), 124.1 (**C-13**), 116.2 (d, J = 24.4 Hz, **C-16**), 112.6 (d, J = 18.2 Hz, **C-18**), 71.2 (**C-2**), 40.4 (**C-4**), 40.1 (**C-5**), 38.1 (**C-3**), 34.8 (**C-6**), 31.7 (**C-1**), 28.4 (**C-8**), 25.1 (**C-7**), 20.2 (**C-11**)

¹⁹F NMR (377 MHz, CDCl₃) δ -112.1

HRMS (ESI+) m/z found 286.1603 [$M+H$]⁺, C₁₈H₂₀FNO calculated 286.1607 (Δ = -1.40 ppm).

(3S*,4aS*,12bS*)-10-methoxy-12b-methyl-1,2,3,4,4a,5,6,12b-octahydrobenzo[c]acridin-3-ol



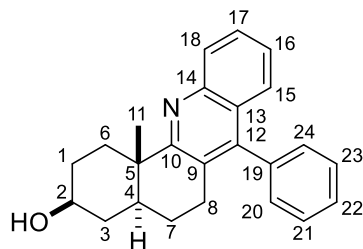
2.25, 4 hours reduction, 20 hours cyclisation, purified by preparative HPLC, desalted (25.0 mg, 0.0841 mmol, 31% yield, white solid)

¹H NMR (400 MHz, CDCl₃) δ 7.72 (s, 1H, **H-12**), 7.56 (d, *J* = 8.9 Hz, 1H, **H-15**), 7.31 (s, 1H, **H-18**), 7.09 (d, *J* = 8.9, 1H, **H-16**), 3.94 (s, 3H, **H-19**), 3.73 (td, *J* = 10.8, 5.9 Hz, 1H, **H-2**), 3.04 (m, 2H, **H-8**), 2.81 (d, *J* = 12.5 Hz, 1H, **H-6**), 2.04 (m, 1H, **H-1**), 1.92 – 1.46 (m, 7H, **H-1**, **H-3**, **H-4**, **H-6**, **H-7**), 1.19 (s, 3H, **H-11**)

¹³C NMR (101 MHz, CDCl₃) δ = 166.8 (**C-10**), 160.0 (**C-17**), 148.3 (**C-14**), 135.3 (**C-12**), 127.8 (**C-15**), 126.6 (**C-9**), 122.4 (**C-13**), 119.0 (**C-16**), 106.9 (**C-18**), 71.2 (**C-2**), 55.6 (**C-19**), 40.5 (**C-4**), 39.9 (**C-5**), 38.2 (**C-3**), 35.0 (**C-6**), 31.8 (**C-1**), 28.3 (**C-8**), 25.3 (**C-7**), 20.2 (**C-11**)

HRMS (ESI+) *m/z* found 298.1800 [*M*+*H*]⁺, C₁₉H₂₃NO₂ calculated 298.1807 (Δ = -2.35 ppm).

(3S*,4aS*,12bS*)-12b-methyl-7-phenyl-1,2,3,4,4a,5,6,12b-octahydrobenzo[c]acridin-3-ol



2.28, method 3 (64.4 mg, 0.187 mmol, 68% yield, off-white solid)

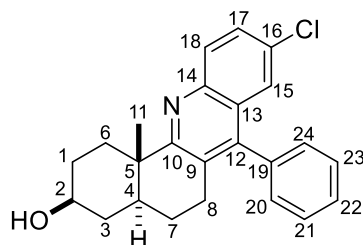
R_f = 0.28 (1:1 ethyl acetate/*n*-heptane)

¹H NMR (400 MHz, DMSO) δ 7.93 (d, *J* = 8.3 Hz, 1H, **H-18**), 7.62 (t, *J* = 7.6 Hz, 1H, **H-17**), 7.59 – 7.47 (m, 3H, **H-21**, **H-22**, **H-23**), 7.37 (t, *J* = 8.2, 6.8, 1.2 Hz, 1H, **H-16**), 7.30 – 7.20 (m, 2H, **H-20**, **H-24**), 7.16 (dd, *J* = 8.5, 1.3 Hz, 1H, **H-15**), 4.58 (d, *J* = 4.6 Hz, 1H, **OH**), 3.47 (tt, *J* = 10.0, 4.7 Hz, 1H, **H-2**), 2.74 – 2.54 (m, 3H, **H-6**, **H-8**), 1.92 – 1.82 (m, 1H, **H-1**), 1.71 – 1.43 (m, 6H, **H-1**, **H-3**, **H-4**, **H-6**, **H-7**), 1.36 (q, *J* = 12.0 Hz, 1H, **H-3**), 1.14 (s, 3H, **H-11**)

¹³C NMR (101 MHz, DMSO) δ 166.2 (**C-10**), 146.2 (**C-12**), 145.5 (**C-14**), 136.8 (**C-19**), 128.9 (**C-20**, **C-21**, **C-23**, **C-24**), 128.7 (**C-18**), 128.1 (**C-17**), 127.8 (**C-22**), 126.2 (**C-9**), 125.8 (**C-13**), 125.7 (**C-16**), 125.0 (**C-15**), 69.1 (**C-2**), 39.9 (**C-5**), 39.2 (**C-4**), 37.9 (**C-3**), 35.0 (**C-6**), 31.4 (**C-1**), 27.2 (**C-8**), 24.6 (**C-7**), 20.2 (**C-11**)

HRMS (ESI+) *m/z* found 334.2007 [*M*+*H*]⁺, C₂₄H₂₅NO calculated 334.2014 (Δ = -2.03 ppm).

(3S*,4aS*,12bS*)-9-chloro-12b-methyl-7-phenyl-1,2,3,4,4a,5,6,12b-octahydrobenzo[c]acridin-3-ol



2.29, method 3 (76.0 mg, 0.201 mmol, 73% yield, pale-yellow solid)

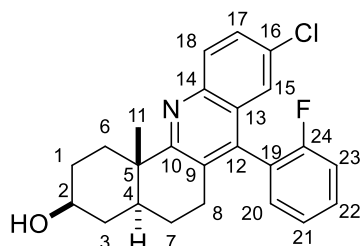
R_f = 0.28 (1:1 ethyl acetate/*n*-heptane)

¹H NMR (400 MHz, DMSO) δ = 7.96 (d, *J* = 8.9 Hz, 1H, **H-18**), 7.68 – 7.48 (m, 5H, **H-17**, **H-21**, **H-22**, **H-23**), 7.33 – 7.23 (m, 2H, **H-20**, **H-24**), 7.08 (d, *J* = 2.4 Hz, 1H, **H-15**), 4.59 (d, *J* = 4.7 Hz, 1H, **OH**), 3.48 (dt, *J* = 10.1, 4.4 Hz, 1H, **H-2**), 2.74 – 2.56 (m, 3H, **H-6**, **H-8**), 1.9 – 1.83 (m, 1H, **H-1**), 1.75 – 1.44 (m, 6H, **H-1**, **H-3**, **H-4**, **H-6**, **H-7**), 1.36 (q, *J* = 12.1 Hz, 1H, **H-3**), 1.14 (s, 3H, **H-11**)

¹³C NMR (101 MHz, DMSO) δ = 166.9 (**C-10**), 145.5 (**C-12**), 143.9 (**C-14**), 136.0 (**C-19**), 131.0 (**C-18**), 130.1 (**C-16**), 129.00 (**C-21/C-23**), 128.97 (**C-21/C-23**), 128.8 (**C-24**), 128.7 (**C-17**, **C-20**), 128.1 (**C-22**), 127.6 (**C-9**), 126.6 (**C-13**), 123.5 (**C-15**), 69.0 (**C-2**), 40.0 (**C-5**), 39.0 (**C-4**), 37.8 (**C-3**), 34.9 (**C-6**), 31.3 (**C-1**), 27.2 (**C-8**), 24.4 (**C-7**), 20.2 (**C-11**)

HRMS (ESI+) m/z found 378.1616 [$M+H$]⁺, C₂₄H₂₄ClNO calculated 378.1624 (Δ = -2.12 ppm).

(3S*,4aS*,12bS*)-9-chloro-7-(2-fluorophenyl)-12b-methyl-1,2,3,4,4a,5,6,12b-octahydrobenzo[c]acridin-3-ol



2.30, method 3 (85.2 mg, 0.216 mmol, 79% yield, pale-yellow solid)

R_f = 0.30 (1:1 ethyl acetate/*n*-heptane)

¹H NMR (400 MHz, DMSO) δ 7.98 (d, J = 9.0 Hz, 1H, **H-18**), 7.67 (dd, J = 9.0, 2.4 Hz, 1H, **H-17**), 7.62 (dtd, J = 7.6, 6.4, 5.3, 1.9 Hz, 1H **H-20/21/22/23**), 7.50 – 7.29 (m, 3H, **H-20/21/22/23**), 7.10 – 7.04 (m, 1H, **H-15**), 3.49 (m, 2H, **H-2**, O-H), 2.77 – 2.52 (m, 3H, **H-6**, **H-8**), 1.86 (m, 1H, **H-1**), 1.77 – 1.60 (m, 3H, **H-3**, **H-4**, **H-7**), 1.59 – 1.43 (m, 3H, **H-1**, **H-6**, **H-7**), 1.36 (q, J = 11.7 Hz, 1H, **H-3**), 1.14 (s, 3H, **H-11**)

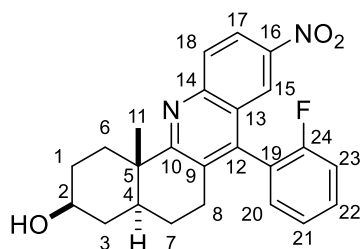
¹³C NMR (101 MHz, DMSO) δ 167.0, 167.0, 159.7, 157.5, 157.3, 143.9, 143.9, 139.5, 139.4, 131.3, 131.2, 131.1, 131.1, 130.6, 129.0, 128.7, 128.7, 126.4, 126.4, 125.3, 123.0, 123.0, 122.9, 122.8, 116.3, 116.3, 116.1, 116.1, 69.8, 69.0, 68.9, 39.0, 37.8, 34.8, 34.8, 31.3, 26.9, 26.5, 24.3, 24.2, 20.2, 20.2

¹⁹F NMR (377 MHz, DMSO) δ -114.9, -115.0

HRMS (ESI+) m/z found 396.1521 [$M+H$]⁺, C₂₄H₂₃ClFNO calculated 396.1530 (Δ = -2.27 ppm).

Note: Compound present as a mixture of conformational isomers. Assignment of carbon atoms was not made owing to complexity of the ¹³C spectrum.

(3S*,4aS*,12bS*)-7-(2-fluorophenyl)-12b-methyl-9-nitro-1,2,3,4,4a,5,6,12b-octahydrobenzo[c]acridin-3-ol



2.31, method 3 (45.3 mg, 0.111 mmol, 41% yield, off-white solid)

R_f = 0.26 (3:2 ethyl acetate/*n*-hexane)

¹H NMR (400 MHz, DMSO) δ 8.38 (dd, J = 9.2, 2.55 Hz, 1H, **H-17**), 8.18 (d, J = 9.2 Hz, 1H, **H-18**), 8.02 (dd, J = 4.9, 2.55 Hz, 1H, **H-15**), 7.71 – 7.64 (m, 1H), 7.56 – 7.38 (m, 3H), 4.62 (dd, J = 4.8, 2.2 Hz, 1H, O-H), 3.56 – 3.40 (m, 1H, **H-2**), 2.81 – 2.54 (m, 3H, **H-6**, **H-8**), 1.88 (m, 1H, **H-1**), 1.82 – 1.64 (m, 3H, **H-3**, **H-4**, **H-7**), 1.63 – 1.48 (m, 3H, **H-1**, **H-6**, **H-7**), 1.37 (q, J = 12.0 Hz, 1H, **H-3**), 1.17 (s, 3H, **H-11**)

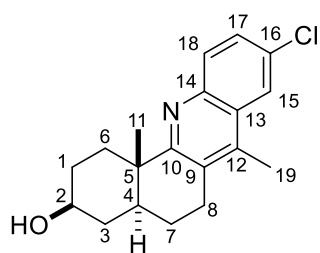
¹³C NMR (101 MHz, DMSO) δ 170.7, 170.6, 147.4, 144.7, 144.7, 142.1, 142.0, 131.5, 131.5, 131.5, 131.3, 131.3, 131.2, 130.8, 130.5, 130.0, 129.9, 125.4, 125.3, 125.3, 125.3, 124.5, 124.5, 122.3, 122.3, 122.2, 122.1, 121.8, 121.0, 121.0, 116.4, 116.3, 116.2, 116.2, 116.1, 68.8, 68.8, 40.4, 40.4, 38.8, 38.6, 37.7, 34.6, 34.6, 31.2, 26.8, 26.5, 24.1, 24.0, 20.1, 20.0

^{19}F NMR (377 MHz, DMSO) δ -114.6, -114.7

HRMS (ESI+) m/z found 407.1765 $[\text{M}+\text{H}]^+$, $\text{C}_{24}\text{H}_{23}\text{FN}_2\text{O}_3$ calculated 407.1771 (Δ = -1.47 ppm).

Note: Compound present as a mixture of conformational isomers. Assignment of carbon atoms was not made owing to complexity of the ^{13}C spectrum.

(3S*,4aS*,12bS*)-9-chloro-7,12b-dimethyl-1,2,3,4,4a,5,6,12b-octahydrobenzo[c]acridin-3-ol



2.32, method 3 (31.4 mg, 0.0994 mmol, 53% yield, pale-yellow solid)

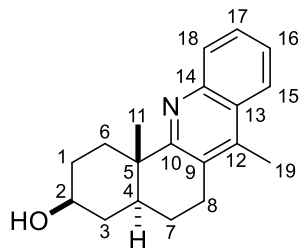
R_f = 0.34 (1:1 ethyl acetate/*n*-hexane)

^1H NMR (400 MHz, DMSO) δ 8.10 (d, J = 2.3 Hz, 1H, **H-15**), 7.85 (d, J = 8.9 Hz, 1H, **H-18**), 7.60 (dd, J = 8.9, 2.3 Hz, 1H, **H-17**), 4.57 (d, J = 4.7 Hz, 1H, O-H), 3.46 (tt, J = 10.1, 4.7 Hz, 1H, **H-2**), 3.02 – 2.79 (m, 2H, **H-8**), 2.63 (dt, J = 13.3, 3.3 Hz, 1H, **H-6**), 2.48 (s, 3H, **H-19**), 1.86 – 1.78 (m, 1H, **H-1**), 1.76 – 1.60 (m, 4H, **H-3**, **H-4**, **H-7**), 1.55 – 1.42 (m, 1H, **H-1**), 1.42 – 1.30 (m, 2H, **H-3**, **H-6**), 1.08 (s, 3H, **H-11**)

^{13}C NMR (101 MHz, DMSO) δ = 166.2 (**C-10**), 143.7 (**C-14**), 140.9 (**C-12**), 131.2 (**C-18**), 130.0 (**C-16**), 128.3 (**C-17**), 128.1 (**C-9**), 127.0 (**C-13**), 122.5 (**C-15**), 69.0 (**C-2**), 39.6 (**C-5**), 38.9 (**C-4**), 37.9 (**C-3**), 35.0 (**C-6**), 31.4 (**C-1**), 26.1 (**C-8**), 24.5 (**C-7**), 20.1 (**C-11**), 13.5 (**C-19**)

HRMS (ESI+) m/z found 316.1464 $[\text{M}+\text{H}]^+$, $\text{C}_{19}\text{H}_{22}\text{ClNO}$ calculated 316.1468 (Δ = -1.27 ppm).

(3S*,4aS*,12bS*)-7,12b-dimethyl-1,2,3,4,4a,5,6,12b-octahydrobenzo[c]acridin-3-ol



2.33, method 3 (25.7 mg, 0.0913 mmol, 67% yield, white solid)

R_f = 0.32 (2:3 ethyl acetate/*n*-hexane)

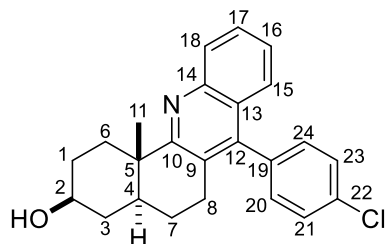
^1H NMR (400 MHz, DMSO) δ 8.07 (d, J = 8.4 Hz, 1H, **H-15**), 7.85 (d, J = 8.3 Hz, 1H, **H-18**), 7.61 (t, J = 7.6 Hz, 1H, **H-16**), 7.50 (t, J = 7.7 Hz, 1H, **H-17**), 4.58 (s, 1H, O-H), 3.47 (tt, J = 10.6, 4.7 Hz, 1H, **H-2**), 3.02 – 2.81 (m, 2H, **H-8**), 2.72 – 2.61 (m, 1H, **H-6**), 2.50 (s, **H-19**), 1.90 – 1.78 (m, 1H, **H-1**), 1.77 – 1.22 (m, 7H, **H-1**, **H-3**, **H-4**, **H-6**, **H-7**), 1.10 (s, 3H, **H-11**)

^{13}C NMR (101 MHz, DMSO) δ = 165.5 (**C-10**), 145.3 (**C-14**), 141.2 (**C-12**), 129.2 (**C-18**), 127.8 (**C-16**), 126.9 (**C-9**), 126.2 (**C-13**), 125.4 (**C-17**), 123.5 (**C-15**), 69.1 (**C-2**), 38.0 (**C-3**), 35.1 (**C-6**), 31.4 (**C-1**), 26.1 (**C-8**), 24.7 (**C-7**), 20.1 (**C-11**), 13.4 (**C-19**)

HRMS (ESI+) m/z found 282.1851 $[\text{M}+\text{H}]^+$, $\text{C}_{19}\text{H}_{23}\text{NO}$ calculated 282.1858 (Δ = -2.48 ppm).

Note: Methyl (C-19) overlaps with the DMSO signal in the ^1H NMR spectrum and signals arising from C-4 and C-5 could not be seen on the 1D- ^{13}C spectrum but could be seen to appear within the residual solvent peak in the HMBC spectrum

(3S*,4aS*,12bS*)-7-(4-chlorophenyl)-12b-methyl-1,2,3,4,4a,5,6,12b-octahydrobenzo[c]acridin-3-ol



2.34, method 3 (61.4 mg, 0.162 mmol, 59% yield, white solid)

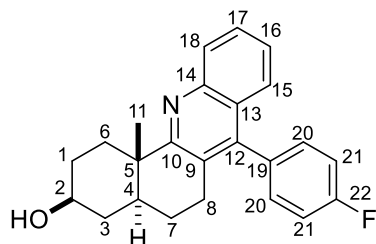
R_f = 0.32 (2:3 ethyl acetate/*n*-hexane)

$^1\text{H NMR}$ (400 MHz, DMSO) δ 7.93 (d, J = 8.7 Hz, 1H, **H-15**), 7.67 – 7.57 (m, 3H, 17, **H-20**, **H-24**), 7.39 (t, J = 8.3 Hz, 1H, **H-16**), 7.34 – 7.24 (m, 2H, **H-21**, **H-23**), 7.16 (d, J = 8.4 Hz, 1H, **H-18**), 4.59 (d, J = 4.6 Hz, 1H, O-H), 3.47 (dt, J = 9.9, 4.7 Hz, 1H, **H-2**), 2.73 – 2.53 (m, 2H, **H-8**), 1.90 – 1.83 (m, 1H, **H-1**), 1.76 – 1.28 (m, 6H, **H-1**, **H-3**, **H-4**, **H-6**, **H-7**), 1.14 (s, 2H, **H-11**)

$^{13}\text{C NMR}$ (101 MHz, DMSO) δ = 166.2 (**C-10**), 145.5 (**C-14**), 144.9 (**C-12**), 135.7 (**C-19**), 132.7 (**C-22**), 130.9 (**C-21/23**), 130.8 (**C-21/23**), 128.92 (**C-20/24**), 128.89 (**C-20/24**), 128.8 (**C-15**), 128.3 (**C-17**), 126.3 (**C-9**), 125.9 (**C-16**), 125.6 (**C-13**), 124.8 (**C-18**), 69.1 (**C-2**), 37.9 (**C-3**), 35.0 (**C-6**), 31.4 (**C-1**), 27.1 (**C-8**), 24.5 (**C-7**), 20.2 (**C-11**)

HRMS (ESI+) m/z found 378.1616 $[\text{M}+\text{H}]^+$, $\text{C}_{24}\text{H}_{24}\text{ClNO}$ calculated 378.1624 (Δ = -2.12 ppm).

(3S*,4aS*,12bS*)-7-(4-fluorophenyl)-12b-methyl-1,2,3,4,4a,5,6,12b-octahydrobenzo[c]acridin-3-ol



2.35, method 3 (58.6 mg, 0.162 mmol, 59% yield, white solid)

R_f = 0.35 (2:3 ethyl acetate/*n*-hexane)

$^1\text{H NMR}$ (400 MHz, DMSO- d_6) δ 7.93 (d, J = 8.4 Hz, 1H, **H-18**), 7.63 (t, J = 7.7 Hz, 1H, **H-17**), 7.44 – 7.25 (m, 5H, **H-16**, **H-20**, **H-21**), 7.16 (d, J = 8.3 Hz, 1H, **H-15**), 3.47 (tt, J = 10.3, 9.9, 4.6 Hz, 1H, **H-2**), 2.76 – 2.53 (m, 3H, **H-6**, **H-8**), 1.92 – 1.83 (m, 1H, **H-1**), 1.76 – 1.60 (m, 3H, **H-3**, **H-4**, **H-7**), 1.60 – 1.46 (m, 3H, **H-1**, **H-6**, **H-7**), 1.36 (q, J = 11.8 Hz, 1H, **H-3**), 1.14 (s, 3H, **H-11**)

$^{13}\text{C NMR}$ (101 MHz, DMSO) δ 166.2 (**C-10**), 161.7 (d, J = 235.9 Hz, **C-22**), 145.5 (**C-12/14**), 145.2 (**C-12/14**), 133.0 (**C-19**), 131.0 (dd, J = 15.4, 8.1 Hz, **C-20**), 128.7 (**C-18**), 128.2 (**C-17**), 126.6 (**C-9**), 125.9 (**C-13**), 125.8 (**C-16**), 124.9 (**C-15**), 115.8 (d, J = 21.5 Hz, **C-21**), 69.1 (**C-2**), 37.9 (**C-3**), 35.0 (**C-6**), 31.4 (**C-1**), 27.2 (**C-8**), 24.6 (**C-7**), 20.2 (**C-11**)

$^{19}\text{F NMR}$ (377 MHz, DMSO) δ -114.4

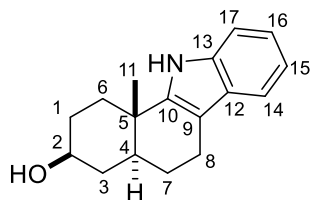
HRMS (ESI+) m/z found 362.1913 $[\text{M}+\text{H}]^+$, $\text{C}_{24}\text{H}_{24}\text{FNO}$ calculated 362.1920 (Δ = -1.93 ppm).

Note: signals arising from C-4 and C-5 could not be seen on the 1D- ^{13}C spectrum but could be seen to appear within the residual solvent peak in the HMBC spectrum

General procedure for the synthesis of indole fused analogues

To a solution of ketone **2.01** (1 equiv.) and *p*-TsOH.H₂O (1.3 equiv.) in absolute ethanol was added the appropriate hydrazine hydrochloride salt (1.3 equiv.) and the reaction mixture refluxed for the indicated time. The reaction was cooled to room temperature, neutralised with saturated aqueous NaHCO₃, and extracted with DCM (3x). The combined organic phases were dried over anhydrous sodium sulfate and the solvent removed to yield a crude solid. Purification of the crude solid via flash chromatography on silica gel afforded the indole products as solids.

(3*S**,4*aS**,11*bS**)-11b-methyl-2,3,4,4*a*,5,6,11,11b-octahydro-1H-benzo[*a*]carbazol-3-ol



2.36, reaction heated for 4 hours (36.5 mg, 0.143 mmol, 52% yield, brown solid)

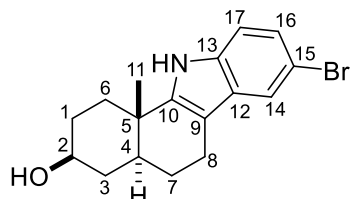
R_f = 0.18 (1:1 ethyl acetate/*n*-heptane)

¹H NMR (400 MHz, CDCl₃) δ 7.71 (s, 1H, **NH**), 7.45 (dd, *J* = 7.5, 1.3 Hz, 1H, **H-17**), 7.30 (dd, *J* = 7.5, 1.3 Hz, 1H, **H-14**), 7.10 (dtd, *J* = 7.5, 1.3 Hz, 2H, **H-15**, **H-16**), 3.75 (tt, *J* = 10.4, 4.8 Hz, 1H, **H-2**), 2.89 – 2.64 (m, 2H, **H-8**), 2.06 – 1.97 (m, 2H, **H-1**, **H-6**), 1.90 – 1.47 (m, 7H, **H-1**, **H-3**, **H-4**, **H-6**, **H-7**), 1.23 (s, 3H, **H-11**)

¹³C NMR (101 MHz, CDCl₃) δ 143.2 (**C-10**), 135.9 (**C-13**), 127.8 (**C-12**), 121.3 (**C-16**), 119.4 (**C-15**), 118.2 (**C-17**), 110.7 (**C-14**), 108.2 (**C-9**), 71.2 (**C-2**), 42.1 (**C-4**), 37.1 (**C-3**), 34.8 (**C-6**), 34.3 (**C-5**), 31.2 (**C-1**), 26.1 (**C-7**), 21.3 (**C-8**), 20.2 (**C-11**)

HRMS (ESI⁺) *m/z* found 256.1711 [M+H]⁺, C₁₇H₂₁NO calculated 256.1701 (Δ = 3.90 ppm).

(3*S**,4*aS**,11*bS**)-8-bromo-11b-methyl-2,3,4,4*a*,5,6,11,11b-octahydro-1H-benzo[*a*]carbazol-3-ol



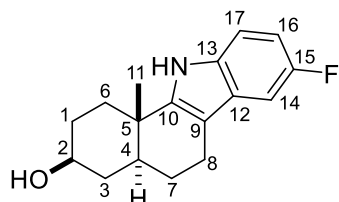
2.37, reaction heated for 20 hours (61.2 mg, 0.183 mmol, 67% yield, tan solid); *R_f* = 0.26 (5% MeOH/DCM)

¹H NMR (400 MHz, CDCl₃) δ 7.76 (s, 1H, **N-H**), 7.56 (d, *J* = 1.8 Hz, 1H, **H-14**), 7.22 – 7.12 (m, 2H, **H-16**, **H-17**), 3.74 (tt, *J* = 10.5, 4.7 Hz, 1H, **H-2**), 2.82 – 2.60 (m, 2H, **H-8**), 2.05 – 1.95 (m, 2H, **H-1**, **H-6**), 1.89 – 1.44 (m, 7H, **H-1**, **H-3**, **H-4**, **H-6**, **H-7**), 1.22 (s, 3H, **H-11**)

¹³C NMR (101 MHz, CDCl₃) δ 144.6 (**C-10**), 134.5 (**C-13**), 129.7 (**C-12**), 123.9 (**C-16**), 120.9 (**C-14**), 112.6 (**C-15**), 112.1 (**C-17**), 108.0 (**C-9**), 71.1 (**C-2**), 42.0 (**C-4**), 37.0 (**C-3**), 34.7 (**C-6**), 34.3 (**C-5**), 31.1 (**C-1**), 25.9 (**C-7**), 21.1 (**C-8**), 20.2 (**C-11**)

HRMS (ESI⁺) *m/z* found 334.0792 [M+H]⁺, C₁₇H₂₁BrNO calculated 334.0806 (Δ = -4.19 ppm).

(3*S**,4*aS**,11*bS**)-8-fluoro-11b-methyl-2,3,4,4*a*,5,6,11,11b-octahydro-1H-benzo[*a*]carbazol-3-ol



2.38, reaction heated for 2.5 hours (37.1 mg, 0.136 mmol, 50% yield, purple solid)

R_f = 0.26 (1:1 ethyl acetate/*n*-pentane)

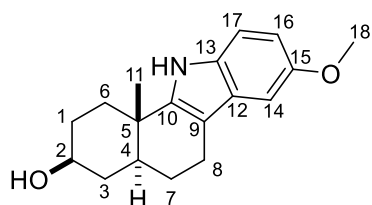
¹H NMR (400 MHz, CDCl₃) δ 7.75 (s, 1H, N-H), 7.19 (dd, *J* = 8.7, 4.3 Hz, 1H, H-17), 7.08 (dd, *J* = 9.6, 2.5 Hz, 1H, H-14), 6.86 (td, *J* = 9.1, 2.5 Hz, 1H, H-16), 3.75 (tt, *J* = 10.6, 4.6 Hz, 1H, H-2), 2.88 – 2.58 (m, 2H, H-8), 2.12 – 1.93 (m, 2H, H-1, H-6), 1.89 – 1.43 (m, 7H, H-1, H-3, H-4, H-6, H-7), 1.23 (s, 3H, H-11)

¹³C NMR (101 MHz, CDCl₃) δ 157.9 (d, *J* = 233.8 Hz, C-15), 145.2 (C-10), 132.3 (C-13), 128.2 (d, *J* = 9.6 Hz, C-12), 111.2 (d, *J* = 9.7 Hz, C-17), 109.2 (d, *J* = 26.2 Hz, C-16), 108.4 (d, *J* = 4.5 Hz, C-9), 103.3 (d, *J* = 23.2 Hz, C-14), 71.2 (C-2), 42.0 (C-4), 37.0 (C-3), 34.7 (C-6), 34.4 (C-5), 31.1 (C-1), 25.9 (C-7), 21.2 (C-8), 20.2 (C-11)

¹⁹F NMR (377 MHz, DMSO-d₆) δ -125.1

HRMS (ESI+) *m/z* found 274.1600 [M+H]⁺, C₁₇H₂₀FNO calculated 274.1607 (Δ = -2.55 ppm).

(3S*,4aS*,11bS*)-8-methoxy-11b-methyl-2,3,4,4a,5,6,11,11b-octahydro-1H-benzo[a]carbazol-3-ol



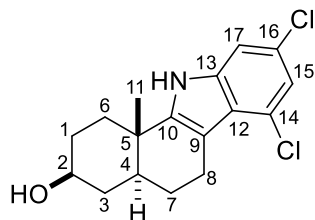
2.39, reaction heated for 24 hours (56.5mg, 0.198 mmol, 72% yield, brown solid); *R_f* = 0.38 (1:1 ethyl acetate/DCM)

¹H NMR (400 MHz, CDCl₃) δ 7.66 (s, 1H, N-H), 7.18 (d, *J* = 8.7 Hz, 1H, H-17), 6.92 (d, *J* = 2.5 Hz, 1H, H-14), 6.79 (dd, *J* = 8.7, 2.5 Hz, 1H, H-16), 3.86 (s, 3H, H-18), 3.81 – 3.68 (m, 1H, H-2), 2.83 – 2.63 (m, 2H, H-8), 2.11 – 1.93 (m, 2H, H-1, H-6), 1.91 – 1.47 (m, 7H, H-1, H-3, H-4, H-6, H-7), 1.22 (s, 3H, H-11)

¹³C NMR (101 MHz, CDCl₃) δ 154.1 (C-15), 144.3 (C-10), 131.0 (C-12), 128.2 (C-13), 111.4 (C-17), 111.0 (C-16), 108.0 (C-9), 100.7 (C-14), 71.2 (C-2), 56.2 (C-18), 42.1 (C-4), 37.1 (C-3), 34.8 (C-6), 34.3 (C-5), 31.1 (C-1), 26.1 (C-7), 21.3 (C-8), 20.2 (C-11)

HRMS (ESI+) *m/z* found 286.1800 [M+H]⁺, C₁₈H₂₃NO₂ calculated 286.1807 (Δ = -2.45 ppm).

(3S*,4aS*,11bS*)-7,9-dichloro-11b-methyl-2,3,4,4a,5,6,11,11b-octahydro-1H-benzo[a]carbazol-3-ol



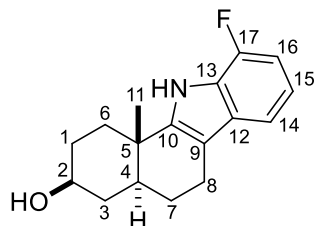
2.40, reaction heated for 48 hours (31.1 mg, 0.0959 mmol, 35% yield, white solid); *R_f* = 0.34 (2:3 ethyl acetate/DCM)

¹H NMR (400 MHz, CDCl₃) δ 7.82 (s, 1H, N-H), 7.15 (d, *J* = 1.65 Hz, 1H, H-17), 7.01 (d, *J* = 1.65 Hz, 1H, H-15), 3.74 (tt, *J* = 10.7, 4.8 Hz, 1H, H-2), 3.21 (dd, *J* = 16.4, 5.8 Hz, 1H, H-8), 3.00 – 2.87 (m, 1H, H-8), 2.05 – 1.94 (m, 2H, H-1, H-6), 1.89 – 1.41 (m, 7H, H-1, H-3, H-4, H-6, H-7), 1.22 (s, 3H, H-11)

¹³C NMR (101 MHz, CDCl₃) δ = 144.6 (C-10), 136.9 (C-13), 126.6 (C-14/C-16), 126.5 (C-14/C-16), 124.0 (C-12), 120.3 (C-15), 109.5 (C-17), 108.7 (C-9), 71.1 (C-2), 41.3 (C-4), 36.9 (C-3), 34.8 (C-6), 34.3 (C-5), 31.0 (C-1), 26.0 (C-7), 23.2 (C-8), 20.2 (C-11)

HRMS (ESI+) *m/z* found 324.0918 [M+H]⁺, C₁₇H₁₉Cl₂NO calculated 324.0922 (Δ = -1.23 ppm).

(3*S,4*aS**,11*bS**)-10-fluoro-11*b*-methyl-2,3,4,4*a*,5,6,11,11*b*-octahydro-1*H*-benzo[*a*]carbazol-3-ol**



2.41, reaction heated for 3 hours (29.6 mg, 0.108 mmol, 39% yield, brown solid)

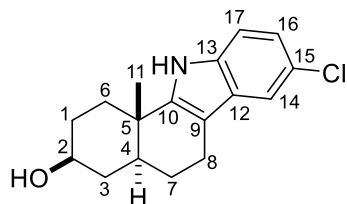
R_f = 0.48 (1:1 ethyl acetate/DCM); $^1\text{H NMR}$ (400 MHz, CDCl_3) δ 7.9 (s, 1H, N-H), 7.2 (d, J = 7.8 Hz, 1H, H-14), 7.0 (tdd, J = 7.8, 4.8, 0.9 Hz, 1H, H-15), 6.8 (ddd, J = 11.3, 7.9, 1.0 Hz, 1H, H-16), 3.8 (tt, J = 10.5, 4.9 Hz, 1H, H-2), 2.8 – 2.7 (m, 2H, H-8), 2.1 – 2.0 (m, 2H, H-1, H-6), 1.9 – 1.5 (m, 7H, H-1, H-3, H-4, H-6, H-7), 1.2 (s, 3H, H-11)

$^{13}\text{C NMR}$ (101 MHz, CDCl_3) δ 149.5 (d, J = 242.5 Hz, C-17), 144.0 (C-10), 131.6 (d, J = 5.5 Hz, C-12), 123.8 (d, J = 12.6 Hz, C-13), 119.6 (d, J = 6.3 Hz, C-15), 114.0 (d, J = 3.2 Hz, C-14), 109.0 (d, J = 2.2 Hz, C-9), 106.4 (d, J = 16.4 Hz, C-16), 71.2 (C-2), 42.1 (C-4), 37.0 (C-3), 34.7 (C-6), 34.4 (C-5), 31.1 (C-1), 26.0 (C-7), 21.4 (C-8), 20.2 (C-11)

$^{19}\text{F NMR}$ (377 MHz, CDCl_3) δ -136.0

HRMS (ESI+) m/z found 274.1600 $[\text{M}+\text{H}]^+$, $\text{C}_{17}\text{H}_{20}\text{FNO}$ calculated 274.1607 (Δ = -2.55 ppm).

(3*S,4*aS**,11*bS**)-8-chloro-11*b*-methyl-2,3,4,4*a*,5,6,11,11*b*-octahydro-1*H*-benzo[*a*]carbazol-3-ol**



2.42, reaction heated for 2.5 hours (29.2 mg, 0.101 mmol, 37% yield, yellow solid)

R_f = 0.26 (1:1 ethyl acetate/*n*-pentane)

$^1\text{H NMR}$ (400 MHz, CDCl_3) δ 7.78 (s, 1H, N-H), 7.40 (d, J = 2.0 Hz, 1H, H-14), 7.19 (d, J = 8.5 Hz, 1H, H-17), 7.06 (dd, J = 8.6, 2.0 Hz, 1H, H-16), 3.78 – 3.68 (m, 1H, H-2), 2.79 – 2.61 (m, 2H, H-8), 2.04 – 1.96 (m, 2H, H-1, H-6), 1.87 – 1.44 (m, 7H, H-1, H-3, H-4, H-6, H-7), 1.22 (s, 3H, H-11)

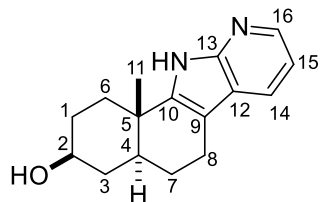
$^{13}\text{C NMR}$ (101 MHz, CDCl_3) δ = 144.8 (C-10), 134.2 (C-13), 129.0 (C-12), 125.0 (C-15), 121.4 (C-16), 117.8 (C-14), 111.6 (C-17), 108.0 (C-9), 71.1 (C-2), 42.0 (C-4), 37.0 (C-3), 34.7 (C-6), 34.3 (C-5), 31.1 (C-1), 25.9 (C-7), 21.1 (C-8), 20.2 (C-11)

HRMS (ESI+) m/z found 290.1305 $[\text{M}+\text{H}]^+$, $\text{C}_{17}\text{H}_{20}\text{ClNO}$ calculated 290.1311 (Δ = -2.07 ppm).

General procedure for the synthesis of 7-azaindole fused analogues

Ketone **2.01** (1 equiv.) and the hydrazinopyridine or hydrazinopyridine hydrochloride salt (1.5 equiv.) were suspended in diethylene glycol in a Biotage microwave vial, and the vial heated at 250 °C via microwave irradiation for 3 hours. The reaction was poured into saturated aqueous NaHCO_3 and extracted with DCM (3x). The combined organic phases were dried over anhydrous sodium sulfate and concentrated to yield a crude oil. Purification of the crude oil via either flash chromatography on silica gel or preparative HPLC afforded the azaindole products as solids.

(3S*,4aS*,11bS*)-11b-methyl-2,3,4,4a,5,6,11,11b-octahydro-1H-benzo[g]pyrido[2,3-b]indol-3-ol



2.49, (27.8 mg, 0.108 mmol, 39% yield, yellow solid)

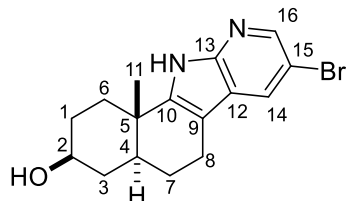
R_f = 0.22 (5.0% MeOH/DCM)

¹H NMR (400 MHz, CDCl₃) δ 10.98 (s, 1H, N-H), 8.19 (dd, *J* = 4.9, 1.5 Hz, 1H, **H-16**), 7.77 (dd, *J* = 7.8, 1.5 Hz, 1H, **H-14**), 7.03 (dd, *J* = 7.7, 4.9 Hz, 1H, **H-15**), 3.77 (tt, *J* = 11.2, 5.1 Hz, 1H, **H-2**), 2.83 – 2.66 (m, 2H, **H-8**), 2.28 (dt, *J* = 12.8, 3.2 Hz, 1H, **H-6**), 2.09 – 1.99 (m, 1H, **H-1**), 1.90 – 1.51 (m, 7H, **H-1**, **H-3**, **H-4**, **H-6**, **H-7**), 1.29 (s, 3H, **H-11**)

¹³C NMR (101 MHz, CDCl₃) δ = 149.0 (**C-13**), 144.7 (**C-10**), 140.8 (**C-16**), 126.4 (**C-14**), 121.0 (**C-12**), 115.2 (**C-15**), 106.2 (**C-9**), 71.2 (**C-2**), 42.1 (**C-4**), 37.1 (**C-3**), 34.8 (**C-6**), 34.5 (**C-5**), 31.2 (**C-1**), 25.9 (**C-7**), 21.2 (**C-8**), 19.9 (**C-11**)

HRMS (ESI+) *m/z* found 257.1647 [M+H]⁺, C₁₆H₂₀N₂O calculated 257.1654 (Δ = -2.72 ppm).

(3S*,4aS*,11bS*)-8-bromo-11b-methyl-2,3,4,4a,5,6,11,11b-octahydro-1H-benzo[g]pyrido[2,3-b]indol-3-ol



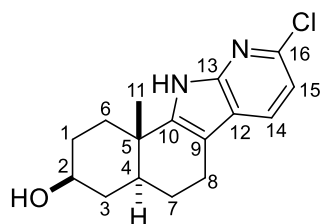
2.50, (18.0 mg, 0.0537 mmol, 10% yield, brown solid)

¹H NMR (400 MHz, CDCl₃) δ 10.50 (s, 1H, N-H), 8.19 (d, *J* = 2.05 Hz, 1H, **H-16**), 7.93 (d, *J* = 2.05 Hz, 1H, **H-14**), 3.77 (tt, *J* = 10.2, 5.1 Hz, 1H, **H-2**), 2.70 (m, 2H, **H-8**), 2.21 (m, 1H, **H-6**), 2.10 – 1.98 (m, 1H, **H-1**), 1.92 – 1.48 (m, 7H, **H-1**, **H-3**, **H-4**, **H-6**, **H-7**), 1.27 (s, 3H, **H-11**)

¹³C NMR (101 MHz, CDCl₃) δ = 147.2 (**C-10**), 145.7 (**C-13**), 139.4 (**C-16**), 129.9 (**C-14**), 123.5 (**C-12**), 110.6 (**C-15**), 106.6 (**C-9**), 71.0 (**C-2**), 41.9 (**C-4**), 36.9 (**C-3**), 34.6 (**C-5**), 34.5 (**C-6**), 31.0 (**C-1**), 25.6 (**C-7**), 20.9 (**C-8**), 19.9 (**C-11**)

HRMS (ESI+) *m/z* found 335.0751 [M+H]⁺, C₁₆H₁₉BrN₂O calculated 335.0759 (Δ = -2.39 ppm).

(3S*,4aS*,11bS*)-9-chloro-11b-methyl-2,3,4,4a,5,6,11,11b-octahydro-1H-benzo[g]pyrido[2,3-b]indol-3-ol



2.51, (39.6 mg, 0.136 mmol, 25% yield, yellow solid)

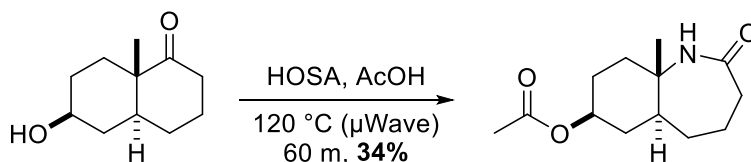
R_f = 0.28 (4.5% MeOH/DCM)

¹H NMR (400 MHz, CDCl₃) δ 9.03 (s, 1H, N-H), 7.68 (d, *J* = 8.1 Hz, 1H, **H-14**), 7.03 (d, *J* = 8.1 Hz, 1H, **H-15**), 3.75 (tt, *J* = 10.6, 4.9 Hz, 1H, **H-2**), 2.71 (m, 2H, **H-8**), 2.07 (dt, *J* = 12.7, 3.4 Hz, 1H, **H-6**), 2.04 – 1.95 (m, 1H, **H-1**), 1.90 – 1.46 (m, 7H, **H-1**, **H-3**, **H-4**, **H-6**, **H-7**), 1.24 (s, 3H, **H-11**)

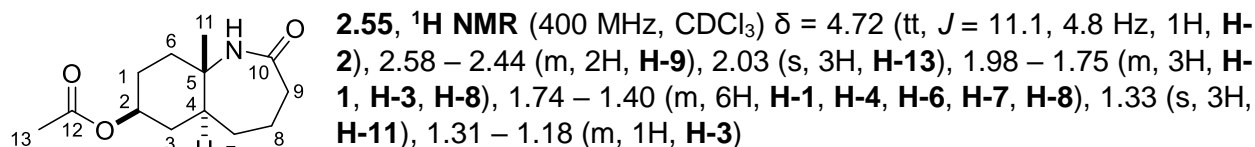
¹³C NMR (101 MHz, CDCl₃) δ = 147.4 (**C-13**), 144.5 (**C-10**), 142.7 (**C-16**), 128.7 (**C-14**), 119.4 (**C-12**), 115.4 (**C-15**), 107.0 (**C-9**), 71.1 (**C-2**), 41.9 (**C-4**), 36.9 (**C-3**), 34.4 (**C-5**), 34.4 (**C-6**), 31.0 (**C-1**), 25.6 (**C-7**), 21.1 (**C-8**), 19.9 (**C-11**)

HRMS (ESI+) m/z found 291.1250 [M+H]⁺, C₁₆H₁₉ClN₂O calculated 291.1264 (Δ = -4.81 ppm).

(5aS*,7S*,9aS*)-9a-methyl-2-oxodecahydro-1H-benzo[b]azepin-7-yl acetate



To a solution of ketone **2.01** (50.7 mg, 0.278 mmol) in glacial AcOH (3 mL) in a 2.0 – 5.0 mL Biotage microwave vial was added hydroxylamine-o-sulfonic acid (33.1 mg, 0.293 mmol). The vial was capped and heated at 120 °C for 60 minutes. The reaction mixture was quenched via addition of 2M aqueous NaOH, extracted with DCM (3x), and the organic phase dried over anhydrous Na₂SO₄, before concentration under reduced pressure. The crude compound was purified via flash chromatography on silica gel (1.5% MeOH/DCM) to yield the product as a white solid (22.8 mg, 0.0953 mmol, 34%)



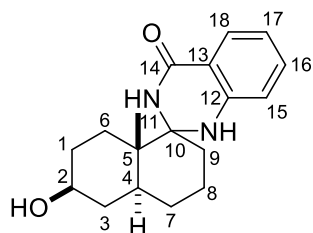
¹³C NMR (101 MHz, CDCl₃) δ = 177.3 (**C-10**), 170.6 (**C-12**), 71.9 (**C-2**), 54.3 (**C-5**), 44.7 (**C-4**), 40.2 (**C-6**), 37.4 (**C-9**), 36.6 (**C-3**), 33.7 (**C-7**), 27.4 (**C-8/C-1**), 23.7 (**C-1/C-8**), 21.4 (**C-13**), 19.2 (**C-11**)

HRMS (ESI+) m/z found 240.1594 [M+H]⁺, C₁₃H₂₁NO₃ calculated 240.1599 (Δ = -2.08 ppm).

General procedure for the synthesis of spirocyclic dihydroquinazolinone analogues

To a solution of ketone **2.01** (1.0 equiv.) in ethanol (2.0 mL) was added the appropriate 2-aminobenzamide (1.05 equiv.) and ammonium chloride (1.00 equiv.) and the solution heated at reflux for 24 hours. After 24 hours, an additional 0.3 equiv. of both the 2-aminobenzamide and ammonium chloride were added and the reactions heated at reflux for a further 8 hours (at this stage, an aliquot of the reaction was taken for determination of the diastereoisomeric ratio). The reaction was concentrated, dissolved in ethyl acetate, washed once with water, and dried over anhydrous Na₂SO₄ to afford a crude solid. The crude solid was purified by flash chromatography on silica gel (6% MeOH/DCM), yielding the product as an inseparable mixture of diastereoisomers.

(4aS*,6S*,8aS*)-6-hydroxy-8a-methyl-3,4,4a,5,6,7,8,8a-octahydro-1'H,2H-spiro[naphthalene-1,2'-quinazolin]-4'(3'H)-one



2.56, (14.7 mg, 0.288 mmol, 18% yield, white solid)

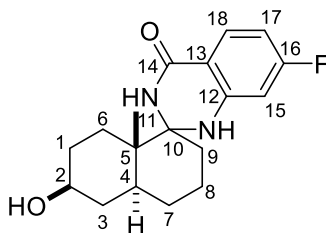
R_f = 0.14 (6% MeOH/DCM); $^1\text{H NMR}$ (400 MHz, MeOD) δ 7.60 (dd, J = 7.8, 1.5 Hz, 1H, **H-18**), 7.24 – 7.19 (t, J = 7.5 Hz, 1H, **H-16**), 6.68 (d, J = 8.2 Hz, 1H, **H-15**), 6.60 (t, J = 7.5 Hz, 1H, **H-17**), 3.50 (td, J = 10.7, 10.2, 5.0 Hz, 1H, **H-2**), 2.03 – 1.87 (m, 2H, **H-9**), 1.79 – 1.56 (m, 5H, **H-1**, **H-3**, **H-4**, **H-8**), 1.50 (m, 2H, **H-6**), 1.42 – 1.23 (m, 4H, **H-1**, **H-3**, **H-7**), 1.05 (s, 3H, **H-11**)

$^{13}\text{C NMR}$ (101 MHz, MeOD) δ 167.2 (**C-14**), 149.2 (**C-12/13**), 135.4 (**C-16**), 128.3 (**C-18**), 117.5 (**C-17**), 114.8 (**C-15**), 113.5 (**C-12/13**), 75.4 (**C-10**), 71.1 (**C-2**), 45.3 (**C-5**), 38.5 (**C-3**), 37.4 (**C-4**), 36.1 (**C-9**), 32.2 (**C-6**), 31.7 (**C-1**), 28.8 (**C-7**), 21.5 (**C-8**), 13.4 (**C-11**)

HRMS (ESI+) m/z found 301.1916 $[\text{M}+\text{H}]^+$, $\text{C}_{18}\text{H}_{24}\text{N}_2\text{O}_2$ calculated 301.1916 (Δ = 0 ppm)

Note: Only signals arising from the isolated diastereoisomer are presented; signals arising from the other diastereoisomer can be seen in the ^1H and ^{13}C spectra, crude d.r. = 1.00:0.85

(4aS*,6S*,8aS*)-7'-fluoro-6-hydroxy-8a-methyl-3,4,4a,5,6,7,8,8a-octahydro-1'H,2H-spiro[naphthalene-1,2'-quinazolin]-4'(3'H)-one



2.57, (69.6 mg, 0.219 mmol, 80% yield, white solid); R_f = 0.26 (6% MeOH/DCM)

$^1\text{H NMR}$ (400 MHz, DMSO) δ 7.57 – 7.47 (m, 1H), 6.62 (dd, J = 11.6, 2.4 Hz, 1H, **H-15***), 6.47 (dd, J = 11.4, 2.4 Hz, 1H, **H-15***), 6.30 (td, J = 8.7, 4.3 Hz, 1H), 4.45 (d, J = 5.2 Hz, 1H, **O-H***), 3.35 – 3.19 (m, 2H, **H-2**, **O-H***), 1.93 (td, J = 14.4, 4.9 Hz, 1H, **C-H***), 1.85 – 1.39 (m, 7H), 1.39 – 1.06 (m, 6H), 0.93 (s, 3H, **H-11***), 0.87 (s, 3H, **H-11***)

$^{13}\text{C NMR}$ (101 MHz, DMSO) δ 167.0, 164.5, 162.5, 162.4, 161.9, 149.3, 149.2, 129.8, 129.7, 129.5, 109.8, 109.7, 102.9, 102.8, 102.7, 102.6, 98.9, 98.8, 98.6, 98.6, 74.0, 73.9, 73.9, 73.8, 68.9, 68.8, 68.7, 68.6, 44.9, 44.1, 37.9, 35.6, 35.2, 35.1, 34.9, 30.8, 30.7, 30.6, 30.5, 27.3, 20.1, 19.7, 13.0, 12.4

$^{19}\text{F NMR}$ (377 MHz, DMSO) δ -107.3

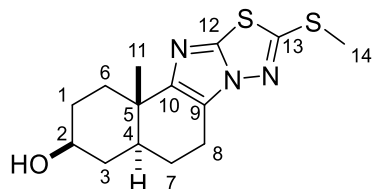
HRMS (ESI+) m/z found 319.1818 $[\text{M}+\text{H}]^+$, $\text{C}_{18}\text{H}_{23}\text{FN}_2\text{O}_2$ calculated 319.1822 (Δ = -1.25 ppm).

Note: Owing to the complexity of the spectral data, assignments are only reported for protons arising from the two diastereoisomers with clear separation, and marked with an asterisk. Data from the ^{13}C spectrum is reported as observed. Crude d.r. = 1.00:0.73

General procedure for the synthesis of imidazothiadiazole fused analogues

To a solution of α -bromoketone **2.10** (1.00 equiv.) in absolute EtOH (1 mL) in a 0.5 – 2.0 mL Biotage microwave vial was added the aminothiadiazole (1.50 equiv.) and the resulting solution heated to 150 °C in a microwave reactor for 2 hours. The reaction mixture was concentrated under reduced pressure and the resulting brown oil purified via flash chromatography on silica gel or via preparative HPLC to yield the products as solids.

(3S*,4aS*,11bS*)-11b-methyl-9-(methylthio)-1,2,3,4,4a,5,6,11b-octahydronaphtho[1',2':4,5]imidazo[2,1-b][1,3,4]thiadiazol-3-ol



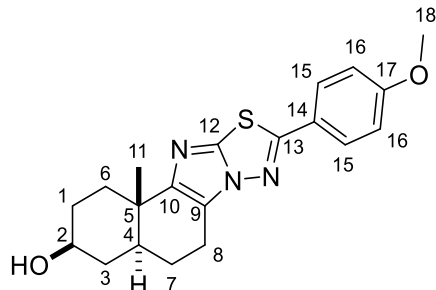
2.60, (21.5 mg, 0.0695 mmol, 36% yield, tan solid)

¹H NMR (400 MHz, CDCl₃) δ 3.71 (tt, *J* = 10.6, 4.9 Hz, 1H, **H-2**), 2.94 – 2.73 (m, 2H, **H-8**), 2.70 (s, 3H, **H-14**), 2.28 (dt, *J* = 13.3, 3.4 Hz, 1H, **H-6**), 2.01 – 1.92 (m, 1H, **H-1**), 1.89 – 1.74 (m, 2H, **H-3**, **H-7**), 1.73 – 1.38 (m, 5H, **H-1**, **H-3**, **H-4**, **H-6**, **H-7**), 1.16 (s, 3H, **H-11**)

¹³C NMR (101 MHz, CDCl₃) δ 160.2 (**C-13**), 149.8 (**C-10**), 142.3 (**C-12**), 120.0 (**C-9**), 71.3 (**C-2**), 42.2 (**C-4**), 36.9 (**C-3**), 35.4 (**C-5**), 34.4 (**C-6**), 31.3 (**C-1**), 25.2 (**C-7**), 20.9 (**C-8**), 20.0 (**C-11**), 16.7 (**C-14**)

HRMS (ESI+) *m/z* found 310.1037 [M+H]⁺, C₁₄H₁₉N₃OS₂ calculated 310.1048 (Δ = -3.55 ppm).

(3S*,4aS*,11bS*)-9-(4-methoxyphenyl)-11b-methyl-1,2,3,4,4a,5,6,11b-octahydronaphtho[1',2':4,5]imidazo[2,1-b][1,3,4]thiadiazol-3-ol



2.61, (24.0 mg, 0.0650 mmol, 39% yield, brown solid)

¹H NMR (400 MHz, CDCl₃) δ = 7.79 (d, *J* = 8.8 Hz, 2H, **H-15**), 6.98 (d, *J* = 8.8 Hz, 2H, **H-16**), 3.87 (s, 3H, **H-18**), 3.74 (dt, *J* = 10.9, 5.6 Hz, 1H, **H-2**), 3.02 – 2.80 (m, 2H, **H-8**), 2.33 (dt, *J* = 13.3, 3.4 Hz, 1H, **H-6**), 2.04 – 1.94 (m, 1H, **H-1**), 1.93 – 1.45 (m, 7H, **H-1**, **H-3**, **H-4**, **H-6**, **H-7**), 1.21 (s, 3H, **H-11**)

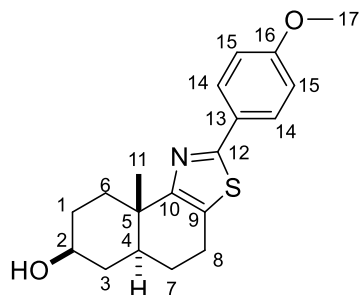
¹³C NMR (101 MHz, CDCl₃) δ = 162.4 (**C-17**), 161.6 (**C-13**), 149.4 (**C-10**), 142.3 (**C-12**), 128.5 (**C-15**), 123.0 (**C-14**), 120.0 (**C-9**), 114.8 (**C-16**), 71.3 (**C-2**), 55.7 (**C-18**), 42.2 (**C-4**), 36.9 (**C-3**), 35.4 (**C-5**), 34.3 (**C-6**), 31.2 (**C-1**), 25.2 (**C-7**), 20.9 (**C-8**), 19.9 (**C-11**)

HRMS (ESI+) *m/z* found 370.1579 [M+H]⁺, C₂₀H₂₃ClN₃O₂S calculated 370.1589 (Δ = -2.70 ppm).

General procedure for the synthesis of thiazole fused analogues

To a solution of α-bromoketone **2.10** (1 equiv.) in EtOH (2.5 mL) was added the appropriate thiourea (1.05 – 3.0 equiv.) and the reaction mixture heated at reflux for the indicated time (in some cases an additional 1.05 equiv. of the substituted thiourea was added to the reaction mixture). Reaction mixtures were concentrated under reduced pressure and purified either by flash chromatography on silica gel or by preparative HPLC, yielding the corresponding thiazoles as solids.

(5aS*,7S*,9aS*)-2-(4-methoxyphenyl)-9a-methyl-4,5,5a,6,7,8,9,9a-octahydronaphtho[1,2-d]thiazol-7-ol



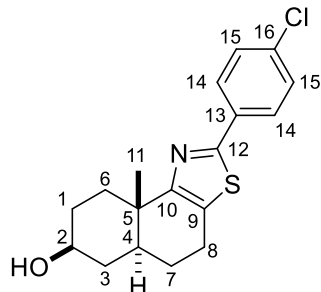
2.63, (25.0 mg, 0.0759 mmol, 26% yield, white solid) 3.00 equiv. of substituted thiourea, 3h reflux

¹H NMR (400 MHz, CDCl₃) δ 7.81 (d, *J* = 8.75 Hz, 2H, **H-14**), 6.91 (d, *J* = 8.75 Hz, 2H, **H-15**), 3.83 (s, 3H, **H-17**), 3.71 (tt, *J* = 10.6, 4.9 Hz, 1H, **H-2**), 2.90 – 2.75 (m, 2H, **H-8**), 2.49 (dt, *J* = 13.5, 3.4 Hz, 1H, **H-6**), 2.03 – 1.90 (m, 1H, **H-1**), 1.89 – 1.57 (m, 5H, **H-1**, **H-3**, **H-4**, **H-7**), 1.55 – 1.41 (m, 2H, **H-3**, **H-6**), 1.18 (s, 3H, **H-11**)

¹³C NMR (101 MHz, CDCl₃) δ 164.9 (**C-12**), 160.8 (**C-16**), 160.5 (**C-10**), 127.8 (**C-14**), 127.4 (**C-13**), 127.0 (**C-9**), 114.2 (**C-15**), 71.3 (**C-2**), 55.5 (**C-17**), 41.5 (**C-4**), 37.0 (**C-3**, **C-5**), 35.0 (**C-6**), 31.4 (**C-1**), 25.9 (**C-7**), 23.9 (**C-8**), 19.5 (**C-11**)

HRMS (ESI+) *m/z* found 330.1522 [*M*+*H*]⁺, C₁₉H₂₃NO₂S calculated 330.1527 (Δ = -1.51 ppm).

(5aS*,7S*,9aS*)-2-(4-chlorophenyl)-9a-methyl-4,5,5a,6,7,8,9,9a-octahydronaphtho[1,2-d]thiazol-7-ol



2.64, (39.0 mg, 0.117 mmol, 61% yield, pale yellow solid) additional 1.05 equiv. of substituted thiourea added after 24h, 48h reflux

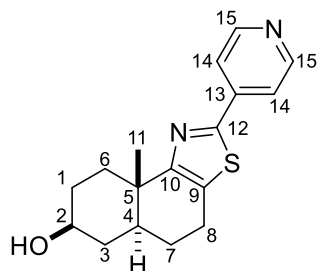
R_f = 0.4 (5% MeOH in DCM)

¹H NMR (400 MHz, CDCl₃) δ 7.89 – 7.80 (m, 2H, **H-14**), 7.40 – 7.34 (m, 2H, **H-15**), 3.72 (tt, *J* = 10.6, 4.9 Hz, 1H, **H-2**), 2.94 – 2.78 (m, 2H, **H-8**), 2.56 (dt, *J* = 13.5, 3.5 Hz, 1H, **H-6**), 2.03 – 1.93 (m, 1H, **H-1**), 1.90 – 1.76 (m, 2H, **H-3**, **H-7**), 1.73 – 1.58 (m, 3H, **H-1**, **H-4**, **H-7**), 1.55 – 1.44 (m, 2H, **H-3**, **H-6**), 1.21 (s, 3H, **H-11**)

¹³C NMR (101 MHz, CDCl₃) δ 164.1 (**C-12**), 160.7 (**C-10**), 135.7 (**C-13**), 132.2 (**C-16**), 129.2 (**C-15**), 128.7 (**C-9**), 127.8 (**C-14**), 71.3 (**C-2**), 41.5 (**C-4**), 37.2 (**C-5**), 37.0 (**C-3**), 34.9 (**C-6**), 31.4 (**C-1**), 25.8 (**C-7**), 24.0 (**C-8**), 19.5 (**C-11**)

HRMS (ESI+) *m/z* found 334.1024 [*M*+*H*]⁺, C₁₈H₂₁N₃O₂ calculated 334.1032 (Δ = -2.39 ppm).

(5aS*,7S*,9aS*)-9a-methyl-2-(pyridin-4-yl)-4,5,5a,6,7,8,9,9a-octahydronaphtho[1,2-d]thiazol-7-ol



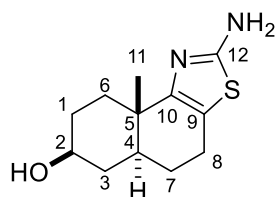
2.65, (25.0 mg, 0.083 mmol, 43% yield, light brown solid) additional 1.05 equiv. of substituted thiourea added after 24h, 48h reflux

¹H NMR (400 MHz, DMSO-*d*₆) δ 8.75 – 8.56 (m, 2H, **H-15**), 7.84 – 7.68 (m, 2H, **H-14**), 4.61 (d, *J* = 4.8 Hz, 1H, O-H), 3.47 (tt, *J* = 10.7, 5.2 Hz, 1H, **H-2**), 2.98 – 2.79 (m, 2H, **H-8**), 2.30 (dt, *J* = 13.0, 3.3 Hz, 1H, **H-6**), 1.85 – 1.27 (m, 8H, **H-1**, **H-3**, **H-4**, **H-6**, **H-7**), 1.10 (s, 3H, **H-11**)

¹³C NMR (101 MHz, DMSO-d₆) δ 161.8 (C-10), 160.9 (C-12), 150.6 (C-15), 139.9 (C-13), 130.8 (C-9), 119.6 (C-14), 69.2 (C-2), 40.6 (C-4), 36.8 (C-5), 36.7 (C-3), 34.8 (C-6), 31.0 (C-1), 25.2 (C-7), 23.3 (C-8), 19.5 (C-11)

HRMS (ESI+) m/z found 301.1382 [M+H]⁺, C₁₇H₂₀N₂OS calculated 301.1374 (Δ = 2.66 ppm).

(5aS*,7S*,9aS*)-2-amino-9a-methyl-4,5,5a,6,7,8,9,9a-octahydronaphtho[1,2-d]thiazol-7-ol



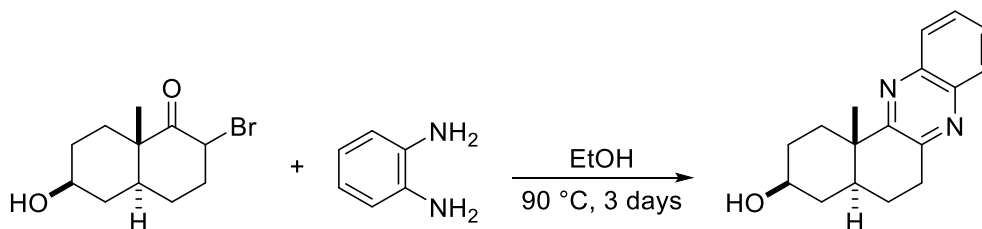
2.66, (23.7 mg, 0.0994 mmol, 67% yield, white solid) 2.00 equiv. of thiourea added, 4h reflux, reaction dissolved in DCM and washed twice with water, dried over anhydrous Na₂SO₄, and concentrated to yield the product

¹H NMR (400 MHz, MeOD) δ 3.61 (tt, *J* = 11.0, 5.7 Hz, 1H, H-2), 2.69 – 2.50 (m, 2H, H-8), 2.12 (dt, *J* = 13.2, 7.1, 3.6 Hz, 1H, H-6), 1.91 – 1.82 (m, 1H, H-1), 1.82 – 1.64 (m, 2H, H-3, H-7), 1.67 – 1.27 (m, 5H, H-1, H-3, H-4, H-6, H-7), 1.10 (s, 3H, H-11)

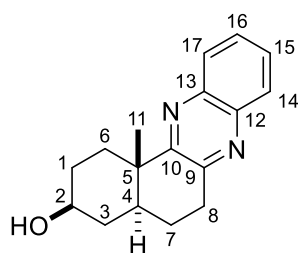
¹³C NMR (101 MHz, MeOD) δ = 169.7 (C-12), 153.6 (C-10), 116.6 (C-9), 71.6 (C-2), 42.8 (C-4), 37.7 (C-3), 37.6 (C-5), 35.7 (C-6), 31.8 (C-1), 27.0 (C-7), 24.2 (C-8), 19.1 (C-11)

HRMS (ESI+) m/z found 239.1212 [M+H]⁺, C₁₂H₁₈N₂OS calculated 239.1218 (Δ = -2.51 ppm).

(3S*,4aS*,12bS*)-12b-methyl-1,2,3,4,4a,5,6,12b-octahydrobenzo[a]phenazin-3-ol



To a solution of α-bromoketone **2.10** (55.6 mg, 0.217 mmol) in absolute ethanol was added o-phenylenediamine (23.1 mg, 0.214 mmol) and the solution refluxed at 90 °C for 3 days. The reaction was concentrated and purified directly by preparative HPLC, yielding the product as a brown solid (1.9 mg, 0.00710 mmol, 3%)



2.67, ¹H NMR (400 MHz, MeOD) δ 8.03 – 7.98 (m, 1H, H-14), 7.95 – 7.88 (m, 1H, H-17), 7.75 – 7.68 (m, 2H, H-15, H-16), 3.67 (tt, *J* = 10.7, 4.8 Hz, 1H, H-2), 3.27 – 3.15 (m, 2H, H-8), 2.75 – 2.67 (m, 1H, H-6), 2.07 – 1.78 (m, 5H, H-1, H-3, H-4, H-7), 1.74 – 1.46 (m, 3H, H-1, H-3, H-6), 1.22 (s, 3H, H-11)

¹³C NMR (101 MHz, MeOD) δ = 163.0 (C-10), 154.4 (C-9), 142.4 (C-13), 141.6 (C-12), 130.5 (C-15), 130.2 (C-16), 129.8 (C-14), 128.4 (C-17), 71.3 (C-2), 41.1 (C-5), 41.0 (C-4), 38.5 (C-3), 35.5 (C-6), 33.0 (C-8), 31.9 (C-1), 25.8 (C-7), 20.3 (C-11)

HRMS (ESI+) m/z found 269.1652 [M+H]⁺, C₁₇H₂₀N₂O calculated 269.1652 (Δ = -0.74 ppm).

Generalised procedures for the synthesis of pyrazole fused analogues

Method 1

To a solution of MEM-protected hydroxymethylene **2.13** (1 equiv.) in glacial AcOH was added the substituted hydrazine (10 equiv.). The reaction was then heated at reflux for three hours and cooled to room temperature. The orange solution was poured into water, extracted with ethyl acetate, the organic phase washed with saturated aqueous NaHCO₃ (3 x), dried over anhydrous MgSO₄, and the solvent removed under reduced pressure to yield an amber-red oil.

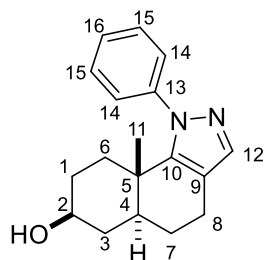
Method 2

To a solution of MEM-protected hydroxymethylene **2.13** (1 equiv.) in a mixture of MeOH:AcOH (4:1) was added the appropriate hydrazine (1.1 – 2.0 equiv.) and the reaction left stirring at room temperature for the indicated amount of time. The reaction was then diluted with water, extracted with ethyl acetate, washed sequentially with saturated aqueous NaHCO₃, water, brine, dried over anhydrous MgSO₄, and the solvent removed to yield the crude pyrazole as a mixture of regioisomers.

Deprotection

The crude mixture of pyrazole regioisomers was dissolved in THF (5 mL) before addition of 6M aqueous HCl (1 mL) and the reaction left stirring at room temperature for 18 hours. The reaction was neutralised with saturated aqueous NaHCO₃, extracted with ethyl acetate, and the organic phase washed sequentially with water, brine, and dried over anhydrous MgSO₄. The solvent was removed to afford an oily residue which was purified by preparative HPLC (MeCN/H₂O + 0.1% HCO₂H) yielding the pyrazole-fused analogues.

(5aS*,7S*,9aS*)-9a-methyl-1-phenyl-4,5,5a,6,7,8,9,9a-octahydro-1H-benzo[g]indazol-7-ol



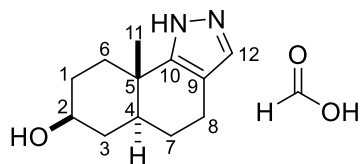
2.73a, method 1, (8.8 mg, 0.0312 mmol, 12% yield over two steps)

¹H NMR (400 MHz, CDCl₃) δ 7.47 – 7.40 (m, 3H, **H-14**, **H-16**), 7.39 – 7.32 (m, 3H, **H-15**, **H-12**), 3.58 (tt, *J* = 10.4, 4.8 Hz, 1H, **H-2**), 2.71 – 2.54 (m, 2H, **H-8**), 1.82 – 1.60 (m, 4H, **H-1**, **H-3**, **H-7**, **H-4**), 1.58 – 1.48 (m, 1H, **H-7**), 1.47 – 1.22 (m, 4H, **H-1**, **H-3**, **H-6**), 1.20 (s, 3H, **H-11**)

¹³C NMR (101 MHz, CDCl₃) δ 148.3 (**C-10**), 142.5 (**C-13**), 138.1 (**C-12**), 129.0 (**C-16**), 128.9 (**C-14**), 128.2 (**C-15**), 115.4 (**C-9**), 70.6 (**C-2**), 43.1 (**C-4**), 37.2 (**C-3**), 35.3 (**C-5**), 34.1 (**C-6**), 31.0 (**C-1**), 26.3 (**C-7**), 20.9 (**C-8**), 20.0 (**C-11**)

HRMS (ESI+) *m/z* found 283.1797 [M+H]⁺, C₁₈H₂₂N₂O calculated 283.1810 (Δ = -4.59 ppm)

(5aS*,7S*,9aS*)-9a-methyl-4,5,5a,6,7,8,9,9a-octahydro-1H-benzo[g]indazol-7-ol, formate salt



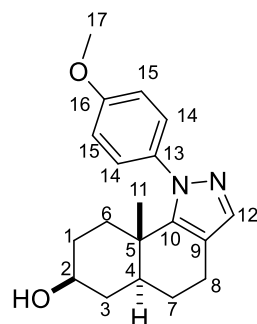
2.74, method 2, (17.3 mg, 0.0686 mmol, 27% yield over two steps)

¹H NMR (400 MHz, CDCl₃) δ 7.24 (s, 1H, **H-12**), 3.71 (tt, *J* = 10.6, 4.8 Hz, 1H, **H-2**), 2.70 – 2.47 (m, 2H, **H-8**), 2.17 (ddd, *J* = 12.7, 2.8 Hz, 1H, **H-6**), 2.01 – 1.89 (m, 1H, **H-1**), 1.86 – 1.76 (m, 1H, **H-3**), 1.76 – 1.42 (m, 6H, **H-1**, **H-3**, **H-4**, **H-6**, **H-7**), 1.15 (s, 3H, **H-11**)

¹³C NMR (101 MHz, CDCl₃) δ 153.9 (**C-10**), 130.5 (**C-12**), 113.6 (**C-9**), 71.1 (**C-2**), 41.8 (**C-4**), 36.9 (**C-3**), 34.6 (**C-6**), 34.0 (**C-5**), 31.2 (**C-1**), 26.0 (**C-7**), 20.4 (**C-8**), 20.3 (**C-11**)

HRMS (ESI+) m/z found 207.1498 [M+H]⁺, C₁₂H₁₉N₂O calculated 207.1497 (Δ = 0.48 ppm).

(5a*S,7*S**,9a*S**)-1-(4-methoxyphenyl)-9a-methyl-4,5,5a,6,7,8,9,9a-octahydro-1H-benzo[*g*]indazol-7-ol**



2.75, method 2, (5.9 mg, 0.0189 mmol, 8% yield over two steps)

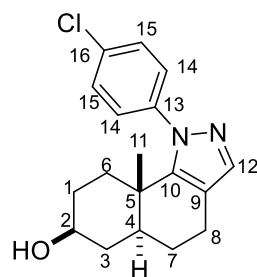
¹H NMR (400 MHz, CDCl₃) δ 7.34 (s, 1H, **H-12**), 7.30 – 7.17 (m, 2H, **H-14**), 6.96 – 6.88 (m, 2H, **H-15**), 3.86 (s, 3H, **H-17**), 3.59 (tt, *J* = 10.6, 4.8 Hz, 1H, **H-2**), 2.69 – 2.54 (m, 2H, **H-8**), 1.81 – 1.59 (m, 4H, **H-1**, **H-3**, **H-4**, **H-7**), 1.58 – 1.19 (m, 5H, **H-1**, **H-3**, **H-6**, **H-7**), 1.17 (s, 3H, **H-11**)

¹³C NMR (101 MHz, CDCl₃) δ 159.9 (**C-16**), 148.5 (**C-10**), 137.7 (**C-12**), 135.1 (**C-13**), 129.3 (**C-14**), 115.2 (**C-9**), 114.0 (**C-15**), 70.7 (**C-2**), 55.7 (**C-17**), 43.0 (**C-4**), 37.2 (**C-3**), 35.3 (**C-5**), 34.1 (**C-6**), 31.1 (**C-1**), 26.4 (**C-7**),

21.0 (**C-8**), 19.9 (**C-11**)

HRMS (ESI+) m/z found 313.1907 [M+H]⁺, C₁₉H₂₄N₂O₂ calculated 313.1916 (Δ = -2.87 ppm).

(5a*S,7*S**,9a*S**)-1-(4-chlorophenyl)-9a-methyl-4,5,5a,6,7,8,9,9a-octahydro-1H-benzo[*g*]indazol-7-ol**



2.76, method 2, (26.0 mg, 0.0821 mmol, 47% yield over two steps)

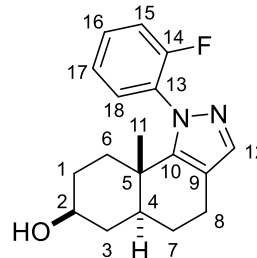
¹H NMR (400 MHz, CDCl₃) δ 7.45 – 7.39 (m, 1H, **H-14**), 7.37 (s, 1H, **H-12**), 7.34 – 7.27 (m, 2H, **H-15**), 3.60 (tt, *J* = 4.9, 10.5 Hz, 1H, **H-2**), 2.69 – 2.54 (m, 2H, **H-8**), 1.83 – 1.21 (m, 8H, **H-1**, **H-3**, **H-6**, **H-7**), 1.19 (s, 3H, **H-11**)

¹³C NMR (101 MHz, CDCl₃) δ 148.8 (**C-10**), 140.7 (**C-13**), 138.4 (**C-12**), 135.3 (**C-16**), 129.6 (**C-15**), 129.4 (**C-14**), 116.0 (**C-9**), 70.7 (**C-2**), 43.2 (**C-4**), 37.3 (**C-3**), 35.4 (**C-5**), 34.3 (**C-6**), 31.1 (**C-1**), 26.4 (**C-7**), 21.0 (**C-8**),

20.2 (**C-11**)

HRMS (ESI+) m/z found 317.1426 [M+H]⁺, C₁₈H₂₁ClN₂O calculated 317.1420 (Δ = 1.89 ppm).

(5a*S,7*S**,9a*S**)-1-(2-fluorophenyl)-9a-methyl-4,5,5a,6,7,8,9,9a-octahydro-1H-benzo[*g*]indazol-7-ol**



2.77 (Astercin-1), method 2, (18.0 mg, 0.0600 mmol, 27% yield over two steps)

¹H NMR (400 MHz, CDCl₃) δ 7.49 – 7.35 (m, 3H, **H-12**, **H-16**, **H-17**), 7.21 (q, *J* = 8.6, 7.9 Hz, 2H, **H-15**, **H-18**), 3.58 (tt, *J* = 10.2, 4.9 Hz, 1H, **H-2**), 2.69 – 2.55 (m, 2-1H, **H-8**), 1.86 (s, 1H, O-H), 1.79 – 1.61 (m, 4H, **H-1**, **H-3**, **H-4**, **H-7**), 1.54 (m, 1H, **H-7**), 1.45 – 1.35 (m, 2H, **H-3**, **H-6**), 1.34 – 1.23 (m, 2H, **H-1**, **H-6**), 1.13 (s, 3H, **H-11**), 1.09 (s, 3H, **H-11** (minor isomer))

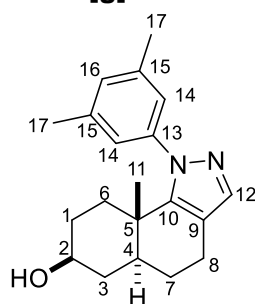
¹³C NMR (101 MHz, CDCl₃) δ 158.82 (d, *J* = 252.4 Hz, **C-14**), 158.53 (d, *J* = 251.7 Hz, **C-14'**), 149.2 (**C-10'**), 148.9 (**C-10**), 139.0 (**C-12**), 131.5 – 131.2 (**C13**, **C-16**), 130.3 (**C-17**), 124.30 (**C-18**), 124.25 (**C-18'**), 116.7 (d, *J* = 19.9 Hz, **C-15**), 115.6 (**C-9'**), 115.5 (**C-9**), 70.6 (**C-2'**), 70.5 (**C-2**), 42.9 (**C-4'**), 42.7 (**C-4**), 37.0 (**C-3**), 35.2 (**C-5'**), 35.1 (**C-5**), 34.5 (**C-6'**), 32 (**C-6**), 31.0 (**C-1'**), 30.9 (**C-1**), 26.33 (**C-7**), 26.28 (**C-7'**), 20.9 (**C-8**), 19.7 (**C-11**), 18.4 (**C-11'**)

¹⁹F NMR (377 MHz, DMSO) δ -120.9, -121.2

HRMS (ESI+) *m/z* found 301.1705 [M+H]⁺, C₁₈H₂₁FN₂O calculated 301.1716 (Δ = -3.65 ppm).

Note: Compound present as a mixture of conformational isomers. ¹³C NMR data is reported as the chemical shifts and coupling constants of the major conformational isomer, except in cases when there is clear separation of the two peaks. Peaks arising from the minor isomer are reported as C-X'.

(5a*S,7*S**,9a*S**)-1-(3,5-dimethylphenyl)-9a-methyl-4,5,5a,6,7,8,9,9a-octahydro-1H-benzo[*g*]indazol-7-ol**



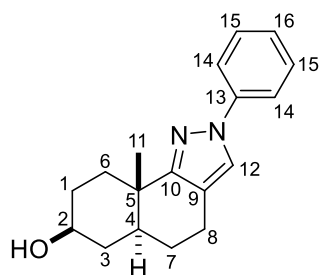
2.78a, method 2, (18.9 mg, 0.0609 mmol, 30% yield over two steps)

¹H NMR (400 MHz, CDCl₃) δ 7.32 (s, 1H, **H-12**), 7.05 (s, 1H, **H-16**), 6.96 (s, 2H, **H-14**), 3.56 (tt, *J* = 10.8, 5.2 Hz, 1H, **H-2**), 2.69 – 2.53 (m, 2H, **H-8**), 2.34 (s, 6H, **H-17**), 1.79 – 1.58 (m, 4H, **H-1**, **H-3**, **H-4**, **H-7**), 1.56 – 1.49 (m, 1H, **H-7**), 1.46 – 1.38 (m, 2H, **H-3**, **H-6**), 1.36 – 1.20 (m, 2H, **H-1**, **H-6**), 1.19 (s, 3H, **H-11**)

¹³C NMR (101 MHz, CDCl₃) δ 148.1 (**C-10**), 142.3 (**C-13**), 138.5 (**C-15**), 137.8 (**C-12**), 130.6 (**C-16**), 125.8 (**C-14**), 115.1 (**C-9**), 70.6 (**C-2**), 43.1 (**C-4**), 37.2 (**C-3**), 35.2 (**C-5**), 34.0 (**C-6**), 31.0 (**C-1**), 26.3 (**C-7**), 21.3 (**C-17**), 20.9 (**C-8**), 19.9 (**C-11**)

HRMS (ESI+) *m/z* found 311.2128 [M+H]⁺, C₂₀H₂₆N₂O calculated 311.2123 (Δ = 1.61 ppm).

(5a*S,7*S**,9a*S**)-9a-methyl-2-phenyl-4,5,5a,6,7,8,9,9a-octahydro-2H-benzo[*g*]indazol-7-ol**



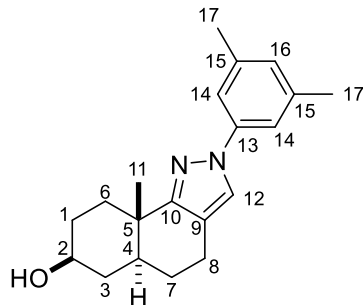
2.73I, method 1, (3.5 mg, 0.0124 mmol, 5% yield over two steps)

¹H NMR (400 MHz, CDCl₃) δ 7.66 – 7.59 (m, 2H, **H-14**), 7.55 (s, 1H, **H-12**), 7.45 – 7.34 (m, 2H, **H-15**), 7.24 – 7.16 (m, 1H, **H-16**), 3.72 (tt, *J* = 10.6, 4.9 Hz, 1H, **H-2**), 2.79 – 2.56 (m, 2H, **H-8**), 2.45 – 2.36 (m, 1H, **H-6**), 2.03 – 1.93 (m, 1H, **H-1**), 1.86 – 1.44 (m, 7H, **H-1**, **H-3**, **H-4**, **H-6**, **H-7**), 1.21 (s, 3H, **H-11**)

¹³C NMR (101 MHz, CDCl₃) δ 160.4 (**C-10**), 140.5 (**C-13**), 129.3 (**C-15**), 125.6 (**C-16**), 123.7 (**C-12**), 118.9 (**C-14**), 116.2 (**C-9**), 71.2 (**C-4**), 41.7 (**C-4**), 37.1 (**C-3**), 34.53 (**C-5**), 34.51 (**C-6**), 31.3 (**C-1**), 25.7 (**C-7**), 20.3 (**C-8**), 20.2 (**C-11**)

HRMS (ESI+) *m/z* found 283.1797 [M+H]⁺, C₁₈H₂₂N₂O calculated 283.1810 (Δ = -4.59 ppm).

(5aS*,7S*,9aS*)-2-(3,5-dimethylphenyl)-9a-methyl-4,5,5a,6,7,8,9,9a-octahydro-2H-benzo[g]indazol-7-ol



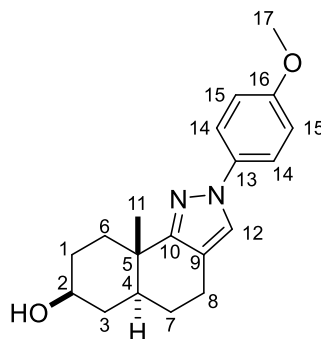
2.78I, method 2, (11.5 mg, 0.0370 mmol, 18% yield over two steps)

¹H NMR (400 MHz, CDCl₃) δ 7.51 (s, 1H, **H-12**), 7.22 (s, 2H, **H-14**), 6.85 (s, 1H, **H-16**), 3.72 (tt, *J* = 10.5, 5.2 Hz, 1H, **H-2**), 2.75 – 2.56 (m, 2H, **H-8**), 2.43 – 2.37 (m, 1H, **H-6**), 2.34 (s, 6H, **H-17**), 2.00 – 1.94 (m, 1H, **H-1**), 1.86 – 1.43 (m, 6H, **H-1**, **H-3**, **H-4**, **H-6**, **H-7**), 1.21 (s, 3H, **H-11**)

¹³C NMR (101 MHz, CDCl₃) δ 160.3 (**C-10**), 140.6 (**C-13**), 139.1 (**C-15**), 127.6 (**C-16**), 124.1 (**C-12**), 117.1 (**C-14**), 116.0 (**C-9**), 71.4 (**C-2**), 41.9 (**C-4**), 37.3 (**C-3**), 34.68 (**C-5**), 34.66 (**C-6**), 31.4 (**C-1**), 25.9 (**C-7**), 21.5 (**C-17**), 20.5 (**C-8**), 20.3 (**C-11**)

HRMS (ESI+) *m/z* found 311.2118 [**M+H**]⁺, C₂₀H₂₆N₂O calculated 311.2123 (Δ = -1.60 ppm).

(5aS*,7S*,9aS*)-2-(4-methoxyphenyl)-9a-methyl-4,5,5a,6,7,8,9,9a-octahydro-2H-benzo[g]indazol-7-ol



2.75I, method 2, (4.7 mg, 0.0150 mmol, 6% yield over two steps)

¹H NMR (400 MHz, CDCl₃) δ 7.53 – 7.48 (m, 2H, **H-14**), 7.45 (s, 1H, **H-12**), 6.95 – 6.88 (m, 2H, **H-15**), 3.82 (s, 3H, **H-17**), 3.72 (tt, *J* = 10.5, 5.0 Hz, 1H, **H-2**), 2.76 – 2.56 (m, 2H, **H-8**), 2.41 – 2.35 (m, 1H, **H-6**), 2.01 – 1.93 (m, 1H, **H-1**), 1.85 – 1.43 (m, 7H, **H-1**, **H-3**, **H-4**, **H-6**, **H-7**), 1.20 (s, 3H, **H-11**)

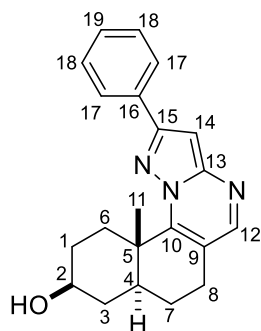
¹³C NMR (101 MHz, CDCl₃) δ 160.2 (**C-10**), 158.0 (**C-16**), 134.8 (**C-13**), 124.1 (**C-12**), 120.9 (**C-14**), 116.0 (**C-9**), 114.7 (**C-15**), 71.6 (**C-2**), 55.8 (**C-17**), 42.1 (**C-4**), 37.4 (**C-3**), 34.9 (**C-6**), 34.8 (**C-5**), 31.6 (**C-1**), 26.1 (**C-7**), 20.6 (**C-8**), 20.5 (**C-11**)

HRMS (ESI+) *m/z* found 313.1901 [**M+H**]⁺, C₁₉H₂₄N₂O₂ calculated 313.1916 (Δ = -4.79 ppm).

General procedure for the synthesis of pyrazolo[1,5-*a*]pyrimidine fused analogues

To a solution of hydroxymethylene **2.11** (1 equiv.) and the appropriate aminopyrazole (1.05 equiv.) in toluene was added *p*-TsOH·H₂O (0.05 equiv.) before fitting the flask with a Dean-Stark trap. The reaction was heated at reflux for two hours, cooled to room temperature, and the solvent removed under reduced pressure to afford an oily residue. The residue was dissolved in ethyl acetate and washed sequentially with saturated aqueous NaHCO₃, water, brine, dried over anhydrous MgSO₄, and the solvent removed under reduce pressure to yield the crude pyrazolopyrimidine fused compounds as a mixture of the “angular” and “linear” regioisomers. Purification of the crude material by preparative HPLC (MeCN/H₂O + 0.1% HCO₂H) afforded the two regioisomers in separate fractions.

(7aS*,9S*,11aS*)-11a-methyl-2-phenyl-6,7,7a,8,9,10,11,11a-octahydrobenzo[h]pyrazolo[1,5-a]quinazolin-9-ol



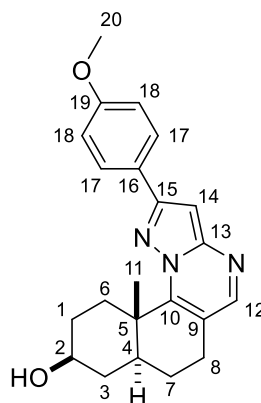
2.68a, (20.8 mg, 0.0624 mmol, 19% yield)

¹H NMR (400 MHz, CDCl₃) δ 8.18 (s, 1H, **H-12**), 8.05 – 7.91 (m, 2H, **H-17**), 7.50 – 7.42 (m, 2H, **H-18**), 7.41 – 7.33 (m, 1H, **H-19**), 6.91 (s, 1H, **H-14**), 4.04 (ddd, *J* = 13.7, 3.8 Hz, 1H, **H-6**), 3.76 (tt, *J* = 10.5, 5.1 Hz, 1H, **H-2**), 2.99 – 2.75 (m, 2H, **H-8**), 2.10 – 2.00 (m, 1H, **H-1**), 1.97 – 1.59 (m, 6H, **H-1**, **H-3**, **H-4**, **H-7**), 1.56 (s, 3H, **H-11**), 1.38 (ddd, *J* = 13.7, 3.8 Hz, 1H, **H-6**)

¹³C NMR (101 MHz, CDCl₃) δ 153.8 (**C-15**), 151.8 (**C-12**), 151.1 (**C-10**), 150.3 (**C-13**), 133.6 (**C-16**), 128.93 (**C-18**), 128.85 (**C-19**), 126.6 (**C-17**), 116.2 (**C-9**), 92.9 (**C-14**), 70.8 (**C-2**), 42.8 (**C-4**), 39.1 (**C-5**), 37.4 (**C-3**), 31.7 (**C-6**), 31.4 (**C-1**), 26.9 (**C-8**), 25.0 (**C-7**), 14.5 (**C-11**)

HRMS (ESI+) *m/z* found 334.1908 [M+H]⁺, C₂₁H₂₃N₃O calculated 334.1919 (Δ = -3.29 ppm).

(7aS*,9S*,11aS*)-2-(4-methoxyphenyl)-11a-methyl-6,7,7a,8,9,10,11,11a-octahydrobenzo[h]pyrazolo[1,5-a]quinazolin-9-ol



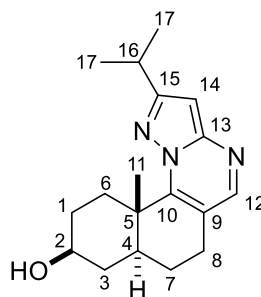
2.69a, (29.7 mg, 0.0817 mmol, 22% yield)

¹H NMR (400 MHz, CDCl₃) δ 8.14 (s, 1H, **H-12**), 7.96 – 7.89 (m, 2H, **H-17**), 7.03 – 6.95 (m, 2H, **H-18**), 6.82 (s, 1H, **H-14**), 4.02 (ddd, *J* = 13.7, 3.75 Hz, 1H, **H-6**), 3.85 (s, 3H, **H-20**), 3.75 (tt, *J* = 10.4, 5.0 Hz, 1H, **H-2**), 2.95 – 2.75 (m, 2H, **H-8**), 2.09 – 1.59 (m, 7H, **H-1**, **H-3**, **H-4**, **H-7**), 1.54 (s, 3H, **H-11**), 1.36 (ddd, *J* = 13.7, 3.75 Hz, 1H, **H-6**)

¹³C NMR (101 MHz, CDCl₃) δ 160.2 (**C-19**), 153.5 (**C-15**), 151.5 (**C-12**), 150.9 (**C-10**), 150.2 (**C-13**), 127.8 (**C-17**), 126.2 (**C-16**), 115.7 (**C-9**), 114.2 (**C-18**), 92.0 (**C-14**), 70.7 (**C-2**), 55.5 (**C-20**), 42.7 (**C-4**), 39.0 (**C-5**), 37.3 (**C-3**), 31.5 (**C-6**), 31.2 (**C-1**), 26.7 (**C-8**), 24.9 (**C-7**), 14.4 (**C-11**)

HRMS (ESI+) *m/z* found 364.2035 [M+H]⁺, C₂₂H₂₅N₃O₂ calculated 364.2052 (Δ = -4.67 ppm).

(7aS*,9S*,11aS*)-2-isopropyl-11a-methyl-6,7,7a,8,9,10,11,11a-octahydrobenzo[h]pyrazolo[1,5-a]quinazolin-9-ol



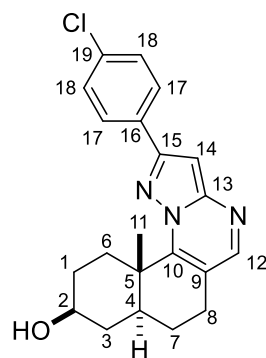
2.70a, (21.0 mg, 0.0701 mmol, 22% yield);

¹H NMR ¹H NMR (400 MHz, CDCl₃) δ 8.12 (s, 1H, **H-12**), 6.40 (s, 1H, **H-14**), 3.95 (ddd, *J* = 13.7, 3.7 Hz, 1H, **H-6**), 3.75 (tt, *J* = 10.1, 5.1 Hz, 1H, **H-2**), 3.14 (sept, *J* = 6.9 Hz, 1H, **H-16**), 2.93 – 2.74 (m, 2H, **H-8**), 2.05 – 1.97 (m, 1H, **H-1**), 1.89 – 1.83 (m, 1H, **H-3**), 1.80 – 1.58 (m, 6H, **H-1**, **H-3**, **H-4**, **H-7**), 1.49 (s, 3H, **H-11**), 1.38 – 1.25 (m, 7H, **H-6**, **H-17**)

¹³C NMR (101 MHz, CDCl₃) δ 162.8 (**C-15**), 151.1 (**C-12**), 150.9 (**C-10**), 149.5 (**C-13**), 115.0 (**C-9**), 92.5 (**C-14**), 70.9 (**C-2**), 42.9 (**C-4**), 39.0 (**C-5**), 37.5 (**C-3**), 31.5 (**C-6**), 31.4 (**C-1**), 28.9 (**C-16**), 26.8 (**C-8**), 25.1 (**C-7**), 23.02 (**C-17**), 23.00 (**C-17**), 14.4 (**C-11**)

HRMS (ESI+) *m/z* found 300.2071 [M+H]⁺, C₁₈H₂₅N₃O calculated 300.2076 (Δ = -1.67 ppm).

(7aS*,9S*,11aS*)-2-(4-chlorophenyl)-11a-methyl-6,7,7a,8,9,10,11,11a-octahydrobenzo[h]pyrazolo[1,5-a]quinazolin-9-ol



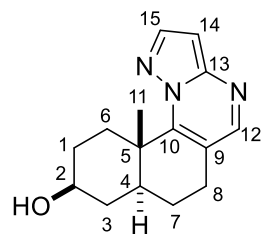
2.71a, (14.8 mg, 0.0402 mmol, 13% yield)

¹H NMR (400 MHz, CDCl₃) δ 8.19 (s, 1H, **H-12**), 7.94 – 7.86 (m, 2H, **H-17**), 7.46 – 7.36 (m, 2H, **H-18**), 6.87 (s, 1H, **H-14**), 3.98 (m, 1H, **H-6**), 3.77 (tt, *J* = 10.4, 5.0 Hz, 1H, **H-2**), 2.97 – 2.78 (m, 2H, **H-8**), 2.10 – 2.01 (m, 1H, **H-1**), 1.93 – 1.61 (m, 6H, **H-1**, **H-3**, **H-4**, **H-7**), 1.55 (s, 3H, **H-11**), 1.38 (ddd, *J* = 13.65, 3.8 Hz, 1H, **H-6**)

¹³C NMR (101 MHz, CDCl₃) δ 152.5 (**C-15**), 151.9 (**C-12**), 151.0 (**C-10**), 150.2 (**C-13**), 134.5 (**C-19**), 132.0 (**C-16**), 129.0 (**C-18**), 127.8 (**C-17**), 116.3 (**C-9**), 92.8 (**C-14**), 70.7 (**C-2**), 42.7 (**C-4**), 39.0 (**C-5**), 37.3 (**C-3**), 31.6 (**C-6**), 31.2 (**C-1**), 26.8 (**C-8**), 24.9 (**C-7**), 14.4 (**C-11**)

HRMS (ESI+) *m/z* found 368.1544 [*M*+*H*]⁺, C₂₁H₂₂ClN₃O calculated 368.1529 (Δ = 4.07 ppm).

(7aS*,9S*,11aS*)-11a-methyl-6,7,7a,8,9,10,11,11a-octahydrobenzo[h]pyrazolo[1,5-a]quinazolin-9-ol



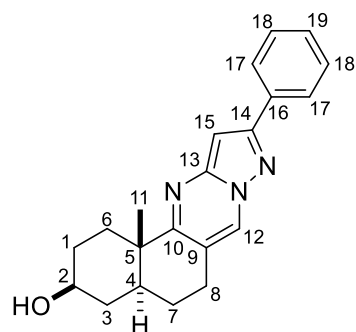
2.72a, (15.5 mg, 0.0602 mmol, 17% yield)

¹H NMR (400 MHz, CDCl₃) δ 8.21 (s, 1H, **H-12**), 8.01 (d, *J* = 2.35 Hz, 1H, **H-15**), 6.62 (d, *J* = 2.35 Hz, 1H, **H-14**), 3.88 (ddd, *J* = 13.7, 3.85 Hz, 1H, **H-6**), 3.75 (tt, *J* = 10.6, 5.1 Hz, 1H, **H-2**), 2.98 – 2.78 (m, 2H, **H-8**), 2.07 – 1.61 (m, 7H, **H-1**, **H-3**, **H-4**, **H-7**), 1.50 (s, 3H, **H-11**), 1.32 (td, *J* = 13.7, 3.85 Hz, 1H, **H-6**)

¹³C NMR (101 MHz, CDCl₃) δ 151.7 (**C-12**), 151.2 (**C-10**), 148.9 (**C-13**), 142.5 (**C-15**), 116.0 (**C-9**), 96.2 (**C-14**), 70.6 (**C-2**), 42.8 (**C-4**), 38.9 (**C-5**), 37.3 (**C-3**), 31.4 (**C-6**), 31.1 (**C-1**), 26.7 (**C-8**), 24.8 (**C-7**), 14.4 (**C-11**)

HRMS (ESI+) *m/z* found 258.1597 [*M*+*H*]⁺, C₁₅H₁₉N₃O calculated 258.1606 (Δ = -3.49 ppm).

(3S*,4aS*,12bS*)-12b-methyl-10-phenyl-1,2,3,4,4a,5,6,12b-octahydrobenzo[h]pyrazolo[5,1-b]quinazolin-3-ol



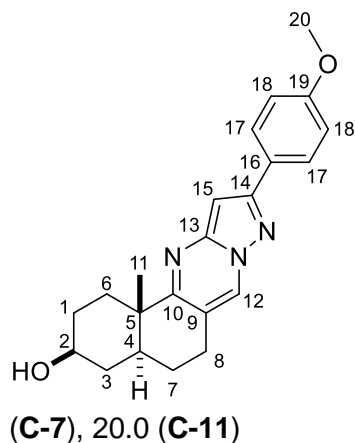
2.68I, (7.8 mg, 0.0234 mmol, 7% yield)

¹H NMR (400 MHz, CDCl₃) δ 8.38 (s, 1H, **H-12**), 7.99 – 7.77 (m, 2H, **H-17**), 7.54 – 7.41 (m, 2H, **H-18**), 7.42 – 7.32 (m, 1H, **H-19**), 6.83 (s, 1H, **H-15**), 3.72 (tt, *J* = 10.7, 4.8 Hz, 1H, **H-2**), 3.01 – 2.83 (m, 2H, **H-8**), 2.63 (ddd, *J* = 13.2, 2.7 Hz, 1H, **H-6**), 2.07 – 1.96 (m, 1H, **H-1**), 1.93 – 1.46 (m, 7H, **H-1**, **H-3**, **H-4**, **H-6**, **H-7**), 1.19 (s, 3H, **H-11**)

¹³C NMR (101 MHz, CDCl₃) 167.3 (**C-10**), 156.1 (**C-14**), 148.8 (**C-13**), 133.4 (**C-16**), 133.0 (**C-12**), 129.04 (**C-18**), 129.00 (**C-19**), 126.7 (**C-17**), 116.5 (**C-9**), 92.4 (**C-15**), 71.0 (**C-2**), 40.18 (**C-4**), 40.16 (**C-5**), 37.9 (**C-3**), 34.4 (**C-6**), 31.6 (**C-1**), 25.5 (**C-8**), 24.8 (**C-7**), 20.0 (**C-11**)

HRMS (ESI+) *m/z* found 334.1915 [*M*+*H*]⁺, C₂₁H₂₃N₃O calculated 334.1919 (Δ = -1.20 ppm).

(3S*,4aS*,12bS*)-10-(4-methoxyphenyl)-12b-methyl-1,2,3,4,4a,5,6,12b-octahydrobenzo[h]pyrazolo[5,1-b]quinazolin-3-ol



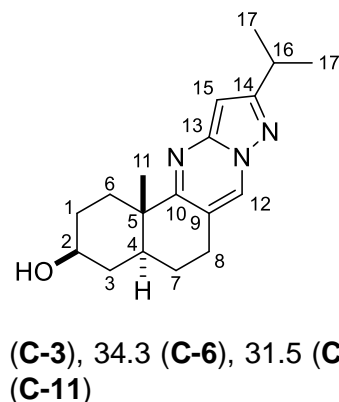
2.69I, (6.6 mg, 0.0182 mmol, 5% yield)

¹H NMR (400 MHz, CDCl₃) δ 8.37 (s, 1H, **H-12**), 7.91 – 7.84 (m, 2H, **H-17**), 7.01 – 6.95 (m, 2H, **H-18**), 6.75 (s, 1H, **H-15**), 3.86 (s, 3H, **H-20**), 3.72 (tt, *J* = 10.7, 4.7 Hz, 1H, **H-2**), 3.01 – 2.83 (m, 2H, **H-8**), 2.63 (ddd, *J* = 13.2, 2.8 Hz, 1H, **H-6**), 2.09 – 1.97 (m, 1H, **H-1**), 1.93 – 1.45 (m, 7H, **H-1**, **H-3**, **H-4**, **H-6**, **H-7**), 1.19 (s, 3H, **H-11**)

¹³C NMR (101 MHz, CDCl₃) 167.3 (**C-10**), 160.5 (**C-19**), 155.9 (**C-14**), 148.8 (**C-13**), 133.0 (**C-12**), 128.0 (**C-17**), 125.9 (**C-16**), 116.2 (**C-9**), 114.5 (**C-18**), 91.8 (**C-15**), 71.0 (**C-2**), 55.7 (**C-20**), 40.21 (**C-4**), 40.17 (**C-5**), 38.0 (**C-3**), 34.4 (**C-6**), 31.6 (**C-1**), 25.5 (**C-8**), 24.8

HRMS (ESI+) *m/z* found 364.2034 [*M*+*H*]⁺, C₂₂H₂₅N₃O₂ calculated 364.2052 (Δ = -4.94 ppm).

(3S*,4aS*,12bS*)-10-isopropyl-12b-methyl-1,2,3,4,4a,5,6,12b-octahydrobenzo[h]pyrazolo[5,1-b]quinazolin-3-ol



2.70I, (2.4 mg, 0.00802 mmol, 3% yield)

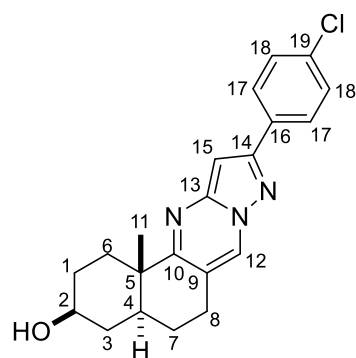
¹H NMR (400 MHz, CDCl₃) δ 8.31 (s, 1H, **H-12**), 6.35 (s, 1H, **H-15**), 3.70 (tt, *J* = 10.8, 5.2 Hz, 1H, **H-2**), 3.14 (sept, *J* = 6.9 Hz, 1H, **H-16**), 2.97 – 2.81 (m, 2H, **H-8**), 2.61 (ddd, *J* = 13.5, 3.1 Hz, 1H, **H-6**), 2.05 – 1.98 (m, 1H, **H-1**), 1.91 – 1.45 (m, 7H, **H-1**, **H-3**, **H-4**, **H-6**, **H-7**), 1.35 (d, *J* = 6.9 Hz, 6H, **H-17**), 1.16 (s, 3H, **H-11**)

¹³C NMR (101 MHz, CDCl₃) δ 166.8 (**C-10**), 148.0 (**C-13**), 132.8 (**C-12**), 115.5 (**C-9**), 91.8 (**C-15**), 70.9 (**C-2**), 40.1 (**C-4**), 39.9 (**C-5**), 37.8 (**C-3**), 34.3 (**C-6**), 31.5 (**C-1**), 28.8 (**C-16**), 25.3 (**C-8**), 24.7 (**C-7**), 23.0 (**C-17**), 22.9 (**C-17**), 19.9 (**C-11**)

HRMS (ESI+) *m/z* found 300.2065 [*M*+*H*]⁺, C₁₈H₂₅N₃O calculated 300.2076 (Δ = -3.66 ppm).

Note: C-14 is not visible in the ¹³C spectrum however HMBC correlations can be observed, indicating that C-14 should be present at δ = 165.0 ppm

(3*S,4*aS**,12*bS**)-10-(4-chlorophenyl)-12*b*-methyl-1,2,3,4,4*a*,5,6,12*b*-octahydrobenzo[*h*]pyrazolo[5,1-*b*]quinazolin-3-ol**



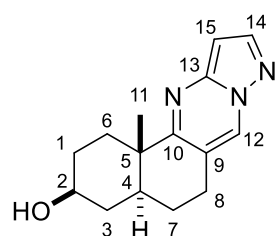
2.71I, (9.2 mg, 0.0250 mmol, 8% yield)

¹H NMR (400 MHz, CDCl₃) δ 8.35 (s, 1H, **H-12**), 7.91 – 7.73 (m, 2H, **H-17**), 7.52 – 7.33 (m, 2H, **H-18**), 6.79 (s, 1H, **H-15**), 3.72 (m, 1H, **H-2**), 3.00 – 2.85 (m, 2H, **H-8**), 2.62 (m, 1H, **H-6**), 2.07 – 1.97 (m, 1H, **H-1**), 1.92 – 1.85 (m, 1H, **H-3**), 1.84 – 1.45 (m, 6H, **H-1**, **H-3**, **H-4**, **H-6**, **H-7**), 1.18 (s, 3H, **H-11**)

¹³C NMR (101 MHz, CDCl₃) δ 167.3 (**C-10**), 154.7 (**C-14**), 148.7 (**C-13**), 134.7 (**C-16**), 132.9 (**C-12**), 131.8 (**C-19**), 129.1 (**C-18**), 127.7 (**C-17**), 116.6 (**C-9**), 92.3 (**C-15**), 70.9 (**C-2**), 40.1 (**C-4**), 40.0 (**C-5**), 37.8 (**C-3**), 34.2 (**C-6**), 31.5 (**C-1**), 25.4 (**C-8**), 24.6 (**C-7**), 19.9 (**C-11**)

HRMS (ESI+) *m/z* found 368.1519 [M+H]⁺, C₂₁H₂₂ClN₃O calculated 368.1529 (Δ = -2.72 ppm).

(3*S,4*aS**,12*bS**)-12*b*-methyl-1,2,3,4,4*a*,5,6,12*b*-octahydrobenzo[*h*]pyrazolo[5,1-*b*]quinazolin-3-ol**



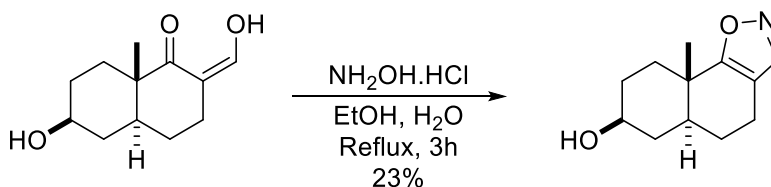
2.72I, (4.5 mg, 0.0175 mmol, 5% yield)

¹H NMR (400 MHz, CDCl₃) δ 8.38 (s, 1H, **H-12**), 8.00 (d, *J* = 2.3 Hz, 1H, **H-14**), 6.53 (d, *J* = 2.3 Hz, 1H, **H-15**), 3.77 – 3.66 (tt, *J* = 10.8, 5.5 Hz, 1H, **H-2**), 2.99 – 2.86 (m, 2H, **H-8**), 2.62 (ddd, *J* = 13.3, 2.8 Hz, 1H, **H-6**), 2.06 – 1.98 (m, 1H, **H-1**), 1.95 – 1.45 (m, 7H, **H-1**, **H-3**, **H-4**, **H-6**, **H-7**), 1.17 (s, 3H, **H-11**)

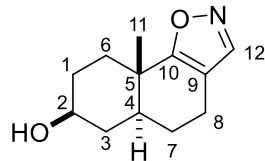
¹³C NMR (101 MHz, CDCl₃) δ 167.2 (**C-10**), 147.6 (**C-13**), 144.7 (**C-14**), 133.3 (**C-12**), 116.5 (**C-9**), 95.5 (**C-15**), 71.0 (**C-2**), 40.2 (**C-4**, **C-5**), 37.9 (**C-3**), 34.4 (**C-6**), 31.6 (**C-1**), 25.4 (**C-8**), 24.8 (**C-7**), 20.0 (**C-11**)

HRMS (ESI+) *m/z* found 258.1598 [M+H]⁺, C₁₅H₁₉N₃O calculated 258.1606 (Δ = -3.10 ppm).

(5*aS,7*S**,9*aS**)-9*a*-methyl-4,5,5*a*,6,7,8,9,9*a*-octahydronaphtho[2,1-*d*]isoxazol-7-ol**



To a solution of hydroxymethylene **2.11** (38 mg, 0.181 mmol) in a mixture of ethanol:H₂O (98:2) was added hydroxylamine hydrochloride (12.6 mg, 0.181 mmol). The resulting mixture was heated at 80 °C for three hours then cooled to room temperature and concentrated to yield a crude oil. The crude oil was dissolved in DCM and washed with saturated aqueous NaHCO₃, the organic phase dried over anhydrous Na₂SO₄ and concentrated to yield a yellow residue. Purification of the residue via flash chromatography on silica gel (1:1 ethyl acetate/*n*-hexane) yielded the product as a colourless oil (19.0 mg, 0.0917 mmol, 60%)



2.79, $R_f = 0.20$ (1:1 ethyl acetate/*n*-hexane)

^1H NMR (400 MHz, CDCl_3) δ 7.99 (s, 1H, **H-12**), 3.70 (tt, $J = 10.7, 5.0$ Hz, 1H, **H-2**), 2.55 – 2.39 (m, 2H, **H-8**), 2.23 (dt, $J = 13.1, 3.2$ Hz, 1H, **H-6**), 2.01 – 1.94 (m, 1H, **H-1**), 1.88 – 1.78 (m, 1H, **H-3**), 1.74 – 1.44 (m, 6H, **H-1, H-3, H-4, H-6, H-7**), 1.18 (s, 3H, **H-11**)

^{13}C NMR (101 MHz, CDCl_3) δ 174.8 (**C-10**), 149.7 (**C-12**), 109.9 (**C-9**), 70.9 (**C-2**), 42.0 (**C-4**), 36.1 (**C-3**), 35.4 (**C-5**), 32.6 (**C-6**), 30.7 (**C-1**), 25.6 (**C-7**), 19.7 (**C-8**), 18.5 (**C-14**)

HRMS (ESI+) m/z found 208.1330 $[\text{M}+\text{H}]^+$, $\text{C}_{12}\text{H}_{17}\text{N}_2\text{O}$ calculated 208.1337 ($\Delta = 1.89$ ppm).

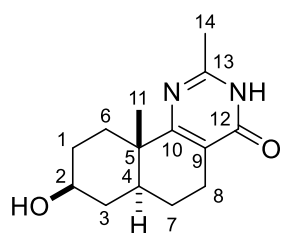
General procedure for the synthesis of MEM-protected 4-pyrimidone fused analogues

To a solution of β -ketoester **2.14** (1 equiv.) in dry MeOH (1.5 mL) was added the appropriate amidine (1.3 – 1.95 equiv.) and anhydrous K_2CO_3 (1.3 – 1.95 equiv.). The resulting solution was heated at reflux for 24 hours before reaching completion. The reaction was diluted with saturated aqueous NH_4Cl and extracted twice with DCM. The combined organic phases were dried over anhydrous magnesium sulfate and the solvent removed to yield the products as oils. The products were used immediately in the subsequent deprotection (Yields between 74 – 90%)

General procedure for the deprotection of MEM-protected 4-pyrimidone fused analogues

The MEM-protected 4-pyrimidones were dissolved in THF (2 mL) before addition of 6M aqueous HCl (0.5 mL) and stirred at room temperature for 24 hours. The reactions were neutralised via addition of either saturated aqueous NaHCO_3 or Na_2CO_3 to a neutral and basic pH respectively. The aqueous phases were extracted three times with either DCM or $i\text{PrOH}:\text{CHCl}_3$ (1:9) and the combined organic phases dried over anhydrous magnesium sulfate. Removal of the solvent under reduced pressure yielded the crude 4-pyrimidones as solids. The crude 4-pyrimidones were dry loaded onto Celite and purified via flash chromatography on silica gel (MeOH/DCM), affording the products as either white solids or colourless oils. (Yields between 48 – 90%)

(6aS*,8S*,10aS*)-8-hydroxy-2,10a-dimethyl-5,6,6a,7,8,9,10,10a-octahydrobenzo[h]quinazolin-4(3H)-one



2.81, (16.1 mg, 0.0648 mmol, 42% yield over two steps, colourless oil)
1.95 equiv. of amidine.HCl and base

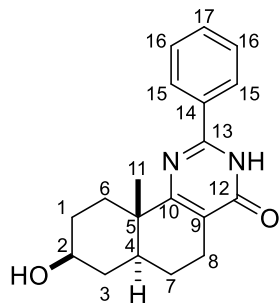
$R_f = 0.38$ (10% MeOH in DCM)

^1H NMR (400 MHz, CD_3OD) δ 3.60 (tt, $J = 10.6, 4.9$ Hz, 1H, **H-2**), 2.62 – 2.51 (m, 1H, **H-8**), 2.48 – 2.27 (m, 5H, **H-6, H-8, H-14**), 1.95 – 1.85 (m, 1H, **H-1**), 1.80 – 1.71 (m, 1H, **H-3**), 1.68 – 1.49 (m, 4H, **H-1, H-7, H-18**), 1.43 (q, $J = 11.7$ Hz, 1H, **H-3**), 1.28 (td, $J = 13.8, 4.0$ Hz, 1H, **H-6**), 1.11 (s, 3H, **H-11**)

^{13}C NMR (101 MHz, CD_3OD) δ 170.6 (**C-10**), 166.0 (**C-12**), 156.7 (**C-13**), 118.2 (**C-9**), 71.4 (**C-2**), 41.6 (**C-4**), 39.7 (**C-5**), 38.3 (**C-3**), 34.6 (**C-6**), 31.8 (**C-1**), 25.2 (**C-7**), 23.4 (**C-8**), 21.1 (**C-14**), 18.9 (**C-11**)

HRMS (ESI+) m/z found 249.1603 $[\text{M}+\text{H}]^+$, $\text{C}_{14}\text{H}_{20}\text{N}_2\text{O}_2$ calculated 249.1611 ($\Delta = 3.21$ ppm).

(6aS*,8S*,10aS*)-8-hydroxy-10a-methyl-2-phenyl-5,6,6a,7,8,9,10,10a-octahydrobenzo[h]quinazolin-4(3H)-one



2.82, (35.7 mg, 0.115 mmol, 76% yield over two steps, white solid) 1.5 equiv. of amidine and base

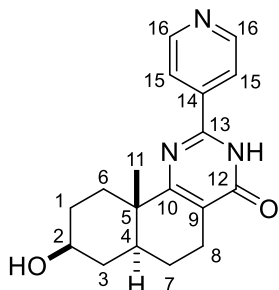
$R_f = 0.17$ (5% MeOH in DCM)

^1H NMR (400 MHz, CDCl_3) δ 8.43 – 7.99 (m, 2H, **H-15**), 7.60 – 7.39 (m, 3H, **H-16**, **H-17**), 3.72 (dt, $J = 11.0, 5.7$ Hz, 1H, **H-2**), 2.76 (m, 1H, **H-8**), 2.64 – 2.47 (m, 2H, **H-6**, **H-8**), 2.06 – 1.93 (m, 1H, **H-1**), 1.90 – 1.76 (m, 1H, **H-3**), 1.75 – 1.56 (m, 4H, **H-1**, **H-4**, **H-7**), 1.55 – 1.35 (m, 2H, **H-3**, **H-6**), 1.18 (s, 3H, **H-11**)

^{13}C NMR (101 MHz, CDCl_3) δ 169.6 (**C-10**), 165.1 (**C-11**), 152.8 (**C-13**), 132.6 (**C-14**), 131.6 (**C-17**), 129.0 (**C-16**), 127.4 (**C-15**), 118.5 (**C-9**), 71.1 (**C-2**), 40.3 (**C-4**), 39.0 (**C-5**), 37.7 (**C-3**), 33.7 (**C-6**), 31.4 (**C-1**), 24.3 (**C-7**), 22.5 (**C-8**), 19.1 (**C-11**)

HRMS (ESI+) m/z found 311.1759 $[\text{M}+\text{H}]^+$, $\text{C}_{19}\text{H}_{22}\text{N}_2\text{O}_2$ calculated 311.1756 ($\Delta = -0.96$ ppm).

(6aS*,8S*,10aS*)-8-hydroxy-10a-methyl-2-(pyridin-4-yl)-5,6,6a,7,8,9,10,10a-octahydrobenzo[h]quinazolin-4(3H)-one



2.83, (25.5 mg, 0.0819 mmol, 54% yield over two steps, yellow solid) 1.75 equiv. of amidine.HCl and base

$R_f = 0.26$ (7% MeOH in DCM)

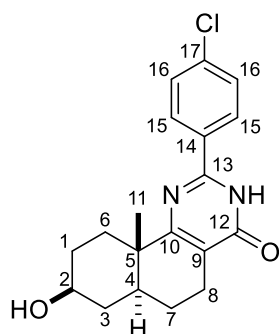
^1H NMR (400 MHz, CDCl_3) δ 8.80 – 8.68 (d, $J = 6.4$ Hz, 2H, **H-16**), 8.19 (d, $J = 5.7$ Hz, 2H, **H-15**), 3.63 (tt, $J = 10.6, 4.9$ Hz, 1H, **H-2**), 2.70 (m, 1H, **H-8**), 2.62 – 2.47 (m, 2H, **H-6**, **H-8**), 1.95 (m, 1H, **H-1**), 1.80 (m, 1H, **H-3**), 1.74 – 1.56 (m, 4H, **H-1**, **H-4**, **H-7**), 1.54 – 1.35 (m, 2H, **H-3**, **H-6**), 1.19 (s, 1H, **H-11**)

11)

^{13}C NMR (101 MHz, CDCl_3) δ 171.2 (**C-10**), 166.4 (**C-12**), 153.3 (**C-13**), 149.7 (**C-16**), 144.8 (**C-14**), 123.4 (**C-15**), 120.7 (**C-9**), 71.4 (**C-2**), 41.4 (**C-4**), 40.0 (**C-5**), 38.3 (**C-3**), 34.8 (**C-6**), 31.8 (**C-1**), 25.1 (**C-7**), 23.6 (**C-8**), 19.3 (**C-11**)

HRMS (ESI+) m/z found 312.1707 $[\text{M}+\text{H}]^+$, $\text{C}_{18}\text{H}_{21}\text{N}_3\text{O}_2$ calculated 312.1712 ($\Delta = -1.60$ ppm).

(6aS*,8S*,10aS*)-2-(4-chlorophenyl)-8-hydroxy-10a-methyl-5,6,6a,7,8,9,10,10a-octahydrobenzo[h]quinazolin-4(3H)-one



2.84, (35.7 mg, 0.104 mmol, 69% yield over two steps, white solid) 1.3 equiv. of amidine.HCl and base

$R_f = 0.48$ (10% MeOH in DCM)

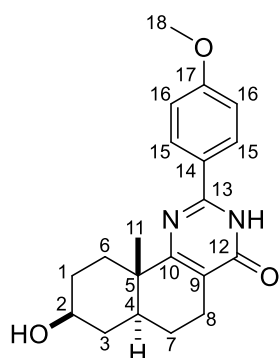
^1H NMR (400 MHz, CDCl_3) δ 8.21 (d, $J = 8.5$ Hz, 2H, **H-15**), 7.48 (d, $J = 8.5$ Hz, 2H, **H-16**), 3.77 – 3.66 (m, 1H, **H-2**), 2.75 (m, 1H, **H-8**), 2.63 – 2.49 (m, 2H, **H-6**, **H-8**), 2.04 – 1.81 (m, 2H, **H-1**, **H-3**), 1.77 – 1.32 (m, 6H, **H-1**, **H-3**, **H-4**, **H-6**, **H-7**), 1.18 (s, 3H, **H-11**)

¹³C NMR (101 MHz, CDCl₃) δ 170.1 (C-10), 165.3 (C-12), 152.0 (C-13), 138.1 (C-14), 130.8 (C-17), 129.2 (C-16), 128.9 (C-15), 118.6 (C-9), 71.1 (C-2), 40.3 (C-4), 39.1 (C-5), 37.6 (C-3), 33.6 (C-6), 31.3 (C-1), 24.2 (C-7), 22.5 (C-8), 19.1 (C-11)

HRMS (ESI+) m/z found 345.1375 [M+H]⁺, C₁₉H₂₁ClN₂O₂ calculated 345.1370 (Δ = 1.45 ppm).

Note: Some ¹³C signals do not appear, but can be seen, and thus assigned via the HMBC spectrum

(6aS*,8S*,10aS*)-8-hydroxy-2-(4-methoxyphenyl)-10a-methyl-5,6,6a,7,8,9,10,10a-octahydrobenzo[h]quinazolin-4(3H)-one



2.85, (44.0 mg, 0.129 mmol, 62% yield over two steps, white solid) 1.3 equiv. of amidine.HCl and base

R_f = 0.38 (10% MeOH in DCM)

¹H NMR (400 MHz, CDCl₃) δ 8.16 (d, *J* = 8.9 Hz, 2H, H-15), 7.00 (d, *J* = 8.9 Hz, 2H, H-16), 3.88 (s, 3H, H-18), 3.77 – 3.65 (m, 1H, H-2), 2.79 – 2.69 (m, 1H, H-8), 2.64 – 2.47 (m, 2H, H-6, H-8), 2.06 – 1.78 (m, 2H, H-1, H-3), 1.72 – 1.33 (m, 6H, H-1, H-3, H-4, H-6, H-7), 1.19 (s, 3H, H-11)

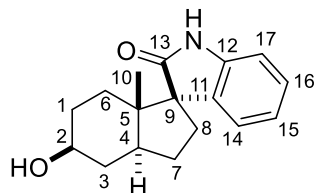
¹³C NMR (101 MHz, CDCl₃) δ 169.8 (C-10), 165.0 (C-12), 162.6 (C-17), 152.7 (C-13), 129.2 (C-15), 124.6 (C-14), 117.4 (C-9), 114.4 (C-16), 71.1 (C-2), 55.7 (C-18), 40.3 (C-4), 39.0 (C-5), 37.7 (C-3), 33.7 (C-6), 31.4 (C-1), 24.3 (C-7), 22.4 (C-8), 19.0 (C-11)

HRMS (ESI+) m/z found 341.1859 [M+H]⁺, C₂₀H₂₄N₂O₃ calculated 341.1865 (Δ = -1.76 ppm).

General procedure for the synthesis of spirooxindole analogues

The appropriate indole-fused analogue (1.00 equiv.) and *N*-bromosuccinimide (1.10 equiv.) were dissolved in a 1:1:1 mixture of AcOH:THF:H₂O and stirred at room temperature for 30 minutes. The reaction mixture was poured into saturated Na₂CO₃, extracted twice with DCM, and the organic phase washed with water. The organic phase was dried over anhydrous sodium sulfate and concentrated to a crude yellow oil. Purification of the crude compounds by flash chromatography on silica gel (3% MeOH in DCM) afforded the products as single diastereoisomers.

(1S*,3aS*,5S*,7aS*)-5-hydroxy-7a-methyl-2,3,3a,4,5,6,7,7a-octahydrospiro[indene-1,3'-indolin]-2'-one



2.52, (19.2 mg, 0.0708 mmol, 45% yield, white solid)

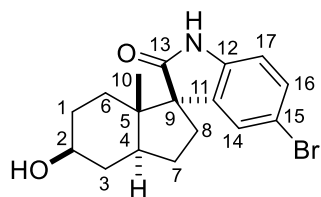
R_f = 0.18 (3% MeOH/DCM); ¹H NMR (400 MHz, MeOD) δ 7.24 (d, *J* = 7.5 Hz, 1H, H-14), 7.17 (t, *J* = 7.7 Hz, 1H, H-16), 6.99 (t, *J* = 7.6 Hz, 1H, H-15), 6.84 (d, *J* = 7.7 Hz, 1H, H-17), 3.42 (tt, *J* = 10.7, 5.1 Hz, 1H, H-2), 2.48 – 2.39 (m, 1H, H-8), 2.24 (m, 1H, H-4), 1.98 – 1.83 (m, 3H, H-3, H-7, H-8), 1.66 (m, H-7), 1.59 – 1.50 (m, 1H, H-1), 1.49 – 1.36 (m, 2H, H-1, H-3), 1.12 – 1.01 (m, 4H, H-6, H-10), 0.72 (td, *J* = 13.3, 4.5 Hz, 1H, H-6)

¹³C NMR (101 MHz, MeOD) δ 183.8 (C-13), 142.5 (C-12), 136.5 (C-11), 128.7 (C-16), 125.5 (C-14), 122.7 (C-15), 110.3 (C-17), 71.9 (C-2), 62.1 (C-9), 50.4 (C-5), 45.4 (C-4), 35.4 (C-3), 32.8 (C-8), 31.4 (C-6), 31.3 (C-1), 27.5 (C-7), 15.5 (C-10).

HRMS (ESI+) m/z found 272.1647 [M+H]⁺, C₁₇H₂₁NO₂ calculated 272.1650 (Δ = -1.10 ppm)

Note: formed alongside ~10% of inseparable C-15 brominated spiro-oxindole **2.53**

(1S*,3aS*,5S*,7aS*)-5'-bromo-5-hydroxy-7a-methyl-2,3,3a,4,5,6,7,7a-octahydrospiro[indene-1,3'-indolin]-2'-one



2.53, (26.7 mg, 0.0760 mmol, 63% yield, white solid)

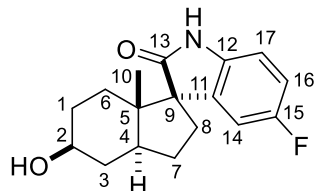
R_f = 0.20 (3% MeOH/DCM)

¹H NMR (400 MHz, MeOD) δ 7.38 (d, *J* = 1.9 Hz, 1H, H-14), 7.34 (dd, *J* = 8.2, 1.9 Hz, 1H, H-16), 6.78 (d, *J* = 8.2 Hz, 1H, H-17), 3.45 (tt, *J* = 10.8, 5.1 Hz, 1H, H-2), 2.52 – 2.38 (m, 1H, H-8), 2.22 – 2.05 (m, 1H, H-4), 2.00 – 1.83 (m, 3H, H-3, H-7, H-8), 1.71 – 1.54 (m, 2H, H-1, H-7), 1.50 – 1.36 (m, 2H, H-1, H-3), 1.10 (dt, *J* = 13.2, 4.05 Hz, 1H, H-6), 1.06 (s, 3H, H-10), 0.72 (td, *J* = 13.2, 4.05 Hz, 1H, H-6)

¹³C NMR (101 MHz, MeOD) δ 183.0 (C-13), 141.9 (C-12), 138.9 (C-11), 131.6 (C-16), 128.5 (C-14), 115.1 (C-15), 111.8 (C-17), 71.7 (C-2), 62.5 (C-9), 50.7 (C-5), 45.6 (C-4), 35.3 (C-3), 32.8 (C-8), 31.5 (C-6), 31.2 (C-1), 27.4 (C-7), 15.5 (C-10)

HRMS (ESI+) m/z found 350.0754 [M+H]⁺, C₁₇H₂₀BrNO₂ calculated 350.0755 (Δ = -0.29 ppm)

(1S*,3aS*,5S*,7aS*)-5'-fluoro-5-hydroxy-7a-methyl-2,3,3a,4,5,6,7,7a-octahydrospiro[indene-1,3'-indolin]-2'-one



2.54, (37.0 mg, 0.128 mmol, 88% yield, white solid)

¹H NMR (400 MHz, MeOD) δ 7.08 (dd, *J* = 9.0, 2.6 Hz, 1H, H-14), 6.93 (td, *J* = 8.9, 2.5 Hz, 1H, H-16), 6.81 (dd, *J* = 8.5, 4.5 Hz, 1H, H-17), 3.46 (tt, *J* = 10.7, 5.1 Hz, 1H, H-2), 2.49 – 2.40 (m, 1H, H-8), 2.23 – 2.11 (m, 1H, H-4), 2.00 – 1.83 (m, 3H, H-3, H-7, H-8), 1.72 – 1.53 (m, 2H, H-1, H-7), 1.51 – 1.37 (m, 2H, H-1, H-3), 1.12 – 1.03 (m, 4H, H-6, H-10), 0.73 (td, *J* = 13.2, 4.4 Hz, 1H, H-6)

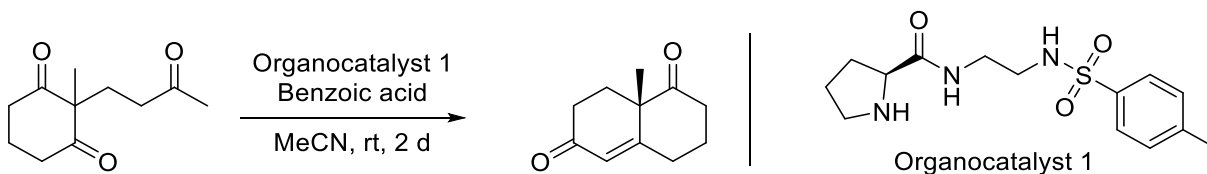
¹³C NMR (101 MHz, MeOD) δ 183.5 (C-13), 160.1 (d, *J* = 237.7 Hz, C-15), 138.6 (d, *J* = 1.9 Hz, C-12), 138.2 (d, *J* = 7.6 Hz, C-11), 114.7 (d, *J* = 23.5 Hz, C-16), 113.5 (d, *J* = 25.3 Hz, C-14), 110.8 (d, *J* = 8.2 Hz, C-17), 71.8 (C-2), 62.8 (d, *J* = 1.7 Hz, C-9), 50.7 (C-5), 45.5 (C-4), 35.3 (C-3), 32.8 (C-8), 31.4 (C-6), 31.2 (C-1), 27.4 (C-7), 15.5 (C-10)

¹⁹F NMR (377 MHz, MeOD) δ -123.7

HRMS (ESI+) m/z found 290.1552 [M+H]⁺, C₁₇H₂₀FNO₂ calculated 290.1556 (Δ = -1.38 ppm)

Synthesis of (-)-Astercin 1 and (+)-Astercin 1

(S)-8a-methyl-3,4,8a-tetrahydronaphthalene-1,6(2H,7H)-dione (S)-2.02



Triketone **2.03** (1.0 g, 5.10 mmol), organocatalyst **3.01** (0.22 g, 0.71 mmol), and benzoic acid (0.087 g, 0.71 mmol) were dissolved in MeCN (10 mL) and stirred at room temperature for 48 hours. The reaction was diluted with saturated aqueous ammonium chloride (25 mL), extracted with EtOAc (3 x 30 mL), the combined organic phases dried over anhydrous sodium sulfate, and concentrated to a brown-green oil. The crude product was purified by flash chromatography on silica gel (2:3 ethyl acetate/*n*-hexane) to yield the product as a pale yellow oil (0.732 g, 4.06 mmol, 80% yield)

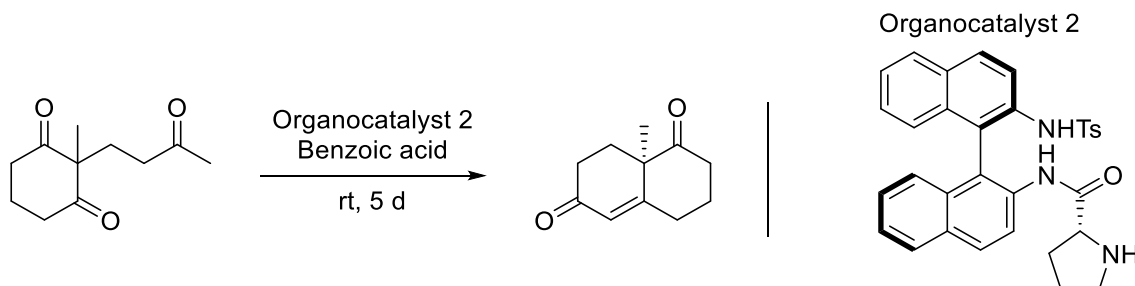
¹H NMR (400 MHz, CDCl₃) δ 5.86 (d, *J* = 1.8 Hz, 1H), 2.77 – 2.66 (m, 2H), 2.55 – 2.43 (m, 4H), 2.20 – 2.09 (m, 3H), 1.77 – 1.65 (m, 1H), 1.45 (s, 3H)

¹³C NMR (101 MHz, CDCl₃) δ 211.2, 198.5, 166.0, 126.0, 50.8, 37.8, 33.8, 31.9, 29.8, 23.4, 23.1.

Organocatalyst 1 was prepared according to the procedure of Pedrosa *et al*¹⁵⁰

The ¹H and ¹³C spectra are in agreement with those reported in the literature¹²¹

(*R*)-8a-methyl-3,4,8,8a-tetrahydronaphthalene-1,6(2H,7H)-dione (*R*)-2.02



Triketone **2.03** (21.9 g, 0.112 mol), organocatalyst **3.02** (0.6 g, 0.00112 mol), and benzoic acid (0.341 g, 0.0028 mol) were added to a flask and stirred at room temperature for 5 days. The crude oil was dissolved in ethyl acetate (150 mL), activated carbon (5 g) added, and the suspension stirred at room temperature for 2 hours. The suspension was diluted with *n*-hexane (150 mL) and filtered through a silica plug, eluting with a 1:1 mixture of ethyl acetate:*n*-hexane. The filtrate was concentrated and the amber oil purified by flash chromatography on silica gel (10 → 30 → 50% EtOAc/*n*-hexane) to yield the product as an off-white solid. (16.3 g, 0.0915 mol, 82% yield)

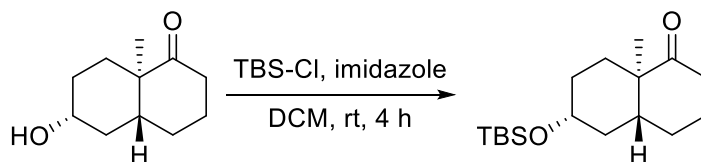
¹H NMR (400 MHz, CDCl₃) δ 5.85 (d, *J* = 1.8 Hz, 1H), 2.78 – 2.64 (m, 2H), 2.54 – 2.41 (m, 4H), 2.21 – 2.09 (m, 3H), 1.78 – 1.60 (m, 1H), 1.44 (s, 3H)

¹³C NMR (101 MHz, CDCl₃) δ 211.2, 198.4, 165.9, 126.0, 50.7, 37.8, 33.7, 31.9, 29.8, 23.4, 23.0.

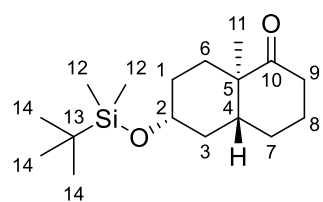
Organocatalyst 2 was prepared according to the procedure of Bradshaw *et al*¹²²

The ¹H and ¹³C spectra are in agreement with those reported in the literature¹²¹

(4a*R*,6*R*,8a*R*)-6-((*tert*-butyldimethylsilyl)oxy)-8a-methyloctahydronaphthalen-1(2*H*)-one (+)-3.08



(+)-**2.01** (1.47 g, 8.07 mmol) was dissolved in dry DCM (100 mL) before addition of imidazole (1.10 g, 16.1 mmol) and TBS-Cl (1.46, 9.68 mmol), and the suspension stirred at room temperature for 4 hours. Water (75 mL) was added to the suspension, the phases separated, the organic phase dried over anhydrous magnesium sulfate, and concentrated to a yellow oil. Purification of the crude product by flash chromatography on silica gel (1:9 ethyl acetate/*n*-heptane) to yield the product as a colourless oil that solidified to a white solid upon storage at – 20 °C (2.02 g, 6.81 mmol, 84% yield)



$R_f = 0.30$ (1:9 ethyl acetate/*n*-heptane)

^1H NMR (400 MHz, CDCl_3) δ 3.51 (m, 1H, **H-2**), 2.63 (td, $J = 13.8, 6.9$ Hz, 1H, **H-9**), 2.25 – 2.16 (m, 1H, **H-9**), 2.08 – 1.95 (m, 1H, **H-8**), 1.82 – 1.73 (m, 1H, **H-1**), 1.73 – 1.54 (m, 4H, **H-3**, **H-6**, **H-8**), 1.54 – 1.36 (m, 5H, **H-1**, **H-3**, **H-6**, **H-7**), 1.12 (s, 3H, **H-11**), 0.88 (s, 9H, **H-14**), 0.05

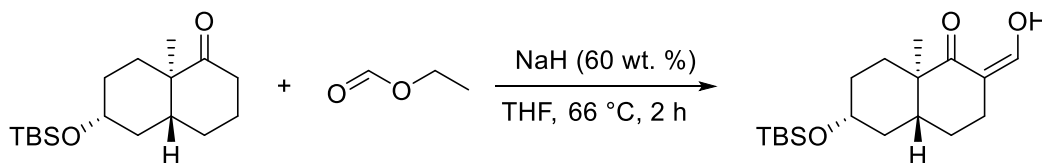
(s, 6H, **H-12**)

^{13}C NMR (101 MHz, CDCl_3) δ 216.1 (**C-10**), 71.4 (**C-2**), 47.8 (**C-5**), 44.1 (**C-4**), 37.63 (**C-9/3**), 37.59 (**C-9/3**), 31.3 (**C-1**), 31.1 (**C-6**), 27.6 (**C-7**), 26.4 (**C-8**), 26.0 (**C-14**), 18.4 (**C-13**), 16.0 (**C-11**), –4.4 (**C-12**), –4.5 (**C-12**)

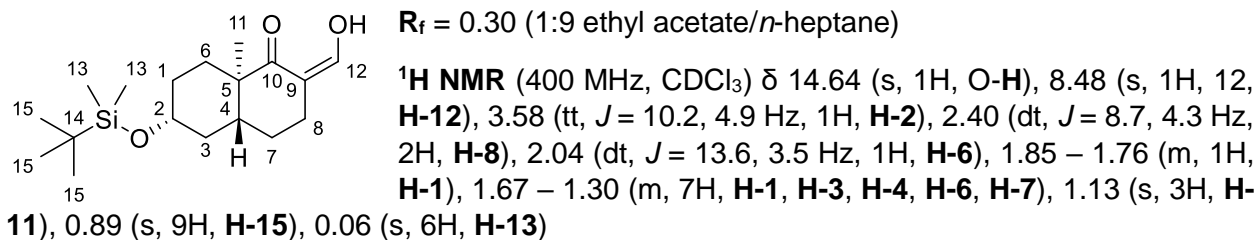
HRMS (ESI+) m/z found 297.2246 $[\text{M}+\text{H}]^+$, $\text{C}_{17}\text{H}_{32}\text{O}_2\text{Si}$ calculated 297.2250 ($\Delta = -1.35$ ppm)

$[\alpha]_D^{23} = +38.5$ ($c = 1.0$, CHCl_3)

(4a*R*,6*R*,8a*R*,*Z*)-6-((*tert*-butyldimethylsilyl)oxy)-2-(hydroxymethylene)-8a-methyloctahydronaphthalen-1(2*H*)-one (-)-3.09



A solution of (+)-**3.08** (1.00 g, 3.37 mmol) in anhydrous THF (50 mL) was cooled to 0 °C in an ice-bath before addition of ethyl formate (2.73 mL, 33.7 mmol), and sodium hydride (60 wt% in mineral oil, 0.40 g, 10.1 mmol), and the resulting suspension heated at reflux for 2 hours. The bright orange reaction was quenched via the addition of saturated aqueous NH_4Cl before dilution with ethyl acetate. The organic phase was separated, washed with water, dried over anhydrous sodium sulfate, and concentrated to yield a pale-yellow solid. The crude solid was purified via flash chromatography on silica gel (1:9 ethyl acetate/*n*-heptane) to afford the product as a tan solid (0.85 g, 2.62 mmol, 78% yield).

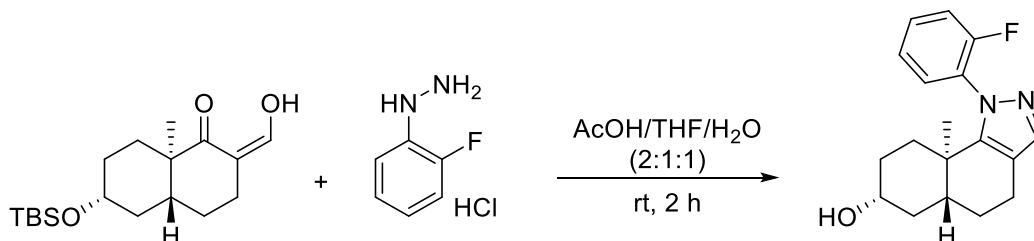


¹³C NMR (101 MHz, CDCl₃) δ 193.7 (**C-10**), 185.9 (**C-12**), 106.1 (**C-9**), 71.5 (**C-2**), 40.7 (**C-5**), 39.4 (**C-4**), 37.6 (**C-3**), 31.6 (**C-6**), 31.3 (**C-1**), 26.0 (**C-15**), 24.9 (**C-7**), 23.1 (**C-8**), 18.4 (**C-14**), 17.7 (**C-11**), -4.4 (**C-13**), -4.5 (**C-13**)

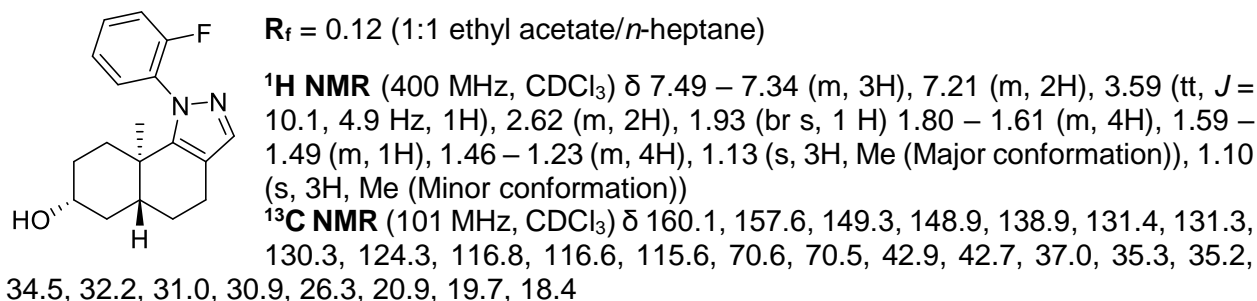
HRMS (ESI+) *m/z* found 325.2206 [M+H]⁺, C₁₈H₃₂O₃Si calculated 325.2199 (Δ = 2.15 ppm)

[α]_D²³ = - 24.3 (*c* = 1.0, CHCl₃).

(5aR,7R,9aR)-1-(2-fluorophenyl)-9a-methyl-4,5,5a,6,7,8,9,9a-octahydro-1H-benzo[*g*]indazol-7-ol, (-)-2.77, (-)-Astercin 1



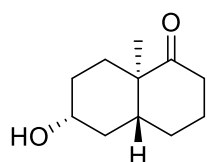
(-)-**3.09** (250 mg, 0.77 mmol) and 2-fluorophenylhydrazine HCl (162 mg, 1.00 mmol) were suspended in a 2:1:1 mixture of glacial AcOH/THF/H₂O and stirred at room temperature for 1 hour, with complete dissolution observed after 5 minutes. The reaction was neutralised by addition of 2M aqueous NaOH and extracted with ethyl acetate (2x). The organic phases were dried over anhydrous magnesium sulfate and concentrated to a crude yellow solid. Purification of the solid by flash chromatography on silica gel (1:1 ethyl acetate/*n*-heptane) afforded (-)-Astercin 1 as a pale-yellow solid. (137 mg, 0.46 mmol, 60% yield) with e.r. = 95.0:5.0(-):(+).



(HRMS (ESI+)) *m/z* found 301.1719 [M+H]⁺, C₁₈H₂₁FN₂O calculated 301.1716 (Δ = 1.00 ppm)

[α]_D²³ = - 67.0 (*c* = 1.0, CHCl₃)

(4aR,6R,8aR)-6-hydroxy-8a-methyloctahydronaphthalen-1(2H)-one, (+)-2.01



Synthesised according to the procedures of **(±)-2.01**

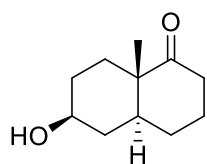
¹H NMR (400 MHz, CDCl₃) δ 3.63 – 3.51 (m, 1H), 2.71 – 2.55 (m, 1H), 2.28 – 2.16 (m, 1H), 2.07 – 1.97 (m, 1H), 1.93 – 1.85 (m, 1H), 1.78 – 1.59 (m, 4H), 1.59 – 1.37 (m, 5H), 1.13 (s, 3H)

¹³C NMR (101 MHz, CDCl₃) δ 215.8, 70.6, 47.8, 43.9, 37.6, 37.0, 31.0, 30.9, 27.6, 26.3, 15.9

HRMS (ESI+) m/z found 183.1391 [M+H]⁺, C₁₁H₁₈O₂ calculated 183.1385 (Δ = 3.28 ppm)

[α]_D²³ = + 59.8 (c = 1.84, CHCl₃).

(4aS,6S,8aS)-6-hydroxy-8a-methyloctahydronaphthalen-1(2H)-one, (-)-2.01



Synthesised according to the procedures of **(±)-2.01**

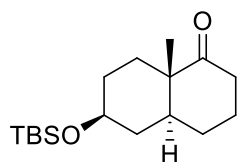
¹H NMR (400 MHz, CDCl₃) δ 3.58 (tt, J = 9.9, 4.8 Hz, 1H), 2.71 – 2.55 (m, 1H), 2.27 – 2.17 (m, 1H), 2.10 – 1.95 (m, 1H), 1.95 – 1.82 (m, 1H), 1.79 – 1.58 (m, 4H), 1.58 – 1.37 (m, 5H), 1.13 (s, 3H)

¹³C NMR (101 MHz, CDCl₃) δ 215.9, 70.6, 47.7, 43.9, 37.6, 36.9, 31.0, 30.9, 27.5, 26.3, 15.9

HRMS (ESI+) m/z found 183.1391 [M+H]⁺, C₁₁H₁₈O₂ calculated 183.1385 (Δ = 3.28 ppm)

[α]_D²³ = - 61.2 (c = 1.82, CHCl₃)

(4aS,6S,8aS)-6-((tert-butyldimethylsilyl)oxy)-8a-methyloctahydronaphthalen-1(2H)-one, (-)-3.08



Synthesised according to the procedure of **(+)-3.08**, affording **(-)-3.08** as a white solid in 80% yield.

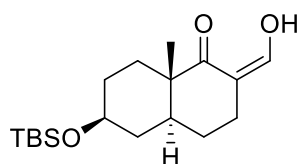
¹H NMR (400 MHz, CDCl₃) δ 3.58 – 3.45 (m, 1H), 2.70 – 2.57 (m, 1H), 2.25 – 2.16 (m, 1H), 2.06 – 1.96 (m, 1H), 1.81 – 1.72 (m, 1H), 1.72 – 1.58 (m, 4H), 1.55 – 1.38 (m, 5H), 1.12 (s, 3H), 0.88 (s, 9H), 0.05 (s, 6H)

¹³C NMR (101 MHz, CDCl₃) δ 216.1, 71.4, 47.8, 44.1, 37.6, 37.6, 31.3, 31.1, 27.6, 26.4, 26.0, 18.3, 16.0, -4.5, -4.5

HRMS (ESI+) m/z found 297.2255 [M+H]⁺, C₁₇H₃₂O₂Si calculated 297.2250 (Δ = 1.68 ppm)

[α]_D²³ = - 36.0 (c = 1.00, CHCl₃)

(4aS,6S,8aS,Z)-6-((tert-butyldimethylsilyl)oxy)-2-(hydroxymethylene)-8a-methyloctahydronaphthalen-1(2H)-one



Synthesised according to the procedure of **(-)-3.09**, affording **(+)-3.09** as a tan solid in 61% yield.

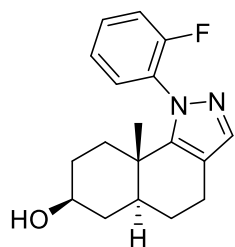
¹H NMR (400 MHz, CDCl₃) δ 14.64 (s, 1H), 8.50 – 8.45 (m, 1H), 3.58 (tt, J = 10.2, 4.9 Hz, 1H), 2.46 – 2.33 (m, 2H), 2.04 (dt, J = 13.6, 3.5 Hz, 1H), 1.84 – 1.76 (m, 1H), 1.67 – 1.30 (m, 7H), 1.13 (s, 3H), 0.89 (s, 9H), 0.06 (s, 6H)

¹³C NMR (101 MHz, CDCl₃) δ 193.7, 185.9, 106.1, 71.5, 40.7, 39.4, 37.6, 31.6, 31.3, 26.0, 24.9, 23.1, 18.4, 17.7, -4.4, -4.5

HRMS (ESI+) m/z found 325.2200 [M+H]⁺, C₁₈H₃₂O₃Si calculated 325.2199 (Δ = 0.31 ppm)

[α]_D²³ = + 24.0 (c = 1.00, CHCl₃)

(5a*S*,7*S*,9a*S*)-1-(2-fluorophenyl)-9a-methyl-4,5,5a,6,7,8,9,9a-octahydro-1H-benzo[*g*]indazol-7-ol, (+)-2.77, (+)-Astercin 1



Synthesised according to the procedure of (-)-Astercin 1, affording (+)-Astercin 1 as a pale-yellow solid in 13% yield (purified by preparative HPLC), with e.r. = 95.5:4.5 (+):(-)

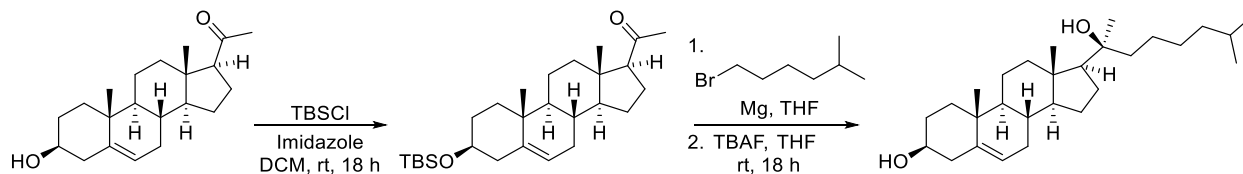
¹H NMR (400 MHz, CDCl₃) δ 7.50 – 7.35 (m, 3H), 7.25 – 7.16 (q, *J* = 8.9, 8.0 Hz, 2H), 3.61 (tt, *J* = 10.0, 4.7 Hz, 1H), 2.70 – 2.58 (m, 2H), 1.82 – 1.22 (m, 9H), 1.14 (s, 3H, Me (Major conformation)), 1.10 (s, 3H, Me (Minor conformation))

¹³C NMR (101 MHz, CDCl₃) δ 148.9, 139.1, 131.4, 131.3, 130.4, 124.3, 116.8, 116.6, 115.5, 70.7, 70.6, 42.9, 42.7, 37.1, 35.2, 34.5, 32.2, 31.0, 30.9, 26.4, 21.0, 19.7, 18.4

HRMS (ESI+) m/z found 301.1721 [M+H]⁺, C₁₈H₂₁FN₂O calculated 301.1716 (Δ = 1.66 ppm)

[α]_D²³ = + 87.0 (c = 0.92, CHCl₃)

Aster inhibitor synthesis

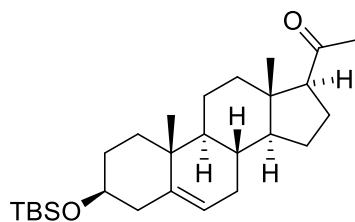


Compound **AI-11** was synthesised according to the procedures of Xiao *et al*¹¹⁰

1-((3*S*,8*S*,9*S*,10*R*,13*S*,14*S*,17*S*)-3-((*tert*-butyldimethylsilyl)oxy)-10,13-dimethyl-2,3,4,7,8,9,10,11,12,13,14,15,16,17-tetradecahydro-1H-cyclopenta[*a*]phenanthren-17-yl)ethan-1-one

To a suspension of pregnenolone (1.00 g, 3.16 mmol) and imidazole (0.43 g, 6.32 mmol) in anhydrous DCM was added *tert*-butyldimethylsilyl chloride (0.57 g, 3.79 mmol) and the suspension stirred at room temperature for 18 hours. The reaction was concentrated and the resulting white solid was partitioned between diethyl ether and water, separated, and the organic phase washed once with brine before drying over anhydrous magnesium sulfate. Removal of solvent under reduced pressure afforded the desired product as a white solid (1.00 g, 2.32 mmol, 73% yield)

The ¹H and ¹³C spectra are in agreement with those reported in the literature¹¹⁰



$R_f = 0.58$ (1:4 ethyl acetate/*n*-hexane)

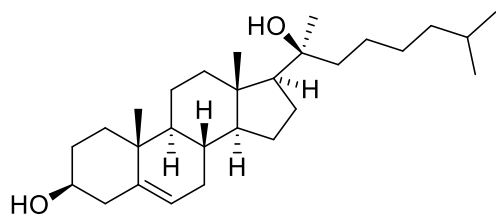
$^1\text{H NMR}$ (400 MHz, CDCl_3) δ 5.31 (dt, $J = 4.8, 2.0$ Hz, 1H), 3.48 (ddd, $J = 11.0, 6.1, 4.6$ Hz, 1H), 2.53 (t, $J = 9.0$ Hz, 1H), 2.30 – 2.13 (m, 3H), 2.12 (s, 3H), 2.06 – 1.95 (m, 2H), 1.82 (dt, $J = 13.2, 3.5$ Hz, 1H), 1.75 – 1.38 (m, 9H), 1.28 – 1.01 (m, 3H), 1.00 (s, 3H), 0.99 – 0.93 (m, 1H), 0.89 (s, 9H), 0.63 (s, 3H), 0.06 (s, 6H)

$^{13}\text{C NMR}$ (101 MHz, CDCl_3) δ 209.7, 141.7, 121.0, 72.7, 63.9, 57.1, 50.2, 44.2, 42.9, 39.0, 37.5, 36.8, 32.19, 32.02, 32.0, 31.7, 26.1, 24.6, 23.0, 21.2, 19.6, 18.4, 13.4, -4.44.

(3S,8S,9S,10R,13S,14S,17S)-17-((S)-2-hydroxy-7-methyloctan-2-yl)-10,13-dimethyl-2,3,4,7,8,9,10,11,12,13,14,15,16,17-tetradecahydro-1H-cyclopenta[a]phenanthren-3-ol

To a suspension of magnesium turnings (0.102 g, 4.18 mmol) in anhydrous THF (5 mL) was added 1-bromo-5-methylhexane (0.449 mL, 2.76 mmol) and the suspension heated at reflux for 2 hours. The solution of the Grignard reagent was cooled to 0 °C in an ice bath before the dropwise addition of a solution of TBS-pregnenolone (99.1 mg, 0.23 mmol) in anhydrous THF (5 mL). The resulting solution was stirred at room temperature for 18 hours before reaching completion. The reaction was quenched via addition of saturated aqueous ammonium chloride and stirred until destruction of excess magnesium was observed, after which, the reaction mixture was extracted with ethyl acetate. The organic phase was dried over anhydrous magnesium sulfate, concentrated to a crude solid, and used immediately in the deprotection.

The crude solid obtained from the previous step was dissolved in THF (15 mL) before addition of 1 M TBAF in THF (2 mL) and the resulting solution stirred at room temperature for 18 hours. The reaction was partitioned between brine and ethyl acetate, the combined organic phase dried over anhydrous magnesium sulfate, and concentrated to a crude yellow oil. Purification of the crude oil by flash chromatography on silica gel (1:4 ethyl acetate/*n*-hexane) afforded the desired product **AI-11** as a white solid (45 mg, 0.108 mmol, 47% yield)



$R_f = 0.14$ (1:4 ethyl acetate/*n*-hexane)

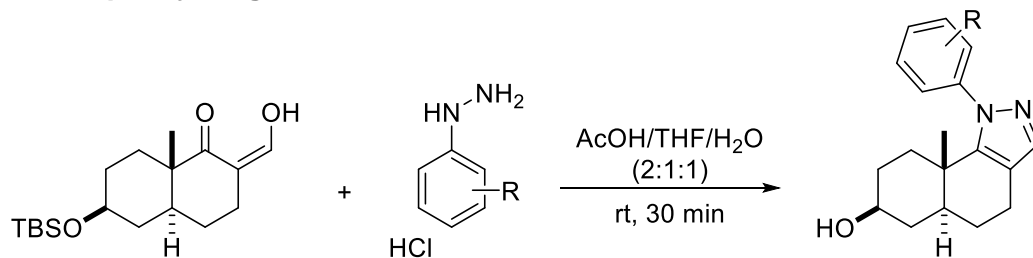
$^1\text{H NMR}$ (400 MHz, CDCl_3) δ 5.39 – 5.32 (m, 1H), 3.55 – 3.46 (m, 1H), 2.29 (s, 2H), 2.09 (dt, $J = 12.5, 3.5$ Hz, 1H), 1.98 (dtd, $J = 16.2, 4.6, 2.4$ Hz, 1H), 1.88 – 1.78 (m, 2H), 1.78 – 1.41 (m, 10H), 1.40 (s, 3H), 1.37 – 1.03 (m, 10H), 1.01 (s, 3H), 1.00 – 0.89 (m, 2H), 0.88 – 0.86 (m, 6H),

0.85 (s, 3H)

$^{13}\text{C NMR}$ (101 MHz, CDCl_3) δ 140.9, 121.8, 75.4, 71.9, 57.7, 57.1, 50.2, 44.2, 42.8, 42.4, 40.3, 39.2, 37.4, 36.7, 31.9, 31.8, 31.5, 28.2, 28.1, 26.6, 24.7, 23.9, 22.81, 22.78, 22.5, 21.1, 19.5, 13.8.

General procedure for the synthesis of pyrazole-fused analogues

Exploration of phenyl ring substitution



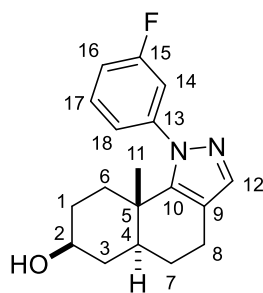
TBS-protected hydroxymethylene **3.09** (1 equiv.) and the appropriate phenylhydrazine HCl salt (1.05 equiv.) were suspended in a 2:1:1 mixture of AcOH/H₂O/THF and stirred at room temperature for 30 minutes, after which both starting materials had fully dissolved. The reaction was cooled in an ice-bath and basified via addition of 2M aq. NaOH. The reaction mixture was extracted with ethyl acetate (3x), the combined organic phases dried over anhydrous sodium sulfate, and concentrated to a crude yellow oil. The crude compounds were purified by flash chromatography on silica gel (1:1 ethyl acetate/*n*-heptane, unless otherwise stated) to afford the products as solids.

Notes: Single enantiomers of (±)-Astercin 1 analogues were synthesised in an identical procedure from the enantiopure TBS-protected hydroxymethylene (–)-**3.09**.

¹³C NMR spectra for Astercin 1 analogues are often complex owing to splitting of carbon signals by fluorine and the presence of conformational isomers, therefore spectral data reported are the main identifiable signals. 2D NMR experiments support the identification of the products and number of carbons present. Methyl signals in the ¹H NMR spectra are reported as “major” and “minor” with an integral of 3H despite the real integrals reflecting the ratio of conformers. Integrating the two peaks as one produces an integral accounting for the expected 3H of the methyl group.

Some hydrazines yielded isolable amounts of the corresponding linear regioisomers. Characterisation data for these compounds is reported after the respective angular regioisomer.

(5a*S**,7*S**,9a*S**)-1-(3-fluorophenyl)-9a-methyl-4,5,5a,6,7,8,9,9a-octahydro-1H-benzo[*g*]indazol-7-ol



3.10, isolated as a yellow solid (23.6 mg, 0.0786 mmol, 57% yield)

R_f = 0.13 (1:1 ethyl acetate/ *n*-heptane)

¹H NMR (400 MHz, CDCl₃) δ 7.45 – 7.36 (m, 2H, **H-12**, **H-17**), 7.21 – 7.14 (m, 2H, **H-16**, **H-18**), 7.13 – 7.08 (m, 1H, **H-14**), 3.58 (tt, *J* = 10.3, 4.9 Hz, 1H, **H-2**), 2.70 – 2.54 (m, 2H, **H-8**), 1.81 – 1.60 (m, 4H, **H-1**, **H-3**, **H-4**, **H-7**), 1.58 – 1.50 (m, 1H, **H-7**), 1.47 – 1.23 (m, 4H, **H-1**, **H-3**, **H-6**), 1.21 (s, 3H, **H-11**).

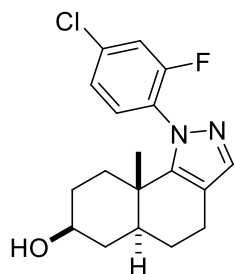
¹³C NMR (101 MHz, CDCl₃) δ 162.4 (d, *J* = 248.9 Hz, **C-15**), 148.6 (**C-10**), 143.6 (d, *J* = 9.7 Hz, **C-13**), 138.3 (**C-12**), 130.1 (d, *J* = 9.0 Hz, **C-17**), 124.0 (d, *J* = 3.3 Hz, **C-18**), 116.4 (d, *J* = 20.9

Hz, **C-16**), 115.9 (d, $J = 22.7$ Hz, **C-14**), 115.8 (**C-9**), 70.5 (**C-2**), 43.0 (**C-4**), 37.1 (**C-3**), 35.3 (**C-5**), 34.1 (**C-6**), 30.9 (**C-1**), 26.2 (**C-7**), 20.8 (**C-8**), 20.0 (**C-11**).

^{19}F NMR (377 MHz, CDCl_3) δ -110.60.

HRMS (ESI+) m/z found 301.1718 $[\text{M}+\text{H}]^+$, $\text{C}_{18}\text{H}_{21}\text{FN}_2\text{O}$ calculated 301.1716 ($\Delta = 0.66$ ppm)

(5aS*,7S*,9aS*)-1-(4-chloro-2-fluorophenyl)-9a-methyl-4,5,5a,6,7,8,9,9a-octahydro-1H-benzo[g]indazol-7-ol



3.11, isolated as a light yellow solid (27.5 mg, 0.082 mmol, 52% yield)

$R_f = 0.16$ (2:3 ethyl acetate/ *n*-heptane)

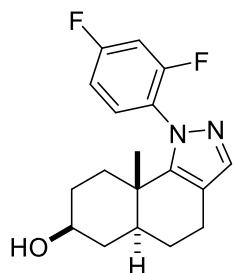
^1H NMR (400 MHz, CDCl_3) δ 7.42 (s, 1H), 7.36 – 7.28 (m, 1H), 7.27 – 7.21 (m, 2H), 3.66 – 3.55 (m, 1H), 2.69 – 2.54 (m, 2H), 1.92 (br s, 1H), 1.82 – 1.64 (m, 4H), 1.60 – 1.50 (m, 1H), 1.49 – 1.21 (m, 4H), 1.12 (s, 3H, **Me** major), 1.09 (s, 3H, **Me** minor).

^{13}C NMR (101 MHz, CDCl_3) δ 149.5, 149.1, 145.5, 139.3, 136.5, 136.4, 132.0, 131.0, 124.8, 117.7, 117.5, 115.9, 70.5, 70.5, 42.9, 42.7, 37.0, 35.2, 34.6, 32.3, 31.0, 30.9, 26.3, 20.9, 19.8, 18.5

^{19}F NMR (377 MHz, CDCl_3) δ -116.4, -116.8

HRMS (ESI+) m/z found 335.1327 $[\text{M}+\text{H}]^+$, $\text{C}_{18}\text{H}_{20}\text{ClFN}_2\text{O}$ calculated 335.1326 ($\Delta = 0.30$ ppm)

(5aS*,7S*,9aS*)-1-(2,4-difluorophenyl)-9a-methyl-4,5,5a,6,7,8,9,9a-octahydro-1H-benzo[g]indazol-7-ol



3.12, isolated as a pale yellow solid (23.0 mg, 0.072 mmol, 47% yield)

$R_f = 0.18$ (1:1 ethyl acetate/ *n*-heptane)

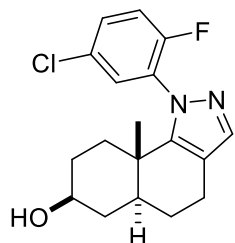
^1H NMR (400 MHz, CDCl_3) δ 7.42 (s, 1H), 7.40 – 7.32 (m, 1H), 7.01 – 6.92 (m, 2H), 3.68 – 3.56 (m, 1H), 2.70 – 2.51 (m, 2H), 1.93 (br s, 1H), 1.83 – 1.63 (m, 4H), 1.61 – 1.50 (m, 1H), 1.50 – 1.23 (m, 4H), 1.12 (s, 3H, **Me** major), 1.10 (s, 3H, **Me** minor).

^{13}C NMR (101 MHz, CDCl_3) δ 164.6, 164.5, 162.1, 162.0, 149.4, 149.1, 139.1, 132.3, 132.2, 131.2, 131.1, 115.9, 115.8, 111.8, 111.6, 111.5, 105.5, 105.2, 105.1, 70.6, 70.5, 42.9, 42.7, 37.0, 35.3, 35.2, 34.6, 32.3, 31.0, 30.9, 26.3, 26.2, 20.9, 19.8, 18.54, 18.51

^{19}F NMR (377 MHz, CDCl_3) δ -106.25 (d, $J = 8.5$ Hz), -106.33, -114.43 (d, $J = 8.5$ Hz), -114.81 (d, $J = 8.6$ Hz)

HRMS (ESI+) m/z found 319.1626 $[\text{M}+\text{H}]^+$, $\text{C}_{18}\text{H}_{20}\text{F}_2\text{N}_2\text{O}$ calculated 319.1622 ($\Delta = 1.25$ ppm).

(5aS*,7S*,9aS*)-1-(5-chloro-2-fluorophenyl)-9a-methyl-4,5,5a,6,7,8,9,9a-octahydro-1H-benzo[g]indazol-7-ol



3.13, isolated as a yellow solid (15.0 mg, 0.045 mmol, 29% yield)

R_f = 0.24 (1:1 ethyl acetate/ *n*-heptane)

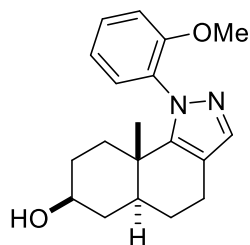
$^1\text{H NMR}$ (400 MHz, CDCl_3) δ 7.47 – 7.35 (m, 3H), 7.16 (t, J = 8.8 Hz, 1H), 3.61 (tt, J = 10.2, 4.9 Hz, 1H), 2.70 – 2.53 (m, 2H), 1.94 – 1.62 (m, 5H), 1.60 – 1.51 (m, 1H), 1.49 – 1.23 (m, 4H), 1.15 (s, 3H, **Me** major), 1.11 (s, 3H, **Me** minor).

$^{13}\text{C NMR}$ (101 MHz, CDCl_3) δ 149.4, 149.1, 139.4, 131.4, 131.3, 130.5, 129.1, 117.9, 117.7, 115.9, 70.5, 42.9, 42.7, 37.0, 35.2, 34.5, 32.4, 30.9, 26.2, 20.9, 19.9, 18.5

$^{19}\text{F NMR}$ (377 MHz, CDCl_3) δ -121.5, -122.1

HRMS (ESI+) m/z found 335.1322 $[\text{M}+\text{H}]^+$, $\text{C}_{18}\text{H}_{20}\text{ClFN}_2\text{O}$ calculated 335.1326 (Δ = - 1.19 ppm)

(5aS*,7S*,9aS*)-1-(2-methoxyphenyl)-9a-methyl-4,5,5a,6,7,8,9,9a-octahydro-1H-benzo[g]indazol-7-ol



3.14, isolated as a yellow solid (10.4 mg, 0.033 mmol, 21% yield)

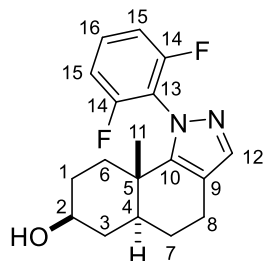
R_f = 0.10 (1:1 ethyl acetate/ *n*-heptane)

$^1\text{H NMR}$ (400 MHz, CDCl_3) δ 7.47 – 7.39 (m, 2H), 7.34 – 7.23 (m, 1H), 7.05 – 6.96 (m, 2H), 3.79 (s, 3H, **OMe** major), 3.77 (s, 3H, **OMe** minor), 3.59 (tt, J = 10.2, 4.9 Hz, 1H), 2.70 – 2.57 (m, 2H), 1.80 – 1.59 (m, 4H), 1.59 – 1.49 (m, 1H), 1.46 – 1.20 (m, 5H), 1.12 (s, 3H, **Me** major), 1.04 (s, 3H, **Me** minor)

$^{13}\text{C NMR}$ (101 MHz, CDCl_3) δ 156.3, 155.9, 149.1, 148.8, 137.8, 137.7, 131.11, 131.05, 131.00, 129.9, 120.43, 120.35, 115.2, 115.0, 112.12, 112.06, 70.7, 70.6, 55.9, 55.7, 42.9, 42.6, 37.1, 35.4, 35.2, 34.5, 31.6, 31.1, 31.0, 26.4, 26.3, 21.00, 20.97, 19.6, 18.2

HRMS (ESI+) m/z found 313.1916 $[\text{M}+\text{H}]^+$, $\text{C}_{19}\text{H}_{24}\text{N}_2\text{O}_2$ calculated 313.1916.

(5aS*,7S*,9aS*)-1-(2,6-difluorophenyl)-9a-methyl-4,5,5a,6,7,8,9,9a-octahydro-1H-benzo[g]indazol-7-ol



3.15, isolated as a yellow solid (8.2 mg, 0.026 mmol, 17% yield)

R_f = 0.18 (1:1 ethyl acetate/ *n*-heptane)

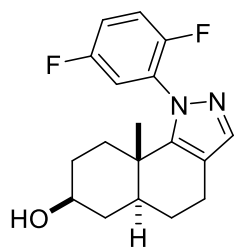
$^1\text{H NMR}$ (400 MHz, CDCl_3) δ 7.48 (s, 1H, **H-12**), 7.47 – 7.40 (m, 1H, **H-16**), 7.09 – 6.99 (m, 2H, **H-15**), 3.63 (tt, J = 10.6, 4.9 Hz, 1H, **H-2**), 2.70 – 2.54 (m, 2H, **H-8**), 1.86 – 1.65 (m, 5H, **H-1**, **H-3**, **H-4**, **H-7**, O-H), 1.60 – 1.24 (m, 5H, **H-1**, **H-3**, **H-6**, **H-7**), 1.09 (s, 3H, **H-11**)

$^{13}\text{C NMR}$ (101 MHz, CDCl_3) δ 159.8 (dd, J = 254.3, 3.3 Hz, **C-14**), 159.5 (dd, J = 254.3, 3.3 Hz, **C-14**), 149.59 (**C-10**), 140.06 (**C-12**), 131.30 (t, J = 9.9 Hz, **C-16**), 119.93 (**C-13**), 115.96 (**C-9**), 112.20 (ddd, J = 20.1, 13.7, 3.6 Hz, **C-15**), 70.58 (**C-2**), 42.65 (**C-4**), 37.01 (**C-3**), 35.09 (**C-5**), 32.31 (**C-6**), 30.92 (**C-1**), 26.26 (**C-7**), 20.95 (**C-8**), 18.42 (d, J = 3.1 Hz, **C-11**)

¹⁹F NMR (377 MHz, CDCl₃) δ -116.80 (dd, *J* = 45.0, 2.7 Hz)

HRMS (ESI+) *m/z* found 319.1618 [M+H]⁺, C₁₈H₂₀F₂N₂O calculated 319.1622 (Δ = - 1.25 ppm).

(5a*S,7*S**,9a*S**)-1-(2,5-difluorophenyl)-9a-methyl-4,5,5a,6,7,8,9,9a-octahydro-1H-benzo[*g*]indazol-7-ol**



3.16, isolated as a yellow solid (28 mg, 0.088 mmol, 57% yield)

*R*_f = 0.20 (1:1 ethyl acetate/ *n*-heptane)

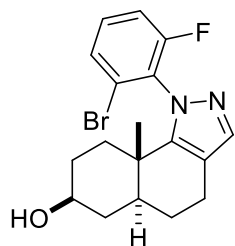
¹H NMR (400 MHz, CDCl₃) δ 7.43 (s, 1H), 7.21 – 7.15 (m, 2H), 7.15 – 7.10 (m, 1H), 3.61 (tt, *J* = 10.2, 4.9 Hz, 1H), 2.70 – 2.53 (m, 2H), 1.92 – 1.61 (m, 6H), 1.60 – 1.51 (m, 1H), 1.49 – 1.24 (m, 4H), 1.15 (s, 3H, **Me** major), 1.11 (s, 3H, **Me** minor)

¹³C NMR (101 MHz, CDCl₃) δ 148.9, 139.3, 130.6, 118.2, 117.6, 117.5, 117.3, 117.3, 115.9, 70.5, 42.8, 42.6, 37.0, 35.2, 34.6, 32.3, 30.9, 26.2, 20.9, 19.8, 18.5

¹⁹F NMR (377 MHz, CDCl₃) δ -116.91 (d, *J* = 16.0 Hz), -117.05 (d, *J* = 16.3 Hz), -124.77 (d, *J* = 16.2 Hz), -125.41 (d, *J* = 16.3 Hz)

HRMS (ESI+) *m/z* found 319.1623 [M+H]⁺, C₁₈H₂₀F₂N₂O calculated 319.1622 (Δ = 0.31 ppm).

(5a*S,7*S**,9a*S**)-1-(2-bromo-6-fluorophenyl)-9a-methyl-4,5,5a,6,7,8,9,9a-octahydro-1H-benzo[*g*]indazol-7-ol**



3.17, isolated as a yellow solid (12.7 mg, 0.034 mmol, 22% yield)

*R*_f = 0.14 (1:1 ethyl acetate/ *n*-heptane)

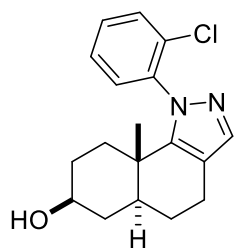
¹H NMR (400 MHz, CDCl₃) δ 7.53 – 7.44 (m, 2H), 7.39 – 7.29 (m, 1H), 7.25 – 7.11 (m, 1H), 3.63 (dt, *J* = 11.0, 5.7 Hz, 1H), 2.70 – 2.55 (m, 2H), 1.84 – 1.23 (m, 10H), 1.15 (s, 3H, **Me** minor), 1.11 (s, 3H, **Me** major)

¹³C NMR (101 MHz, CDCl₃) δ 159.9 (d, *J* = 252.5 Hz), 159.5 (d, *J* = 252.5 Hz), 149.0, 148.9, 139.91, 139.88, 131.8, 131.74, 131.65, 129.04, 129.00, 128.93, 128.90, 126.1, 125.3, 116.1, 116.0, 115.9, 115.9, 115.7, 115.5, 70.6, 42.7, 37.1, 35.3, 35.1, 32.2, 32.1, 31.0, 26.29, 26.27, 21.0, 20.9, 19.5, 18.7 (d, *J* = 3.9 Hz)

¹⁹F NMR (377 MHz, CDCl₃) δ -113.2, -113.6

HRMS (ESI+) *m/z* found 379.0823 [M+H]⁺, C₁₈H₂₀BrFN₂O calculated 379.0821 (Δ = 0.53 ppm).

(5a*S,7*S**,9a*S**)-1-(2-chlorophenyl)-9a-methyl-4,5,5a,6,7,8,9,9a-octahydro-1H-benzo[*g*]indazol-7-ol**



3.18, isolated as a light-yellow solid (28.6 mg, 0.090 mmol, 58% yield)

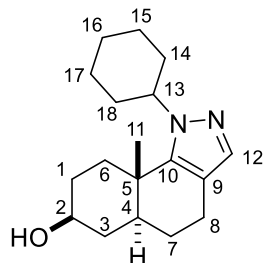
*R*_f = 0.16 (1:1 ethyl acetate/*n*-heptane)

¹H NMR (400 MHz, CDCl₃) δ 7.53 – 7.49 (m, 1H), 7.46 – 7.40 (m, 3H), 7.39 – 7.31 (m, 1H), 3.60 (t, *J* = 5.1 Hz, 1H), 2.70 – 2.56 (m, 2H), 1.81 – 1.16 (m, 10H), 1.15 (s, 3H, **Me** major), 1.10 (s, 3H, **Me** minor)

¹³C NMR (101 MHz, CDCl₃) δ 148.8, 148.5, 139.8, 139.6, 138.7, 138.6, 134.2, 133.9, 131.7, 130.9, 130.8, 130.5, 130.4, 130.2, 127.3, 127.0, 115.6, 115.4, 70.6, 70.5, 42.9, 42.7, 37.12, 37.06, 35.4, 35.1, 35.0, 31.7, 31.0, 30.9, 26.3, 21.0, 20.9, 20.0, 19.0

HRMS (ESI+) m/z found 317.1418 [M+H]⁺, C₁₈H₂₁ClN₂O calculated 317.1420 (Δ = - 0.63 ppm).

(5aS*,7S*,9aS*)-1-cyclohexyl-9a-methyl-4,5,5a,6,7,8,9,9a-octahydro-1H-benzo[g]indazol-7-ol



3.19, isolated as a white solid (17.0 mg, 0.059 mmol, 38% yield)

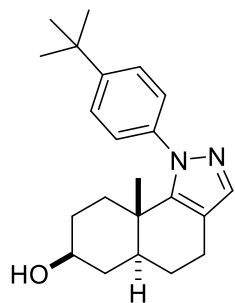
R_f = 0.22 (1:1 ethyl acetate/*n*-heptane)

¹H NMR (400 MHz, CDCl₃) δ 7.26 (s, 1H, **H-12**), 4.13 – 4.02 (m, 1H, **H-13**), 3.72 (tt, *J* = 10.4, 5.0 Hz, 1H, **H-2**), 2.59 – 2.40 (m, 2H, **H-8**), 2.32 – 2.22 (m, 1H, **H-6**), 2.17 – 2.03 (m, 1H, **H-14/18**), 2.02 – 1.24 (m, 17H, **H-1**, **H-3**, **H-4**, **H-6**, **H-7**, **H-14**, **H-15**, **H-16**, **H-17**, **H-18**), 1.19 (s, 3H, **H-11**)

¹³C NMR (101 MHz, CDCl₃) δ 145.4 (**C10**), 136.5 (**C12**), 114.5 (**C9**), 70.6 (**C2**), 59.9 (**C13**), 44.0 (**C4**), 37.2 (**C3**), 35.4 (**C5**), 34.5 (**C6**), 33.9 (**C14/18**), 33.3 (**C14/18**), 31.3 (**C1**), 26.8 (**C7**), 26.3 (**C15/17**), 26.1 (**C15/17**), 25.4 (**C16**), 21.7 (**C8**), 18.1 (**C11**)

HRMS (ESI+) m/z found 289.2272 [M+H]⁺, C₁₈H₂₈N₂O calculated 289.2280 (Δ = - 2.77 ppm).

(5aS*,7S*,9aS*)-1-(4-(tert-butyl)phenyl)-9a-methyl-4,5,5a,6,7,8,9,9a-octahydro-1H-benzo[g]indazol-7-ol



3.20a, purified by flash chromatography on silica gel (3:7 ethyl acetate/*n*-heptane), isolated as a yellow solid (6.8 mg, 0.020 mmol, 13% yield)

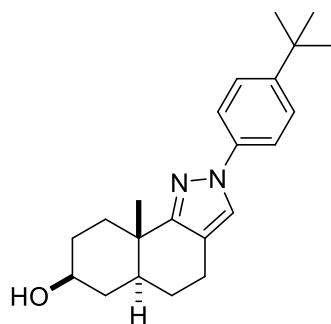
R_f = 0.22 (3:7 ethyl acetate/*n*-heptane)

¹H NMR (400 MHz, CDCl₃) δ 7.46 – 7.39 (m, 2H), 7.35 (s, 1H), 7.30 – 7.22 (m, 2H), 3.58 (tt, *J* = 10.7, 4.8 Hz, 1H), 2.71 – 2.52 (m, 2H), 1.81 – 1.49 (m, 6H), 1.48 – 1.24 (m, 13H), 1.24 – 1.15 (m, 3H)

¹³C NMR (101 MHz, CDCl₃) δ 152.2, 148.3, 139.7, 137.8, 127.6, 125.8, 115.3, 70.7, 43.1, 37.2, 35.3, 34.9, 34.0, 31.5, 31.1, 26.3, 21.0, 19.9

HRMS (ESI+) m/z found 339.2437 [M+H]⁺, C₂₂H₃₀N₂O calculated 339.2436 (Δ = 0.29 ppm).

(5aS*,7S*,9aS*)-2-(4-(tert-butyl)phenyl)-9a-methyl-4,5,5a,6,7,8,9,9a-octahydro-2H-benzo[g]indazol-7-ol



3.20I, purified by flash chromatography on silica gel (3:7 ethyl acetate/*n*-heptane), isolated as a yellow solid (11.3 mg, 0.033 mmol, 22% yield)

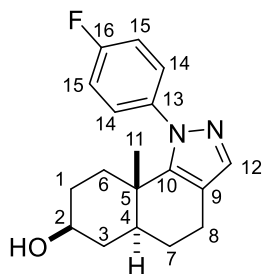
R_f = 0.28 (1:1 ethyl acetate/*n*-heptane)

¹H NMR (400 MHz, CDCl₃) δ 7.54 – 7.49 (m, 3H), 7.42 – 7.38 (m, 2H), 3.71 (tt, *J* = 10.4, 4.9 Hz, 1H), 2.75 – 2.56 (m, 2H), 2.44 – 2.33 (m, 1H), 2.03 – 1.89 (m, 1H), 1.84 – 1.42 (m, 8H), 1.32 (s, 9H), 1.20 (s, 3H)

¹³C NMR (101 MHz, CDCl₃) δ 160.3, 148.8, 138.4, 126.2, 123.8, 118.9, 116.0, 77.5, 77.2, 76.8, 71.4, 41.9, 37.3, 34.67, 34.65, 34.6, 31.49, 31.46, 25.9, 20.5, 20.4

HRMS (ESI+) m/z found 339.2443 [M+H]⁺, C₂₂H₃₀N₂O calculated 339.2436 (Δ = 2.06 ppm).

(5a*S,7*S**,9a*S**)-1-(4-fluorophenyl)-9a-methyl-4,5,5a,6,7,8,9,9a-octahydro-1H-benzo[*g*]indazol-7-ol**



3.21a, isolated as a yellow solid (10.3 mg, 0.034 mmol, 22% yield)

R_f = 0.14 (1:1 ethyl acetate/*n*-heptane)

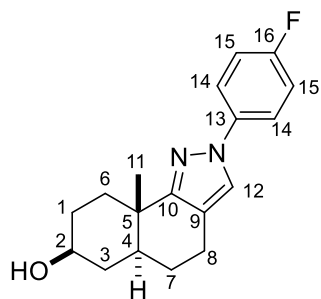
¹H NMR (400 MHz, CDCl₃) δ 7.37 – 7.30 (m, 3H, **H-12**, **H-14**), 7.15 – 7.09 (m, 2H, **H-15**), 3.57 (tt, *J* = 10.4, 4.8 Hz, 1H, **H-2**), 2.68 – 2.52 (m, 2H, **H-8**), 1.97 (br s, 1H, O-H), 1.80 – 1.58 (m, 4H, **H-1**, **H-3**, **H-4**, **H-7**), 1.56 – 1.50 (m, 1H, **H-7**), 1.45 – 1.19 (m, 4H, **H-1**, **H-3**, **H-6**), 1.17 (s, 3H, **H-11**)

¹³C NMR (101 MHz, CDCl₃) δ 162.73 (d, *J* = 249.1 Hz, **C-16**), 148.58 (**C-10**), 138.40 (d, *J* = 3.3 Hz, **C-13**), 138.15 (**C-12**), 129.98 (d, *J* = 8.8 Hz, **C-14**), 115.90 (d, *J* = 22.9 Hz, **C-15**), 115.60 (**C-9**), 70.51 (**C-2**), 42.99 (**C-4**), 37.10 (**C-3**), 35.26 (**C-5**), 34.21 (**C-6**), 30.95 (**C-1**), 26.26 (**C-7**), 20.89 (**C-8**), 19.99 (**C-11**)

¹⁹F NMR (377 MHz, CDCl₃) δ -111.75

HRMS (ESI+) m/z found 301.1718 [M+H]⁺, C₁₈H₂₁FN₂O calculated 301.1716 (Δ = 0.66 ppm).

(5a*S,7*S**,9a*S**)-2-(4-fluorophenyl)-9a-methyl-4,5,5a,6,7,8,9,9a-octahydro-2H-benzo[*g*]indazol-7-ol**



3.21I, isolated as a yellow solid (7.4 mg, 0.025 mmol, 16% yield)

R_f = 0.22 (1:1 ethyl acetate/*n*-heptane)

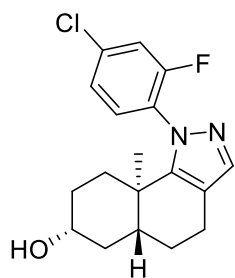
¹H NMR (400 MHz, CDCl₃) δ 7.59 – 7.53 (m, 2H, **H-14**), 7.48 (s, 1H, **H-12**), 7.13 – 7.04 (m, 2H, **H-15**), 3.71 (dt, *J* = 9.7, 4.9 Hz, 1H, **H-2**), 2.76 – 2.57 (m, 2H, **H-8**), 2.41 – 2.30 (m, 1H, **H-6**), 2.02 – 1.89 (m, 1H, **H-1**), 1.85 – 1.42 (m, 7H, **H-1**, **H-3**, **H-4**, **H-6**, **H-7**), 1.20 (s, 3H, **H-11**)

¹³C NMR (101 MHz, CDCl₃) δ 160.8 (d, *J* = 244.6 Hz, **C-16**), 160.7 (**C-10**), 137.1 (d, *J* = 2.9 Hz, **C-13**), 124.0 (**C-12**), 120.7 (d, *J* = 8.2 Hz, **C-14**), 116.5 (**C-9**), 116.1 (d, *J* = 22.8 Hz, **C-15**), 71.3 (**C-2**), 41.9 (**C-4**), 37.2 (**C-3**), 34.7 (**C-6**, **C-5**), 31.4 (**C-1**), 25.8 (**C-7**), 20.42 (**C-8**), 20.35 (**C-11**)

¹⁹F NMR (377 MHz, CDCl₃) δ -117.34

HRMS (ESI+) m/z found 301.1713 [M+H]⁺, C₁₈H₂₁FN₂O calculated 301.1716 (Δ = - 1.00 ppm).

(5a*R*,7*R*,9a*R*)-1-(4-chloro-2-fluorophenyl)-9a-methyl-4,5,5a,6,7,8,9,9a-octahydro-1*H*-benzo[*g*]indazol-7-ol



(-)-3.11, (Astercin-2), isolated as a yellow solid (63 mg, 0.188 mmol, 64% yield),

R_f = 0.16 (2:3 ethyl acetate/*n*-heptane);

^1H NMR (400 MHz, CDCl_3) δ 7.44 (s, 1H), 7.39 – 7.27 (m, 1H), 7.28 – 7.21 (m, 2H), 3.67 – 3.55 (m, 1H), 2.69 – 2.54 (m, 2H), 1.82 – 1.64 (m, 4H), 1.60 – 1.51 (m, 1H), 1.48 – 1.24 (m, 4H), 1.13 (s, 3H, **Me** major), 1.10 (s, 3H, **Me** minor).

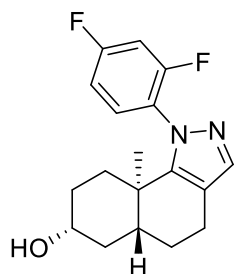
^{13}C NMR (101 MHz, CDCl_3) δ 159.9, 157.3, 149.7, 149.3, 139.0, 136.7, 136.6, 132.0, 131.0, 128.8, 128.7, 125.0, 124.9, 117.8, 117.7, 117.5, 117.5, 116.0, 116.0, 70.5, 70.5, 42.8, 42.6, 37.0, 35.3, 35.2, 34.5, 32.3, 31.0, 30.8, 26.2, 26.1, 20.9, 19.8, 18.5.

^{19}F NMR (377 MHz, CDCl_3) δ -116.3, -116.7.

HRMS (ESI+) m/z found 335.1325 $[\text{M}+\text{H}]^+$, $\text{C}_{18}\text{H}_{20}\text{ClFN}_2\text{O}$ calculated 335.1326 (Δ = - 0.30 ppm).

$[\alpha]_D^{23}$ = - 58.9 (c = 1.13, CHCl_3)

(5a*R*,7*R*,9a*R*)-1-(2,4-difluorophenyl)-9a-methyl-4,5,5a,6,7,8,9,9a-octahydro-1*H*-benzo[*g*]indazol-7-ol



(-)-3.12, isolated as a yellow solid (48 mg, 0.151 mmol, 65% yield),

R_f = 0.18 (1:1 ethyl acetate/*n*-heptane);

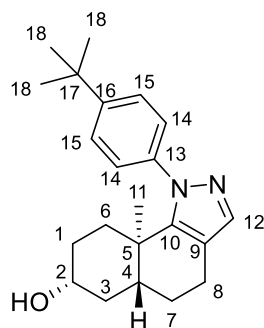
^1H NMR (400 MHz, CDCl_3) δ 7.43 (s, 1H), 7.42 – 7.33 (m, 1H), 7.00 – 6.93 (m, 2H), 3.67 – 3.56 (m, 1H), 2.69 – 2.53 (m, 2H), 1.82 – 1.63 (m, 4H), 1.61 – 1.51 (m, 1H), 1.49 – 1.22 (m, 4H), 1.13 (s, 3H, **Me** major), 1.10 (s, 3H, **Me** minor).

^{13}C NMR (101 MHz, CDCl_3) δ 164.7, 164.5, 162.1, 162.0, 149.7, 149.3, 138.9, 132.3, 132.2, 131.2, 131.1, 116.0, 115.9, 111.9, 111.7, 111.7, 111.5, 105.5, 105.4, 105.3, 105.1, 105.0, 70.5, 70.5, 42.9, 42.6, 37.0, 35.3, 35.2, 34.5, 32.2, 31.0, 30.9, 26.3, 26.2, 20.9, 19.8, 18.5.

^{19}F NMR (377 MHz, CDCl_3) δ -106.06 (d, J = 8.5 Hz), -106.12 (d, J = 8.4 Hz), -114.37 (d, J = 8.5 Hz), -114.74 (d, J = 8.5 Hz).

HRMS (ESI+) m/z found 319.1619 $[\text{M}+\text{H}]^+$, $\text{C}_{18}\text{H}_{20}\text{F}_2\text{N}_2\text{O}$ calculated 319.1622 (Δ = - 0.94 ppm).

(5a*R*,7*R*,9a*R*)-1-(4-(*tert*-butyl)phenyl)-9a-methyl-4,5,5a,6,7,8,9,9a-octahydro-1*H*-benzo[*g*]indazol-7-ol



(-)-3.20a, isolated as a yellow solid (12 mg, 0.0355 mmol, 23% yield),

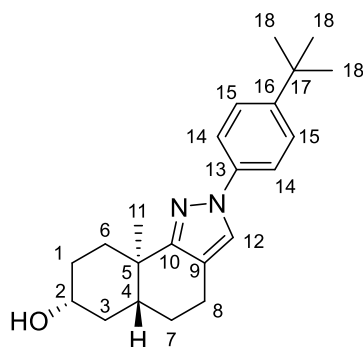
$R_f = 0.10$ (3:7 ethyl acetate/*n*-heptane);

$^1\text{H NMR}$ (400 MHz, CDCl_3) δ 7.45 – 7.40 (m, 2H, **H-14**), 7.35 (s, 1H, **H-12**), 7.28 – 7.23 (m, 2H, **H-15**), 3.56 (tt, $J = 10.6, 4.9$ Hz, 1H, **H-2**), 2.72 – 2.53 (m, 2H, **H-8**), 1.80 – 1.59 (m, 4H, **H-1**, **H-3**, **H-4**, **H-7**), 1.58 – 1.47 (m, 1H, **H-7**), 1.45 – 1.22 (m, 13H, **H-1**, **H-3**, **H-6**, **H-18**), 1.20 (s, 3H, **H-11**).

$^{13}\text{C NMR}$ (101 MHz, CDCl_3) δ 152.3 (**C-16**), 148.4 (**C-10**), 139.5 (**C-13**), 137.6 (**C-12**), 127.5 (**C-15**), 125.8 (**C-14**), 115.3 (**C-9**), 70.6 (**C-2**), 43.0 (**C-4**), 37.2 (**C-3**), 35.3 (**C-5**), 34.9 (**C-17**), 34.0 (**C-6**), 31.5 (**C-18**), 31.0 (**C-1**), 26.3 (**C-7**), 20.9 (**C-8**), 19.9 (**C-11**).

HRMS (ESI+) m/z found 339.2433 $[\text{M}+\text{H}]^+$, $\text{C}_{22}\text{H}_{30}\text{N}_2\text{O}$ calculated 339.2436 ($\Delta = -0.88$ ppm).

(5a*R*,7*R*,9a*R*)-2-(4-(*tert*-butyl)phenyl)-9a-methyl-4,5,5a,6,7,8,9,9a-octahydro-2*H*-benzo[*g*]indazol-7-ol



(-)-3.20I, isolated as a yellow solid (25 mg, 0.0739 mmol, 48% yield),

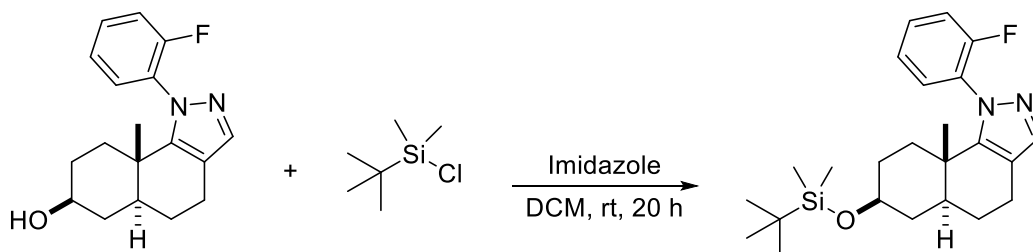
$R_f = 0.16$ (3:7 ethyl acetate/*n*-heptane);

$^1\text{H NMR}$ (400 MHz, CDCl_3) δ 7.54 – 7.49 (m, 3H, **H-12**, **H-14**), 7.43 – 7.39 (m, 2H, **H-15**), 3.71 (tt, $J = 10.6, 5.1$ Hz, 1H, **H-2**), 2.77 – 2.56 (m, 2H, **H-8**), 2.46 – 2.37 (m, 1H, **H-6**), 2.00 – 1.91 (m, 1H, **H-1**), 1.84 – 1.42 (m, 7H, **H-1**, **H-3**, **H-4**, **H-6**, **H-7**), 1.32 (s, 9H, **H-18**), 1.21 (s, 3H, **H-11**).

$^{13}\text{C NMR}$ (101 MHz, CDCl_3) δ 160.2 (**C-10**), 149.0 (**C-16**), 138.2 (**C-13**), 126.3 (**C-15**), 124.0 (**C-12**), 119.0 (**C-14**), 116.0 (**C-9**), 71.4 (**C-2**), 41.9 (**C-4**), 37.3 (**C-3**), 34.68 (**C-5/C-6/C-17**), 34.65 (**C-5/C-6/C-17**), 34.60 (**C-5/C-6/C-17**), 31.49 (**C-18**), 31.45 (**C-1**), 25.9 (**C-7**), 20.5 (**C-8**), 20.3 (**C-11**).

HRMS (ESI+) m/z found 339.2437 $[\text{M}+\text{H}]^+$, $\text{C}_{22}\text{H}_{30}\text{N}_2\text{O}$ calculated 339.2436 ($\Delta = 0.29$ ppm).

(5a*S,7*S**,9a*S**)-7-((*tert*-butyldimethylsilyl)oxy)-1-(2-fluorophenyl)-9a-methyl-4,5,5a,6,7,8,9,9a-octahydro-1*H*-benzo[*g*]indazole, 3.38**



(\pm)-Astercin 1 (105.6 mg, 0.352 mmol), *tert*-butyldimethylsilyl chloride (63.6 mg, 0.422 mmol), and imidazole (47.9 mg, 0.703 mmol) were suspended in dry DCM (5 mL) and stirred at room

temperature for 20 hours. The reaction was diluted with water and the two phases separated. The organic phase was dried over anhydrous magnesium sulfate and concentrated to a crude yellow oil. Purification by flash chromatography on silica gel (1:4 ethyl acetate/*n*-heptane) afforded the product as a yellow solid (116 mg, 0.280 mmol, 80% yield).

R_f = 0.32 (1:4 ethyl acetate/*n*-heptane) – UV and KMnO_4 staining

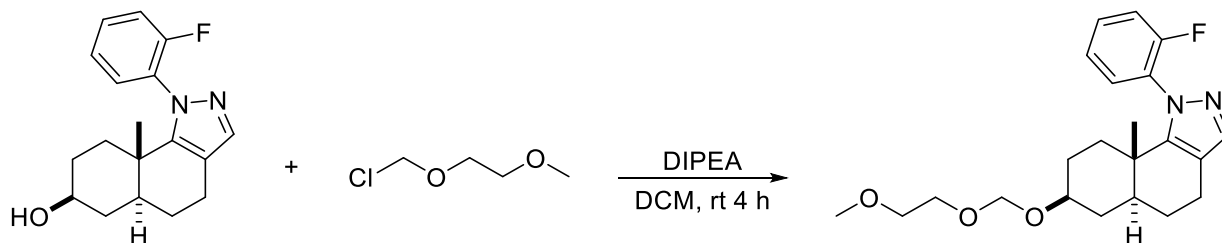
^1H NMR (400 MHz, CDCl_3) δ 7.49 – 7.43 (m, 1H), 7.42 (s, 1H), 7.42 – 7.35 (m, 1H), 7.25 – 7.17 (m, 2H), 3.57 (tt, J = 11.2, 5.4 Hz, 1H), 2.69 – 2.55 (m, 2H), 1.76 – 1.22 (m, 9H), 1.14 (s, 3H, **Me** major), 1.10 (s, 3H, **Me** minor), 0.86 (s, 9H), 0.03 (s, 3H), 0.02 (s, 3H).

^{13}C NMR (101 MHz, CDCl_3) δ 157.6, 157.4, 149.6, 149.2, 138.9, 131.34, 131.26, 130.4, 124.31, 124.27, 116.8, 116.6, 115.6, 115.5, 71.5, 71.4, 43.1, 42.8, 37.7, 35.2, 34.7, 32.4, 32.0, 31.6, 31.5, 29.2, 26.4, 26.0, 22.8, 21.0, 19.8, 18.3, 14.3, -4.5.

^{19}F NMR (377 MHz, CDCl_3) δ -119.22, -119.83.

HRMS (ESI+) m/z found 415.2579 $[\text{M}+\text{H}]^+$, $\text{C}_{24}\text{H}_{35}\text{FN}_2\text{OSi}$ calculated 415.2581 (Δ = - 0.48 ppm).

(5a*S,7*S**,9a*S**)-1-(2-fluorophenyl)-7-((2-methoxyethoxy)methoxy)-9a-methyl-4,5,5a,6,7,8,9,9a-octahydro-1H-benzo[*g*]indazole, 3.26**



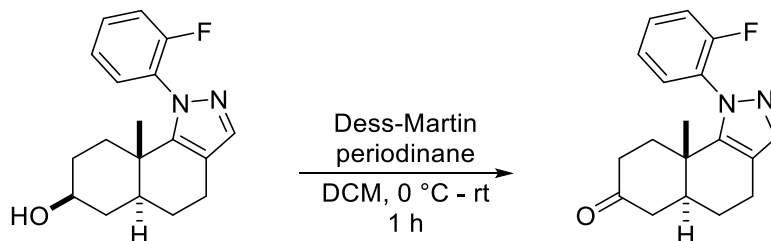
(\pm)-Astercin 1 (40 mg, 0.133 mmol) was dissolved in dry DCM (2 mL) before addition of DIPEA (70 μL , 0.399 mmol) and 2-methoxyethoxymethyl chloride (30 μL , 0.266 mmol) and the resulting yellow solution stirred at room temperature for 4 hours. The reaction was quenched via addition of saturated aqueous ammonium chloride and extracted twice with DCM. The combined organic phases were dried over anhydrous magnesium sulfate and concentrated to a crude residue. Purification by flash chromatography on silica gel (2:3 ethyl acetate/*n*-heptane) to yield the product as a pale yellow oil (32.6 mg, 0.084 mmol, 63% yield).

^1H NMR (400 MHz, CDCl_3) δ 7.49 – 7.42 (m, 2H), 7.42 – 7.35 (m, 1H), 7.25 – 7.15 (m, 2H), 4.74 (q, J = 7.0 Hz, 2H), 3.73 – 3.63 (m, 2H), 3.59 – 3.50 (m, 3H), 3.38 (s, 3H), 2.69 – 2.54 (m, 2H), 1.89 – 1.82 (m, 1H), 1.79 – 1.62 (m, 3H), 1.58 – 1.23 (m, 5H), 1.14 (s, 3H, **Me** major), 1.10 (s, 3H, **Me** minor).

^{13}C NMR (101 MHz, CDCl_3) δ 159.92, 157.6, 149.3, 148.9, 139.0, 131.41, 131.36, 131.3, 130.3, 124.3, 116.8, 116.6, 115.62, 115.55, 93.8, 75.7, 75.6, 71.9, 66.9, 59.2, 42.9, 42.7, 35.4, 35.3, 34.5, 34.3, 32.3, 28.4, 28.3, 26.42, 26.37, 20.9, 19.7, 18.4.

HRMS (ESI+) m/z found 389.2241 $[\text{M}+\text{H}]^+$, $\text{C}_{22}\text{H}_{29}\text{FN}_2\text{O}_3$ calculated 389.2240 (Δ = - 0.26 ppm).

(5aS*,9aS*)-1-(2-fluorophenyl)-9a-methyl-1,4,5,5a,6,8,9,9a-octahydro-7H-benzo[g]indazol-7-one, 3.36



(±)-Astercin 1 (20 mg, 0.666 mmol) was dissolved in DCM (1 mL) and stirred at room temperature until fully dissolved. The solution was cooled in an ice bath before the addition Dess-Martin periodinane (0.3 M in DCM, 0.332 mL, 0.999 mmol). The reaction was returned to room temperature and stirred for 1 hour. The reaction was neutralised via addition of saturated aqueous NaHCO₃ and extracted with DCM (2x), the combined organic phases dried over anhydrous MgSO₄, and concentrated to yield a crude solid. Purification of the crude material by flash chromatography on silica gel (1:1 ethyl acetate/ *n*-heptane) afforded the product as a colourless oil (14.6 mg, 0.0489 mmol, 73% yield)

R_f = 0.24 (1:1 ethyl acetate/ *n*-heptane) – UV and KMnO₄ staining

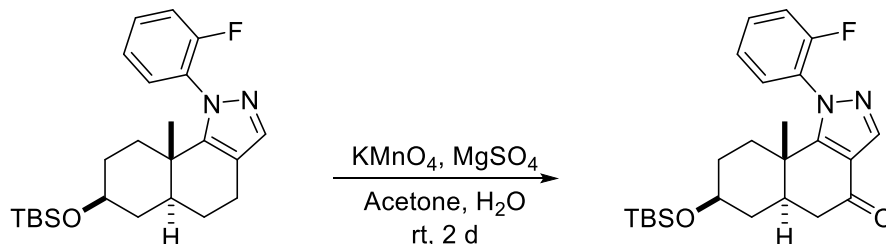
¹H NMR (400 MHz, CDCl₃) δ 7.53 – 7.46 (m, 2H), 7.46 – 7.37 (m, 1H), 7.30 – 7.19 (m, 2H), 2.76 – 2.57 (m, 2H), 2.43 – 2.20 (m, 4H), 2.20 – 2.04 (m, 1H), 1.86 – 1.56 (m, 4H), 1.31 (s, 3H, **Me** major), 1.28 (s, 3H, **Me** minor).

¹³C NMR (101 MHz, CDCl₃) δ 209.5, 138.8, 131.8, 131.7, 131.4, 130.4, 124.6, 124.5, 117.1, 116.9, 116.7, 115.9, 44.4, 44.1, 43.8, 37.7, 37.6, 35.3, 35.2, 33.1, 26.4, 20.8, 18.8.

¹⁹F NMR (377 MHz, CDCl₃) δ - 119.36, - 119.82.

HRMS (ESI+) *m/z* found 299.1558 [M+H]⁺, C₁₈H₁₉FN₂O calculated 299.1558 (Δ = - 0.33 ppm)

(5aR*,7S*,9aS*)-7-((tert-butyldimethylsilyl)oxy)-1-(2-fluorophenyl)-9a-methyl-1,5,5a,6,7,8,9,9a-octahydro-4H-benzo[g]indazol-4-one



TBS-protected Astercin **3.38** (93.8 mg, 0.226 mmol) and magnesium sulfate (56 mg, 0.482 mmol) were suspended in a 1:1 mixture of acetone:H₂O and cooled in an ice-bath to 0 °C before addition of potassium permanganate (114.3 mg, 0.724 mmol) and the resulting purple solution stirred at room temperature for 1 day. After 1 day, an addition 0.5 equiv. of magnesium sulfate and potassium permanganate were added and stirring continued for another day. The reaction was quenched by addition of aqueous sodium disulfite and extracted with DCM (2x). The combined organic phases were dried over anhydrous sodium sulfate and concentrated to a crude oil.

Purification by flash chromatography on silica gel (1:4 ethyl acetate/*n*-heptane) afforded the product as a colourless oil (26 mg, 0.061 mmol, 27% yield).

R_f = 0.12 (1:4 ethyl acetate/ *n*-heptane) – UV

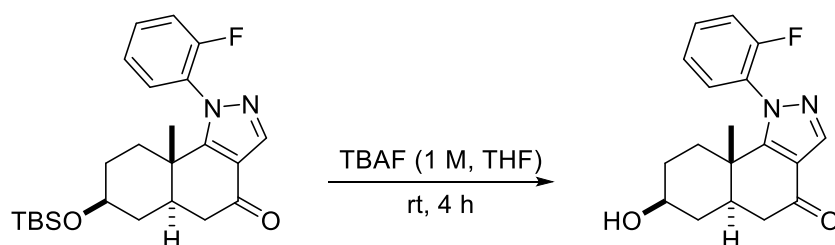
^1H NMR (400 MHz, CDCl_3) δ 8.05 – 8.01 (m, 1H), 7.57 – 7.50 (m, 1H), 7.45 – 7.36 (m, 1H), 7.31 – 7.24 (m, 2H), 3.57 (qt, J = 10.6, 4.9 Hz, 1H), 2.59 – 2.45 (m, 1H), 2.34 – 2.15 (m, 2H), 1.72 – 1.23 (m, 10H), 0.85 (s, 9H), 0.04 – -0.01 (m, 6H).

^{13}C NMR (101 MHz, CDCl_3) δ 192.9, 192.7, 159.61, 159.56, 159.2, 157.0, 156.7, 138.93, 138.91, 132.32, 132.25, 132.2, 132.1, 130.6, 129.6, 128.8, 128.7, 128.6, 128.5, 124.81, 124.78, 124.73, 124.69, 119.4, 119.3, 117.2, 117.0, 116.8, 70.5, 70.4, 43.3, 42.9, 42.1, 36.9, 36.1, 35.9, 33.6, 32.0, 31.4, 31.3, 31.2, 26.0, 22.8, 18.3, 17.0, 16.9, 14.3, -4.52, -4.53.

^{19}F NMR (377 MHz, CDCl_3) δ -119.72, -119.95.

HRMS (ESI+) m/z found 429.2375 $[\text{M}+\text{H}]^+$, $\text{C}_{24}\text{H}_{33}\text{FN}_2\text{O}_2\text{Si}$ calculated 429.2373 (Δ = 0.47 ppm)

(5aR*,7S*,9aS*)-1-(2-fluorophenyl)-7-hydroxy-9a-methyl-1,5,5a,6,7,8,9,9a-octahydro-4H-benzo[g]indazol-4-one, 3.39



The 7-keto analogue (9.1 mg, 0.0212 mmol) was dissolved in THF (0.75 mL) before addition of TBAF (1 M in THF, 53.1 μL , 0.0531 mmol) and the reaction stirred at room temperature for 4 hours. The reaction was quenched by addition of saturated aqueous ammonium chloride, extracted with chloroform (2 x). The combined organic phases were dried over anhydrous sodium sulfate and concentrated to yield a crude residue. Purification by flash chromatography on silica gel (ethyl acetate) afforded the product as a colourless oil (4.9 mg, 0.0156 mmol, 74% yield).

R_f = 0.18 (ethyl acetate) – UV and KMnO_4 staining

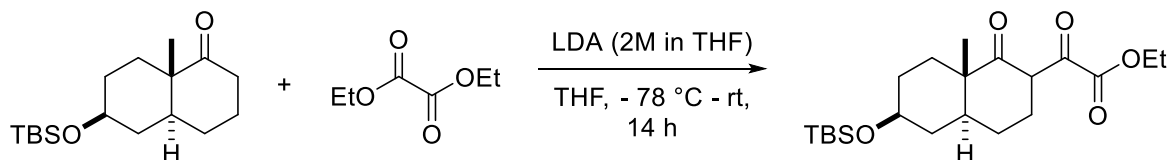
^1H NMR (400 MHz, CDCl_3) δ 8.06 – 8.02 (m, 1H), 7.58 – 7.50 (m, 1H), 7.45 – 7.36 (m, 1H), 7.33 – 7.24 (m, 2H), 3.65 (tq, J = 11.1, 6.1, 5.5 Hz, 1H), 2.61 – 2.46 (m, 1H), 2.39 – 2.17 (m, 2H), 1.87 – 1.68 (m, 2H), 1.64 (s, 1H), 1.58 – 1.43 (m, 2H), 1.43 – 1.23 (m, 7H).

^{13}C NMR (101 MHz, CDCl_3) δ 192.5, 159.4, 159.0, 138.97, 138.95, 132.4, 132.34, 132.28, 132.2, 130.6, 129.6, 124.8, 119.3, 117.2, 117.1, 116.9, 69.8, 69.7, 43.1, 42.7, 42.0, 36.4, 36.3, 36.1, 35.9, 33.4, 31.2, 30.7, 30.5, 18.3.

^{19}F NMR (377 MHz, CDCl_3) δ -119.73, -119.90.

HRMS (ESI+) m/z found 301.1711 $[\text{M}+\text{H}]^+$, $\text{C}_{18}\text{H}_{19}\text{FN}_2\text{O}_2$ calculated 315.1509 (Δ = - 0.32 ppm)

Ethyl 2-((4a*S,6*S**,8a*S**)-6-((*tert*-butyldimethylsilyl)oxy)-8a-methyl-1-oxodecahydronaphthalen-2-yl)-2-oxoacetate, **3.29****



(±)-TBS-ketone **3.08** (0.5 g, 1.69 mmol) was dissolved in dry THF (30 mL) and the resulting solution cooled to $-78\text{ }^{\circ}\text{C}$ in a dry ice bath. A 2M solution of LDA in THF (1.01 mL, 2.02 mmol) was added dropwise to the solution and stirred at the same temperature for 15 minutes. Diethyl oxalate (0.28 mL, 2.02 mmol) was added dropwise to the reaction at $-78\text{ }^{\circ}\text{C}$ before returning to room temperature and allowing to stir for 14 hours. The reaction was partitioned between saturated aqueous NH_4Cl and ethyl acetate, extracting the aqueous phase further with ethyl acetate (2X). Combined organic phases were dried over anhydrous magnesium sulfate and concentrated to yield a crude oil. Purification by flash chromatography on silica gel (1:9 ethyl acetate/*n*-heptane) afforded the product as an orange oil (0.397 g, 1.00 mmol, 59% yield).

Note: Diketoester **3.29** was isolated as a mixture of keto-enol tautomers, with the enol-form predominating in solution. The NMR spectra of diketoester **3.29** appear complex because of this, thus presented NMR data is that corresponding to the major enol tautomer.

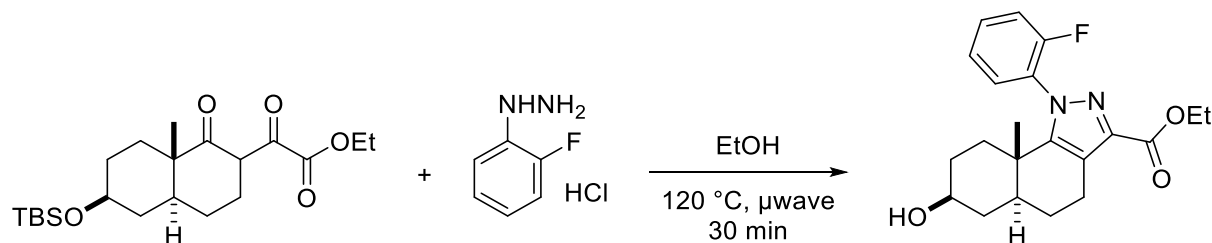
$R_f = 0.34$ (1:9 ethyl acetate/*n*-heptane) – UV and KMnO_4 staining

^1H NMR (400 MHz, CDCl_3) δ 15.57 (s, 1H), 4.33 (q, $J = 7.2\text{ Hz}$, 2H), 3.58 (tt, $J = 10.5, 4.9\text{ Hz}$, 1H), 2.62 – 2.46 (m, 2H), 2.07 (dt, $J = 13.6, 3.5\text{ Hz}$, 1H), 1.88 – 1.74 (m, 1H), 1.68 – 1.41 (m, 7H), 1.39 – 1.33 (m, 4H), 1.14 (s, 3H), 0.88 (s, 9H), 0.06 (s, 6H).

^{13}C NMR (101 MHz, CDCl_3) δ 200.3, 177.3, 163.4, 105.1, 71.3, 62.0, 41.9, 38.8, 37.6, 31.8, 31.2, 26.0, 24.5, 23.0, 18.3, 17.7, 14.2, -4.4, -4.5.

HRMS (ESI+) m/z found 397.2409 $[\text{M}+\text{H}]^+$, $\text{C}_{21}\text{H}_{36}\text{O}_5\text{Si}$ calculated 397.2410 ($\Delta = -0.25\text{ ppm}$).

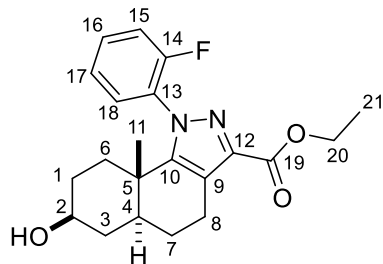
ethyl (5a*S,7*S**,9a*S**)-1-(2-fluorophenyl)-7-hydroxy-9a-methyl-4,5,5a,6,7,8,9,9a-octahydro-1H-benzo[g]indazole-3-carboxylate, **3.27****



Diketoester **3.29** (397 mg, 1.00 mmol) and 2-fluorophenylhydrazine hydrochloride (195 mg, 1.20 mmol) were suspended in absolute ethanol (3 mL) in a 2 – 5 mL Biotage microwave vial. The vial was capped and heated in a microwave reaction at $120\text{ }^{\circ}\text{C}$ for 30 minutes. The reaction mixture was diluted with ethyl acetate and washed with 5% aqueous HCl , and the aqueous phase further extracted with ethyl acetate (2X). The combined organic phases were dried over anhydrous magnesium sulfate and concentrated to a crude residue. Purification by flash chromatography on

silica gel (1:1 – 2:1 ethyl acetate/*n*-heptane) afforded the product as a light yellow solid (276 mg, 0.741 mmol, 74% yield).

Note: NMR assignment of pyrazole **x** has been made for the major conformation only, however, the methyl signal for both conformations has been presented. The signal arising from the H-11 hydrogens in the minor conformation appears as a doublet ($J = 1.3$ Hz) as well as the C-11 carbon ($J = 3.9$ Hz) due a through space coupling to fluorine, suggesting the minor conformation has the fluorine place in close proximity to the axial methyl group. The major conformation likely has the fluorine placed away from the methyl group, with an NOESY correlation seen between H-11 and H-18.



$R_f = 0.12$ (1:1 ethyl acetate/*n*-heptane) – UV and KMnO_4 staining

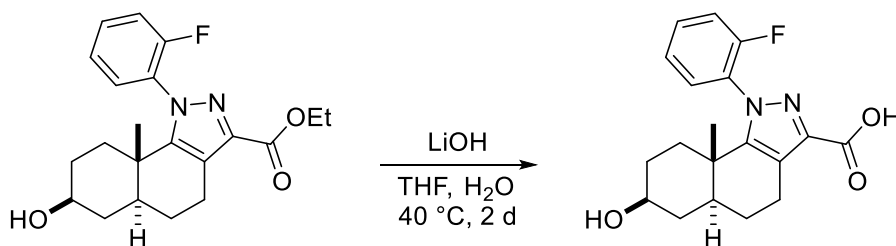
^1H NMR (400 MHz, CDCl_3) δ 7.51 – 7.44 (m, 1H, **H-16**), 7.42 – 7.35 (m, 1H, **H-18**), 7.26 – 7.16 (m, 2H, **H-15**, **H-17**), 4.38 (q, $J = 7.1$ Hz, 2H, **H-20**), 3.67 – 3.55 (m, 1H, **H-2**), 3.06 – 2.95 (m, 1H, **H-8**), 2.81 – 2.68 (m, 1H, **H-8**), 1.83 – 1.56 (m, 6H, O-H, **H-1**, **H-3**, **H-4**, **H-7**), 1.46 – 1.33 (m, 5H, **H-3**, **H-6**, **H-21**), 1.33 – 1.21 (m, 2H, **H-1**, **H-6**), 1.13 (s, 3H, **H-11**, **Me** major conformation), 1.12

(d, $J = 1.3$ Hz, 3H, **H-11**, **Me** minor conformation).

^{13}C NMR (101 MHz, CDCl_3) δ 163.01 (**C-19**), 158.61 (d, $J = 253.3$ Hz, **C-14**), 150.85 (**C-10**), 141.17 (**C-12**), 131.88 (d, $J = 7.9$ Hz, **C-16**), 130.17 (**C-18**), 129.80 (d, $J = 12.9$ Hz, **C-13**), 124.32 (d, $J = 4.1$ Hz, **C-17**), 119.32 (**C-9**), 116.78 (d, $J = 19.4$ Hz, **C-15**), 70.38 (**C-2**), 60.80 (**C-20**), 42.20 (**C-4**), 36.91 (**C-3**), 35.33 (**C-5**), 34.35 (**C-6**), 30.75 (**C-1**), 25.96 (**C-7**), 22.00 (**C-8**), 19.62 (**C-11**, major conformation), 18.36 (d, $J = 3.9$ Hz, **C-11**, minor conformation), 14.60 (**C-21**).

HRMS (ESI+) m/z found 373.1923 $[\text{M}+\text{H}]^+$, $\text{C}_{21}\text{H}_{25}\text{FN}_2\text{O}_3$ calculated 373.1927 ($\Delta = -1.07$ ppm).

(5a*S,7*S**,9a*S**)-1-(2-fluorophenyl)-7-hydroxy-9a-methyl-4,5,5a,6,7,8,9,9a-octahydro-1H-benzo[*g*]indazole-3-carboxylic acid, 3.28**



Pyrazole **x** (20 mg, 0.054 mmol) was dissolved in a 1:1 mixture of THF: H_2O (2 mL) before addition of LiOH (3.2 mg, 0.134 mmol) and the reaction stirred at room temperature for 1 day before a further addition of LiOH (3.2 mg, 0.134 mmol) and increasing the reaction temperature to 40 °C, reaching completion after a further day. The reaction was acidified with dilute aqueous HCl and extracted with ethyl acetate (2x). The combined organic phases were dried over anhydrous sodium sulfate and concentrated to yield to product as a colourless oil, becoming a fluffy white solid upon drying under high vacuum (14.5 mg, 0.042 mmol, 78% yield).

$R_f = 0.10$ (1:1 ethyl acetate/*n*-heptane) – UV and KMnO_4 staining

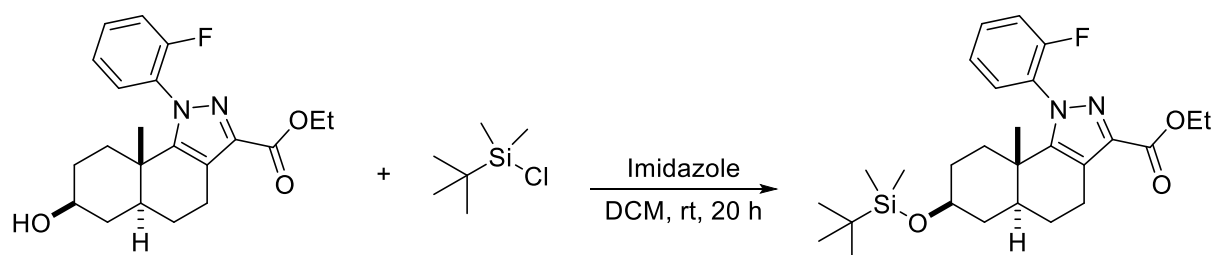
¹H NMR (400 MHz, MeOD) δ 7.67 – 7.59 (m, 1H), 7.52 (qd, J = 7.8, 1.8 Hz, 1H), 7.41 – 7.30 (m, 2H), 3.60 – 3.48 (m, 1H), 3.08 – 2.93 (m, 1H), 2.83 – 2.67 (m, 1H), 1.84 – 1.56 (m, 5H), 1.46 – 1.21 (m, 4H), 1.19 (s, 3H, **Me** major), 1.13 (d, J = 1.3 Hz, 3H, **Me** minor).

¹³C NMR (101 MHz, MeOD) δ 165.5, 152.9, 152.6, 142.3, 133.6, 133.5, 132.4, 131.3, 125.8, 120.2, 117.8, 117.6, 70.84, 70.80, 43.6, 43.5, 37.5, 36.6, 36.5, 35.5, 33.3, 31.4, 31.2, 26.92, 26.89, 23.0, 19.8, 18.7.

¹⁹F NMR (377 MHz, CDCl₃) δ – 119.29, -119.76.

HRMS (ESI+) m/z found 345.1610 [M+H]⁺, C₁₉H₂₁FN₂O₃ calculated 345.1614 (Δ = - 1.16 ppm).

ethyl (5a*S,7*S**,9a*S**)-7-((*tert*-butyldimethylsilyl)oxy)-1-(2-fluorophenyl)-9a-methyl-4,5,5a,6,7,8,9,9a-octahydro-1*H*-benzo[*g*]indazole-3-carboxylate, 3.34**



Ester **3.27** (150 mg, 0.403 mmol), *tert*-butyldimethylsilyl chloride (73 mg, 0.483 mmol), and imidazole (55 mg, 0.306 mmol) were suspended in dry DCM (10 mL) and stirred at room temperature for 24 hours, after which an additional 0.2 equivalents of *tert*-butyldimethylsilyl chloride and imidazole were added, and the reaction stirred for a further 4 hours. The reaction was diluted with water and the phases separated. The organic phase was dried over anhydrous magnesium sulfate and concentrated to a crude oil. Purification by flash chromatography on silica gel (1:4 ethyl acetate/*n*-heptane) afforded the product as a fluffy white solid (71.1 mg, 0.146 mmol, 36% yield).

R_f = 0.16 (1:1 ethyl acetate/*n*-heptane) – UV and KMnO₄

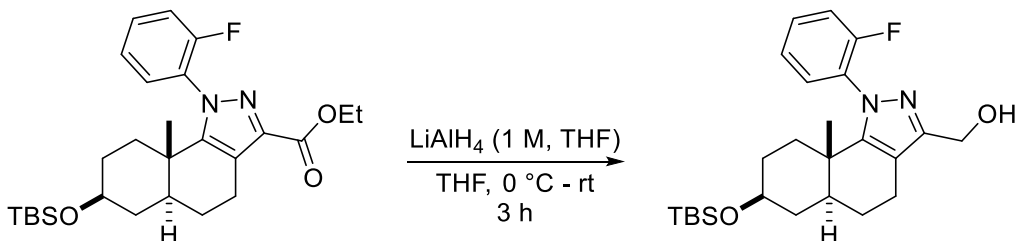
¹H NMR (400 MHz, CDCl₃) δ 7.51 – 7.43 (m, 1H), 7.42 – 7.36 (m, 1H), 7.25 – 7.16 (m, 2H), 4.43 – 4.35 (q, J = 7.1 Hz, 2H), 3.61 – 3.49 (m, 1H), 3.06 – 2.94 (m, 1H), 2.82 – 2.68 (m, 1H), 1.76 – 1.52 (m, 5H), 1.50 – 1.18 (m, 7H), 1.13 (s, 3H, **Me** major), 1.11 (s, 3H, **Me** minor), 0.86 (s, 9H), 0.02 (d, J = 5.3 Hz, 6H).

¹³C NMR (101 MHz, CDCl₃) δ 163.1, 159.9, 151.3, 151.1, 141.2, 131.9, 131.8, 131.3, 130.2, 124.3, 124.3, 124.3, 119.4, 119.3, 116.8, 116.7, 71.3, 71.2, 60.8, 42.7, 42.4, 37.5, 35.5, 35.4, 34.6, 32.1, 31.5, 31.4, 26.0, 25.9, 22.0, 19.7, 18.5, 18.4, 18.3, 14.6, -4.5, -4.5.

¹⁹F NMR (377 MHz, CDCl₃) δ -119.2, -119.6.

HRMS (ESI+) m/z found 487.2787 [M+H]⁺, C₂₇H₃₉FN₂O₃Si calculated 487.2792 (Δ = - 1.03 ppm).

((5a*S,7*S**,9a*S**)-7-((tert-butyldimethylsilyl)oxy)-1-(2-fluorophenyl)-9a-methyl-4,5,5a,6,7,8,9,9a-octahydro-1H-benzo[*g*]indazol-3-yl)methanol**



TBS-protected ester **3.34** (47.1 mg, 0.0968 mmol) was dissolved in dry THF (4 mL) and cooled in an ice bath to 0 °C before the dropwise addition of a 1 M solution of LiAlH₄ in THF (0.116 mL, 0.116 mmol). The reaction was kept at 0 °C for 15 minutes and then stirred at room temperature for 3 hours. The reaction was diluted with aqueous 2 M NaOH and the resulting suspension filtered through a short pad of celite, eluting with DCM. The organic phase was dried over anhydrous sodium sulfate and concentrated to a crude oil. Purification by flash chromatography on silica gel (1:1 ethyl acetate/*n*-heptane) afforded the product as a fluffy white solid (24.7 mg, 0.0555 mmol, 57% yield)

R_f = 0.14 (1:1 ethyl acetate/*n*-heptane) – UV and KMnO₄

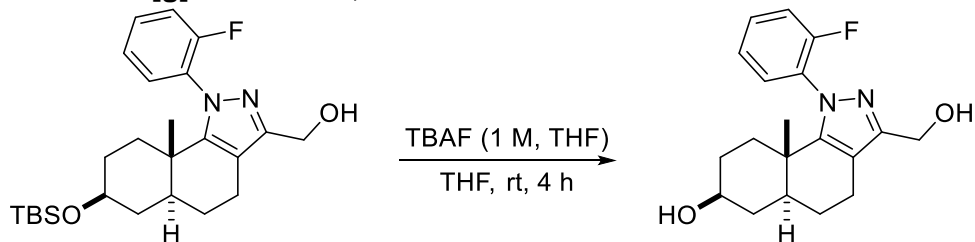
¹H NMR (400 MHz, CDCl₃) δ 7.52 – 7.44 (m, 1H), 7.44 – 7.35 (m, 1H), 7.27 – 7.17 (m, 2H), 4.66 (s, 2H), 3.61 – 3.46 (m, 1H), 2.70 – 2.50 (m, 2H), 1.78 – 1.52 (m, 5H), 1.52 – 1.20 (m, 5H), 1.14 (s, 3H, **Me** major), 1.11 (s, 3H, **Me** minor), 0.86 (s, 9H), 0.02 (d, *J* = 5.0 Hz, 6H).

¹³C NMR (101 MHz, CDCl₃) δ 151.3, 150.8, 149.6, 131.8, 131.7, 131.3, 130.4, 129.5, 124.5, 116.9, 116.7, 113.7, 71.4, 71.3, 57.8, 57.7, 42.7, 42.5, 37.5, 35.5, 35.4, 34.5, 32.2, 31.5, 31.4, 26.0, 20.2, 19.7, 18.3, -4.48, -4.49.

¹⁹F NMR (377 MHz, CDCl₃) δ -119.35, -119.92.

HRMS (ESI+) *m/z* found 445.2688 [M+H]⁺, C₂₅H₃₇FN₂O₂Si calculated 445.2686 (Δ = - 0.45 ppm).

(5a*S,7*S**,9a*S**)-1-(2-fluorophenyl)-3-(hydroxymethyl)-9a-methyl-4,5,5a,6,7,8,9,9a-octahydro-1H-benzo[*g*]indazol-7-ol, **3.35****



TBS protected primary alcohol (24.7 mg, 0.0555 mmol) was dissolved in THF (1 mL) before addition of a 1 M solution of TBAF in THF (0.11 mL, 0.11 mmol) and the reaction stirred at room temperature for 5 hours. The reaction was diluted with water and ethyl acetate, and the organic phase washed with water (3 x). The aqueous phase was back extracted with ethyl acetate and the organic phases combined. The combined organic phases were washed with brine, dried

over anhydrous sodium sulfate, and concentrated to a crude residue. Purification by flash chromatography afforded the product as a colourless oil (6.4 mg, 0.0194 mmol, 35% yield).

R_f = 0.18 (ethyl acetate) – UV and KMnO_4

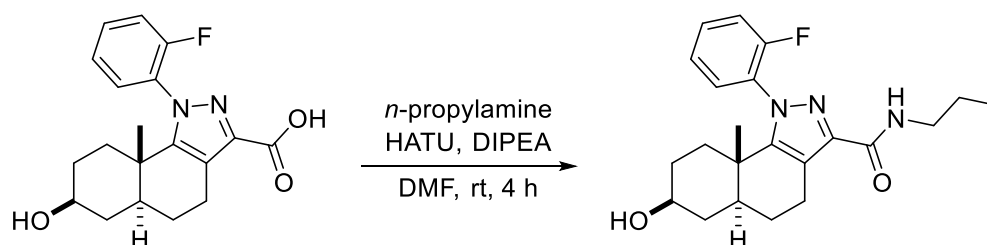
^1H NMR (400 MHz, CDCl_3) δ 7.53 – 7.46 (m, 1H), 7.46 – 7.36 (m, 1H), 7.27 – 7.18 (m, 2H), 4.67 (s, 2H), 3.61 (dt, J = 11.0, 6.1 Hz, 1H), 2.71 – 2.52 (m, 2H), 1.82 – 1.51 (m, 5H), 1.52 – 1.23 (m, 4H), 1.15 (s, 3H, **Me** major), 1.12 (s, 3H, **Me** minor).

^{13}C NMR (101 MHz, CDCl_3) δ 149.6, 132.0, 131.9, 131.3, 130.4, 124.6, 117.0, 116.8, 114.0, 113.9, 70.5, 70.4, 57.7, 57.6, 42.6, 42.4, 36.9, 35.4, 34.3, 32.0, 30.9, 30.8, 25.9, 25.8, 20.2, 19.7, 18.4.

^{19}F NMR (377 MHz, CDCl_3) δ -119.09, -119.59.

HRMS (ESI+) m/z found 331.1823 $[\text{M}+\text{H}]^+$, $\text{C}_{19}\text{H}_{23}\text{FN}_2\text{O}_2$ calculated 331.1822 (Δ = 0.30 ppm).

(5aS*,7S*,9aS*)-1-(2-fluorophenyl)-7-hydroxy-9a-methyl-N-propyl-4,5,5a,6,7,8,9,9a-octahydro-1H-benzo[g]indazole-3-carboxamide, 3.31



Carboxylic acid **3.28** (13.7 mg, 0.0398 mmol) was dissolved in dry DMF (1 mL) before addition of DIPEA (20.7 μL , 0.119 mmol) and HATU (30.3 mg, 0.0796 mmol) and the solution stirred at room temperature for 15 minutes, turning from colourless to brown. *N*-propylamine (3.6 μL , 0.0438 mmol) was added and the reaction stirred for 3.75 hours at room temperature. The reaction was diluted with water, extracted with ethyl acetate (2x), and the combined organic phases washed with 5 % aqueous LiCl (2 x) and dried over anhydrous sodium sulfate. The dried organic phases were concentrated to a brown residue that was purified by preparative HPLC, affording the product as a white solid (3.1 mg, 0.0080 mmol, 20% yield).

R_f = 0.46 (5% MeOH in DCM) – UV and KMnO_4

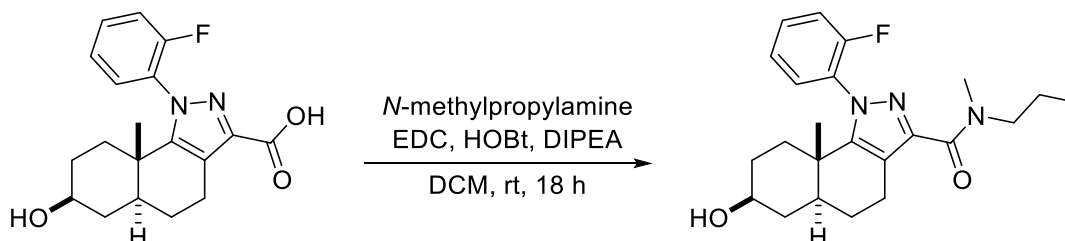
^1H NMR (400 MHz, CDCl_3) δ 7.55 – 7.48 (m, 1H), 7.42 – 7.36 (m, 1H), 7.30 – 7.22 (m, 2H), 6.94 – 6.83 (m, 1H), 3.63 (dt, J = 11.0, 5.6 Hz, 1H), 3.37 – 3.27 (m, 2H), 3.15 – 3.07 (m, 1H), 2.86 – 2.72 (m, 1H), 1.85 – 1.51 (m, 8H), 1.48 – 1.22 (m, 4H), 1.15 (s, 3H, **Me** major), 1.13 – 1.11 (m, 1H, **Me** minor), 0.94 (t, J = 7.4 Hz, 3H).

^{13}C NMR (101 MHz, CDCl_3) δ 162.8, 157.2, 151.2, 143.3, 132.0, 131.9, 131.1, 130.1, 124.6, 117.9, 117.1, 116.9, 70.6, 70.5, 42.5, 42.2, 40.8, 37.0, 35.5, 35.4, 34.4, 32.1, 30.9, 30.8, 26.1, 23.1, 21.8, 19.7, 18.5, 11.7.

^{19}F NMR (377 MHz, CDCl_3) δ -119.16, -119.72.

HRMS (ESI+) m/z found 385.2166 $[\text{M}+\text{H}]^+$, $\text{C}_{22}\text{H}_{28}\text{FN}_3\text{O}_2$ calculated 386.2244 (Δ = - 0.52 ppm).

(5a*S,7*S**,9a*S**)-1-(2-fluorophenyl)-7-hydroxy-*N*,9a-dimethyl-*N*-propyl-4,5,5a,6,7,8,9,9a-octahydro-1*H*-benzo[*g*]indazole-3-carboxamide, 3.32**



Carboxylic acid **3.28** (17.5 mg, 0.0510 mmol), *N*-methylpropylamine (6.31 μ L, 0.0610 mmol), EDC hydrochloride (11.7 mg, 0.0610 mmol), HOBT monohydrate (9.3 mg, 0.0610 mmol), and DIPEA (22.1 μ L, 0.127 mmol) were dissolved in dry DCM (1.5 mL) and stirred at room temperature for 18 hours. The reaction was further diluted with DCM, washed with water, dried over anhydrous magnesium sulfate, and concentrated to a crude solid. Purification by flash chromatography on silica gel (3.5% MeOH in DCM) afforded the product as a fluffy white solid (14.6 mg, 0.0365 mmol, 72% yield).

R_f = 0.26 (3.5% MeOH in DCM) – UV and KMnO_4

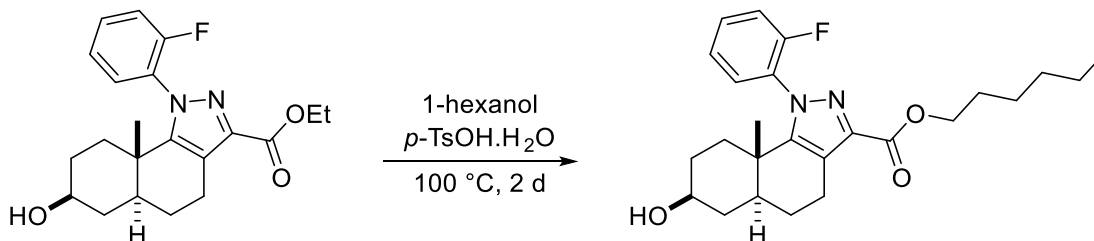
^1H NMR (400 MHz, CDCl_3) δ 7.52 – 7.43 (m, 1H), 7.39 – 7.33 (m, 1H), 7.25 – 7.16 (m, 2H), 3.68 – 3.35 (m, 3H), 3.24 – 2.99 (m, 3H), 2.96 – 2.86 (m, 1H), 2.79 – 2.54 (m, 1H), 1.89 – 1.49 (m, 8H), 1.49 – 1.22 (m, 4H), 1.15 (s, 3H, **Me** major), 1.10 (s, 3H, **Me** minor), 0.98 – 0.69 (m, 3H).

^{13}C NMR (101 MHz, CDCl_3) δ 160.0, 159.7, 157.5, 157.2, 150.2, 149.8, 144.6, 131.6, 131.5, 131.3, 130.2, 124.4, 116.9, 116.7, 70.5, 52.8, 49.6, 42.5, 42.4, 37.0, 35.4, 35.3, 34.4, 33.4, 32.2, 30.9, 30.8, 26.1, 21.8, 21.2, 20.3, 19.7, 18.5, 11.4, 11.0.

^{19}F NMR (377 MHz, CDCl_3) δ -119.69, -120.06, -120.13, -120.65.

HRMS (ESI+) m/z found 400.2396 $[\text{M}+\text{H}]^+$, $\text{C}_{23}\text{H}_{30}\text{FN}_3\text{O}_2$ calculated 400.2400 (Δ = - 1.00 ppm).

hexyl (5a*S,7*S**,9a*S**)-1-(2-fluorophenyl)-7-hydroxy-9a-methyl-4,5,5a,6,7,8,9,9a-octahydro-1*H*-benzo[*g*]indazole-3-carboxylate, 3.33**



Ester **3.27** (19.4 mg, 0.0521 mmol) and *p*-toluenesulfonic acid monohydrate (5.0 mg, 0.0261 mmol) were dissolved in 1-hexanol (1 mL) and heated at 100 $^{\circ}\text{C}$ for 2 days, adding an extra 0.5 eq. of *p*-toluenesulfonic acid monohydrate after 1 day. A majority of the 1-hexanol was removed under reduced pressure and the residue dissolved in ethyl acetate, washed with water, the organic phase dried over anhydrous sodium sulfate, and concentrated to a crude residue.

Purification by flash chromatography on silica gel (1:1 ethyl acetate/*n*-heptane) afforded the product as a colourless oil (10.3 mg, 0.0240 mmol, 46% yield).

R_f = 0.18 (1:1 ethyl acetate/*n*-heptane) – UV and KMnO_4

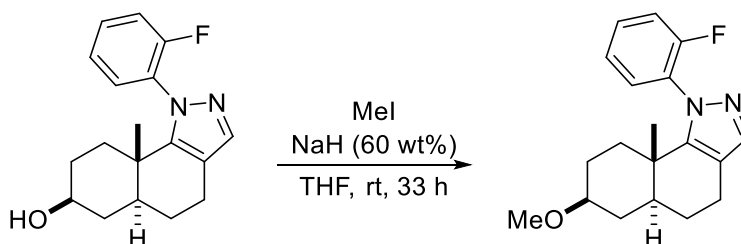
^1H NMR (400 MHz, CDCl_3) δ 7.51 – 7.45 (m, 1H), 7.42 – 7.35 (m, 1H), 7.26 – 7.17 (m, 2H), 4.31 (t, J = 7.0 Hz, 2H), 3.67 – 3.57 (m, 1H), 3.05 – 2.95 (m, 1H), 2.81 – 2.68 (m, 1H), 1.84 – 1.57 (m, 7H), 1.54 (br s, 1H), 1.48 – 1.22 (m, 10H), 1.14 (s, 3H, **Me** major), 1.13 (d, J = 1.4 Hz, 3H, **Me** minor), 0.94 – 0.82 (m, 3H)

^{13}C NMR (101 MHz, CDCl_3) δ 163.2, 159.9, 159.5, 157.4, 157.0, 151.2, 150.8, 141.3, 131.9, 131.8, 131.2, 130.2, 124.43, 124.38, 124.33, 124.29, 119.23, 119.16, 116.9, 116.7, 70.5, 70.4, 65.0, 42.5, 42.2, 36.9, 35.4, 35.3, 34.4, 32.0, 31.6, 30.9, 30.8, 28.9, 26.0, 25.9, 25.7, 22.7, 22.1, 19.6, 18.4, 18.4, 14.1.

^{19}F NMR (377 MHz, CDCl_3) δ -119.18, -119.63.

HRMS (ESI+) m/z found 429.2545 $[\text{M}+\text{H}]^+$, $\text{C}_{25}\text{H}_{33}\text{FN}_2\text{O}_3$ calculated 429.2553 (Δ = - 1.86 ppm).

(5a*S,7*S**,9a*S**)-1-(2-fluorophenyl)-7-methoxy-9a-methyl-4,5,5a,6,7,8,9,9a-octahydro-1H-benzo[*g*]indazole, 3.37**



(\pm)-Astercin 1 (17.5 mg, 0.0583 mmol) was dissolved in dry THF (1 mL) before addition of NaH (60 wt%, 9.32 mg, 0.233 mmol) and iodomethane (7.3 μL , 0.117 mmol). The reaction was stirred at room temperature for 1 day before addition of extra NaH (60 wt%, 9.32 mg, 0.233 mmol) and iodomethane (14.6 μL , 0.234 mmol) and stirred for an additional 9 hours. The reaction was cooled to 0 $^\circ\text{C}$ in an ice bath, quenched by addition of saturated aqueous ammonium chloride, and extracted with ethyl acetate. The organic phase was dried over anhydrous magnesium sulfate and concentrated to a crude solid. Purification by flash chromatography on silica gel (1:1 ethyl acetate/*n*-heptane) afforded the product as a colourless oil (14.1 mg, 0.0448 mmol, 77% yield).

R_f = 0.40 (1:1 ethyl acetate/*n*-heptane) – UV and KMnO_4

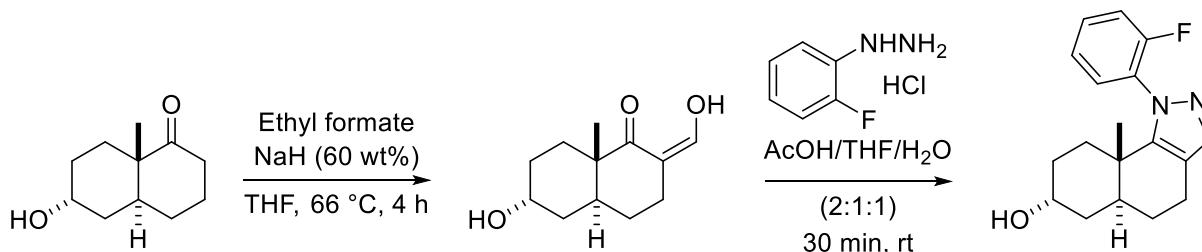
^1H NMR (400 MHz, CDCl_3) δ 7.50 – 7.42 (m, 2H), 7.42 – 7.35 (m, 1H), 7.26 – 7.17 (m, 2H), 3.32 (s, 3H), 3.19 – 3.10 (m, 1H), 2.71 – 2.55 (m, 2H), 1.93 – 1.84 (m, 1H), 1.81 – 1.51 (m, 4H), 1.45 – 1.19 (m, 4H), 1.14 (s, 3H, **Me** major), 1.10 (s, 3H, **Me** minor).

^{13}C NMR (101 MHz, CDCl_3) δ 160.0, 157.5, 149.5, 149.1, 138.8, 131.5, 131.4, 130.4, 124.4, 124.3, 116.8, 116.6, 115.7, 115.6, 79.1, 55.8, 42.9, 42.6, 35.6, 35.5, 34.4, 33.4, 32.2, 27.6, 27.4, 26.5, 21.0, 19.7, 18.3.

^{19}F NMR (377 MHz, CDCl_3) δ -119.50, -120.18.

HRMS (ESI+) m/z found 315.1873 $[M+H]^+$, $C_{19}H_{23}FN_2O$ calculated 315.1872 (Δ = 0.32 ppm).

(5a*S,7*R**,9a*S**)-1-(2-fluorophenyl)-9a-methyl-4,5,5a,6,7,8,9,9a-octahydro-1H-benzo[*g*]indazol-7-ol, 3.40**



Ketone **2.09** (159 mg, 0.872 mmol) and ethyl formate (0.67 mL, 8.23 mmol) were dissolved in dry THF (7.5 mL) before addition of sodium hydride (60 wt%, 98.8 mg, 2.47 mmol) and the reaction heated at reflux for 4 hours. The reaction was cooled to room temperature, quenched by addition of saturated aqueous ammonium chloride, and extracted with ethyl acetate (3 x). The combined organic phases were dried over anhydrous magnesium sulfate and concentrated to a brown oil. The brown oil was dissolved in a 2:1:1 mixture of AcOH/THF/H₂O before addition of 2-fluorophenylhydrazine hydrochloride (141.8 mg, 0.872 mmol) and stirred at room temperature for 3 hours. The reaction was cooled in an ice-bath and basified via addition of 2M aq. NaOH. The reaction mixture was extracted with ethyl acetate (3x), the combined organic phases dried over anhydrous sodium sulfate, and concentrated to a crude yellow oil. Purification by flash chromatography on silica gel (2:3 ethyl acetate/*n*-heptane) afforded the product as a yellow solid (69 mg, 0.230 mmol, 26% yield).

R_f = 0.08 (2:3 ethyl acetate/*n*-heptane) – UV and KMnO₄

¹H NMR (400 MHz, CDCl₃) δ 7.50 – 7.36 (m, 3H), 7.24 – 7.16 (m, 2H), 4.02 (p, J = 2.9 Hz, 1H), 2.71 – 2.60 (m, 2H), 2.26 – 2.11 (m, 1H), 1.81 – 1.39 (m, 7H), 1.16 – 1.00 (m, 4H).

¹³C NMR (101 MHz, CDCl₃) δ 160.1, 159.7, 149.7, 149.2, 138.7, 131.6, 131.4, 131.3, 130.3, 124.4, 124.2, 116.8, 116.7, 116.5, 115.7, 65.9, 36.7, 36.6, 35.8, 35.1, 35.0, 30.2, 28.7, 28.0, 26.0, 20.8, 18.7, 17.4.

¹⁹F NMR (377 MHz, CDCl₃) δ -119.70, -119.74.

HRMS (ESI+) m/z found 301.1711 $[M+H]^+$, $C_{18}H_{21}FN_2O$ calculated 301.1716 (Δ = - 1.66 ppm).

References

- (1) Dandapani, S.; Rosse, G.; Southall, N.; Salvino, J. M.; Thomas, C. J. Selecting, Acquiring, and Using Small Molecule Libraries for High-Throughput Screening. *Curr. Protoc. Chem. Biol.* **2012**, *4*, 177–191. <https://doi.org/10.1002/9780470559277.ch110252>.
- (2) Drews, J. Drug Discovery: A Historical Perspective. *Science (80-.)*. **2000**, *287* (5460), 1960 LP – 1964. <https://doi.org/10.1126/science.287.5460.1960>.
- (3) Pereira, D. A.; Williams, J. A. Origin and Evolution of High Throughput Screening. *Br. J. Pharmacol.* **2007**, *152* (1), 53–61. <https://doi.org/10.1038/sj.bjp.0707373>.
- (4) Liu, R.; Li, X.; Lam, K. S. Combinatorial Chemistry in Drug Discovery. *Curr. Opin. Chem. Biol.* **2017**, *38*, 117–126. <https://doi.org/https://doi.org/10.1016/j.cbpa.2017.03.017>.
- (5) Kennedy, J. P.; Williams, L.; Bridges, T. M.; Daniels, R. N.; Weaver, D.; Lindsley, C. W. Application of Combinatorial Chemistry Science on Modern Drug Discovery. *J. Comb. Chem.* **2008**, *10* (3), 345–354. <https://doi.org/10.1021/cc700187t>.
- (6) Sauer, W. H. B.; Schwarz, M. K. Molecular Shape Diversity of Combinatorial Libraries: A Prerequisite for Broad Bioactivity. *J. Chem. Inf. Comput. Sci.* **2003**, *43* (3), 987–1003. <https://doi.org/10.1021/ci025599w>.
- (7) Clemons, P. A.; Bodycombe, N. E.; Carrinski, H. A.; Wilson, J. A.; Shamji, A. F.; Wagner, B. K.; Koehler, A. N.; Schreiber, S. L. Small Molecules of Different Origins Have Distinct Distributions of Structural Complexity That Correlate with Protein-Binding Profiles. *Proc. Natl. Acad. Sci.* **2010**, *107* (44), 18787 LP – 18792. <https://doi.org/10.1073/pnas.1012741107>.
- (8) Singh, N.; Guha, R.; Giulianotti, M. A.; Pinilla, C.; Houghten, R. A.; Medina-Franco, J. L. Chemoinformatic Analysis of Combinatorial Libraries, Drugs, Natural Products, and Molecular Libraries Small Molecule Repository. *J. Chem. Inf. Model.* **2009**, *49* (4), 1010–1024. <https://doi.org/10.1021/ci800426u>.
- (9) Wetzel, S.; Schuffenhauer, A.; Roggo, S.; Ertl, P.; Waldmann, H. Cheminformatic Analysis of Natural Products and Their Chemical Space. *Chimia (Aarau)*. **2007**, *61* (6 SE-Scientific Articles), 355. <https://doi.org/10.2533/chimia.2007.355>.
- (10) Newman, D. J.; Cragg, G. M. Natural Products as Sources of New Drugs over the Nearly Four Decades from 01/1981 to 09/2019. *J. Nat. Prod.* **2020**, *83* (3), 770–803. <https://doi.org/10.1021/acs.jnatprod.9b01285>.
- (11) Moss, G. P. Nomenclature of Steroids (Recommendations 1989). *Pure Appl. Chem.* **1989**, *61* (10), 1783–1822. <https://doi.org/doi:10.1351/pac198961101783>.
- (12) Lednicer, D. Steroid Chemistry at a Glance. In *Steroid Chemistry at a Glance*; John Wiley & Sons, Ltd: Chichester, 2010; pp 10–16.
- (13) Turgeon, J. L.; McDonnell, D. P.; Martin, K. A.; Wise, P. M. Hormone Therapy: Physiological Complexity Belies Therapeutic Simplicity. *Science (80-.)*. **2004**, *304* (5675), 1269–1273. <https://doi.org/10.1126/science.1096725>.
- (14) Myers, J. B.; Meacham, R. B. Androgen Replacement Therapy in the Aging Male. *Rev. Urol.* **2003**, *5* (4), 216–226.
- (15) Barshes, N. R.; Goodpastor, S. E.; Goss, J. A. Pharmacologic Immunosuppression. *Frontiers in*

bioscience : a journal and virtual library. Michael E. DeBakey Department of Surgery, Baylor College of Medicine, 6550 Fannin. Suite 1628, Houston, TX 77030, USA. 2004, pp 411–420. <https://doi.org/10.2741/1249>.

- (16) Fizazi, K.; Scher, H. I.; Molina, A.; Logothetis, C. J.; Chi, K. N.; Jones, R. J.; Staffurth, J. N.; North, S.; Vogelzang, N. J.; Saad, F.; Mainwaring, P.; Harland, S.; Goodman, O. B.; Sternberg, C. N.; Li, J. H.; Kheoh, T.; Haqq, C. M.; de Bono, J. S. Abiraterone Acetate for Treatment of Metastatic Castration-Resistant Prostate Cancer: Final Overall Survival Analysis of the COU-AA-301 Randomised, Double-Blind, Placebo-Controlled Phase 3 Study. *Lancet Oncol.* **2012**, *13* (10), 983–992. [https://doi.org/https://doi.org/10.1016/S1470-2045\(12\)70379-0](https://doi.org/https://doi.org/10.1016/S1470-2045(12)70379-0).
- (17) Welsch, M. E.; Snyder, S. A.; Stockwell, B. R. Privileged Scaffolds for Library Design and Drug Discovery. *Curr. Opin. Chem. Biol.* **2010**, *14* (3), 347–361. <https://doi.org/https://doi.org/10.1016/j.cbpa.2010.02.018>.
- (18) Biju, P.; Wang, H.; Anthes, J.; McCormick, K.; Aslanian, R.; Berlin, M.; Bitar, R.; Lim, Y.-H.; Lee, Y. J.; Prelusky, D.; Mcleod, R.; Jia, Y.; Fernandez, X.; Lieber, G.; Jimenez, J.; Eckel, S.; House, A.; Chapman, R.; Phillips, J. Steroidal C-21 Heteroaryl Thioethers. Part 3: Pregn-4-Eno-[3,2-c]Pyrazole Fused A Ring Modified Steroids as Selective Glucocorticoid Receptor Modulators (Dissociated Steroids). *Bioorg. Med. Chem. Lett.* **2012**, *22* (9), 3291–3295. <https://doi.org/https://doi.org/10.1016/j.bmcl.2012.03.015>.
- (19) Cui, H.-W.; Peng, S.; Gu, X.-Z.; Chen, H.; He, Y.; Gao, W.; Lv, F.; Wang, J.-H.; Wang, Y.; Xie, J.; Liu, M.-Y.; Yi, Z.; Qiu, W.-W. Synthesis and Biological Evaluation of D-Ring Fused 1,2,3-Thiadiazole Dehydroepiandrosterone Derivatives as Antitumor Agents. *Eur. J. Med. Chem.* **2016**, *111*, 126–137. <https://doi.org/https://doi.org/10.1016/j.ejmech.2016.01.058>.
- (20) Arenas-González, A.; Mendez-Delgado, L. A.; Merino-Montiel, P.; Padrón, J. M.; Montiel-Smith, S.; Vega-Báez, J. L.; Meza-Reyes, S. Synthesis of Monomeric and Dimeric Steroids Containing [1,2,4]Triazolo[1,5-a]Pyrimidines. *Steroids* **2016**, *116*, 13–19. <https://doi.org/https://doi.org/10.1016/j.steroids.2016.09.014>.
- (21) Tan, D. S. Diversity-Oriented Synthesis: Exploring the Intersections between Chemistry and Biology. *Nat. Chem. Biol.* **2005**, *1* (2), 74–84. <https://doi.org/10.1038/nchembio0705-74>.
- (22) Yi, S.; Varun, B. V.; Choi, Y.; Park, S. B. A Brief Overview of Two Major Strategies in Diversity-Oriented Synthesis: Build/Couple/Pair and Ring-Distortion. *Frontiers in Chemistry*. 2018.
- (23) Huigens III, R. W.; Morrison, K. C.; Hicklin, R. W.; Flood Jr, T. A.; Richter, M. F.; Hergenrother, P. J. A Ring-Distortion Strategy to Construct Stereochemically Complex and Structurally Diverse Compounds from Natural Products. *Nat. Chem.* **2013**, *5* (3), 195–202. <https://doi.org/10.1038/nchem.1549>.
- (24) Ciardiello, J. J.; Stewart, H. L.; Sore, H. F.; Galloway, W. R. J. D.; Spring, D. R. A Novel Complexity-to-Diversity Strategy for the Diversity-Oriented Synthesis of Structurally Diverse and Complex Macrocycles from Quinine. *Bioorg. Med. Chem.* **2017**, *25* (11), 2825–2843. <https://doi.org/https://doi.org/10.1016/j.bmc.2017.02.060>.
- (25) Srinivasulu, V.; Srikanth, G.; Khanfar, M. A.; Abu-Yousef, I. A.; Majdalawieh, A. F.; Mazitschek, R.; Setty, S. C.; Sebastian, A.; Al-Tel, T. H. Stereodivergent Complexity-to-Diversity Strategy En Route to the Synthesis of Nature-Inspired Skeleta. *J. Org. Chem.* **2022**, *87* (2), 1377–1397. <https://doi.org/10.1021/acs.joc.1c02698>.
- (26) Llabani, E.; Hicklin, R. W.; Lee, H. Y.; Motika, S. E.; Crawford, L. A.; Weerapana, E.; Hergenrother, P. J. Diverse Compounds from Pleuromutilin Lead to a Thioredoxin Inhibitor and

- Inducer of Ferroptosis. *Nat. Chem.* **2019**, *11* (6), 521–532. <https://doi.org/10.1038/s41557-019-0261-6>.
- (27) Dobson, C. M. Chemical Space and Biology. *Nature* **2004**, *432* (7019), 824–828. <https://doi.org/10.1038/nature03192>.
- (28) Galloway, W. R. J. D.; Isidro-Llobet, A.; Spring, D. R. Diversity-Oriented Synthesis as a Tool for the Discovery of Novel Biologically Active Small Molecules. *Nat. Commun.* **2010**, *1* (1), 80. <https://doi.org/10.1038/ncomms1081>.
- (29) Galloway, W. R. J. D.; Spring, D. R. Is Synthesis the Main Hurdle for the Generation of Diversity in Compound Libraries for Screening? *Expert Opin. Drug Discov.* **2009**, *4* (5), 467–472. <https://doi.org/10.1517/17460440902916606>.
- (30) Burke, M. D.; Schreiber, S. L. A Planning Strategy for Diversity-Oriented Synthesis. *Angew. Chemie Int. Ed.* **2004**, *43* (1), 46–58. <https://doi.org/10.1002/anie.200300626>.
- (31) Ibbeson, B. M.; Laraia, L.; Alza, E.; O' Connor, C. J.; Tan, Y. S.; Davies, H. M. L.; McKenzie, G.; Venkitaraman, A. R.; Spring, D. R. Diversity-Oriented Synthesis as a Tool for Identifying New Modulators of Mitosis. *Nat. Commun.* **2014**, *5* (1), 3155. <https://doi.org/10.1038/ncomms4155>.
- (32) Hassan, H.; Marsden, S. P.; Nelson, A. Design and Synthesis of a Fragment Set Based on Twisted Bicyclic Lactams. *Bioorg. Med. Chem.* **2018**, *26* (11), 3030–3033. <https://doi.org/https://doi.org/10.1016/j.bmc.2018.02.027>.
- (33) Wawer, M. J.; Li, K.; Gustafsdottir, S. M.; Ljosa, V.; Bodycombe, N. E.; Marton, M. A.; Sokolnicki, K. L.; Bray, M. A.; Kemp, M. M.; Winchester, E.; Taylor, B.; Grant, G. B.; Hon, C. S. Y.; Duvall, J. R.; Wilson, J. A.; Bittker, J. A.; Dančák, V.; Narayan, R.; Subramanian, A.; Winckler, W.; Golub, T. R.; Carpenter, A. E.; Shamji, A. F.; Schreiber, S. L.; Clemons, P. A. Toward Performance-Diverse Small-Molecule Libraries for Cell-Based Phenotypic Screening Using Multiplexed High-Dimensional Profiling. *Proc. Natl. Acad. Sci. U. S. A.* **2014**, *111* (30), 10911–10916. <https://doi.org/10.1073/pnas.1410933111>.
- (34) Pavlinov, I.; Gerlach, E. M.; Aldrich, L. N. Next Generation Diversity-Oriented Synthesis: A Paradigm Shift from Chemical Diversity to Biological Diversity. *Org. Biomol. Chem.* **2019**, *17* (7), 1608–1623. <https://doi.org/10.1039/C8OB02327A>.
- (35) Wetzel, S.; Bon, R. S.; Kumar, K.; Waldmann, H. Biology-Oriented Synthesis. *Angew. Chemie Int. Ed.* **2011**, *50* (46), 10800–10826. <https://doi.org/10.1002/anie.201007004>.
- (36) Laraia, L.; Robke, L.; Waldmann, H. Bioactive Compound Collections: From Design to Target Identification. *Chem* **2018**, *4* (4), 705–730. <https://doi.org/https://doi.org/10.1016/j.chempr.2018.01.012>.
- (37) Koch, M. A.; Schuffenhauer, A.; Scheck, M.; Wetzel, S.; Casaulta, M.; Odermatt, A.; Ertl, P.; Waldmann, H. Charting Biologically Relevant Chemical Space: A Structural Classification of Natural Products (SCONP). *Proc. Natl. Acad. Sci. U. S. A.* **2005**, *102* (48), 17272–17277. <https://doi.org/10.1073/pnas.0503647102>.
- (38) Karageorgis, G.; Waldmann, H. Guided by Evolution: Biology-Oriented Synthesis of Bioactive Compound Classes. *Synthesis (Stuttg.)* **2019**, *51* (01), 55–66.
- (39) Xia, G.; Cao, S.; Chen, L.; Qiu, F. Natural Withanolides, an Update. *Nat. Prod. Rep.* **2022**, *39* (4), 784–813. <https://doi.org/10.1039/D1NP00055A>.

- (40) Švenda, J.; Sheremet, M.; Kremer, L.; Maier, L.; Bauer, J. O.; Strohmamm, C.; Ziegler, S.; Kumar, K.; Waldmann, H. Biology-Oriented Synthesis of a Withanolide-Inspired Compound Collection Reveals Novel Modulators of Hedgehog Signaling. *Angew. Chemie Int. Ed.* **2015**, *54* (19), 5596–5602. <https://doi.org/10.1002/anie.201500112>.
- (41) Sheremet, M.; Kapoor, S.; Schröder, P.; Kumar, K.; Ziegler, S.; Waldmann, H. Small Molecules Inspired by the Natural Product Withanolides as Potent Inhibitors of Wnt Signaling. *ChemBioChem* **2017**, *18* (18), 1797–1806. <https://doi.org/https://doi.org/10.1002/cbic.201700260>.
- (42) Over, B.; Wetzel, S.; Grütter, C.; Nakai, Y.; Renner, S.; Rauh, D.; Waldmann, H. Natural-Product-Derived Fragments for Fragment-Based Ligand Discovery. *Nat. Chem.* **2013**, *5* (1), 21–28. <https://doi.org/10.1038/nchem.1506>.
- (43) Erlanson, D. A. Introduction to Fragment-Based Drug Discovery BT - Fragment-Based Drug Discovery and X-Ray Crystallography; Davies, T. G., Hyvönen, M., Eds.; Springer Berlin Heidelberg: Berlin, Heidelberg, 2012; pp 1–32. https://doi.org/10.1007/128_2011_180.
- (44) Roughley, S. D.; Hubbard, R. E. How Well Can Fragments Explore Accessed Chemical Space? A Case Study from Heat Shock Protein 90. *J. Med. Chem.* **2011**, *54* (12), 3989–4005. <https://doi.org/10.1021/jm200350g>.
- (45) Fink, T.; Reymond, J.-L. Virtual Exploration of the Chemical Universe up to 11 Atoms of C, N, O, F: Assembly of 26.4 Million Structures (110.9 Million Stereoisomers) and Analysis for New Ring Systems, Stereochemistry, Physicochemical Properties, Compound Classes, and Drug Discov. *J. Chem. Inf. Model.* **2007**, *47* (2), 342–353. <https://doi.org/10.1021/ci600423u>.
- (46) Hung, A. W.; Ramek, A.; Wang, Y.; Kaya, T.; Wilson, J. A.; Clemons, P. A.; Young, D. W. Route to Three-Dimensional Fragments Using Diversity-Oriented Synthesis. *Proc. Natl. Acad. Sci. U. S. A.* **2011**, *108* (17), 6799–6804. <https://doi.org/10.1073/pnas.1015271108>.
- (47) Lowe, R. A.; Taylor, D.; Chibale, K.; Nelson, A.; Marsden, S. P. Synthesis and Evaluation of the Performance of a Small Molecule Library Based on Diverse Tropane-Related Scaffolds. *Bioorg. Med. Chem.* **2020**, *28* (9), 115442. <https://doi.org/https://doi.org/10.1016/j.bmc.2020.115442>.
- (48) Xu, H.; Golz, C.; Strohmamm, C.; Antonchick, A. P.; Waldmann, H. Enantiodivergent Combination of Natural Product Scaffolds Enabled by Catalytic Enantioselective Cycloaddition. *Angew. Chemie Int. Ed.* **2016**, *55* (27), 7761–7765. <https://doi.org/https://doi.org/10.1002/anie.201602084>.
- (49) Karageorgis, G.; Foley, D. J.; Laraia, L.; Brakmann, S.; Waldmann, H. Pseudo Natural Products—Chemical Evolution of Natural Product Structure. *Angew. Chemie - Int. Ed.* **2021**, *60* (29), 15705–15723. <https://doi.org/10.1002/anie.202016575>.
- (50) Karageorgis, G.; Reckzeh, E. S.; Ceballos, J.; Schwalfenberg, M.; Sievers, S.; Ostermann, C.; Pahl, A.; Ziegler, S.; Waldmann, H. Chromopynones Are Pseudo Natural Product Glucose Uptake Inhibitors Targeting Glucose Transporters GLUT-1 and -3. *Nat. Chem.* **2018**, *10* (11), 1103–1111. <https://doi.org/10.1038/s41557-018-0132-6>.
- (51) Cremosnik, G. S.; Liu, J.; Waldmann, H. Guided by Evolution: From Biology Oriented Synthesis to Pseudo Natural Products. *Nat. Prod. Rep.* **2020**, *37* (11), 1497–1510. <https://doi.org/10.1039/D0NP00015A>.
- (52) Liu, J.; Cremosnik, G. S.; Otte, F.; Pahl, A.; Sievers, S.; Strohmamm, C.; Waldmann, H. Design, Synthesis, and Biological Evaluation of Chemically and Biologically Diverse Pyrroquinoline Pseudo Natural Products. *Angew. Chemie Int. Ed.* **2021**, *60* (9), 4648–4656. <https://doi.org/https://doi.org/10.1002/anie.202013731>.

- (53) Gally, J.-M.; Pahl, A.; Czodrowski, P.; Waldmann, H. Pseudonatural Products Occur Frequently in Biologically Relevant Compounds. *J. Chem. Inf. Model.* **2021**, *61* (11), 5458–5468. <https://doi.org/10.1021/acs.jcim.1c01084>.
- (54) Christoforow, A.; Wilke, J.; Binici, A.; Pahl, A.; Ostermann, C.; Sievers, S.; Waldmann, H. Design, Synthesis, and Phenotypic Profiling of Pyrano-Furo-Pyridone Pseudo Natural Products. *Angew. Chemie Int. Ed.* **2019**, *58* (41), 14715–14723. <https://doi.org/10.1002/anie.201907853>.
- (55) Niggemeyer, G.; Knyazeva, A.; Gasper, R.; Corkery, D.; Bodenbinder, P.; Holstein, J. J.; Sievers, S.; Wu, Y.-W.; Waldmann, H. Synthesis of 20-Membered Macrocyclic Pseudo-Natural Products Yields Inducers of LC3 Lipidation. *Angew. Chemie Int. Ed.* **2022**, *61* (11), e202114328. <https://doi.org/https://doi.org/10.1002/anie.202114328>.
- (56) Liu, J.; Flegel, J.; Otte, F.; Pahl, A.; Sievers, S.; Strohmman, C.; Waldmann, H. Combination of Pseudo-Natural Product Design and Formal Natural Product Ring Distortion Yields Stereochemically and Biologically Diverse Pseudo-Sesquiterpenoid Alkaloids. *Angew. Chemie Int. Ed.* **2021**, *60* (39), 21384–21395. <https://doi.org/https://doi.org/10.1002/anie.202106654>.
- (57) Alonso, F.; Galilea, A.; Mañez, P. A.; Acebedo, S. L.; Cabrera, G. M.; Otero, M.; Barquero, A. A.; Ramírez, J. A. Beyond Pseudo-Natural Products: Sequential Ugi/Pictet-Spengler Reactions Leading to Steroidal Pyrazinoisoquinolines That Trigger Caspase-Independent Death in HepG2 Cells. *ChemMedChem* **2021**, *16* (12), 1945–1955. <https://doi.org/https://doi.org/10.1002/cmdc.202100052>.
- (58) Krause, M. R.; Regen, S. L. The Structural Role of Cholesterol in Cell Membranes: From Condensed Bilayers to Lipid Rafts. *Acc. Chem. Res.* **2014**, *47* (12), 3512–3521. <https://doi.org/10.1021/ar500260t>.
- (59) Payne, A. H.; Hales, D. B. Overview of Steroidogenic Enzymes in the Pathway from Cholesterol to Active Steroid Hormones. *Endocr. Rev.* **2004**, *25* (6), 947–970. <https://doi.org/10.1210/er.2003-0030>.
- (60) Huang, P.; Nedelcu, D.; Watanabe, M.; Jao, C.; Kim, Y.; Liu, J.; Salic, A. Cellular Cholesterol Directly Activates Smoothed in Hedgehog Signaling. *Cell* **2016**, *166* (5), 1176–1187.e14. <https://doi.org/https://doi.org/10.1016/j.cell.2016.08.003>.
- (61) Sheng, R.; Kim, H.; Lee, H.; Xin, Y.; Chen, Y.; Tian, W.; Cui, Y.; Choi, J.-C.; Doh, J.; Han, J.-K.; Cho, W. Cholesterol Selectively Activates Canonical Wnt Signalling over Non-Canonical Wnt Signalling. *Nat. Commun.* **2014**, *5* (1), 4393. <https://doi.org/10.1038/ncomms5393>.
- (62) van Reyk, D. M.; Brown, A. J.; Hult'en, L. M.; Dean, R. T.; Jessup, W. Oxysterols in Biological Systems: Sources, Metabolism and Pathophysiological Relevance. *Redox Rep.* **2006**, *11* (6), 255–262. <https://doi.org/10.1179/135100006X155003>.
- (63) Vanier, M. T. Niemann-Pick Disease Type C. *Orphanet J. Rare Dis.* **2010**, *5* (1), 16. <https://doi.org/10.1186/1750-1172-5-16>.
- (64) Luo, J.; Yang, H.; Song, B.-L. Mechanisms and Regulation of Cholesterol Homeostasis. *Nat. Rev. Mol. Cell Biol.* **2020**, *21* (4), 225–245. <https://doi.org/10.1038/s41580-019-0190-7>.
- (65) Cerqueira, N. M. F. S. A.; Oliveira, E. F.; Gesto, D. S.; Santos-Martins, D.; Moreira, C.; Moorthy, H. N.; Ramos, M. J.; Fernandes, P. A. Cholesterol Biosynthesis: A Mechanistic Overview. *Biochemistry* **2016**, *55* (39), 5483–5506. <https://doi.org/10.1021/acs.biochem.6b00342>.
- (66) Hampton, R.; Dimster-Denk, D.; Rine, J. The Biology of HMG-CoA Reductase: The Pros of Contra-Regulation. *Trends Biochem. Sci.* **1996**, *21* (4), 140–145.

[https://doi.org/https://doi.org/10.1016/S0968-0004\(96\)80168-X](https://doi.org/https://doi.org/10.1016/S0968-0004(96)80168-X).

- (67) Gill, S.; Stevenson, J.; Kristiana, I.; Brown, A. J. Cholesterol-Dependent Degradation of Squalene Monooxygenase, a Control Point in Cholesterol Synthesis beyond HMG-CoA Reductase. *Cell Metab.* **2011**, *13* (3), 260–273. <https://doi.org/https://doi.org/10.1016/j.cmet.2011.01.015>.
- (68) Ge, L.; Wang, J.; Qi, W.; Miao, H.-H.; Cao, J.; Qu, Y.-X.; Li, B.-L.; Song, B.-L. The Cholesterol Absorption Inhibitor Ezetimibe Acts by Blocking the Sterol-Induced Internalization of NPC1L1. *Cell Metab.* **2008**, *7* (6), 508–519. <https://doi.org/https://doi.org/10.1016/j.cmet.2008.04.001>.
- (69) Betters, J. L.; Yu, L. NPC1L1 and Cholesterol Transport. *FEBS Lett.* **2010**, *584* (13), 2740–2747. <https://doi.org/https://doi.org/10.1016/j.febslet.2010.03.030>.
- (70) Wijers, M.; Kuivenhoven, J. A.; van de Sluis, B. The Life Cycle of the Low-Density Lipoprotein Receptor: Insights from Cellular and in-Vivo Studies. *Curr. Opin. Lipidol.* **2015**, *26* (2).
- (71) Zhang, H. Lysosomal Acid Lipase and Lipid Metabolism: New Mechanisms, New Questions, and New Therapies. *Curr. Opin. Lipidol.* **2018**, *29* (3).
- (72) Li, J.; Pfeiffer, S. R. Lysosomal Membrane Glycoproteins Bind Cholesterol and Contribute to Lysosomal Cholesterol Export. *Elife* **2016**, *5*, e21635. <https://doi.org/10.7554/eLife.21635>.
- (73) Horton, J. D.; Goldstein, J. L.; Brown, M. S. SREBPs: Activators of the Complete Program of Cholesterol and Fatty Acid Synthesis in the Liver. *J. Clin. Invest.* **2002**, *109* (9), 1125–1131. <https://doi.org/10.1172/JCI15593>.
- (74) Yang, T.; Espenshade, P. J.; Wright, M. E.; Yabe, D.; Gong, Y.; Aebersold, R.; Goldstein, J. L.; Brown, M. S. Crucial Step in Cholesterol Homeostasis: Sterols Promote Binding of SCAP to INSIG-1, a Membrane Protein That Facilitates Retention of SREBPs in ER. *Cell* **2002**, *110* (4), 489–500. [https://doi.org/https://doi.org/10.1016/S0092-8674\(02\)00872-3](https://doi.org/https://doi.org/10.1016/S0092-8674(02)00872-3).
- (75) Yabe, D.; Brown, M. S.; Goldstein, J. L. Insig-2, a Second Endoplasmic Reticulum Protein That Binds SCAP and Blocks Export of Sterol Regulatory Element-Binding Proteins. *Proc. Natl. Acad. Sci. U. S. A.* **2002**, *99* (20), 12753–12758. <https://doi.org/10.1073/pnas.162488899>.
- (76) Radhakrishnan, A.; Ikeda, Y.; Hyock, J. K.; Brown, M. S.; Goldstein, J. L. Sterol-Regulated Transport of SREBPs from Endoplasmic Reticulum to Golgi: Oxysterols Block Transport by Binding to Insig. *Proc. Natl. Acad. Sci. U. S. A.* **2007**, *104* (16), 6511–6518. <https://doi.org/10.1073/pnas.0700899104>.
- (77) Espenshade, P. J.; Li, W. P.; Yabe, D. Sterols Block Binding of COPII Proteins to SCAP, Thereby Controlling SCAP Sorting in ER. *Proc. Natl. Acad. Sci. U. S. A.* **2002**, *99* (18), 11694–11699. <https://doi.org/10.1073/pnas.182412799>.
- (78) Sakai, J.; Duncan, E. A.; Rawson, R. B.; Hua, X.; Brown, M. S.; Goldstein, J. L. Sterol-Regulated Release of SREBP-2 from Cell Membranes Requires Two Sequential Cleavages, One Within a Transmembrane Segment. *Cell* **1996**, *85* (7), 1037–1046. [https://doi.org/https://doi.org/10.1016/S0092-8674\(00\)81304-5](https://doi.org/https://doi.org/10.1016/S0092-8674(00)81304-5).
- (79) Amemiya-Kudo, M.; Shimano, H.; Hasty, A. H.; Yahagi, N.; Yoshikawa, T.; Matsuzaka, T.; Okazaki, H.; Tamura, Y.; Iizuka, Y.; Ohashi, K.; Osuga, J.; Harada, K.; Gotoda, T.; Sato, R.; Kimura, S.; Ishibashi, S.; Yamada, N. Transcriptional Activities of Nuclear SREBP-1a, -1c, and -2 to Different Target Promoters of Lipogenic and Cholesterogenic Genes. *J. Lipid Res.* **2002**, *43* (8), 1220–1235. <https://doi.org/https://doi.org/10.1194/jlr.M100417-JLR200>.
- (80) Sorrentino, V.; Zelcer, N. Post-Transcriptional Regulation of Lipoprotein Receptors by the E3-

Ubiquitin Ligase Inducible Degradation of the Low-Density Lipoprotein Receptor. *Curr. Opin. Lipidol.* **2012**, 23 (3).

- (81) Iwayanagi, Y.; Takada, T.; Tomura, F.; Yamanashi, Y.; Terada, T.; Inui, K.; Suzuki, H. Human NPC1L1 Expression Is Positively Regulated by PPAR α . *Pharm. Res.* **2011**, 28 (2), 405–412. <https://doi.org/10.1007/s11095-010-0294-4>.
- (82) Kikuchi, T.; Orihara, K.; Oikawa, F.; Han, S.; Kuba, M.; Okuda, K.; Satoh, A.; Osaki, Y.; Takeuchi, Y.; Aita, Y.; Matsuzaka, T.; Iwasaki, H.; Yatoh, S.; Sekiya, M.; Yahagi, N.; Suzuki, H.; Sone, H.; Nakagawa, Y.; Yamada, N.; Shimano, H. Intestinal CREBH Overexpression Prevents High-Cholesterol Diet-Induced Hypercholesterolemia by Reducing Npc1l1 Expression. *Mol. Metab.* **2016**, 5 (11), 1092–1102. <https://doi.org/10.1016/j.molmet.2016.09.004>.
- (83) Noam, Z.; Cynthia, H.; Rima, B.; Peter, T. LXR Regulates Cholesterol Uptake Through Idol-Dependent Ubiquitination of the LDL Receptor. *Science (80-.)*. **2009**, 325 (5936), 100–104. <https://doi.org/10.1126/science.1168974>.
- (84) Brown, M. S.; Radhakrishnan, A.; Goldstein, J. L. Retrospective on Cholesterol Homeostasis: The Central Role of Scap. *Annu. Rev. Biochem.* **2018**, 87 (1), 783–807. <https://doi.org/10.1146/annurev-biochem-062917-011852>.
- (85) Juhl, A. D.; Wüstner, D. Pathways and Mechanisms of Cellular Cholesterol Efflux—Insight From Imaging . *Frontiers in Cell and Developmental Biology* . 2022.
- (86) Wang, N.; Silver, D. L.; Thiele, C.; Tall, A. R. ATP-Binding Cassette Transporter A1 (ABCA1) Functions as a Cholesterol Efflux Regulatory Protein*. *J. Biol. Chem.* **2001**, 276 (26), 23742–23747. <https://doi.org/10.1074/jbc.M102348200>.
- (87) Olzmann, J. A.; Carvalho, P. Dynamics and Functions of Lipid Droplets. *Nat. Rev. Mol. Cell Biol.* **2019**, 20 (3), 137–155. <https://doi.org/10.1038/s41580-018-0085-z>.
- (88) Thiam, A. R.; Ikonen, E. Lipid Droplet Nucleation. *Trends Cell Biol.* **2021**, 31 (2), 108–118. <https://doi.org/10.1016/j.tcb.2020.11.006>.
- (89) Infante, R. E.; Wang, M. L.; Radhakrishnan, A.; Hyock, J. K.; Brown, M. S.; Goldstein, J. L. NPC2 Facilitates Bidirectional Transfer of Cholesterol between NPC1 and Lipid Bilayers, a Step in Cholesterol Egress from Lysosomes. *Proc. Natl. Acad. Sci. U. S. A.* **2008**, 105 (40), 15287–15292. <https://doi.org/10.1073/pnas.0807328105>.
- (90) Trinh, M. N.; Brown, M. S.; Goldstein, J. L.; Han, J.; Vale, G.; McDonald, J. G.; Seemann, J.; Mendell, J. T.; Lu, F. Last Step in the Path of LDL Cholesterol from Lysosome to Plasma Membrane to ER Is Governed by Phosphatidylserine. *Proc. Natl. Acad. Sci. U. S. A.* **2020**, 117 (31), 18521–18529. <https://doi.org/10.1073/pnas.2010682117>.
- (91) Depta, L.; Whitmarsh-Everiss, T.; Laraia, L. Structure, Function and Small Molecule Modulation of Intracellular Sterol Transport Proteins. *Bioorg. Med. Chem.* **2022**, 116856. <https://doi.org/10.1016/j.bmc.2022.116856>.
- (92) Sandhu, J.; Li, S.; Fairall, L.; Pfisterer, S. G.; Gurnett, J. E.; Xiao, X.; Weston, T. A.; Vashi, D.; Ferrari, A.; Orozco, J. L.; Hartman, C. L.; Strugatsky, D.; Lee, S. D.; He, C.; Hong, C.; Jiang, H.; Bentolila, L. A.; Gatta, A. T.; Levine, T. P.; Ferng, A.; Lee, R.; Ford, D. A.; Young, S. G.; Ikonen, E.; Schwabe, J. W. R.; Tontonoz, P. Aster Proteins Facilitate Nonvesicular Plasma Membrane to ER Cholesterol Transport in Mammalian Cells. *Cell* **2018**, 175 (2), 514-529.e20. <https://doi.org/10.1016/j.cell.2018.08.033>.
- (93) Besprozvannaya, M.; Dickson, E.; Li, H.; Ginburg, K. S.; Bers, D. M.; Auwerx, J.; Nunnari, J.

GRAM Domain Proteins Specialize Functionally Distinct ER-PM Contact Sites in Human Cells. *Elife* **2018**, 7, e31019. <https://doi.org/10.7554/eLife.31019>.

- (94) Trinh, M. N.; Brown, M. S.; Seemann, J.; Vale, G.; McDonald, J. G.; Goldstein, J. L.; Lu, F. Interplay between Asters/GRAMD1s and Phosphatidylserine in Intermembrane Transport of LDL Cholesterol. *Proc. Natl. Acad. Sci. U. S. A.* **2022**, 119 (2), e2120411119. <https://doi.org/10.1073/pnas.2120411119>.
- (95) Naito, T.; Ercan, B.; Krshnan, L.; Triebel, A.; Koh, D. H. Z.; Wei, F.-Y.; Tomizawa, K.; Torta, F. T.; Wenk, M. R.; Saheki, Y. Movement of Accessible Plasma Membrane Cholesterol by the GRAMD1 Lipid Transfer Protein Complex. *Elife* **2019**, 8, e51401. <https://doi.org/10.7554/eLife.51401>.
- (96) Ercan, B.; Naito, T.; Koh, D. H. Z.; Dharmawan, D.; Saheki, Y. Molecular Basis of Accessible Plasma Membrane Cholesterol Recognition by the GRAM Domain of GRAMD1b. *EMBO J.* **2021**, 40 (6), e106524. <https://doi.org/10.15252/emboj.2020106524>.
- (97) Sepalika, B.; Srinivasagan, R.; Sanae, I.; D., T. L.; B., S. O.; Yoshikazu, I.; Johannes, von L. Aster Proteins Mediate Carotenoid Transport in Mammalian Cells. *Proc. Natl. Acad. Sci.* **2022**, 119 (15), e2200068119. <https://doi.org/10.1073/pnas.2200068119>.
- (98) Laraia, L.; Friese, A.; Corkery, D. P.; Konstantinidis, G.; Erwin, N.; Hofer, W.; Karatas, H.; Klewer, L.; Brockmeyer, A.; Metz, M.; Schölermann, B.; Dwivedi, M.; Li, L.; Rios-Munoz, P.; Köhn, M.; Winter, R.; Vetter, I. R.; Ziegler, S.; Janning, P.; Wu, Y.-W.; Waldmann, H. The Cholesterol Transfer Protein GRAMD1A Regulates Autophagosome Biogenesis. *Nat. Chem. Biol.* **2019**, 15 (7), 710–720. <https://doi.org/10.1038/s41589-019-0307-5>.
- (99) Andersen, J.-P.; Zhang, J.; Sun, H.; Liu, X.; Liu, J.; Nie, J.; Shi, Y. Aster-B Coordinates with Arf1 to Regulate Mitochondrial Cholesterol Transport. *Mol. Metab.* **2020**, 42, 101055. <https://doi.org/10.1016/j.molmet.2020.101055>.
- (100) Zhang, J.; Andersen, J.-P.; Sun, H.; Liu, X.; Sonenberg, N.; Nie, J.; Shi, Y. Aster-C Coordinates with COP I Vesicles to Regulate Lysosomal Trafficking and Activation of MTORC1. *EMBO Rep.* **2020**, 21 (9), e49898. <https://doi.org/10.15252/embr.201949898>.
- (101) Wui Ng, M. Y.; Charsou, C.; Lapao, A.; Singh, S.; Trachsel-Moncho, L.; Nakken, S.; Munson, M. J.; Simonsen, A. GRAMD1C Regulates Autophagy Initiation and Mitochondrial Bioenergetics through ER-Mitochondria Cholesterol Transport. *bioRxiv* **2021**, 2021.08.04.455032. <https://doi.org/10.1101/2021.08.04.455032>.
- (102) Khanna, P.; Lee, J. S.; Sereemasapun, A.; Lee, H.; Baeg, G. H. GRAMD1B Regulates Cell Migration in Breast Cancer Cells through JAK/STAT and Akt Signaling. *Sci. Rep.* **2018**, 8 (1), 9511. <https://doi.org/10.1038/s41598-018-27864-6>.
- (103) Hao, H.; Wang, Z.; Ren, S.; Shen, H.; Xian, H.; Ge, W.; W, W. GRAMD1C Expression Correlates to Poor Prognosis and Immune Infiltrates in Kidney Renal Clear Cell Carcinoma. *PeerJ* **2019**. <https://doi.org/10.7717/peerj.8205>.
- (104) Burgett, A. W. G.; Poulsen, T. B.; Wangkanont, K.; Anderson, D. R.; Kikuchi, C.; Shimada, K.; Okubo, S.; Fortner, K. C.; Mimaki, Y.; Kuroda, M.; Murphy, J. P.; Schwalb, D. J.; Petrella, E. C.; Cornella-Taracido, I.; Schirle, M.; Tallarico, J. A.; Shair, M. D. Natural Products Reveal Cancer Cell Dependence on Oxysterol-Binding Proteins. *Nat. Chem. Biol.* **2011**, 7 (9), 639–647. <https://doi.org/10.1038/nchembio.625>.
- (105) Péresse, T.; Kovacs, D.; Subra, M.; Bigay, J.; Tsai, M.-C.; Polidori, J.; Gautier, R.; Desrat, S.;

- Fleuriot, L.; Debayle, D.; Litaudon, M.; Pham, V.-C.; Bignon, J.; Antonny, B.; Roussi, F.; Mesmin, B. Molecular and Cellular Dissection of the Oxysterol-Binding Protein Cycle through a Fluorescent Inhibitor. *J. Biol. Chem.* **2020**, *295* (13), 4277–4288. <https://doi.org/https://doi.org/10.1074/jbc.RA119.012012>.
- (106) Zhong, W.; Xu, M.; Li, C.; Zhu, B.; Cao, X.; Li, D.; Chen, H.; Hu, C.; Li, R.; Luo, C.; Pan, G.; Zhang, W.; Lai, C.; Wang, T.; Du, X.; Chen, H.; Xu, G.; Olkkonen, V. M.; Lei, P.; Xu, J.; Yan, D. ORP4L Extracts and Presents PIP2 from Plasma Membrane for PLC β 3 Catalysis: Targeting It Eradicates Leukemia Stem Cells. *Cell Rep.* **2019**, *26* (8), 2166–2177.e9. <https://doi.org/https://doi.org/10.1016/j.celrep.2019.01.082>.
- (107) Wright, M. B.; Varona Santos, J.; Kemmer, C.; Maugeais, C.; Carralot, J.-P.; Roevers, S.; Molina, J.; Ducasa, G. M.; Mitrofanova, A.; Sloan, A.; Ahmad, A.; Pedigo, C.; Ge, M.; Pressly, J.; Barisoni, L.; Mendez, A.; Sgrignani, J.; Cavalli, A.; Merscher, S.; Prunotto, M.; Fornoni, A. Compounds Targeting OSBPL7 Increase ABCA1-Dependent Cholesterol Efflux Preserving Kidney Function in Two Models of Kidney Disease. *Nat. Commun.* **2021**, *12* (1), 4662. <https://doi.org/10.1038/s41467-021-24890-3>.
- (108) Strating, J. R. P. M.; van der Linden, L.; Albulescu, L.; Bigay, J.; Arita, M.; Delang, L.; Leyssen, P.; van der Schaar, H. M.; Lanke, K. H. W.; Thibaut, H. J.; Ulferts, R.; Drin, G.; Schlinck, N.; Wubboldts, R. W.; Sever, N.; Head, S. A.; Liu, J. O.; Beachy, P. A.; De Matteis, M. A.; Shair, M. D.; Olkkonen, V. M.; Neyts, J.; van Kuppeveld, F. J. M. Itraconazole Inhibits Enterovirus Replication by Targeting the Oxysterol-Binding Protein. *Cell Rep.* **2015**, *10* (4), 600–615. <https://doi.org/https://doi.org/10.1016/j.celrep.2014.12.054>.
- (109) Bauer, L.; Ferla, S.; Head, S. A.; Bhat, S.; Pasunooti, K. K.; Shi, W. Q.; Albulescu, L.; Liu, J. O.; Brancale, A.; van Kuppeveld, F. J. M.; Strating, J. R. P. M. Structure-Activity Relationship Study of Itraconazole, a Broad-Range Inhibitor of Picornavirus Replication That Targets Oxysterol-Binding Protein (OSBP). *Antiviral Res.* **2018**, *156*, 55–63. <https://doi.org/https://doi.org/10.1016/j.antiviral.2018.05.010>.
- (110) Xiao, X.; Kim, Y.; Romartinez-Alonso, B.; Sirvydis, K.; Ory, D. S.; Schwabe, J. W. R.; Jung, M. E.; Tontonoz, P. Selective Aster Inhibitors Distinguish Vesicular and Nonvesicular Sterol Transport Mechanisms. *Proc. Natl. Acad. Sci.* **2021**, *118* (2), e2024149118. <https://doi.org/10.1073/pnas.2024149118>.
- (111) Lapillo, M.; Salis, B.; Palazzolo, S.; Poli, G.; Granchi, C.; Minutolo, F.; Rotondo, R.; Caligiuri, I.; Canzonieri, V.; Tuccinardi, T.; Rizzolio, F. First-of-Its-Kind STARD3 Inhibitor: In Silico Identification and Biological Evaluation as Anticancer Agent. *ACS Med. Chem. Lett.* **2019**, *10* (4), 475–480. <https://doi.org/10.1021/acsmedchemlett.8b00509>.
- (112) Wagle, N.; Xian, J.; Shishova, E. Y.; Wei, J.; Glicksman, M. A.; Cuny, G. D.; Stein, R. L.; Cohen, D. E. Small-Molecule Inhibitors of Phosphatidylcholine Transfer Protein/StarD2 Identified by High-Throughput Screening. *Anal. Biochem.* **2008**, *383* (1), 85–92. <https://doi.org/https://doi.org/10.1016/j.ab.2008.07.039>.
- (113) Samaha, D.; Hamdo, H. H.; Cong, X.; Schumacher, F.; Banhart, S.; Aglar, Ö.; Möller, H. M.; Heuer, D.; Kleuser, B.; Saied, E. M.; Arenz, C. Liposomal FRET Assay Identifies Potent Drug-Like Inhibitors of the Ceramide Transport Protein (CERT). *Chemistry* **2020**, *26* (70), 16616–16621. <https://doi.org/10.1002/chem.202003283>.
- (114) Whitmarsh-Everiss, T.; Olsen, A. H.; Laraia, L. Identification of Inhibitors of Cholesterol Transport Proteins Through the Synthesis of a Diverse, Sterol-Inspired Compound Collection. *Angew. Chemie - Int. Ed.* **2021**, *60* (51), 26755–26761. <https://doi.org/10.1002/anie.202111639>.

- (115) Bukiya, A. N.; Dopico, A. M. Common Structural Features of Cholesterol Binding Sites in Crystallized Soluble Proteins. *J. Lipid Res.* **2017**, *58* (6), 1044–1054. <https://doi.org/https://doi.org/10.1194/jlr.R073452>.
- (116) Foley, D. J.; Waldmann, H. Ketones as Strategic Building Blocks for the Synthesis of Natural Product-Inspired Compounds. *Chem. Soc. Rev.* **2022**. <https://doi.org/10.1039/D2CS00101B>.
- (117) Hulce, J. J.; Cognetta, A. B.; Niphakis, M. J.; Tully, S. E.; Cravatt, B. F. Proteome-Wide Mapping of Cholesterol-Interacting Proteins in Mammalian Cells. *Nat. Methods* **2013**, *10* (3), 259–264. <https://doi.org/10.1038/nmeth.2368>.
- (118) Bradshaw, B.; Bonjoch, J. The Wieland-Miescher Ketone: A Journey from Organocatalysis to Natural Product Synthesis. *Synlett* **2012**, *3*, 337–356. <https://doi.org/10.1055/s-0031-1290107>.
- (119) Kametani, T.; Suzuki, K.; Nemoto, H. Asymmetric Synthesis of (-)-3.β-Hydroxy-17-Methoxy-D-Homo-18-nor-5.α.-Androsta-13,15,17-Triene. *J. Org. Chem.* **1980**, *45* (11), 2204–2207. <https://doi.org/10.1021/jo01299a033>.
- (120) Brown, E.; Lebreton, J. Une Synthèse Totale Stéréospécifique de C-nor d-Homostéroïdes Comportant Six Carbones Asymétriques. *Tetrahedron* **1987**, *43* (24), 5827–5840. [https://doi.org/https://doi.org/10.1016/S0040-4020\(01\)87789-9](https://doi.org/https://doi.org/10.1016/S0040-4020(01)87789-9).
- (121) Bradshaw, B.; Etxebarria-Jardi, G.; Bonjoch, J.; Vióquez, S. F.; Guillena, G.; Nájera, C. Efficient Solvent-Free Robinson Annulation Protocols for the Highly Enantioselective Synthesis of the Wieland–Miescher Ketone and Analogues. *Adv. Synth. Catal.* **2009**, *351* (14-15), 2482–2490. <https://doi.org/10.1002/adsc.200900321>.
- (122) Vióquez, S. F.; Guillena, G.; Nájera, C.; Bradshaw, B.; Etxebarria-Jardi, G.; Bonjoch, J. (Sa,S)-N-[2'-(4-METHYLPHENYLSULFONAMIDO)-1,1'-BINAPHTHYL-2-YL]PYRROLIDINE-2-CARBOXAMIDE: AN ORGANOCATALYST FOR THE DIRECT ALDOL REACTION. *Org. Synth.* **2011**, *88*, 317–329.
- (123) Ciceri, P.; Demnitz, F. W. J. An Efficient, Rapid and Highly Selective Preparation of the Wieland-Miescher Ketone-9-Ethylene Ketal. *Tetrahedron Lett.* **1997**, *38* (3), 389–390. [https://doi.org/10.1016/S0040-4039\(96\)02334-9](https://doi.org/10.1016/S0040-4039(96)02334-9).
- (124) Soai, K.; Ohi, K. Stereoselectivity in the Reduction of Cyclic Ketones with Sodium Borohydride. Effect of the Ratio of the Components of a Mixed Solvent of Tetrahydrofuran and Methanol. *Bull. Chem. Soc. Jpn.* **1985**, *58* (5), 1601–1602. <https://doi.org/10.1246/bcsj.58.1601>.
- (125) Protection for the Hydroxyl Group, Including 1,2- and 1,3-Diols. *Greene's Protective Groups in Organic Synthesis*. October 20, 2006, pp 16–366. <https://doi.org/https://doi.org/10.1002/9780470053485.ch2>.
- (126) Crabtree, S. R.; Chu, W. L. A.; Mander, L. N. C-Acylation of Enolates by Methyl Cyanoformate: An Examination of Site- and Stereoselectivity. *Synlett* **1990**, *3*, 169–170.
- (127) Li, A.-H.; Ahmed, E.; Chen, X.; Cox, M.; Crew, A. P.; Dong, H.-Q.; Jin, M.; Ma, L.; Panicker, B.; Siu, K. W.; Steinig, A. G.; Stolz, K. M.; Tavares, P. A. R.; Volk, B.; Weng, Q.; Werner, D.; Mulvihill, M. J. A Highly Effective One-Pot Synthesis of Quinolines from o-Nitroarylcarbaldehydes. *Org. Biomol. Chem.* **2007**, *5* (1), 61–64. <https://doi.org/10.1039/B613775J>.
- (128) Campbell, N.; McCall, E. B. 558. The Preparation of Tetrahydrocarbazoles from 2-Chloro-Cyclohexanone. *J. Chem. Soc.* **1950**, No. 0, 2870–2874. <https://doi.org/10.1039/JR9500002870>.

- (129) CAMPAIGNE, E.; LAKE, R. D. Synthesis of Tetrahydrocarbazoles and Carbazoles by the Bischler Reaction^{1,2}. *J. Org. Chem.* **1959**, 24 (4), 478–487. <https://doi.org/10.1021/jo01086a010>.
- (130) Kelly, A. H.; Parrick, J. AZAINDOLES: I. PREPARATION OF 7-AZAINDOLES BY THERMAL INDOLIZATION OF 2-PYRIDYLHYDRAZONES. *Can. J. Chem.* **1966**, 44 (21), 2455–2459. <https://doi.org/10.1139/v66-370>.
- (131) Jeanty, M.; Blu, J.; Suzenet, F.; Guillaumet, G. Synthesis of 4- and 6-Azaindoles via the Fischer Reaction. *Org. Lett.* **2009**, 11 (22), 5142–5145. <https://doi.org/10.1021/ol902139r>.
- (132) Yokoyama, N.; Arai, T. Asymmetric Friedel–Crafts Reaction of N-Heterocycles and Nitroalkenes Catalyzed by Imidazoline–Aminophenol–Cu Complex. *Chem. Commun.* **2009**, No. 22, 3285–3287. <https://doi.org/10.1039/B904275J>.
- (133) Liu, F.; Yu, L.-Q.; Jiang, C.; Yang, L.; Wu, W.-T.; You, Q.-D. Discovery of Tetrahydro- β -Carbolines as Inhibitors of the Mitotic Kinesin KSP. *Bioorg. Med. Chem.* **2010**, 18 (12), 4167–4177. <https://doi.org/https://doi.org/10.1016/j.bmc.2010.05.024>.
- (134) Beasley, B. O.; Alli-Balogun, A.; Clarkson, G. J.; Shipman, M. Pictet–Spengler Reactions of Oxetan-3-Ones and Related Heterocycles. *Tetrahedron Lett.* **2014**, 55 (2), 541–543. <https://doi.org/https://doi.org/10.1016/j.tetlet.2013.11.077>.
- (135) Miller, M. M.; Banville, J.; Friends, T. J.; Gagnon, M.; Hangeland, J. J.; Lavallée, J.-F.; Martel, A.; O’Grady, H.; Rémillard, R.; Ruediger, E.; Tremblay, F.; Posy, S. L.; Allegretto, N. J.; Guarino, V. R.; Harden, D. G.; Harper, T. W.; Hartl, K.; Josephs, J.; Malmstrom, S.; Watson, C.; Yang, Y.; Zhang, G.; Wong, P.; Yang, J.; Bouvier, M.; Seiffert, D. A.; Wexler, R. R.; Lawrence, R. M.; Priestley, E. S.; Marinier, A. Discovery of Potent Protease-Activated Receptor 4 Antagonists with in Vivo Antithrombotic Efficacy. *J. Med. Chem.* **2019**, 62 (16), 7400–7416. <https://doi.org/10.1021/acs.jmedchem.9b00186>.
- (136) Paquette, L. A.; Sun, L.-Q.; Friedrich, D.; Savage, P. B. Total Synthesis of (+)-Epoxydictymene. Application of Alkoxy-Directed Cyclization to Diterpenoid Construction. *J. Am. Chem. Soc.* **1997**, 119 (36), 8438–8450. <https://doi.org/10.1021/ja971526v>.
- (137) JIANG, X.; VISNICK, M.; BENDER, C. F.; BOLTON, G.; CAPRATHE, B.; LEE, C.; KORNBERG, B.; O’BRIEN, P.; HOTEMA, M. R. PYRAZOLE AND IMIDAZOLE COMPOUNDS FOR INHIBITION OF IL-17 AND ROR γ , 2019.
- (138) Shultz, M. D.; Cheung, A. K.; Kirby, C. A.; Firestone, B.; Fan, J.; Chen, C. H.-T.; Chen, Z.; Chin, D. N.; DiPietro, L.; Fazal, A.; Feng, Y.; Fortin, P. D.; Gould, T.; Lagu, B.; Lei, H.; Lenoir, F.; Majumdar, D.; Ochala, E.; Palermo, M. G.; Pham, L.; Pu, M.; Smith, T.; Stams, T.; Tomlinson, R. C.; Touré, B. B.; Visser, M.; Wang, R. M.; Waters, N. J.; Shao, W. Identification of NVP-TNKS656: The Use of Structure–Efficiency Relationships To Generate a Highly Potent, Selective, and Orally Active Tankyrase Inhibitor. *J. Med. Chem.* **2013**, 56 (16), 6495–6511. <https://doi.org/10.1021/jm400807n>.
- (139) Ertl, P.; Roggo, S.; Schuffenhauer, A. Natural Product-Likeness Score and Its Application for Prioritization of Compound Libraries. *J. Chem. Inf. Model.* **2008**, 48 (1), 68–74. <https://doi.org/10.1021/ci700286x>.
- (140) Vanii Jayaseelan, K.; Moreno, P.; Truszkowski, A.; Ertl, P.; Steinbeck, C. Natural Product-Likeness Score Revisited: An Open-Source, Open-Data Implementation. *BMC Bioinformatics* **2012**, 13 (1), 106. <https://doi.org/10.1186/1471-2105-13-106>.
- (141) Wishart, D. S.; Feunang, Y. D.; Guo, A. C.; Lo, E. J.; Marcu, A.; Grant, J. R.; Sajed, T.; Johnson,

- D.; Li, C.; Sayeeda, Z.; Assempour, N.; Iynkkaran, I.; Liu, Y.; Maciejewski, A.; Gale, N.; Wilson, A.; Chin, L.; Cummings, R.; Le, D.; Pon, A.; Knox, C.; Wilson, M. DrugBank 5.0: A Major Update to the DrugBank Database for 2018. *Nucleic Acids Res.* **2018**, *46* (D1), D1074–D1082. <https://doi.org/10.1093/nar/gkx1037>.
- (142) Colomer, I.; Empson, C. J.; Craven, P.; Owen, Z.; Doveston, R. G.; Churcher, I.; Marsden, S. P.; Nelson, A. A Divergent Synthetic Approach to Diverse Molecular Scaffolds: Assessment of Lead-Likeness Using LLAMA, an Open-Access Computational Tool. *Chem. Commun.* **2016**, *52* (45), 7209–7212. <https://doi.org/10.1039/C6CC03244C>.
- (143) Weiss, W. A.; Taylor, S. S.; Shokat, K. M. Recognizing and Exploiting Differences between RNAi and Small-Molecule Inhibitors. *Nat. Chem. Biol.* **2007**, *3* (12), 739–744. <https://doi.org/10.1038/nchembio1207-739>.
- (144) Niesen, F. H.; Berglund, H.; Vedadi, M. The Use of Differential Scanning Fluorimetry to Detect Ligand Interactions That Promote Protein Stability. *Nat. Protoc.* **2007**, *2* (9), 2212–2221. <https://doi.org/10.1038/nprot.2007.321>.
- (145) Ciulli, A. Biophysical Screening for the Discovery of Small-Molecule Ligands. *Methods Mol. Biol.* **2013**, *1008*, 357–388. https://doi.org/10.1007/978-1-62703-398-5_13.
- (146) Lo, M.-C.; Aulabaugh, A.; Jin, G.; Cowling, R.; Bard, J.; Malamas, M.; Ellestad, G. Evaluation of Fluorescence-Based Thermal Shift Assays for Hit Identification in Drug Discovery. *Anal. Biochem.* **2004**, *332* (1), 153–159. <https://doi.org/https://doi.org/10.1016/j.ab.2004.04.031>.
- (147) Lea, W. A.; Simeonov, A. Fluorescence Polarization Assays in Small Molecule Screening. *Expert Opin. Drug Discov.* **2011**, *6* (1), 17–32. <https://doi.org/10.1517/17460441.2011.537322>.
- (148) Hall, M. D.; Yasgar, A.; Peryea, T.; Braisted, J. C.; Jadhav, A.; Simeonov, A.; Coussens, N. P. Fluorescence Polarization Assays in High-Throughput Screening and Drug Discovery: A Review. *Methods Appl. Fluoresc.* **2016**, *4* (2), 22001. <https://doi.org/10.1088/2050-6120/4/2/022001>.
- (149) Moerke, N. J. Fluorescence Polarization (FP) Assays for Monitoring Peptide-Protein or Nucleic Acid-Protein Binding. *Curr. Protoc. Chem. Biol.* **2009**, *1* (1), 1–15. <https://doi.org/https://doi.org/10.1002/9780470559277.ch090102>.
- (150) Pedrosa, R.; Andrés, J. M.; Manzano, R.; Pérez-López, C. Novel Supported and Unsupported Prolinamides as Organocatalysts for Enantioselective Cyclization of Triketones. *Tetrahedron Lett.* **2013**, *54* (24), 3101–3104. <https://doi.org/https://doi.org/10.1016/j.tetlet.2013.03.123>.
- (151) An, H.; Eum, S.-J.; Koh, M.; Lee, S. K.; Park, S. B. Diversity-Oriented Synthesis of Privileged Benzopyranyl Heterocycles from s-Cis-Enones. *J. Org. Chem.* **2008**, *73* (5), 1752–1761. <https://doi.org/10.1021/jo702196f>.
- (152) Clegg, R. M. Fluorescence Resonance Energy Transfer. *Curr. Opin. Biotechnol.* **1995**, *6* (1), 103–110. [https://doi.org/https://doi.org/10.1016/0958-1669\(95\)80016-6](https://doi.org/https://doi.org/10.1016/0958-1669(95)80016-6).
- (153) Selvin, P. R. The Renaissance of Fluorescence Resonance Energy Transfer. *Nat. Struct. Biol.* **2000**, *7* (9), 730–734. <https://doi.org/10.1038/78948>.
- (154) Beebe, T. R.; Lin, A. L.; Miller, R. D. Reaction of N-Iodosuccinimide with Secondary Alcohols. *J. Org. Chem.* **1974**, *39* (5), 722–724. <https://doi.org/10.1021/jo00919a035>.
- (155) Williams, D. R.; Sakdarat, S. Opportunities for Selective Removal of Methoxyethoxymethyl (Mem) Ethers. *Tetrahedron Lett.* **1983**, *24* (37), 3965–3968. [https://doi.org/https://doi.org/10.1016/S0040-4039\(00\)88237-4](https://doi.org/https://doi.org/10.1016/S0040-4039(00)88237-4).

- (156) Tanwar, L.; Börgel, J.; Lehmann, J.; Ritter, T. Selective C–H Iodination of (Hetero)Arenes. *Org. Lett.* **2021**, 23 (13), 5024–5027. <https://doi.org/10.1021/acs.orglett.1c01530>.
- (157) Galloway, J. D.; Mai, D. N.; Baxter, R. D. Silver-Catalyzed Minisci Reactions Using Selectfluor as a Mild Oxidant. *Org. Lett.* **2017**, 19 (21), 5772–5775. <https://doi.org/10.1021/acs.orglett.7b02706>.
- (158) Seiple, I. B.; Su, S.; Rodriguez, R. A.; Gianatassio, R.; Fujiwara, Y.; Sobel, A. L.; Baran, P. S. Direct C–H Arylation of Electron-Deficient Heterocycles with Arylboronic Acids. *J. Am. Chem. Soc.* **2010**, 132 (38), 13194–13196. <https://doi.org/10.1021/ja1066459>.
- (159) Lyga, J. W.; Henrie II, R. N.; Meier, G. A.; Creekmore, R. W.; Patera, R. M. ‘Through-Space’ Hydrogen–Fluorine, Carbon–Fluorine and Fluorine–Fluorine Spin–Spin Coupling in 2-Phenyl-3-Alkyl-4,5,6,7-Tetrahydroindazoles. *Magn. Reson. Chem.* **1993**, 31 (4), 323–328. <https://doi.org/https://doi.org/10.1002/mrc.1260310402>.
- (160) Whitmarsh-Everiss, T.; Laraia, L. Small Molecule Probes for Targeting Autophagy. *Nat. Chem. Biol.* **2021**, 17 (6), 653–664. <https://doi.org/10.1038/s41589-021-00768-9>.
- (161) Li, W.; Li, J.; Bao, J. Microautophagy: Lesser-Known Self-Eating. *Cell. Mol. Life Sci.* **2012**, 69 (7), 1125–1136. <https://doi.org/10.1007/s00018-011-0865-5>.
- (162) Kaushik, S.; Bandyopadhyay, U.; Sridhar, S.; Kiffin, R.; Martinez-Vicente, M.; Kon, M.; Orenstein, S. J.; Wong, E.; Cuervo, A. M. Chaperone-Mediated Autophagy at a Glance. *J. Cell Sci.* **2011**, 124 (4), 495 LP – 499. <https://doi.org/10.1242/jcs.073874>.
- (163) Hurley, J. H.; Young, L. N. Mechanisms of Autophagy Initiation. *Annu. Rev. Biochem.* **2017**, 86 (1), 225–244. <https://doi.org/10.1146/annurev-biochem-061516-044820>.
- (164) Tanida, I.; Ueno, T.; Kominami, E. LC3 Conjugation System in Mammalian Autophagy. *Int. J. Biochem. Cell Biol.* **2004**, 36 (12), 2503–2518. <https://doi.org/https://doi.org/10.1016/j.biocel.2004.05.009>.
- (165) Lőrincz, P.; Juhász, G. Autophagosome-Lysosome Fusion. *J. Mol. Biol.* **2020**, 432 (8), 2462–2482. <https://doi.org/https://doi.org/10.1016/j.jmb.2019.10.028>.
- (166) Klionsky, D. J.; Abdel-Aziz, A. K.; Abdelfatah, S.; Abdellatif, M.; Abdoli, A.; Abel, S.; Abeliovich, H.; Abildgaard, M. H.; Abudu, Y. P.; Acevedo-Arozena, A.; Adamopoulos, I. E.; Adeli, K.; Adolph, T. E.; Adornetto, A.; Aflaki, E.; Agam, G.; Agarwal, A.; Aggarwal, B. B.; Agnello, M.; Agostinis, P.; Agrewala, J. N.; Agrotis, A.; Aguilar, P. V.; Ahmad, S. T.; Ahmed, Z. M.; Ahumada-Castro, U.; Aits, S.; Aizawa, S.; Akkoc, Y.; Akoumianaki, T.; Akpinar, H. A.; Al-Abd, A. M.; Al-Akra, L.; Al-Gharaibeh, A.; Alaoui-Jamali, M. A.; Alberti, S.; Alcocer-Gómez, E.; Alessandri, C.; Ali, M.; Alim Al-Bari, M. A.; Aliwaini, S.; Alizadeh, J.; Almacellas, E.; Almasan, A.; Alonso, A.; Alonso, G. D.; Altan-Bonnet, N.; Altieri, D. C.; Álvarez, É. M. C.; Alves, S.; Alves da Costa, C.; Alzaharna, M. M.; Amadio, M.; Amantini, C.; Amaral, C.; Ambrosio, S.; Amer, A. O.; Ammanathan, V.; An, Z.; Andersen, S. U.; Andrabi, S. A.; Andrade-Silva, M.; Andres, A. M.; Angelini, S.; Ann, D.; Anozie, U. C.; Ansari, M. Y.; Antas, P.; Antebi, A.; Antón, Z.; Anwar, T.; Apetoh, L.; Apostolova, N.; Araki, T.; Araki, Y.; Arasaki, K.; Araújo, W. L.; Araya, J.; Arden, C.; Arévalo, M.-A.; Arguelles, S.; Arias, E.; Arikath, J.; Arimoto, H.; Ariosa, A. R.; Armstrong-James, D.; Arnauné-Pelloquin, L.; Aroca, A.; Arroyo, D. S.; Arsov, I.; Artero, R.; Asaro, D. M. L.; Aschner, M.; Ashrafizadeh, M.; Ashur-Fabian, O.; Atanasov, A. G.; Au, A. K.; Auberger, P.; Auner, H. W.; Aurelian, L.; Autelli, R.; Avagliano, L.; Ávalos, Y.; Aveic, S.; Aveleira, C. A.; Avin-Wittenberg, T.; Aydin, Y.; Ayton, S.; Ayyadevara, S.; Azzopardi, M.; Baba, M.; Backer, J. M.; Backues, S. K.; Bae, D.-H.; Bae, O.-N.; Bae, S. H.; Baehrecke, E. H.; Baek, A.;

Baek, S.-H.; Baek, S. H.; Bagetta, G.; Bagniewska-Zadworna, A.; Bai, H.; Bai, J.; Bai, X.; Bai, Y.; Bairagi, N.; Baksi, S.; Balbi, T.; Baldari, C. T.; Balduini, W.; Ballabio, A.; Ballester, M.; Balazadeh, S.; Balzan, R.; Bandopadhyay, R.; Banerjee, S.; Banerjee, S.; Bánréti, Á.; Bao, Y.; Baptista, M. S.; Baracca, A.; Barbati, C.; Bargiela, A.; Barilà, D.; Barlow, P. G.; Barmada, S. J.; Barreiro, E.; Barreto, G. E.; Bartek, J.; Bartel, B.; Bartolome, A.; Barve, G. R.; Basagoudanavar, S. H.; Bassham, D. C.; Bast, R. C.; Basu, A.; Batoko, H.; Batten, I.; Baulieu, E. E.; Baumgarner, B. L.; Bayry, J.; Beale, R.; Beau, I.; Beaumatin, F.; Bechara, L. R. G.; Beck, G. R.; Beers, M. F.; Begun, J.; Behrends, C.; Behrens, G. M. N.; Bei, R.; Bejarano, E.; Bel, S.; Behl, C.; Belaid, A.; Belgareh-Touzé, N.; Bellarosa, C.; Belleudi, F.; Belló Pérez, M.; Bello-Morales, R.; Beltran, J. S. de O.; Beltran, S.; Benbrook, D. M.; Bendorius, M.; Benitez, B. A.; Benito-Cuesta, I.; Bensalem, J.; Berchtold, M. W.; Berezowska, S.; Bergamaschi, D.; Bergami, M.; Bergmann, A.; Berliocchi, L.; Berlioz-Torrent, C.; Bernard, A.; Berthoux, L.; Besirli, C. G.; Besteiro, S.; Betin, V. M.; Beyaert, R.; Bezbradica, J. S.; Bhaskar, K.; Bhatia-Kissova, I.; Bhattacharya, R.; Bhattacharya, S.; Bhattacharyya, S.; Bhuiyan, M. S.; Bhutia, S. K.; Bi, L.; Bi, X.; Biden, T. J.; Bijian, K.; Billes, V. A.; Binart, N.; Bincoletto, C.; Birgisdottir, A. B.; Bjorkoy, G.; Blanco, G.; Blas-Garcia, A.; Blasiak, J.; Blomgran, R.; Blomgren, K.; Blum, J. S.; Boada-Romero, E.; Boban, M.; Boesze-Battaglia, K.; Boeuf, P.; Boland, B.; Bomont, P.; Bonaldo, P.; Bonam, S. R.; Bonfili, L.; Bonifacino, J. S.; Boone, B. A.; Bootman, M. D.; Bordi, M.; Borner, C.; Bornhauser, B. C.; Borthakur, G.; Bosch, J.; Bose, S.; Botana, L. M.; Botas, J.; Boulanger, C. M.; Boulton, M. E.; Bourdenx, M.; Bourgeois, B.; Bourke, N. M.; Bousquet, G.; Boya, P.; Bozhkov, P. V.; Bozi, L. H. M.; Bozkurt, T. O.; Brackney, D. E.; Brandts, C. H.; Braun, R. J.; Braus, G. H.; Bravo-Sagua, R.; Bravo-San Pedro, J. M.; Brest, P.; Bringer, M.-A.; Briones-Herrera, A.; Broaddus, V. C.; Brodersen, P.; Brodsky, J. L.; Brody, S. L.; Bronson, P. G.; Bronstein, J. M.; Brown, C. N.; Brown, R. E.; Brum, P. C.; Brumell, J. H.; Brunetti-Pierri, N.; Bruno, D.; Bryson-Richardson, R. J.; Bucci, C.; Buchrieser, C.; Bueno, M.; Buitrago-Molina, L. E.; Buraschi, S.; Buch, S.; Buchan, J. R.; Buckingham, E. M.; Budak, H.; Budini, M.; Bultynck, G.; Burada, F.; Burgoyne, J. R.; Burón, M. I.; Bustos, V.; Büttner, S.; Butturini, E.; Byrd, A.; Cabas, I.; Cabrera-Benitez, S.; Cadwell, K.; Cai, J.; Cai, L.; Cai, Q.; Cairó, M.; Calbet, J. A.; Caldwell, G. A.; Caldwell, K. A.; Call, J. A.; Calvani, R.; Calvo, A. C.; Calvo-Rubio Barrera, M.; Camara, N. O. S.; Camonis, J. H.; Camougrand, N.; Campanella, M.; Campbell, E. M.; Campbell-Valois, F.-X.; Campello, S.; Campesi, I.; Campos, J. C.; Camuzard, O.; Cancino, J.; Candido de Almeida, D.; Canesi, L.; Caniggia, I.; Canonico, B.; Cantí, C.; Cao, B.; Caraglia, M.; Caramés, B.; Carchman, E. H.; Cardenal-Muñoz, E.; Cardenas, C.; Cardenas, L.; Cardoso, S. M.; Carew, J. S.; Carle, G. F.; Carleton, G.; Carloni, S.; Carmona-Gutierrez, D.; Carneiro, L. A.; Carnevali, O.; Carosi, J. M.; Carra, S.; Carrier, A.; Carrier, L.; Carroll, B.; Carter, A. B.; Carvalho, A. N.; Casanova, M.; Casas, C.; Casas, J.; Cassioli, C.; Castillo, E. F.; Castillo, K.; Castillo-Lluva, S.; Castoldi, F.; Castori, M.; Castro, A. F.; Castro-Caldas, M.; Castro-Hernandez, J.; Castro-Obregon, S.; Catz, S. D.; Cavadas, C.; Cavaliere, F.; Cavallini, G.; Cavinato, M.; Cayuela, M. L.; Cebollada Rica, P.; Cecarini, V.; Cecconi, F.; Cechowska-Pasko, M.; Cenci, S.; Ceperuelo-Mallafré, V.; Cerqueira, J. J.; Cerutti, J. M.; Cervia, D.; Cetintas, V. B.; Cetrullo, S.; Chae, H.-J.; Chagin, A. S.; Chai, C.-Y.; Chakrabarti, G.; Chakrabarti, O.; Chakraborty, T.; Chakraborty, T.; Chami, M.; Chamilos, G.; Chan, D. W.; Chan, E. Y. W.; Chan, E. D.; Chan, H. Y. E.; Chan, H. H.; Chan, H.; Chan, M. T. V.; Chan, Y. S.; Chandra, P. K.; Chang, C.-P.; Chang, C.; Chang, H.-C.; Chang, K.; Chao, J.; Chapman, T.; Charlet-Berguerand, N.; Chatterjee, S.; Chaube, S. K.; Chaudhary, A.; Chauhan, S.; Chaum, E.; Checler, F.; Cheetham, M. E.; Chen, C.-S.; Chen, G.-C.; Chen, J.-F.; Chen, L. L.; Chen, L.; Chen, L.; Chen, M.; Chen, M.-K.; Chen, N.; Chen, Q.; Chen, R.-H.; Chen, S.; Chen, W.; Chen, W.; Chen, X.-M.; Chen, X.-W.; Chen, X.; Chen, Y.; Chen, Y.-G.; Chen, Y.; Chen, Y.; Chen, Y.-J.; Chen, Y.-Q.; Chen, Z. S.; Chen, Z.; Chen, Z.-H.; Chen, Z. J.; Chen, Z.; Cheng, H.; Cheng, J.; Cheng, S.-Y.; Cheng, W.; Cheng, X.; Cheng, X.-T.; Cheng, Y.; Cheng, Z.; Chen, Z.; Cheong, H.; Cheong, J. K.; Chernyak, B. V.; Cherry, S.; Cheung, C. F. R.; Cheung, C. H. A.; Cheung, K.-H.; Chevet, E.; Chi, R. J.; Chiang, A. K. S.; Chiaradonna, F.; Chiarelli, R.; Chiariello, M.; Chica, N.;

Chiocca, S.; Chiong, M.; Chiou, S.-H.; Chiramel, A. I.; Chiurchiù, V.; Cho, D.-H.; Choe, S.-K.; Choi, A. M. K.; Choi, M. E.; Choudhury, K. R.; Chow, N. S.; Chu, C. T.; Chua, J. P.; Chua, J. J. E.; Chung, H.; Chung, K. P.; Chung, S.; Chung, S.-H.; Chung, Y.-L.; Cianfanelli, V.; Ciechomska, I. A.; Cifuentes, M.; Cinque, L.; Cirak, S.; Cirone, M.; Clague, M. J.; Clarke, R.; Clementi, E.; Coccia, E. M.; Codogno, P.; Cohen, E.; Cohen, M. M.; Colasanti, T.; Colasuonno, F.; Colbert, R. A.; Colell, A.; Čolić, M.; Coll, N. S.; Collins, M. O.; Colombo, M. I.; Colón-Ramos, D. A.; Combaret, L.; Comincini, S.; Cominetti, M. R.; Consiglio, A.; Conte, A.; Conti, F.; Contu, V. R.; Cookson, M. R.; Coombs, K. M.; Coppens, I.; Corasaniti, M. T.; Corkery, D. P.; Cordes, N.; Cortese, K.; Costa, M. do C.; Costantino, S.; Costelli, P.; Coto-Montes, A.; Crack, P. J.; Crespo, J. L.; Criollo, A.; Crippa, V.; Cristofani, R.; Csizmadia, T.; Cuadrado, A.; Cui, B.; Cui, J.; Cui, Y.; Cui, Y.; Culetto, E.; Cumino, A. C.; Cybulsky, A. V.; Czaja, M. J.; Czuczwar, S. J.; D'Adamo, S.; D'Amelio, M.; D'Arcangelo, D.; D'Lugos, A. C.; D'Orazi, G.; da Silva, J. A.; Dafsari, H. S.; Dagda, R. K.; Dagdas, Y.; Daglia, M.; Dai, X.; Dai, Y.; Dai, Y.; Dal Col, J.; Dalhaimer, P.; Dalla Valle, L.; Dallenga, T.; Dalmasso, G.; Damme, M.; Dando, I.; Dantuma, N. P.; Darling, A. L.; Das, H.; Dasarathy, S.; Dasari, S. K.; Dash, S.; Daumke, O.; Dauphinee, A. N.; Davies, J. S.; Dávila, V. A.; Davis, R. J.; Davis, T.; Dayalan Naidu, S.; De Amicis, F.; De Bosscher, K.; De Felice, F.; De Franceschi, L.; De Leonibus, C.; de Mattos Barbosa, M. G.; De Meyer, G. R. Y.; De Milito, A.; De Nunzio, C.; De Palma, C.; De Santi, M.; De Virgilio, C.; De Zio, D.; Debnath, J.; DeBosch, B. J.; Decuypere, J.-P.; Deehan, M. A.; Deflorian, G.; DeGregori, J.; Dehay, B.; Del Rio, G.; Delaney, J. R.; Delbridge, L. M. D.; Delorme-Axford, E.; Delpino, M. V.; Demarchi, F.; Dembitz, V.; Demers, N. D.; Deng, H.; Deng, Z.; Dengjel, J.; Dent, P.; Denton, D.; DePamphilis, M. L.; Der, C. J.; Deretic, V.; Descoteaux, A.; Devis, L.; Devkota, S.; Devuyt, O.; Dewson, G.; Dharmasivam, M.; Dhiman, R.; di Bernardo, D.; Di Cristina, M.; Di Domenico, F.; Di Fazio, P.; Di Fonzo, A.; Di Guardo, G.; Di Guglielmo, G. M.; Di Leo, L.; Di Malta, C.; Di Nardo, A.; Di Rienzo, M.; Di Sano, F.; Diallinas, G.; Diao, J.; Diaz-Araya, G.; Díaz-Laviada, I.; Dickinson, J. M.; Diederich, M.; Dieudé, M.; Dikic, I.; Ding, S.; Ding, W.-X.; Dini, L.; Dinić, J.; Dinic, M.; Dinkova-Kostova, A. T.; Dionne, M. S.; Distler, J. H. W.; Diwan, A.; Dixon, I. M. C.; Djavaheri-Mergny, M.; Dobrinski, I.; Dobrovinskaya, O.; Dobrowolski, R.; Dobson, R. C. J.; Đokić, J.; Dokmeci Emre, S.; Donadelli, M.; Dong, B.; Dong, X.; Dong, Z.; Dorn, G. W.; Dotsch, V.; Dou, H.; Dou, J.; Dowaidar, M.; Dridi, S.; Drucker, L.; Du, A.; Du, C.; Du, G.; Du, H.-N.; Du, L.-L.; du Toit, A.; Duan, S.-B.; Duan, X.; Duarte, S. P.; Dubrovskaya, A.; Dunlop, E. A.; Dupont, N.; Durán, R. V.; Dwarakanath, B. S.; Dyshlovoy, S. A.; Ebrahimi-Fakhari, D.; Eckhart, L.; Edelstein, C. L.; Efferth, T.; Eftekharpour, E.; Eichinger, L.; Eid, N.; Eisenberg, T.; Eissa, N. T.; Eissa, S.; Ejarque, M.; El Andaloussi, A.; El-Hage, N.; El-Naggar, S.; Eleuteri, A. M.; El-Shafey, E. S.; Elgendy, M.; Eliopoulos, A. G.; Elizalde, M. M.; Elks, P. M.; Elsasser, H.-P.; Elsherbiny, E. S.; Emerling, B. M.; Emre, N. C. T.; Eng, C. H.; Engedal, N.; Engelbrecht, A.-M.; Engelsens, A. S. T.; Enserink, J. M.; Escalante, R.; Esclatine, A.; Escobar-Henriques, M.; Eskelinen, E.-L.; Espert, L.; Eusebio, M.-O.; Fabrias, G.; Fabrizi, C.; Facchiano, A.; Facchiano, F.; Fadeel, B.; Fader, C.; Faesen, A. C.; Fairlie, W. D.; Falcó, A.; Falkenburger, B. H.; Fan, D.; Fan, J.; Fan, Y.; Fang, E. F.; Fang, Y.; Fang, Y.; Fanto, M.; Farfel-Becker, T.; Faure, M.; Fazeli, G.; Fedele, A. O.; Feldman, A. M.; Feng, D.; Feng, J.; Feng, L.; Feng, Y.; Feng, Y.; Feng, W.; Fenz Araujo, T.; Ferguson, T. A.; Fernández, Á. F.; Fernandez-Checa, J. C.; Fernández-Veledo, S.; Fernie, A. R.; Ferrante, A. W.; Ferraresi, A.; Ferrari, M. F.; Ferreira, J. C. B.; Ferro-Novick, S.; Figueras, A.; Filadi, R.; Filigheddu, N.; Filippi-Chiela, E.; Filomeni, G.; Fimia, G. M.; Fineschi, V.; Finetti, F.; Finkbeiner, S.; Fisher, E. A.; Fisher, P. B.; Flamigni, F.; Fliesler, S. J.; Flo, T. H.; Florance, I.; Florey, O.; Florio, T.; Fodor, E.; Follo, C.; Fon, E. A.; Forlino, A.; Fornai, F.; Fortini, P.; Fracassi, A.; Fraldi, A.; Franco, B.; Franco, R.; Franconi, F.; Frankel, L. B.; Friedman, S. L.; Fröhlich, L. F.; Frühbeck, G.; Fuentes, J. M.; Fujiki, Y.; Fujita, N.; Fujiwara, Y.; Fukuda, M.; Fulda, S.; Furic, L.; Furuya, N.; Fusco, C.; Gack, M. U.; Gaffke, L.; Galadari, S.; Galasso, A.; Galindo, M. F.; Gallolu Kankanamalage, S.; Galluzzi, L.; Galy, V.; Gammoh, N.; Gan, B.; Ganley, I. G.; Gao, F.; Gao, H.; Gao, M.; Gao, P.; Gao, S.-J.; Gao, W.; Gao, X.; Garcera, A.; Garcia, M. N.; Garcia, V. E.; García-

Del Portillo, F.; Garcia-Escudero, V.; Garcia-Garcia, A.; Garcia-Macia, M.; García-Moreno, D.; Garcia-Ruiz, C.; García-Sanz, P.; Garg, A. D.; Gargini, R.; Garofalo, T.; Garry, R. F.; Gassen, N. C.; Gatica, D.; Ge, L.; Ge, W.; Geiss-Friedlander, R.; Gelfi, C.; Genschik, P.; Gentle, I. E.; Gerbino, V.; Gerhardt, C.; Germain, K.; Germain, M.; Gewirtz, D. A.; Ghasemipour Afshar, E.; Ghavami, S.; Ghigo, A.; Ghosh, M.; Giamas, G.; Giampietri, C.; Giatromanolaki, A.; Gibson, G. E.; Gibson, S. B.; Ginet, V.; Giniger, E.; Giorgi, C.; Girao, H.; Girardin, S. E.; Giridharan, M.; Giuliano, S.; Giulivi, C.; Giuriato, S.; Giustiniani, J.; Gluschnko, A.; Goder, V.; Goginashvili, A.; Golab, J.; Goldstone, D. C.; Golebiewska, A.; Gomes, L. R.; Gomez, R.; Gómez-Sánchez, R.; Gomez-Puerto, M. C.; Gomez-Sintes, R.; Gong, Q.; Goni, F. M.; González-Gallego, J.; Gonzalez-Hernandez, T.; Gonzalez-Polo, R. A.; Gonzalez-Reyes, J. A.; González-Rodríguez, P.; Goping, I. S.; Gorbatyuk, M. S.; Gorbunov, N. V.; Görgülü, K.; Gorojod, R. M.; Gorski, S. M.; Goruppi, S.; Gotor, C.; Gottlieb, R. A.; Gozes, I.; Gozuacik, D.; Graef, M.; Gräler, M. H.; Granatiero, V.; Grasso, D.; Gray, J. P.; Green, D. R.; Greenhough, A.; Gregory, S. L.; Griffin, E. F.; Grinstaff, M. W.; Gros, F.; Grose, C.; Gross, A. S.; Gruber, F.; Grumati, P.; Grune, T.; Gu, X.; Guan, J.-L.; Guardia, C. M.; Guda, K.; Guerra, F.; Guerri, C.; Guha, P.; Guillén, C.; Gujar, S.; Gukovskaya, A.; Gukovsky, I.; Gunst, J.; Günther, A.; Guntur, A. R.; Guo, C.; Guo, C.; Guo, H.; Guo, L.-W.; Guo, M.; Gupta, P.; Gupta, S. K.; Gupta, S.; Gupta, V. B.; Gupta, V.; Gustafsson, A. B.; Gutterman, D. D.; H.B., R.; Haapasalo, A.; Haber, J. E.; Hać, A.; Hadano, S.; Hafrén, A. J.; Haidar, M.; Hall, B. S.; Halldén, G.; Hamacher-Brady, A.; Hamann, A.; Hamasaki, M.; Han, W.; Hansen, M.; Hanson, P. I.; Hao, Z.; Harada, M.; Harhaji-Trajkovic, L.; Hariharan, N.; Haroon, N.; Harris, J.; Hasegawa, T.; Hasima Nagoor, N.; Haspel, J. A.; Haucke, V.; Hawkins, W. D.; Hay, B. A.; Haynes, C. M.; Hayrabedian, S. B.; Hays, T. S.; He, C.; He, Q.; He, R.-R.; He, Y.-W.; He, Y.-Y.; Heakal, Y.; Heberle, A. M.; Hejtmancik, J. F.; Helgason, G. V.; Henkel, V.; Herb, M.; Hergovich, A.; Herman-Antosiewicz, A.; Hernández, A.; Hernandez, C.; Hernandez-Diaz, S.; Hernandez-Gea, V.; Herpin, A.; Herreros, J.; Hervás, J. H.; Hesselson, D.; Hetz, C.; Heussler, V. T.; Higuchi, Y.; Hilfiker, S.; Hill, J. A.; Hlavacek, W. S.; Ho, E. A.; Ho, I. H. T.; Ho, P. W.-L.; Ho, S.-L.; Ho, W. Y.; Hobbs, G. A.; Hochstrasser, M.; Hoet, P. H. M.; Hofius, D.; Hofman, P.; Höhn, A.; Holmberg, C. I.; Hombrebueno, J. R.; Yi-Ren Hong, C.-W. H.; Hooper, L. V.; Hoppe, T.; Horos, R.; Hoshida, Y.; Hsin, I.-L.; Hsu, H.-Y.; Hu, B.; Hu, D.; Hu, L.-F.; Hu, M. C.; Hu, R.; Hu, W.; Hu, Y.-C.; Hu, Z.-W.; Hua, F.; Hua, J.; Hua, Y.; Huan, C.; Huang, C.; Huang, C.; Huang, C.; Huang, C.; Huang, H.; Huang, K.; Huang, M. L. H.; Huang, R.; Huang, S.; Huang, T.; Huang, X.; Huang, Y. J.; Huber, T. B.; Hubert, V.; Hubner, C. A.; Hughes, S. M.; Hughes, W. E.; Humbert, M.; Hummer, G.; Hurley, J. H.; Hussain, S.; Hussain, S.; Hussey, P. J.; Hutabarat, M.; Hwang, H.-Y.; Hwang, S.; Ieni, A.; Ikeda, F.; Imagawa, Y.; Imai, Y.; Imbriano, C.; Imoto, M.; Inman, D. M.; Inoki, K.; Iovanna, J.; Iozzo, R. V.; Ippolito, G.; Irazoqui, J. E.; Iribarren, P.; Ishaq, M.; Ishikawa, M.; Ishimwe, N.; Isidoro, C.; Ismail, N.; Issazadeh-Navikas, S.; Itakura, E.; Ito, D.; Ivankovic, D.; Ivanova, S.; Iyer, A. K. V.; Izquierdo, J. M.; Izumi, M.; Jäättelä, M.; Jabir, M. S.; Jackson, W. T.; Jacobo-Herrera, N.; Jacomin, A.-C.; Jacquín, E.; Jadiya, P.; Jaeschke, H.; Jagannath, C.; Jakobi, A. J.; Jakobsson, J.; Janji, B.; Jansen-Dürr, P.; Jansson, P. J.; Jantsch, J.; Januszewski, S.; Jassey, A.; Jean, S.; Jeltsch-David, H.; Jendelova, P.; Jenny, A.; Jensen, T. E.; Jessen, N.; Jewell, J. L.; Ji, J.; Jia, L.; Jia, R.; Jiang, L.; Jiang, Q.; Jiang, R.; Jiang, T.; Jiang, X.; Jiang, Y.; Jimenez-Sanchez, M.; Jin, E.-J.; Jin, F.; Jin, H.; Jin, L.; Jin, L.; Jin, M.; Jin, S.; Jo, E.-K.; Joffre, C.; Johansen, T.; Johnson, G. V. W.; Johnston, S. A.; Jokitalo, E.; Jolly, M. K.; Joosten, L. A. B.; Jordan, J.; Joseph, B.; Ju, D.; Ju, J.-S.; Ju, J.; Juárez, E.; Judith, D.; Juhász, G.; Jun, Y.; Jung, C. H.; Jung, S.-C.; Jung, Y. K.; Jungbluth, H.; Jungverdorben, J.; Just, S.; Kaarniranta, K.; Kaasik, A.; Kabuta, T.; Kaganovich, D.; Kahana, A.; Kain, R.; Kajimura, S.; Kalamvoki, M.; Kalia, M.; Kalinowski, D. S.; Kaludercic, N.; Kalvari, I.; Kaminska, J.; Kaminsky, V. O.; Kanamori, H.; Kanasaki, K.; Kang, C.; Kang, R.; Kang, S. S.; Kaniyappan, S.; Kanki, T.; Kanneganti, T.-D.; Kanthasamy, A. G.; Kanthasamy, A.; Kantorow, M.; Kapuy, O.; Karamouzis, M. V.; Karim, M. R.; Karmakar, P.; Katare, R. G.; Kato, M.; Kaufmann, S. H. E.; Kauppinen, A.; Kaushal, G. P.; Kaushik, S.; Kawasaki, K.; Kazan, K.; Ke, P.-Y.; Keating, D. J.; Keber, U.; Kehrl,

J. H.; Keller, K. E.; Keller, C. W.; Kemper, J. K.; Kenific, C. M.; Kepp, O.; Kermorgant, S.; Kern, A.; Ketteler, R.; Keulers, T. G.; Khalfin, B.; Khalil, H.; Khambu, B.; Khan, S. Y.; Khandelwal, V. K. M.; Khandia, R.; Kho, W.; Khobreakar, N. V.; Khuansuwan, S.; Khundadze, M.; Killackey, S. A.; Kim, D.; Kim, D. R.; Kim, D.-H.; Kim, D.-E.; Kim, E. Y.; Kim, E.-K.; Kim, H.-R.; Kim, H.-S.; Kim, H.-R.; Kim, J. H.; Kim, J. K.; Kim, J.-H.; Kim, J.; Kim, J. H.; Kim, K. Il; Kim, P. K.; Kim, S.-J.; Kimball, S. R.; Kimchi, A.; Kimmelman, A. C.; Kimura, T.; King, M. A.; Kinghorn, K. J.; Kinsey, C. G.; Kirkin, V.; Kirshenbaum, L. A.; Kiselev, S. L.; Kishi, S.; Kitamoto, K.; Kitaoka, Y.; Kitazato, K.; Kitsis, R. N.; Kittler, J. T.; Kjaerulff, O.; Klein, P. S.; Klopstock, T.; Klucken, J.; Knævelsrud, H.; Knorr, R. L.; Ko, B. C. B.; Ko, F.; Ko, J.-L.; Kobayashi, H.; Kobayashi, S.; Koch, I.; Koch, J. C.; Koenig, U.; Kögel, D.; Koh, Y. H.; Koike, M.; Kohlwein, S. D.; Kocaturk, N. M.; Komatsu, M.; König, J.; Kono, T.; Kopp, B. T.; Korcsmaros, T.; Korkmaz, G.; Korolchuk, V. I.; Korsnes, M. S.; Koskela, A.; Kota, J.; Kotake, Y.; Kotler, M. L.; Kou, Y.; Koukourakis, M. I.; Koustas, E.; Kovacs, A. L.; Kovács, T.; Koya, D.; Kozako, T.; Kraft, C.; Krainc, D.; Krämer, H.; Krasnodembskaya, A. D.; Kretz-Remy, C.; Kroemer, G.; Ktistakis, N. T.; Kuchitsu, K.; Kuenen, S.; Kuerschner, L.; Kukar, T.; Kumar, A.; Kumar, A.; Kumar, D.; Kumar, D.; Kumar, S.; Kume, S.; Kumsta, C.; Kundu, C. N.; Kundu, M.; Kunnumakkara, A. B.; Kurgan, L.; Kutateladze, T. G.; Kutlu, O.; Kwak, S.; Kwon, H. J.; Kwon, T. K.; Kwon, Y. T.; Kyrmizi, I.; La Spada, A.; Labonté, P.; Ladoire, S.; Laface, I.; Lafont, F.; Lagace, D. C.; Lahiri, V.; Lai, Z.; Laird, A. S.; Lakkaraju, A.; Lamark, T.; Lan, S.-H.; Landajuela, A.; Lane, D. J. R.; Lane, J. D.; Lang, C. H.; Lange, C.; Langel, Ü.; Langer, R.; Lapaquette, P.; Laporte, J.; LaRusso, N. F.; Lastres-Becker, I.; Lau, W. C. Y.; Laurie, G. W.; Lavandero, S.; Law, B. Y. K.; Law, H. K.; Layfield, R.; Le, W.; Le Stunff, H.; Leary, A. Y.; Lebrun, J.-J.; Leck, L. Y. W.; Leduc-Gaudet, J.-P.; Lee, C.; Lee, C.-P.; Lee, D.-H.; Lee, E. B.; Lee, E. F.; Lee, G. M.; Lee, H.-J.; Lee, H. K.; Lee, J. M.; Lee, J. S.; Lee, J.-A.; Lee, J.-Y.; Lee, J. H.; Lee, M.; Lee, M. G.; Lee, M. J.; Lee, M.-S.; Lee, S. Y.; Lee, S.-J.; Lee, S. Y.; Lee, S. B.; Lee, W. H.; Lee, Y.-R.; Lee, Y.; Lee, Y.; Lefebvre, C.; Legouis, R.; Lei, Y. L.; Lei, Y.; Leikin, S.; Leitinger, G.; Lemus, L.; Leng, S.; Lenoir, O.; Lenz, G.; Lenz, H. J.; Lenzi, P.; León, Y.; Leopoldino, A. M.; Leschczyk, C.; Leskelä, S.; Letellier, E.; Leung, C.-T.; Leung, P. S.; Leventhal, J. S.; Levine, B.; Lewis, P. A.; Ley, K.; Li, B.; Li, D.-Q.; Li, J.; Li, J.; Li, J.; Li, K.; Li, L.; Li, M.; Li, M.; Li, M.; Li, M.; Li, M.; Li, P.-L.; Li, M.-Q.; Li, Q.; Li, S.; Li, T.; Li, W.; Li, W.; Li, X.; Li, Y.-P.; Li, Y.; Li, Z.; Li, Z.; Li, Z.; Lian, J.; Liang, C.; Liang, Q.; Liang, W.; Liang, Y.; Liang, Y.; Liao, G.; Liao, L.; Liao, M.; Liao, Y.-F.; Librizzi, M.; Lie, P. P. Y.; Lilly, M. A.; Lim, H. J.; Lima, T. R. R.; Limana, F.; Lin, C.; Lin, C.-W.; Lin, D.-S.; Lin, F.-C.; Lin, J. D.; Lin, K. M.; Lin, K.-H.; Lin, L.-T.; Lin, P.-H.; Lin, Q.; Lin, S.; Lin, S.-J.; Lin, W.; Lin, X.; Lin, Y.-X.; Lin, Y.-S.; Linden, R.; Lindner, P.; Ling, S.-C.; Lingor, P.; Linnemann, A. K.; Liou, Y.-C.; Lipinski, M. M.; Lipovšek, S.; Lira, V. A.; Lisiak, N.; Liton, P. B.; Liu, C.; Liu, C.-H.; Liu, C.-F.; Liu, C. H.; Liu, F.; Liu, H.; Liu, H.-S.; Liu, H.; Liu, H.; Liu, J.; Liu, J.; Liu, J.; Liu, L.; Liu, L.; Liu, M.; Liu, Q.; Liu, W.; Liu, W.; Liu, X.-H.; Liu, X.; Liu, X.; Liu, X.; Liu, X.; Liu, Y.; Liu, Y.; Liu, Y.; Liu, Y.; Liu, Y.; Livingston, J. A.; Lizard, G.; Lizcano, J. M.; Ljubojevic-Holzer, S.; LLeonart, M. E.; Llobet-Navàs, D.; Llorente, A.; Lo, C. H.; Lobato-Márquez, D.; Long, Q.; Long, Y. C.; Loos, B.; Loos, J. A.; López, M. G.; López-Doménech, G.; López-Guerrero, J. A.; López-Jiménez, A. T.; López-Pérez, Ó.; López-Valero, I.; Lorenowicz, M. J.; Lorente, M.; Lorincz, P.; Lossi, L.; Lotersztajn, S.; Lovat, P. E.; Lovell, J. F.; Lovy, A.; Löw, P.; Lu, G.; Lu, H.; Lu, J.-H.; Lu, J.-J.; Lu, M.; Lu, S.; Luciani, A.; Lucocq, J. M.; Ludovico, P.; Luftig, M. A.; Luhr, M.; Luis-Ravelo, D.; Lum, J. J.; Luna-Dulcey, L.; Lund, A. H.; Lund, V. K.; Lünemann, J. D.; Lüningschrör, P.; Luo, H.; Luo, R.; Luo, S.; Luo, Z.; Luparello, C.; Lüscher, B.; Luu, L.; Lyakhovich, A.; Lyamzaev, K. G.; Lystad, A. H.; Lytvynchuk, L.; Ma, A. C.; Ma, C.; Ma, M.; Ma, N.-F.; Ma, Q.-H.; Ma, X.; Ma, Y.; Ma, Z.; MacDougald, O. A.; Macian, F.; MacIntosh, G. C.; MacKeigan, J. P.; Macleod, K. F.; Maday, S.; Madeo, F.; Madesh, M.; Madl, T.; Madrigal-Matute, J.; Maeda, A.; Maejima, Y.; Magarinos, M.; Mahavadi, P.; Maiani, E.; Maiese, K.; Maiti, P.; Maiuri, M. C.; Majello, B.; Major, M. B.; Makareeva, E.; Malik, F.; Mallilankaraman, K.; Malorni, W.; Maloyan, A.; Mammadova, N.; Man, G. C. W.; Manai, F.;

Mancias, J. D.; Mandelkow, E.-M.; Mandell, M. A.; Manfredi, A. A.; Manjili, M. H.; Manjithaya, R.; Manque, P.; Manshian, B. B.; Manzano, R.; Manzoni, C.; Mao, K.; Marchese, C.; Marchetti, S.; Marconi, A. M.; Marcucci, F.; Mardente, S.; Mareninova, O. A.; Margeta, M.; Mari, M.; Marinelli, S.; Marinelli, O.; Mariño, G.; Mariotto, S.; Marshall, R. S.; Marten, M. R.; Martens, S.; Martin, A. P. J.; Martin, K. R.; Martin, S.; Martín-Segura, A.; Martín-Acebes, M. A.; Martin-Burriel, I.; Martin-Rincon, M.; Martin-Sanz, P.; Martina, J. A.; Martinet, W.; Martinez, A.; Martinez, A.; Martinez, J.; Martinez Velazquez, M.; Martinez-Lopez, N.; Martinez-Vicente, M.; Martins, D. O.; Martins, J. O.; Martins, W. K.; Martins-Marques, T.; Marzetti, E.; Masaldan, S.; Masclaux-Daubresse, C.; Mashek, D. G.; Massa, V.; Massieu, L.; Masson, G. R.; Masuelli, L.; Masyuk, A. I.; Masyuk, T. V.; Matarrese, P.; Matheu, A.; Matoba, S.; Matsuzaki, S.; Mattar, P.; Matte, A.; Mattosco, D.; Mauriz, J. L.; Mauthe, M.; Mauvezin, C.; Maverakis, E.; Maycotte, P.; Mayer, J.; Mazzocchi, G.; Mazzoni, C.; Mazzulli, J. R.; McCarty, N.; McDonald, C.; McGill, M. R.; McKenna, S. L.; McLaughlin, B.; McLoughlin, F.; McNiven, M. A.; McWilliams, T. G.; Mechta-Grigoriou, F.; Medeiros, T. C.; Medina, D. L.; Megeney, L. A.; Megyeri, K.; Mehrpour, M.; Mehta, J. L.; Meijer, A. J.; Meijer, A. H.; Mejlvang, J.; Meléndez, A.; Melk, A.; Memisoglu, G.; Mendes, A. F.; Meng, D.; Meng, F.; Meng, T.; Menna-Barreto, R.; Menon, M. B.; Mercer, C.; Mercier, A. E.; Mergny, J.-L.; Merighi, A.; Merkley, S. D.; Merla, G.; Meske, V.; Mestre, A. C.; Metur, S. P.; Meyer, C.; Meyer, H.; Mi, W.; Mialet-Perez, J.; Miao, J.; Micale, L.; Miki, Y.; Milan, E.; Milczarek, M.; Miller, D. L.; Miller, S. I.; Miller, S.; Millward, S. W.; Milosevic, I.; Minina, E. A.; Mirzaei, H.; Mirzaei, H. R.; Mirzaei, M.; Mishra, A.; Mishra, N.; Mishra, P. K.; Misirkic Marjanovic, M.; Misasi, R.; Misra, A.; Misso, G.; Mitchell, C.; Mitou, G.; Miura, T.; Miyamoto, S.; Miyazaki, M.; Miyazaki, M.; Miyazaki, T.; Miyazawa, K.; Mizushima, N.; Mogenssen, T. H.; Mograbi, B.; Mohammadinejad, R.; Mohamud, Y.; Mohanty, A.; Mohapatra, S.; Möhlmann, T.; Mohammed, A.; Moles, A.; Moley, K. H.; Molinari, M.; Mollace, V.; Møller, A. B.; Mollereau, B.; Mollinedo, F.; Montagna, C.; Monteiro, M. J.; Montella, A.; Montes, L. R.; Montico, B.; Mony, V. K.; Monzio Compagnoni, G.; Moore, M. N.; Moosavi, M. A.; Mora, A. L.; Mora, M.; Morales-Alamo, D.; Moratalla, R.; Moreira, P. I.; Morelli, E.; Moreno, S.; Moreno-Blas, D.; Moresi, V.; Morga, B.; Morgan, A. H.; Morin, F.; Morishita, H.; Moritz, O. L.; Moriyama, M.; Moriyasu, Y.; Morleo, M.; Morselli, E.; Moruno-Manchon, J. F.; Moscat, J.; Mostowy, S.; Motori, E.; Moura, A. F.; Moustaid-Moussa, N.; Mrakovcic, M.; Muciño-Hernández, G.; Mukherjee, A.; Mukhopadhyay, S.; Mulcahy Levy, J. M.; Mulero, V.; Muller, S.; Münch, C.; Munjal, A.; Munoz-Canoves, P.; Muñoz-Galdeano, T.; Münz, C.; Murakawa, T.; Muratori, C.; Murphy, B. M.; Murphy, J. P.; Murthy, A.; Myöhänen, T. T.; Mysorekar, I. U.; Mytych, J.; Nabavi, S. M.; Nabissi, M.; Nagy, P.; Nah, J.; Nahimana, A.; Nakagawa, I.; Nakamura, K.; Nakatogawa, H.; Nandi, S. S.; Nanjundan, M.; Nanni, M.; Napolitano, G.; Nardacci, R.; Narita, M.; Nassif, M.; Nathan, I.; Natsumeda, M.; Naude, R. J.; Naumann, C.; Naveiras, O.; Navid, F.; Nawrocki, S. T.; Nazarko, T. Y.; Nazio, F.; Negoita, F.; Neill, T.; Neisch, A. L.; Neri, L. M.; Netea, M. G.; Neubert, P.; Neufeld, T. P.; Neumann, D.; Neutzner, A.; Newton, P. T.; Ney, P. A.; Nezis, I. P.; Ng, C. C. W.; Ng, T. B.; Nguyen, H. T. T.; Nguyen, L. T.; Ni, H.-M.; Ní Cheallaigh, C.; Ni, Z.; Nicolao, M. C.; Nicoli, F.; Nieto-Diaz, M.; Nilsson, P.; Ning, S.; Niranjana, R.; Nishimune, H.; Niso-Santano, M.; Nixon, R. A.; Nobili, A.; Nobrega, C.; Noda, T.; Nogueira-Recalde, U.; Nolan, T. M.; Nombela, I.; Novak, I.; Novoa, B.; Nozawa, T.; Nukina, N.; Nussbaum-Krammer, C.; Nylandsted, J.; O'Donovan, T. R.; O'Leary, S. M.; O'Rourke, E. J.; O'Sullivan, M. P.; O'Sullivan, T. E.; Oddo, S.; Oehme, I.; Ogawa, M.; Ogier-Denis, E.; Ogmundsdottir, M. H.; Ogretmen, B.; Oh, G. T.; Oh, S.-H.; Oh, Y. J.; Ohama, T.; Ohashi, Y.; Ohmuraya, M.; Oikonomou, V.; Ojha, R.; Okamoto, K.; Okazawa, H.; Oku, M.; Oliván, S.; Oliveira, J. M. A.; Ollmann, M.; Olzmann, J. A.; Omari, S.; Omary, M. B.; Önal, G.; Ondrej, M.; Ong, S.-B.; Ong, S.-G.; Onnis, A.; Orellana, J. A.; Orellana-Muñoz, S.; Ortega-Villaizán, M. D. M.; Ortiz-Gonzalez, X. R.; Ortona, E.; Osiewacz, H. D.; Osman, A.-H. K.; Osta, R.; Otegui, M. S.; Otsu, K.; Ott, C.; Ottobri, L.; Ou, J. J.; Outeiro, T. F.; Oynebraten, I.; Ozturk, M.; Pagès, G.; Pahari, S.; Pajares, M.; Pajvani, U. B.; Pal, R.; Paladino, S.; Pallet, N.; Palmieri, M.; Palmisano,

G.; Palumbo, C.; Pampaloni, F.; Pan, L.; Pan, Q.; Pan, W.; Pan, X.; Panasyuk, G.; Pandey, R.; Pandey, U. B.; Pandya, V.; Paneni, F.; Pang, S. Y.; Panzarini, E.; Papademetrio, D. L.; Papaleo, E.; Papinski, D.; Papp, D.; Park, E. C.; Park, H. T.; Park, J.-M.; Park, J.-I.; Park, J. T.; Park, J.; Park, S. C.; Park, S.-Y.; Parola, A. H.; Parys, J. B.; Pasquier, A.; Pasquier, B.; Passos, J. F.; Pastore, N.; Patel, H. H.; Patschan, D.; Patingre, S.; Pedraza-Alva, G.; Pedraza-Chaverri, J.; Pedrozo, Z.; Pei, G.; Pei, J.; Peled-Zehavi, H.; Pellegrini, J. M.; Pelletier, J.; Peñalva, M. A.; Peng, D.; Peng, Y.; Penna, F.; Pennuto, M.; Pentimalli, F.; Pereira, C. M. F.; Pereira, G. J. S.; Pereira, L. C.; Pereira de Almeida, L.; Perera, N. D.; Pérez-Lara, Á.; Perez-Oliva, A. B.; Pérez-Pérez, M. E.; Periyasamy, P.; Perl, A.; Perrotta, C.; Perrotta, I.; Pestell, R. G.; Petersen, M.; Petrache, I.; Petrovski, G.; Pfirrmann, T.; Pfister, A. S.; Philips, J. A.; Pi, H.; Picca, A.; Pickrell, A. M.; Picot, S.; Pierantoni, G. M.; Pierdominici, M.; Pierre, P.; Pierrefite-Carle, V.; Pierzynowska, K.; Pietrocola, F.; Pietruczuk, M.; Pignata, C.; Pimentel-Muñíos, F. X.; Pinar, M.; Pinheiro, R. O.; Pinkas-Kramarski, R.; Pinton, P.; Piracs, K.; Piya, S.; Pizzo, P.; Plantinga, T. S.; Platta, H. W.; Plaza-Zabala, A.; Plomann, M.; Plotnikov, E. Y.; Plun-Favreau, H.; Pluta, R.; Pocock, R.; Pöggeler, S.; Pohl, C.; Poirot, M.; Poletti, A.; Ponpuak, M.; Popelka, H.; Popova, B.; Porta, H.; Porte Alcon, S.; Portilla-Fernandez, E.; Post, M.; Potts, M. B.; Poulton, J.; Powers, T.; Prahlad, V.; Prajsnar, T. K.; Praticò, D.; Prencipe, R.; Priault, M.; Proikas-Cezanne, T.; Promponas, V. J.; Proud, C. G.; Puertollano, R.; Puglielli, L.; Pulinilkunnil, T.; Puri, D.; Puri, R.; Puyal, J.; Qi, X.; Qi, Y.; Qian, W.; Qiang, L.; Qiu, Y.; Quadrilatero, J.; Quarleri, J.; Raben, N.; Rabinowich, H.; Ragona, D.; Ragusa, M. J.; Rahimi, N.; Rahmati, M.; Raia, V.; Raimundo, N.; Rajasekaran, N.-S.; Ramachandra Rao, S.; Rami, A.; Ramírez-Pardo, I.; Ramsden, D. B.; Randow, F.; Rangarajan, P. N.; Ranieri, D.; Rao, H.; Rao, L.; Rao, R.; Rathore, S.; Ratnayaka, J. A.; Ratovitski, E. A.; Ravanan, P.; Ravegnini, G.; Ray, S. K.; Razani, B.; Rebecca, V.; Reggiori, F.; Régnier-Vigouroux, A.; Reichert, A. S.; Reigada, D.; Reiling, J. H.; Rein, T.; Reipert, S.; Rekha, R. S.; Ren, H.; Ren, J.; Ren, W.; Renault, T.; Renga, G.; Reue, K.; Rewitz, K.; Ribeiro de Andrade Ramos, B.; Riazuddin, S. A.; Ribeiro-Rodrigues, T. M.; Ricci, J.-E.; Ricci, R.; Riccio, V.; Richardson, D. R.; Rikihisa, Y.; Risbud, M. V.; Risueño, R. M.; Ritis, K.; Rizza, S.; Rizzuto, R.; Roberts, H. C.; Roberts, L. D.; Robinson, K. J.; Roccheri, M. C.; Rocchi, S.; Rodney, G. G.; Rodrigues, T.; Rodrigues Silva, V. R.; Rodriguez, A.; Rodriguez-Barrueco, R.; Rodriguez-Henche, N.; Rodriguez-Rocha, H.; Roelofs, J.; Rogers, R. S.; Rogov, V. V.; Rojo, A. I.; Rolka, K.; Romanello, V.; Romani, L.; Romano, A.; Romano, P. S.; Romeo-Guitart, D.; Romero, L. C.; Romero, M.; Roney, J. C.; Rongo, C.; Roperto, S.; Rosenfeldt, M. T.; Rosenstiel, P.; Rosenwald, A. G.; Roth, K. A.; Roth, L.; Roth, S.; Rouschop, K. M. A.; Roussel, B. D.; Roux, S.; Rovere-Querini, P.; Roy, A.; Rozieres, A.; Ruano, D.; Rubinsztein, D. C.; Rubtsova, M. P.; Ruckdeschel, K.; Ruckenstuhl, C.; Rudolf, E.; Rudolf, R.; Ruggieri, A.; Ruparelia, A. A.; Rusmini, P.; Russell, R. R.; Russo, G. L.; Russo, M.; Russo, R.; Ryabaya, O. O.; Ryan, K. M.; Ryu, K.-Y.; Sabater-Arcis, M.; Sachdev, U.; Sacher, M.; Sachse, C.; Sadhu, A.; Sadoshima, J.; Safren, N.; Saftig, P.; Sagona, A. P.; Sahay, G.; Sahebkar, A.; Sahin, M.; Sahin, O.; Sahn, S.; Saito, N.; Saito, S.; Saito, T.; Sakai, R.; Sakai, Y.; Sakamaki, J.-I.; Saksela, K.; Salazar, G.; Salazar-Degracia, A.; Salekdeh, G. H.; Saluja, A. K.; Sampaio-Marques, B.; Sanchez, M. C.; Sanchez-Alcazar, J. A.; Sanchez-Vera, V.; Sancho-Shimizu, V.; Sanderson, J. T.; Sandri, M.; Santaguida, S.; Santambrogio, L.; Santana, M. M.; Santoni, G.; Sanz, A.; Sanz, P.; Saran, S.; Sardiello, M.; Sargeant, T. J.; Sarin, A.; Sarkar, C.; Sarkar, S.; Sarrias, M.-R.; Sarkar, S.; Sarmah, D. T.; Sarparanta, J.; Sathyanarayan, A.; Sathyanarayanan, R.; Scaglione, K. M.; Scatozza, F.; Schaefer, L.; Schafer, Z. T.; Schaible, U. E.; Schapira, A. H. V.; Scharl, M.; Schatzl, H. M.; Schein, C. H.; Scheper, W.; Scheuring, D.; Schiaffino, M. V.; Schiappacassi, M.; Schindl, R.; Schlattner, U.; Schmidt, O.; Schmitt, R.; Schmidt, S. D.; Schmitz, I.; Schmukler, E.; Schneider, A.; Schneider, B. E.; Schober, R.; Schoijet, A. C.; Schott, M. B.; Schramm, M.; Schröder, B.; Schuh, K.; Schüller, C.; Schulze, R. J.; Schürmanns, L.; Schwamborn, J. C.; Schwarten, M.; Scialo, F.; Sciarretta, S.; Scott, M. J.; Scotto, K. W.; Scovassi, A. I.; Scrima, A.; Scrivo, A.; Sebastian, D.; Sebt, S.; Sedej, S.; Segatori, L.; Segev, N.; Seglen, P. O.; Seiliez, I.; Seki, E.; Selleck, S. B.; Sellke, F. W.; Selsby, J. T.; Sendtner,

M.; Senturk, S.; Seranova, E.; Sergi, C.; Serra-Moreno, R.; Sesaki, H.; Settembre, C.; Setty, S. R. G.; Sgarbi, G.; Sha, O.; Shacka, J. J.; Shah, J. A.; Shang, D.; Shao, C.; Shao, F.; Sharbati, S.; Sharkey, L. M.; Sharma, D.; Sharma, G.; Sharma, K.; Sharma, P.; Sharma, S.; Shen, H.-M.; Shen, H.; Shen, J.; Shen, M.; Shen, W.; Shen, Z.; Sheng, R.; Sheng, Z.; Sheng, Z.-H.; Shi, J.; Shi, X.; Shi, Y.-H.; Shiba-Fukushima, K.; Shieh, J.-J.; Shimada, Y.; Shimizu, S.; Shimozaawa, M.; Shintani, T.; Shoemaker, C. J.; Shojaei, S.; Shoji, I.; Shravage, B. V.; Shridhar, V.; Shu, C.-W.; Shu, H.-B.; Shui, K.; Shukla, A. K.; Shutt, T. E.; Sica, V.; Siddiqui, A.; Sierra, A.; Sierra-Torre, V.; Signorelli, S.; Sil, P.; Silva, B. J. de A.; Silva, J. D.; Silva-Pavez, E.; Silvente-Poirot, S.; Simmonds, R. E.; Simon, A. K.; Simon, H.-U.; Simons, M.; Singh, A.; Singh, L. P.; Singh, R.; Singh, S. V.; Singh, S. K.; Singh, S. B.; Singh, S.; Singh, S. P.; Sinha, D.; Sinha, R. A.; Sinha, S.; Sirko, A.; Sirohi, K.; Sivridis, E. L.; Skendros, P.; Skirycz, A.; Slaninová, I.; Smaili, S. S.; Smertenko, A.; Smith, M. D.; Soenen, S. J.; Sohn, E. J.; Sok, S. P. M.; Solaini, G.; Soldati, T.; Soleimanpour, S. A.; Soler, R. M.; Solovchenko, A.; Somarelli, J. A.; Sonawane, A.; Song, F.; Song, H. K.; Song, J.-X.; Song, K.; Song, Z.; Soria, L. R.; Sorice, M.; Soukas, A. A.; Soukup, S.-F.; Sousa, D.; Sousa, N.; Spagnuolo, P. A.; Spector, S. A.; Srinivas Bharath, M. M.; St. Clair, D.; Stagni, V.; Staiano, L.; Stalneck, C. A.; Stankov, M. V.; Stathopoulos, P. B.; Stefan, K.; Stefan, S. M.; Stefanis, L.; Steffan, J. S.; Steinkasserer, A.; Stenmark, H.; Sterneckert, J.; Stevens, C.; Stoka, V.; Storch, S.; Stork, B.; Strappazzon, F.; Strohecker, A. M.; Stupack, D. G.; Su, H.; Su, L.-Y.; Su, L.; Suarez-Fontes, A. M.; Subauste, C. S.; Subbian, S.; Subirada, P. V.; Sudhandiran, G.; Sue, C. M.; Sui, X.; Summers, C.; Sun, G.; Sun, J.; Sun, K.; Sun, M.; Sun, Q.; Sun, Y.; Sun, Z.; Sunahara, K. K. S.; Sundberg, E.; Susztak, K.; Sutovsky, P.; Suzuki, H.; Sweeney, G.; Symons, J. D.; Sze, S. C. W.; Szewczyk, N. J.; Tabęcka-Łonczynska, A.; Tabolacci, C.; Tacke, F.; Taegtmeier, H.; Tafani, M.; Tagaya, M.; Tai, H.; Tait, S. W. G.; Takahashi, Y.; Takats, S.; Talwar, P.; Tam, C.; Tam, S. Y.; Tampellini, D.; Tamura, A.; Tan, C. T.; Tan, E.-K.; Tan, Y.-Q.; Tanaka, M.; Tanaka, M.; Tang, D.; Tang, J.; Tang, T.-S.; Tanida, I.; Tao, Z.; Taouis, M.; Tatenhorst, L.; Tavernarakis, N.; Taylor, A.; Taylor, G. A.; Taylor, J. M.; Tchetina, E.; Tee, A. R.; Tegeder, I.; Teis, D.; Teixeira, N.; Teixeira-Clerc, F.; Tekirdag, K. A.; Tencomnao, T.; Tenreiro, S.; Tepikin, A. V.; Testillano, P. S.; Tettamanti, G.; Tharaux, P.-L.; Thedieck, K.; Thekkinghat, A. A.; Thellung, S.; Thinwa, J. W.; Thirumalaikumar, V. P.; Thomas, S. M.; Thomes, P. G.; Thorburn, A.; Thukral, L.; Thum, T.; Thumm, M.; Tian, L.; Tichy, A.; Till, A.; Timmerman, V.; Titorenko, V. I.; Todi, S. V.; Todorova, K.; Toivonen, J. M.; Tomaipitina, L.; Tomar, D.; Tomas-Zapico, C.; Tomić, S.; Tong, B. C.-K.; Tong, C.; Tong, X.; Tooze, S. A.; Torgersen, M. L.; Torii, S.; Torres-López, L.; Torriglia, A.; Towers, C. G.; Towns, R.; Toyokuni, S.; Trajkovic, V.; Tramontano, D.; Tran, Q.-G.; Travassos, L. H.; Trelford, C. B.; Tremel, S.; Triola, G.; Trougakos, I. P.; Tsao, B. P.; Tschan, M. P.; Tse, H.-F.; Tse, T. F.; Tsugawa, H.; Tsvetkov, A. S.; Tumbarello, D. A.; Tumtas, Y.; Tuñón, M. J.; Turcotte, S.; Turk, B.; Turk, V.; Turner, B. J.; Tuxworth, R. I.; Tyler, J. K.; Tyutereva, E. V.; Uchiyama, Y.; Ugun-Klusek, A.; Uhlig, H. H.; Ułamek-Kozioł, M.; Ulasov, I. V.; Umekawa, M.; Ungermann, C.; Unno, R.; Urbe, S.; Uribe-Carretero, E.; Üstün, S.; Uversky, V. N.; Vaccari, T.; Vaccaro, M. I.; Vahsen, B. F.; Vakifahmetoglu-Norberg, H.; Valdor, R.; Valente, M. J.; Valko, A.; Vallee, R. B.; Valverde, A. M.; Van den Berghe, G.; van der Veen, S.; Van Kaer, L.; van Loosdregt, J.; van Wijk, S. J. L.; Vandenberghe, W.; Vanhorebeek, I.; Vannier-Santos, M. A.; Vannini, N.; Vanrell, M. C.; Vantaggiato, C.; Varano, G.; Varela-Nieto, I.; Varga, M.; Vasconcelos, M. H.; Vats, S.; Vavvas, D. G.; Vega-Naredo, I.; Vega-Rubin-de-Celis, S.; Velasco, G.; Velázquez, A. P.; Vellai, T.; Vellenga, E.; Velotti, F.; Verdier, M.; Verginis, P.; Vergne, I.; Verkade, P.; Verma, M.; Verstreken, P.; Vervliet, T.; Vervoorts, J.; Vessoni, A. T.; Victor, V. M.; Vidal, M.; Vidoni, C.; Vieira, O. V.; Vierstra, R. D.; Viganó, S.; Vihinen, H.; Vijayan, V.; Vila, M.; Vilar, M.; Villalba, J. M.; Villalobo, A.; Villarejo-Zori, B.; Villarroya, F.; Villarroya, J.; Vincent, O.; Vindis, C.; Viret, C.; Viscomi, M. T.; Visnjic, D.; Vitale, I.; Vocadlo, D. J.; Voitsekhovskaja, O. V.; Volonté, C.; Volta, M.; Vomero, M.; Von Haefen, C.; Vooijs, M. A.; Voos, W.; Vucicevic, L.; Wade-Martins, R.; Waguri, S.; Waite, K. A.; Wakatsuki, S.; Walker, D. W.; Walker, M. J.; Walker, S. A.; Walter, J.; Wandosell, F. G.; Wang, B.; Wang, C.-Y.; Wang, C.;

Wang, C.; Wang, C.; Wang, C.-Y.; Wang, D.; Wang, F.; Wang, F.; Wang, F.; Wang, G.; Wang, H.; Wang, H.; Wang, H.; Wang, H.-G.; Wang, J.; Wang, J.; Wang, J.; Wang, J.; Wang, K.; Wang, L.; Wang, L.; Wang, M. H.; Wang, M.; Wang, N.; Wang, P.; Wang, P.; Wang, P.; Wang, P.; Wang, Q. J.; Wang, Q.; Wang, Q. K.; Wang, Q. A.; Wang, W.-T.; Wang, W.; Wang, X.; Wang, X.; Wang, Y.; Wang, Y.; Wang, Y.; Wang, Y.-Y.; Wang, Y.; Wang, Y.; Wang, Y.; Wang, Y.; Wang, Z.; Wang, Z.; Wang, Z.; Warnes, G.; Warnsmann, V.; Watada, H.; Watanabe, E.; Watchon, M.; Wawrzyńska, A.; Weaver, T. E.; Wegrzyn, G.; Wehman, A. M.; Wei, H.; Wei, L.; Wei, T.; Wei, Y.; Weiergräber, O. H.; Weihl, C. C.; Weindl, G.; Weiskirchen, R.; Wells, A.; Wen, R. H.; Wen, X.; Werner, A.; Weykopf, B.; Wheatley, S. P.; Whitton, J. L.; Whitworth, A. J.; Wiktorska, K.; Wildenberg, M. E.; Wileman, T.; Wilkinson, S.; Willbold, D.; Williams, B.; Williams, R. S. B.; Williams, R. L.; Williamson, P. R.; Wilson, R. A.; Winner, B.; Winsor, N. J.; Witkin, S. S.; Wodrich, H.; Woehlbier, U.; Wollert, T.; Wong, E.; Wong, J. H.; Wong, R. W.; Wong, V. K. W.; Wong, W. W.-L.; Wu, A.-G.; Wu, C.; Wu, J.; Wu, J.; Wu, K. K.; Wu, M.; Wu, S.-Y.; Wu, S.; Wu, S.-Y.; Wu, S.; Wu, W. K. K.; Wu, X.; Wu, X.; Wu, Y.-W.; Wu, Y.; Xavier, R. J.; Xia, H.; Xia, L.; Xia, Z.; Xiang, G.; Xiang, J.; Xiang, M.; Xiang, W.; Xiao, B.; Xiao, G.; Xiao, H.; Xiao, H.; Xiao, J.; Xiao, L.; Xiao, S.; Xiao, Y.; Xie, B.; Xie, C.-M.; Xie, M.; Xie, Y.; Xie, Z.; Xie, Z.; Xilouri, M.; Xu, C.; Xu, E.; Xu, H.; Xu, J.; Xu, J.; Xu, L.; Xu, W. W.; Xu, X.; Xue, Y.; Yakhine-Diop, S. M. S.; Yamaguchi, M.; Yamaguchi, O.; Yamamoto, A.; Yamashina, S.; Yan, S.; Yan, S.-J.; Yan, Z.; Yanagi, Y.; Yang, C.; Yang, D.-S.; Yang, H.; Yang, H.-T.; Yang, H.; Yang, J.-M.; Yang, J.; Yang, J.; Yang, L.; Yang, L.; Yang, M.; Yang, P.-M.; Yang, Q.; Yang, S.; Yang, S.; Yang, S.-F.; Yang, W.; Yang, W. Y.; Yang, X.; Yang, X.; Yang, Y.; Yang, Y.; Yao, H.; Yao, S.; Yao, X.; Yao, Y.-G.; Yao, Y.-M.; Yasui, T.; Yazdankhah, M.; Yen, P. M.; Yi, C.; Yin, X.-M.; Yin, Y.; Yin, Z.; Yin, Z.; Ying, M.; Ying, Z.; Yip, C. K.; Yiu, S. P. T.; Yoo, Y. H.; Yoshida, K.; Yoshii, S. R.; Yoshimori, T.; Yousefi, B.; Yu, B.; Yu, H.; Yu, J.; Yu, J.; Yu, L.; Yu, M.-L.; Yu, S.-W.; Yu, V. C.; Yu, W. H.; Yu, Z.; Yu, Z.; Yuan, J.; Yuan, L.-Q.; Yuan, S.; Yuan, S.-S. F.; Yuan, Y.; Yuan, Z.; Yue, J.; Yue, Z.; Yun, J.; Yung, R. L.; Zacks, D. N.; Zaffagnini, G.; Zambelli, V. O.; Zanella, I.; Zang, Q. S.; Zanivan, S.; Zappavigna, S.; Zaragoza, P.; Zarbalis, K. S.; Zarebkohan, A.; Zarrouk, A.; Zeitlin, S. O.; Zeng, J.; Zeng, J.; Žerovnik, E.; Zhan, L.; Zhang, B.; Zhang, D. D.; Zhang, H.; Zhang, H.; Zhang, H.; Zhang, H.; Zhang, H.; Zhang, H.; Zhang, H.-L.; Zhang, J.; Zhang, J.; Zhang, J.-P.; Zhang, K. Y. B.; Zhang, L. W.; Zhang, L.; Zhang, L.; Zhang, L.; Zhang, L.; Zhang, M.; Zhang, P.; Zhang, S.; Zhang, W.; Zhang, X.; Zhang, X.-W.; Zhang, X.; Zhang, X.; Zhang, X.; Zhang, X.; Zhang, X. D.; Zhang, Y.; Zhang, Y.; Zhang, Y.; Zhang, Y.-D.; Zhang, Y.; Zhang, Y.-Y.; Zhang, Y.; Zhang, Z.; Zhang, Z.; Zhang, Z.; Zhang, Z.; Zhang, Z.; Zhang, Z.; Zhao, H.; Zhao, L.; Zhao, S.; Zhao, T.; Zhao, X.-F.; Zhao, Y.; Zhao, Y.; Zhao, Y.; Zhao, Y.; Zheng, G.; Zheng, K.; Zheng, L.; Zheng, S.; Zheng, X.-L.; Zheng, Y.; Zheng, Z.-G.; Zhivotovsky, B.; Zhong, Q.; Zhou, A.; Zhou, B.; Zhou, C.; Zhou, G.; Zhou, H.; Zhou, H.; Zhou, H.; Zhou, J.; Zhou, J.; Zhou, J.; Zhou, J.; Zhou, K.; Zhou, R.; Zhou, X.-J.; Zhou, Y.; Zhou, Y.; Zhou, Y.; Zhou, Z.-Y.; Zhou, Z.; Zhu, B.; Zhu, C.; Zhu, G.-Q.; Zhu, H.; Zhu, H.; Zhu, H.; Zhu, W.-G.; Zhu, Y.; Zhu, Y.; Zhuang, H.; Zhuang, X.; Zientara-Rytter, K.; Zimmermann, C. M.; Ziviani, E.; Zoladek, T.; Zong, W.-X.; Zorov, D. B.; Zorzano, A.; Zou, W.; Zou, Z.; Zou, Z.; Zuryn, S.; Zwerschke, W.; Brand-Saberi, B.; Dong, X. C.; Kenchappa, C. S.; Li, Z.; Lin, Y.; Oshima, S.; Rong, Y.; Sluimer, J. C.; Stallings, C. L.; Tong, C.-K. Guidelines for the Use and Interpretation of Assays for Monitoring Autophagy (4th Edition)1. *Autophagy* **2021**, *17* (1), 1–382. <https://doi.org/10.1080/15548627.2020.1797280>.

- (167) Schoop, V.; Martello, A.; Eden, E. R.; Höglinger, D. Cellular Cholesterol and How to Find It. *Biochim. Biophys. Acta - Mol. Cell Biol. Lipids* **2021**, *1866* (9), 158989. <https://doi.org/https://doi.org/10.1016/j.bbalip.2021.158989>.
- (168) Bolard, J. How Do the Polyene Macrolide Antibiotics Affect the Cellular Membrane Properties? *Biochim. Biophys. Acta - Rev. Biomembr.* **1986**, *864* (3), 257–304.

[https://doi.org/https://doi.org/10.1016/0304-4157\(86\)90002-X](https://doi.org/https://doi.org/10.1016/0304-4157(86)90002-X).

- (169) K., T. R. Cholesterol-Dependent Cytolysins, a Family of Versatile Pore-Forming Toxins. *Infect. Immun.* **2005**, *73* (10), 6199–6209. <https://doi.org/10.1128/IAI.73.10.6199-6209.2005>.
- (170) Fam, T. K.; Klymchenko, A. S.; Collot, M. Recent Advances in Fluorescent Probes for Lipid Droplets. *Materials* . 2018. <https://doi.org/10.3390/ma11091768>.
- (171) Listenberger, L. L.; Studer, A. M.; Brown, D. A.; Wolins, N. E. Fluorescent Detection of Lipid Droplets and Associated Proteins. *Curr. Protoc. Cell Biol.* **2016**, *71* (1), 4.31.1-4.31.14. <https://doi.org/https://doi.org/10.1002/cpcb.7>.
- (172) Aits, S.; Kricker, J.; Liu, B.; Ellegaard, A.-M.; Hämälistö, S.; Tvingsholm, S.; Corcelle-Termeau, E.; Høgh, S.; Farkas, T.; Holm Jonassen, A.; Gromova, I.; Mortensen, M.; Jäättelä, M. Sensitive Detection of Lysosomal Membrane Permeabilization by Lysosomal Galectin Puncta Assay. *Autophagy* **2015**, *11* (8), 1408–1424. <https://doi.org/10.1080/15548627.2015.1063871>.
- (173) Jia, J.; Claude-Taupin, A.; Gu, Y.; Choi, S. W.; Peters, R.; Bissa, B.; Mudd, M. H.; Allers, L.; Pallikkuth, S.; Lidke, K. A.; Salemi, M.; Phinney, B.; Mari, M.; Reggiori, F.; Deretic, V. Galectin-3 Coordinates a Cellular System for Lysosomal Repair and Removal. *Dev. Cell* **2020**, *52* (1), 69-87.e8. <https://doi.org/https://doi.org/10.1016/j.devcel.2019.10.025>.
- (174) Sarkar, S.; Carroll, B.; Buganim, Y.; Maetzel, D.; Ng, A. H. M.; Cassady, J. P.; Cohen, M. A.; Chakraborty, S.; Wang, H.; Spooner, E.; Ploegh, H.; Gsponer, J.; Korolchuk, V. I.; Jaenisch, R. Impaired Autophagy in the Lipid-Storage Disorder Niemann-Pick Type C1 Disease. *Cell Rep.* **2013**, *5* (5), 1302–1315. <https://doi.org/https://doi.org/10.1016/j.celrep.2013.10.042>.
- (175) Herms, A.; Bosch, M.; Ariotti, N.; Reddy, B. J. N.; Fajardo, A.; Fernández-Vidal, A.; Alvarez-Guaita, A.; Fernández-Rojo, M. A.; Rentero, C.; Tebar, F.; Enrich, C.; Geli, M.-I.; Parton, R. G.; Gross, S. P.; Pol, A. Cell-to-Cell Heterogeneity in Lipid Droplets Suggests a Mechanism to Reduce Lipotoxicity. *Curr. Biol.* **2013**, *23* (15), 1489–1496. <https://doi.org/https://doi.org/10.1016/j.cub.2013.06.032>.
- (176) Gocze, P. M.; Freeman, D. A. Factors Underlying the Variability of Lipid Droplet Fluorescence in MA-10 Leydig Tumor Cells. *Cytometry* **1994**, *17* (2), 151–158. <https://doi.org/https://doi.org/10.1002/cyto.990170207>.
- (177) Nguyen, T. B.; Louie, S. M.; Daniele, J. R.; Tran, Q.; Dillin, A.; Zoncu, R.; Nomura, D. K.; Olzmann, J. A. DGAT1-Dependent Lipid Droplet Biogenesis Protects Mitochondrial Function during Starvation-Induced Autophagy. *Dev. Cell* **2017**, *42* (1), 9-21.e5. <https://doi.org/https://doi.org/10.1016/j.devcel.2017.06.003>.
- (178) Singh, R.; Kaushik, S.; Wang, Y.; Xiang, Y.; Novak, I.; Komatsu, M.; Tanaka, K.; Cuervo, A. M.; Czaja, M. J. Autophagy Regulates Lipid Metabolism. *Nature* **2009**, *458* (7242), 1131–1135. <https://doi.org/10.1038/nature07976>.
- (179) LaPensee, C. R.; Mann, J. E.; Rainey, W. E.; Crudo, V.; Hunt III, S. W.; Hammer, G. D. ATR-101, a Selective and Potent Inhibitor of Acyl-CoA Acyltransferase 1, Induces Apoptosis in H295R Adrenocortical Cells and in the Adrenal Cortex of Dogs. *Endocrinology* **2016**, *157* (5), 1775–1788. <https://doi.org/10.1210/en.2015-2052>.
- (180) Zweytick, D.; Athenstaedt, K.; Daum, G. Intracellular Lipid Particles of Eukaryotic Cells. *Biochim. Biophys. Acta - Rev. Biomembr.* **2000**, *1469* (2), 101–120. [https://doi.org/https://doi.org/10.1016/S0005-2736\(00\)00294-7](https://doi.org/https://doi.org/10.1016/S0005-2736(00)00294-7).
- (181) Pistor, S.; Chakraborty, T.; Niebuhr, K.; Domann, E.; Wehland, J. The ActA Protein of *Listeria*

- Monocytoenes Acts as a Nucleator Inducing Reorganization of the Actin Cytoskeleton. *EMBO J.* **1994**, *13* (4), 758–763. <https://doi.org/https://doi.org/10.1002/j.1460-2075.1994.tb06318.x>.
- (182) Höglinger, D.; Burgoyne, T.; Sanchez-Heras, E.; Hartwig, P.; Colaco, A.; Newton, J.; Futter, C. E.; Spiegel, S.; Platt, F. M.; Eden, E. R. NPC1 Regulates ER Contacts with Endocytic Organelles to Mediate Cholesterol Egress. *Nat. Commun.* **2019**, *10* (1), 4276. <https://doi.org/10.1038/s41467-019-12152-2>.
- (183) Lee, J.; Jefcoate, C. Monitoring of Dual CRISPR/Cas9-Mediated Steroidogenic Acute Regulatory Protein Gene Deletion and Cholesterol Accumulation Using High-Resolution Fluorescence In Situ Hybridization in a Single Cell . *Frontiers in Endocrinology* . 2017.